UNIVERSITY OF CALIFORNIA SAN DIEGO

Insights into ocean-to-atmosphere transfer of humic-like substances and bacteria

A dissertation submitted in partial satisfaction of the requirements for the degree

Doctor of Philosophy

in

Chemistry

by

Mitchell Valte Santander

Committee in charge:

Professor Kimberly A. Prather, Chair
Professor Lihini A. Aluwihare
Professor Gourisankar Ghosh
Professor Amitabha Sinha
Professor Michael J. Tauber

2022

The dissertation of Mitchell Valte Santander is approved, and it is acceptable in quality and form for publication on microfilm and electronically.

University of California San Diego

2022

DEDICATION

To my family,

for loving and believing in me always

EPIGRAPH

"Give the best you have, and it will never be enough.
Give your best anyway"

St. Teresa of Calcutta (Mother Teresa)

TABLE OF CONTENTS

LIST OF ILLUSTRATIONS

LIST OF FIGURES

LIST OF TABLES

ACKNOWLEDGEMENTS

First and foremost, I would like to thank my advisor and mentor, Professor Kim Prather, for providing me with the many opportunities to grow and to learn as part of my doctoral program at UC San Diego. As a very introverted person, I entered my graduate program lacking experience and ideal communication skills. It was with Kim's passion, guidance, support, and opportunities provided that I was able make vast improvements on my greatest weaknesses as a scientist and as a person. In Kim's group, I learned the importance of thinking about how my work fits into the big picture and how to communicate the science more effectively. I now have more confidence to connect with a wider audience including my family and friends. These are life lessons that I will always remember and I am grateful to have had the chance to learn under her.

I would also like to thank Francesca Malfatti who has been a tremendous source of guidance, support, and encouragement throughout the entire process of completing this dissertation. As a collaborator, Francesca has been there to help resolve issues with our experiments, to give guidance on marine biology, provide feedback on multiple projects, and write papers with me. I am also grateful for the meals we shared and for keeping the atmosphere light-hearted and humorous during difficult times. This dissertation would not be possible without her dedication and support.

I would like to also acknowledge my committee members: Prof. Mike Tauber, Prof. Lihini Aluwihare, Prof. Amit Sinha, and Prof. Gouri Ghosh. I am especially grateful to Mike and Lihini, for providing a source of feedback and support throughout my program. As my first-year advisor, I am grateful for Mike Tauber's dedication to helping me find a research group to join. I

would also like to thank Lihini for inviting me to her group meetings, in which she provided great feedback on my projects, snacks, and encouragement. I am very grateful that they dedicated much of their time to help provide me with feedback and insightful discussions.

This dissertation would also not be possible without the advice and support of both past and present members of the Prather Lab. I would like to especially acknowledge Monica Castrejón, Dr. Chris Lee, Dr. Olivia Ryder, Dr. Xiaofei Wang, and Dr. Jamie Schiffer. Monica Castrejón, our group's administrative assistant, was a tremendous source of support during my graduate program. One of my favorite parts of my time in the group was stopping by Monica's office to chat with her while munching on candy. Dr. Chris Lee shared an office with me for my first few years in the group and has been a great source of support and humor throughout my entire time in graduate school. Dr. Olivia Ryder was also always very funny and supportive through difficult and stressful times. Dr. Xiaofei Wang often accompanied me for lunch, provided me feedback on papers and experiments, and sometimes helped me with last-minute requests. I am grateful to have the chance to work with him during my graduate program. Dr. Jamie Schiffer worked with me on and helped me submit my first paper. Her dedication, positive attitude, and humor were vital during this paper-writing process and beyond.

In addition to those mentioned above, many other Prather Lab members helped support me during my time in the group. My first mentor, Dr. Jess Axson, provided guidance on spectroscopy, experimental design, and experiment interpretation when I first joined the group. I am grateful for her guidance as well as for the many times she offered me a ride home, making a quick stop at Chipotle on the way. Dr. Doug Collins, Dr. Jack Cahill, Matt Ruppel, and Dr. Camille Sultana were also very supportive in mentoring me when I first joined the group. I am especially grateful for Camille's sense of humor and always creating a positive atmosphere. Joe

Mayer was also supportive and allowed me to carry out great science. I would also like to acknowledge the graduate students, post-docs, and lab technicians who I also had the joy of meeting, including Dr. Luis Cuadra-Rodriguez, Dr. Andrew Martin, Dr. Kaitlyn Suski, Hash Al-mashat, Dr. Gavin Cornwell, Kathryn Moore, Matt Pendergraft, Clare Morris, Dr. Charlotte Dewald, Dr. Luisa Galgani, Dolan Lucero, Dr. Kathryn Mayer, Dr. Jon Sauer, Brock Mitts, Dr. Louise Kristensen, Alexia Moore, Dr. Linh Anh Cat, Ke'La Kimble, and Lucia Cancelada. There are many other Prather group members and alumni who I wasn't able to name here, who I am also grateful to have met during my graduate program. I am grateful for all the interaction and fun times we've shared throughout my time at UCSD.

All of the work presented in this dissertation was accomplished through the NSF Center for Aerosol Impacts on Chemistry of the Environment (CAICE). Through this research center, I was able to participate in many intensive campaigns and highly collaborative projects. I am grateful for the many colleagues and collaborators that I was able to work with through CAICE. I would like to give special acknowledgment to Dr. Tom Hill, also commonly referred to as "His Excellency, Thomas Hill, the most brilliant, magnanimous and gracious." Tom's support, humor, and up-to-date knowledge of penguin-related current events always made graduate life lively and entertaining. I am grateful for the opportunity to work with him on several projects, the fun conversations that would come up during CAICE gatherings, and the hilarious email conversations. I also had the pleasure to work with many other CAICE PIs, post-docs, and graduate students, including Dr. Paul DeMott, Dr. Christina McCluskey, Dr. Tim Bertram, Dr. Steven Schill, Dr. Vicki Grassian, Dr. Man Luo, Dr. Mona Shrestha, Dr. Olga Laskina, Dr. Armando Estillore, Dr. Jon Trueblood, Mike Alvez, Victor Or, Liora Mael, Dr. Samantha Doyle, Dr. Skip Pomeroy, Dr. Renee Williams, Dr. Farooq Azam, Dr. Grant Deane, Dr. Dale Stokes,

Dr. Wei Xiong, Dr. Betsy Stone, Dr. Thilina Jayarathne, Dr. Richard Cochran, Dr. Katherine Nadler, Joey Manson. There are many more collaborators that I have interacted with that I am not able to list here. I am also grateful for all of these interactions throughout my involvement in CAICE.

In addition to working with many collaborators, as a member of CAICE I had the opportunity to work as a mentor to many undergraduate students. Josh Cox was the first student that I mentored and I am grateful for the many adventures we had together, such as our late night projects during the IMPACTS campaign and chasing a lost bucket near Scripps Pier. The other undergraduate students I worked with include Nicole Riccobono, Jessica Sustaita, Bas Schaap, Allie Krez, Luis Camarda, Hersh Gupta, Alma Anides-Morales, Sierra Sterling, Young Jeong, Ikran Ibrahim, and Hannah Karp. Their presence especially during summer campaigns made these difficult experiments much brighter.

Lastly I would like to thank the family and friends who have supported me the entire time. First and foremost, I would like to thank my mom and two godmothers for their unconditional love and support. Words can't describe how their cheerfulness and guidance have influenced me before I started graduate school and throughout. They have always been supportive through the good and bad times. I would also like to thank my siblings who have also been extremely supportive. They have always been there for me to share in my joys and pains and sometimes to laugh at my mistakes. I would like to acknowledge my two nephews who always make me smile and sometimes allow me to hug them. I would also like to thank all the aunts, uncles, cousins, and childhood friends who have shown me love and support during my graduate program. Finally, I would like to thank my close friends who have also been supportive

and with whom I've gained so many fun memories. This dissertation would not be possible without my family and friends to keep me sane and happy during my time at UCSD.

Chapter 2 is reproduced with permission from the American Chemical Society: Santander, M.V., Mitts, B.A., Pendergraft, M.A., Dinasquet, J., Lee, C., Moore, A.N., Cancelada, L.B., Kimble, K.A., Malfatti, F., Prather, K.A., "Tandem fluorescence measurements of organic matter and bacteria released in sea spray aerosols", *Environmental Science & Technology*, 55 (8), 5171-5179, 2021. The dissertation author and B.A.M. were co-primary investigators and co-first authors of this paper. The dissertation author was the primary experimenter for studies involving EEMS, primary analyst and figure generator for all EEMS datasets, and lead writer of sections describing EEMS methods and results. B.A.M. was the primary experimenter for studies involving the WIBS, primary analyst and figure generator for all WIBS datasets, and lead writer of sections describing WIBS methods and results. The dissertation author and B.A.M. contributed equally to drafting the introduction, synopsis/abstract, and implications sections of the manuscript, and to revisions of all sections.

Chapter 3 is reproduced with permission from Scientific Reports: Santander, M.V., Schiffer, J.M., Lee, C., Axson, J.L., Tauber, M.J., Prather, K.A., "Factors controlling the transfer of biogenic organic species from seawater to sea spray aerosol", *Scientific Reports*, 12 (1), 3580, 2022. The dissertation author was the primary investigator and author of this paper. M.V.S., M.J.T. and K.A.P. designed the experiments. M.V.S., C.L., J.L.A. performed the experiments. M.V.S. and J. M. S. analyzed the data. M.V.S., J.M.S., M.J.T. and K.A.P. wrote the paper.

Chapter 4 has been submitted to Journal of Geophysical Research: Atmospheres: Santander, M.V.,* Malfatti, F.,* Pendergraft, M.A., Morris, C., Kimble, K.A., Mitts, B.A., Wang, X., Mayer, K.J., Sauer, J.S., Lee, C., Prather, K.A., "Bacterial control of marine humic-

like substance production, composition, size, and transfer to sea spray aerosols during phytoplankton blooms." The dissertation author was the co-primary investigator and co-author of this paper. Authors with * contributed equally. M.V.S., F.M., and K.A.P. designed the experiments. F.M., M.P., C.M., K.A.K. performed enzyme activity measurements, all coauthor participated in the experiments, M.V.S. and F.M. analyzed the data and wrote the paper.

Chapter 5 has been submitted to Environmental Science and Technology: Santander, M.V., Wang, X., Aluwihare, L.I., Prather, K.A., "Assessing Aggregation as a Potential Artifact Impacting the Fluorescence Intensity of Humic Substances in Seawater." The dissertation author was the primary investigator and author of this paper. M.V.S., X.W., L.I.A., and K.A.P designed the experiments. M.V.S performed the fluorescence and particle size distribution measurements and wrote the paper.

Chapter 6 is in preparation: Santander, M.V.,* Malfatti, F.,* Pendergraft, M.A., Dinasquet, J., Mayer, K.J., Sauer, J.S., Lee, C., Prather, K.A., "Metabolically Active Microbes in Sea Spray Aerosols Cycle Inorganic and Organic Carbon Pools: from Single Cells to Bulk Fluorescence-based Analysis During a Phytoplankton Bloom." The dissertation author was the co-primary investigator and co-author of this paper. Authors denoted with * contributed equally. M.V.S., F.M., and K.A.P. designed the experiments. M.V.S. and F.M. analyzed the data, all coauthor participated in the experiments, M.V.S. and F.M. analyzed the data and wrote the paper.

VITA

2010-2011	Research Assistant, University of San Francisco
2011	Teaching Assistant, Department of Chemistry, University of San Francisco
2011-2012	Supplemental Instructor, University of San Francisco
2012	Bachelor of Science, Chemistry, University of San Francisco
2012	Bachelor of Science, Environmental Science, University of San Francisco
2012-2013	Teaching Assistant, Department of Chemistry and Biochemistry, University of California San Diego
2012-2021	Research Assistant, University of California San Diego
2015	Master of Science, Chemistry, University of California San Diego
2022	Doctor of Philosophy, Chemistry, University of California San Diego

PUBLICATIONS

Santander, M.V.*, Malfatti, F.*, Pendergraft, M.A., Dinasquet, J., Mayer, K.J., Sauer, J.S., Lee, C.L., Prather, K.A. Metabolically Active Microbes in Sea Spray Aerosols Cycle Inorganic and Organic Carbon Pools: from Single Cells to Bulk Fluorescence-based Analysis During a Phytoplankton Bloom. In preparation.

Santander, M.V., Luo, M.; Sullivan, M., Grassian, V., Prather, K. A. Molecular Dynamics Model of Marine Humic-like Substances. In preparation.

Mitts, B.A., **Santander, M.V.**, Ibrahim, I., Morris, C.K., Dinasquet, J., Mayer, K.J., Sauer, J.S., Lee, C., Malfatti, F., Prather, K.A. Single-Particle Fluorescence Properties of Oxidized Sea Spray Aerosol. In preparation. 2022

Santander, M.V., Wang, X.; Aluwihare, L., Prather, K. A. Assessing Aggregation as a Potential Artifact Impacting the Fluorescence Intensity of Humic Substances in Seawater. *Environmental Science & Technology*. 2022, submitted.

Santander, M.V.*, Malfatti, F.*, Pendergraft, M.A., Morris, C., Kimble, K.A., Mitts, B.A., Wang, X., Mayer, K.J., Sauer, J.S., Lee, C.L., Prather, K.A. Bacterial Control of Marine Humic-like Substance Production, Composition, Size, and Transfer to Sea Spray Aerosols During Phytoplankton Blooms. *Journal of Geophysical Research: Atmospheres.* **2022**, submitted.

Santander, M.V.; Schiffer, J. M.; Lee, C.; Axson, J. L.; Prather, K. A.; Tauber, M. J., Factors Controlling Transfer of Biogenic Organic Species from Seawater to Sea Spray Aerosol. *Scientific Reports*, 12 (1), 3580, 2022.

Crocker, D. R., Deane, G. B., Cao, R., **Santander, M. V.**, Morris, C. K., Mitts, B. A., Dinasquet, J., Amiri, S., Malfatti, F., Prather, K.A., Thiemens, M.H. Biologically Induced Changes in the Partitioning of Submicron Particulates Between Bulk Seawater and the Sea Surface Microlayer. *Geophysical Research Letters*, 49, 2022

Santander, M.V.*, Mitts, B.A.*, Pendergraft, M.A., Dinasquet, J., Moore, A.N., Cancelada, L.B., Kimble, K.A., Malfatti, F., Prather, K.A. Tandem Fluorescence Measurements of Organic Matter and Bacteria Released in Sea Spray Aerosols, *Environmental Science & Technology*, 55 (8), 5171-5179, 2021.

Pendergraft, M.A., Grimes, D.J., Giddings, S.N., Feddersen, F., Beall, C.M., Lee, C., **Santander, M.V.**, Prather, K.A. Airborne Transmission Pathway for Coastal Water Pollution, *PeerJ*, 2021.

Sauer, J.S., Minich, J.J., Dinasquet, J., Malfatti, F., Mayer, K.J., **Santander, M.V.**, Pendergraft, M., Mitts, B.A., Lee, C., Wang, X. and Rico, B., Knight, R., Bertram, T.H., and Prather, K.A. Production of Dimethyl Sulfide, Methanethiol, and Dimethyl Disulfide During Controlled Phytoplankton-Bacterial Mesocosm Experiments. *Journal of Geophysical Research: Biogeoscience*. In review, 2020.

Mayer, K.J., Wang, X., **Santander, M.V.**, Mitts, B., Sauer, J., Sultana, C. M., Watt, J., Cappa, C.D., and Prather, K.A. Secondary Marine Aerosol Plays a Dominant Role over Primary Sea Spray Aerosol in Cloud Formation, *ACS Central Science*, 6 (12), 2259–2266, 2020.

Hasenecz, E.S., Jayarathne, T., Pendergraft, M.A., **Santander, M.V.**, Mayer, K.J., Sauer, J., Lee, C., Gibson, W.S., Kruse, S.M., Malfatti, F., Prather, K.A., Stone, E.A. Marine Bacteria Affect Saccharide Enrichment in Sea Spray Aerosol During a Phytoplankton Bloom, *ACS Earth and Space Chemistry*, 4 (9), 1638–1649, 2020.

Trueblood, J., Wang, X., Or, V.W., Alves, M.R., **Santander, M.V.**, Prather, K.M., Grassian, V.H. The Old and the New: Aging of Sea Spray Aerosol and Formation of Secondary Marine Aerosol through OH Oxidation Reactions. *ACS Earth and Space Chemistry*, 3 (10), 2307–2314, 2019.

Trueblood, J., Alves, M.R., Power, D., **Santander, M.V.**, Cochran, R.E., Prather, K.M., Grassian, V., Shedding Light on Photosensitized Reactions within Marine-Relevant Organic Thin Films. *ACS Earth and Space Chemistry*, 3 (8), 1614-1623, 2019.

Malfatti, F.*, Lee, C.*, Tinta, T., Pendergraft, M.A., Celussi, M., Zhou, Y., Sultana, C.M., Rotter, A., Axson, J., Collins, D., **Santander, M.V.**, Anides Morales, A.L., Aluwihare, L., Riemer, N., Grassian, V.H., Azam, F. Prather, K.A. Detection of Active Microbial Enzymes in Nascent Sea Spray Aerosol: Implications for Atmospheric Chemistry and Climate. *Environmental Science & Technology Letters*, 6 (3), 171–177, 2019.

Schiffer, J., Luo, M., Dommer, A., Thoron, G., Pendergraft, M., **Santander, M.V.**, Lucero, D., Pecora de Barros, E., Prather, K., Grassian, V., Amaro, R. Impacts of Lipase Enzyme on the Surface Properties of Marine Aerosol. *Journal of Physical Chemistry Letters*, 9, 3839-3849, 2018.

McCluskey, C.S., Hill, T.C.J., Sultana, C.M., Laskina, O., Trueblood, J., **Santander, M.V.**, Beall, C.M., Michaud, J.M., Kreidenweis, S.M, Prather, K.A., Grassian, V.H., DeMott, P.J. A Mesocosm Double Feature: Insights into the Chemical Make-up of Marine Ice Nucleating Particles. *Journal of the Atmospheric Sciences*, 75 (7), 2405-2423, 2018.

Wang, X., Deane, G. B., Moore, K. A., Ryder, O. S., Stokes, M. D., Beall, C. M., Collins, D. B., **Santander, M. V.**, Burrows, S. M., Sultana, C. M., Prather, K. A., The Role of Jet and Film Drops in Controlling the Mixing State of Submicron Sea Spray Aerosol Particles. *Proceedings of the National Academy of Sciences*, 114 (27), 6978, 2017.

Wang, X.F.*, Sultana, C.M.*, Trueblood, J., Hill, T.C.J., Malfatti, F., Lee, C., Laskina, O., Moore, K.A., Beall, C.M., McCluskey, C.S., Cornwell, G.C., Zhou, Y.Y., Cox, J.L., Pendergraft, M.A., **Santander, M.V.**, Bertram, T.H., Cappa, C.D., Azam, F., DeMott, P.J., Grassian, V.H., Prather, K.A., Microbial Control of Sea Spray Aerosol Composition: A Tale of Two Blooms. *ACS Central Science*, 1 (3), 124-31, 2015.

McCluskey, C.S., Hill, T.C.J., Malfatti, F., Sultana, C.M., Lee, C., **Santander, M.V.**, Beall, C.M., Moore, K.A., Cornwell, G.C., Collins, D.B., Prather, K.A., Jayarathne, T., Stone, E.A., Azam, F., Kreidenweis, S.M., DeMott, P.J., A Dynamic Link Between Ice Nucleating Particles Released in Nascent Sea Spray Aerosol and Oceanic Biological Activity during Two Mesocosm Experiments. *Journal of the Atmospheric Sciences*, 74 (1), 151-166, 2017.

Santander, M.V., Cox, J.L., Riccobono, N., Schaap, B., Xiong, W., Grassian, V.H., Prather, K.A., ATR-FT-IR Investigation of the Ocean Surface. *Spectroscopy-Us* 18, 2017.

Lee, C., Sultana, C.M., Collins, D.B., **Santander, M.V.**, Axson, J.L., Malfatti, F., Cornwell, G.C., Grandquist, J.R., Deane, G.B., Stokes, M.D., Azam, F., Grassian, V.H., Prather, K.A., Advancing Model Systems for Fundamental Laboratory Studies of Sea Spray Aerosol Using the Microbial Loop. *Journal of Physical Chemistry A*, 119 (33), 8860-70, 2015.

Pastor, M.B., Kuhn, A.J., Nguyen, P.T., **Santander, M.V.**, Castro, C., Karney, W.L. Hydrogen Shifts and Benzene Ring Contractions in Phenylenes. *Journal of Physical Organic Chemistry*, 26 (9), 750-754, 2013.

Santander, M.V., Pastor, M.B., Nelson, J.N., Castro, C., Karney, W.L. Huckel and Mobius Bond-Shifting Dehydro[4n+2]annulenes. *Journal of Organic Chemistry*, 78 (5), 2033-2039, 2013.

* Authors contributed equally

FIELDS OF STUDY

Major Field of Study: Chemistry

Atmospheric and Analytical Chemistry
Professor Kimberly A. Prather

ABSTRACT OF THE DISSERTATION

Insights into ocean-to-atmosphere transfer of humic-like substances and bacteria

by

Mitchell Valte Santander

Doctor of Philosophy in Chemistry

University of California San Diego, 2022

Professor Kimberly A. Prather, Chair

Sea spray aerosols (SSA) are one of the most abundant aerosols in the atmosphere and strongly influence clouds and climate. The impact of SSA on climate is driven by its chemical composition, in particular the composition of organic matter in SSA; however a full understanding of the factors that control the transfer of organic matter from seawater to SSA has remained elusive. Here we use a combination of fluorescence techniques to examine the chemical composition of seawater, the sea surface microlayer, and SSA in order to identify the factors that give rise to the appearance of species in SSA. Moreover, we use state-of-the-art aerosol generation techniques to study the temporal changes in seawater and isolated SSA over the course of phytoplankton bloom mesocosm experiments that mimic rapid changes in ocean biology and chemistry. In this dissertation, a unique SSA fluorescence signature was characterized and the contribution of marine bacteria to SSA fluorescence was explored. Additional experiments discussed in this dissertation examine the timing of transfer for different classes of molecules in seawater, such as protein-like and humic-like substances (HULIS), and factors that control transfer were identified for each molecular class. Further studies on the HULIS produced during phytoplankton blooms reveal the importance of bacterial enzymes on the sea-air transfer of HULIS. This dissertation also examines the reliability of fluorescence to determine HULIS relative concentration in the presence of aggregation processes. Finally, in this dissertation, a novel approach to study the metabolic activity of marine bacteria is presented and the transfer of metabolically active marine bacteria is discussed. The findings presented herein help to unravel the complex chemical and biological factors that control SSA composition in the real atmosphere.

Chapter 1. Introduction

1.1 Aerosols and Their Impact on Climate

Aerosols are solids or liquids suspended in a gas or more specifically, the atmosphere [*Seinfeld and Pandis, 2006*]. These particles range in size from less than 10 nm to tens of microns [*Seinfeld et al., 2006*]. And while they can be over a hundred times smaller than the width of a human hair, they have profound effects on Earth's climate, atmospheric chemistry, and human health [*Seinfeld et al., 2006*]. In terms of climate, aerosols can interact with solar radiation directly via absorption or scattering of light (known as the direct effect). The ability of aerosols to scatter light depends on factors including their size and refractive index, which in turn is determined by a particle's chemistry [*Seinfeld et al., 2006; Kuniyal and Guleria, 2019*]. Aerosols can also interact with solar radiation indirectly by acting as cloud seeds or forming ice in clouds (ice nucleation), thus controlling cloud properties and lifetime (known as the indirect effect). An aerosol's ability to take up water also depends on multiple factors such as its size and chemical makeup [*Seinfeld et al., 2006; Kuniyal et al., 2019*]. Thus chemistry plays a central role in aerosol's impact on climate. However, because of the vast chemical complexity of atmospheric aerosols, aerosol climate impacts are difficult to study. Therefore, their impact on climate, especially the indirect effect, has been a major uncertainty limiting our understanding of climate change [*IPCC, 2013*]. This uncertainty partially stems from the wide variety of sources for atmospheric aerosols, which can be natural or anthropogenic [*Seinfeld et al., 2006*]. The physicochemical properties of aerosols in the atmosphere can be completely different depending on their source [*Seinfeld et al., 2006*]. One of the most abundant types of aerosols comes from the ocean and is referred to as sea spray aerosol (SSA) [*Gantt and Meskhidze, 2013*].

1.2 Sea Spray Aerosol Climate Impact and Chemical Composition

Oceans cover over 70% of the Earth's surface. The breaking of waves on the ocean surface generates SSA via the bubble bursting process [*Gantt et al., 2013*]. Approximately 2000-10,000 Tg/yr of SSA is ejected from seawater globally; thus, SSA is one of the most abundant types of natural aerosols in the atmosphere [*Gantt et al., 2013*]. SSA can impact climate via both the direct and indirect effect. SSA contains salt which can interact with solar radiation directly by scattering light and contributing to atmospheric cooling [*Haywood et al., 1999; Randles et al., 2004*]. It can also contribute to the indirect effect by forming clouds and affecting cloud properties [*Gantt et al., 2013*]. The SSA impact on the indirect effect is particularly important over remote oceans, where SSA can dominate the aerosol population and cloud formation results in a large change in albedo [*Mccoy et al., 2015*]. SSA can also act as a source for ice nuclei and affect cloud lifetime [*McCluskey et al., 2017*]. While the specific climate-relevant impacts of SSA must be further constrained, it is clear that the SSA impact on climate depends largely on their chemical and biological composition [*Randles et al., 2004; Gantt et al., 2013; Mccoy et al., 2015; McCluskey et al., 2017*].

Because the ocean contains a diverse mixture of organic matter and microscopic organisms, the SSA produced carries with it a unique and complex chemical and biological mixture that is directly controlled by the chemical and biological state of the ocean [*Gantt et al., 2013; Prather et al., 2013; Lee et al., 2015; Wang et al., 2015; Cochran et al., 2017; Bertram et al., 2018; Malfatti et al., 2019; Hasenecz et al., 2020*]. In addition to inorganic components such as sodium chloride, SSA contains a large organic component that is aerosol size-dependent, with a typically high organic fraction at the smaller aerosol sizes [*Prather et al., 2013; Cochran et al., 2017; Bertram et al., 2018*]. The exact nature of this organic fraction has only been recently

heavily studied and has been shown to consist of a wide variety of biomolecules such as lipids, saccharides, proteins, cell fragments, intact microbe cells, and others [*Leck and Bigg, 2005; Facchini et al., 2008; Gantt et al., 2013; Prather et al., 2013; Jayarathne et al., 2016; Cochran et al., 2017; Bertram et al., 2018; Malfatti et al., 2019; Santander et al., 2021*]. While numerous studies have focused on the identification of specific molecular classes in SSA, further questions regarding what compounds are ejected and why still remain [*Bertram et al., 2018*]. What are the ocean biological and chemical factors that control the transfer of organic material from seawater to sea spray? Further investigations into the link between the ocean and the atmosphere are critical to better understand the role of SSA and the oceans on climate.

1.3 The Microbial Loop and the Transfer of Organic Matter and Microbes from Seawater to SSA

Because of the complex chemical composition of SSA, understanding how ocean chemical and biological conditions play a role in SSA composition has been increasingly important in order to predict the role of SSA in climate. Previous field and laboratory studies have shown that the microbial loop [*Azam et al., 1983*] is vital in controlling SSA chemical composition [*Prather et al., 2013; Rinaldi et al., 2013; Lee et al., 2015; O'Dowd et al., 2015; Wang et al., 2015; Malfatti et al., 2019*]. In the microbial loop, marine heterotrophic bacteria degrade and transform the dissolved organic matter produced by phytoplankton [*Azam et al., 1983*]. Following phytoplankton blooms, the increase in heterotrophic bacteria concentrations and their enzyme activities can lead to enhanced transfer of organic matter from seawater to SSA [*Lee et al., 2015; Wang et al., 2015*]. However, the timing and role of bacteria on the transfer of specific classes of molecules requires further studies.

Previous work focusing on specific molecular classes has shown that unique factors may also lead to enhanced sea-air transfer [*Cochran et al., 2016; Jayarathne et al., 2016*]. For example, studies using lipids have shown that differences in surface adsorption can affect the sea-air transfer of lipids, while the binding affinity of cations to these lipids can affect the transfer of divalent cations [*Cochran et al., 2016*]. These findings focused on the air-sea interface has raised interest in the role of the sea surface microlayer (SSML), the 1-1000nm thick layer at the ocean's surface, and how enrichment in the SSML can affect transfer [*Cunliffe et al., 2013*]. While previous work has focused on specific factors that may affect sea-air transfer, questions regarding when and under what types of biological conditions do different molecular classes transfer to SSA remain to be answered.

A milliliter of seawater can contain 10^5 to 10^7 bacteria cells, which can also be directly launched into the atmosphere via SSA [*Patterson et al., 2016; Michaud et al., 2018*]. Previous field studies of microbes in the atmosphere have shown that microbes are abundant in the air and that the ocean is a likely source for airborne bacteria [*Fahlgren et al., 2010; Smets et al., 2016*]. However, only recently has the identification of intact bacteria in SSA been a focus of investigation. Early investigations into isolated SSA produced in the lab have observed a biological component in SSA [*Prather et al., 2013; Cochran et al., 2017*]. Further studies using cryogenic transmission electron microscopy have observed intact cells in SSA [*Patterson et al., 2016*]. Additional studies using extracted DNA have shown that specific bacteria strains are more enriched in SSA and found that factors such as cell wall composition can play a role in more efficient transfer [*Michaud et al., 2018*]. While insights into the transfer of bacteria have been revealed, the properties of microbes after ejection, such as metabolic activity, have yet to be determined. Recent work has shown that airborne bacteria have the potential to be metabolically

active [*Klein et al., 2016*] and to express enzymes [*Malfatti et al., 2019*]. However, no studies have examined the metabolic activity of microbes in SSA or how activity changes due to ocean conditions. Metabolically active microbes in SSA can alter SSA chemistry, affecting their role in climate and atmospheric chemistry [*Smets et al., 2016*]. Thus, uncovering the nature of marine microbes will elucidate their role in climate and human health.

1.4 Laboratory Generation Methods for Producing Atmospherically Relevant SSA

The presence of aerosols from a wide variety of sources makes SSA in the atmosphere a challenge to study in the field and motivates laboratory studies of isolated SSA [*Prather et al., 2013*]. However, SSA has been challenging to study in the laboratory due to the difficulty in generating SSA that accurately mimics the SSA produced over the ocean. SSA observed over the ocean has a unique size distribution that arises from the bursting of bubbles as a wave breaks on the ocean's surface [*Lewis and Schwartz, 2004*]. Additionally, two mechanisms control aerosol production: the rupture of the bubble cap to produce film drops and the collapse of the bubble cavity to eject jet drops [*Lewis et al., 2004*]. The contribution of each of these mechanisms depends on the bubble size distribution created when a wave breaks [*Lewis et al., 2004*]. This bubble bursting process also carries with it a unique chemical and biological composition that depends on the biological state of the ocean [*Prather et al., 2013*]. Thus, in order to capture real, isolated SSA chemistry in the laboratory, the true bubble bursting process must be accurately mimicked.

Three techniques have recently been developed or applied for studies of isolated SSA: 1) the wave channel at Scripps Institution of Oceanography [*Prather et al., 2013*], 2) the Marine Aerosol Reference Tank (MART) [*Stokes et al., 2013*], 3) and the miniature Marine Aerosol

Reference Tank (miniMART) [*Stokes et al., 2016*]. Each of these three SSA generation methods have been shown to accurately mimic the aerosol size distribution generated over the ocean. The SIO wave channel can hold 13,000 L of seawater and produces SSA using a paddle to generate a sinusoidal wave that breaks over an artificial beach. The MART holds approximately 120 L of seawater and generates SSA using a periodic plunging waterfall. The miniMART holds 7 L of seawater and generates aerosols using a water wheel to create a small periodic waterfall. These three generation methods are isolated systems that allow for more controlled experiments where the seawater acting as the source of aerosols can be manipulated to mimic a wide range of ocean chemical and biological states [*Prather et al., 2013; Lee et al., 2015; Wang et al., 2015*]. These experiments can range from simple systems, such as single molecule solutions or bacteria cultures, to extremely complex systems, such as the growth and decline of a phytoplankton bloom. These SSA generation techniques, in combination with tools for chemical characterization of both seawater and SSA, can be used to provide unique insights into the transfer of organic matter and microbes from seawater to SSA.

1.5 Fluorescence Spectroscopy as a Tool for Identifying Links Between Seawater and Aerosol Chemistry

Fluorescence spectroscopy is a powerful tool that can be used to investigate the chemistry of both seawater and SSA. Fluorescence is a phenomenon where a molecule in its excited singlet electronic state relaxes to its ground electronic state through the rapid emission of a photon [*Lakowicz, 2006*]. The fluorescence emission spectra observed depends on the chemical structure of the fluorophores and the solvent in which the fluorophore is dissolved [*Lakowicz, 2006*]. This specificity combined with high sensitivity makes fluorescence ideal for chemical characterization

[*Lakowicz, 2006*]. Two commonly used advancements of fluorescence spectroscopy for the study of aerosol and seawater chemistry include the Wideband Integrated Bioaerosol Sensor (WIBS and excitation-emission matrix (EEM) spectroscopy [*Gabey et al., 2010; Pohlker et al., 2012; Murphy et al., 2013; Toprak and Schnaiter, 2013*].

The WIBS is an instrument designed to detect fluorescence from single particles in real time in order to identify bioaerosols in the atmosphere [*Kaye et al., 2005*]. Rather than full emission spectra, the WIBS integrates the fluorescence over specific wavelength bands at two specific excitation wavelengths targeting the amino acid tryptophan and the cofactor nicotinamide adenine dinucleotide (NADH) [*Kaye et al., 2005*]. In addition to fluorescence, the WIBS also measures particle size and shape. While the WIBS has been used to characterize aerosols in both field studies and laboratory experiments [*Gabey et al., 2010; Toprak et al., 2013; Hernandez et al., 2016; Crawford et al., 2017; Savage et al., 2017*], no studies have used the WIBS to investigate the fluorescence signature of isolated SSA. A WIBS fluorescence characterization of isolated SSA is necessary in order to disentangle their impact in the real atmosphere.

EEM spectroscopy is an extension of fluorescence spectroscopy for improved bulk solution chemical characterization [*Mostofa, 2013; Murphy et al., 2013*]. By examining emission spectra at multiple excitations wavelengths, complex solutions containing multiple fluorophores can be easily studied [*Coble, 1996*]. This technique has been increasingly used to investigate the composition and dynamics of organic matter in a multitude of aquatic environments including wastewater, lakes and the ocean [*Mostofa, 2013; Murphy et al., 2013; Jaffe et al., 2014; Yu et al., 2020*]. EEM spectroscopy is advantageous for studying aquatic environments because it allows for rapid, direct measurements without the need for sample processing or storage [*Coble,*

1996; Zhang et al., 2011]. Additionally, EEM spectroscopy can be used in combination with parallel factor analysis (PARAFAC), a modeling technique used to separate EEMs into individual fluorescent components [*Ishii and Boyer, 2012; Mostofa, 2013; Murphy et al., 2013*]. Both EEMs and PARAFAC analysis have been used previously in numerous studies on marine systems and fewer aerosol studies [*Coble, 1996; Pohlker et al., 2012; Mostofa, 2013; Murphy et al., 2013; Nebbioso and Piccolo, 2013; Chen et al., 2016*]. However, EEM spectroscopy has not been used simultaneously on marine and aerosol systems to examine the transfer of organic matter from seawater to SSA.

In seawater, three classes of fluorescent molecules are commonly detected in EEMs: chlorophyll-a, protein-like substances, and humic-like substances [*Parlanti et al., 2000; Mostofa, 2013*]. Each of these classes fluoresces in a different wavelength region and indicates the presence of different types of biologically-derived constituents in the seawater.

Chlorophyll-a fluoresces in the excitation/emission wavelength region at 400-440 nm / 680-690 nm [*Falkowski and Kiefer, 1985*]. Chlorophyll-a is a common pigment found in every photosynthetic organism, including the microscopic phytoplankton and cyanobacteria found in the marine environment [*Falkowski et al., 1985*]. Chlorophyll-a has been frequently used as a proxy for phytoplankton biomass in the ocean and provides insight into ocean primary productivity and biological activity [*Falkowski et al., 1985; Vignati et al., 2010; Rinaldi et al., 2013; Quinn et al., 2014*]. No studies have reported the detection of this pigment in SSA, thus no studies focus on the factors controlling its sea-air transfer. Because of its unique fluorescence signature and presence in specific types of microbes, chlorophyll-a fluorescence can be used as a useful tool to investigate sea-air transfer.

Protein-like substance fluorescence can originate from a variety of sources, including dissolved proteins, exopolymeric substances (EPS), viruses, bacteria, and phytoplankton [*Determann et al., 1998; Lakowicz, 2006; Mostofa, 2013*]. These fluoresce in the wavelength region of excitation/emission = 275-280 nm / 300-350 nm. It can be further divided into two fluorescence regions: tryptophan-like fluorescence (Ex/Em = 275-280 nm / 330-350 nm) and tyrosine-like fluorescence (Ex/Em = 275 nm / 300-310 nm) [*Determann et al., 1998; Parlanti et al., 2000; Lakowicz, 2006; Mostofa, 2013*]. Because the fluorescence in this region primarily comes from the amino acid tryptophan, observed fluorescence at these excitation or emission wavelengths have been used to identify bioaerosols in the atmosphere [*Despres et al., 2012; Pohlker et al., 2012; Santl-Temkiv et al., 2019*]. Bioaerosols play a critical role in climate and human health.[*Santl-Temkiv et al., 2019*] They can impact cloud properties by acting as cloud seeds or by forming ice in clouds [*Sun and Ariya, 2006; McCluskey et al., 2017; Santl-Temkiv et al., 2019*]. Thus, distinguishing bioaerosols in the atmosphere is vital for a better understanding of their role in climate and health.

Fluorescence in the excitation/emission wavelength region at approximately 320-380 nm / 415-500 nm, are attributed to humic-like substances (HULIS) [*Coble, 1996; Mostofa, 2013*]. HULIS is a complex class of organic molecules that are produced as a result of degrading dead organisms [*Hessen and Tranvik, 1998; Zhang et al., 2009*]. HULIS in the marine environment has been shown to play a role in numerous processes including metal chelation, microbe growth, bioavailability of organic matter for microbe uptake, and production of reactive oxygen species [*Vrana and Votruba, 1995; Hessen et al., 1998; Pouneva, 2005; Laglera and van den Berg, 2009; Gledhill and Buck, 2012*]. HULIS is ubiquitous in the atmosphere and has been the focus of many atmospheric studies due to their potential to act as cloud seeds and contribute to

atmospheric heterogeneous chemistry by acting as photosensitizers [*Graber and Rudich, 2006; Ciuraru et al., 2015; Shrestha et al., 2018; Tsui and McNeill, 2018; Wang et al., 2020*]. While it has been suggested that the ocean is a source for atmospheric HULIS, no studies have focused on the direct sea-air transfer of HULIS in an isolated setting [*Cavalli et al., 2004; Graber et al., 2006*]. Additionally, bacteria are vital for HULIS production in seawater [*Shimotori et al., 2009; Shimotori et al., 2012*]; however, no studies have examined the impact of bacteria or their enzymes on HULIS sea-air transfer. Because of the wide range of roles that HULIS can play in both the seawater and the atmosphere, uncovering the factors that affect the transfer of HULIS from seawater to the atmosphere is critical to better understand its atmospheric chemistry contribution.

1.6 Objectives of Thesis

The overarching goal of the studies in this thesis is to provide unique insights into the transfer of marine organic molecules and microbes from seawater to SSA. While extensive research in the past decade has made great progress in uncovering the chemical composition of SSA [*Cochran et al., 2017; Bertram et al., 2018*], the links between ocean chemistry and SSA composition require further investigation. Specifically, the factors that control sea-air transfer, and how these factors are influenced by marine microbiology, remain elusive. Factors such as concentration, surface activity, and inter-molecular interactions have been suggested to influence the transfer of specific chemical classes [*Cochran et al., 2016*]. However, more studies are necessary to elucidate how these factors play a role in seawater, which is rich in chemical and biological complexity. It is also necessary to elucidate how these factors may change over time and under various ocean biological conditions. Additionally, while it is known that microbes are

transferred from seawater to SSA, the nature of microbes post-ejection requires further investigation. An improved understanding of the microbes in the atmosphere is necessary to elucidate their role in climate and human health. Thus, this dissertation seeks to answer the following questions:

1. What are the fluorescence characteristics of SSA, based on different fluorescence methods? And how do marine bacteria contribute to SSA fluorescence?
2. How does the timing of sea-air transfer for different classes of seawater compare with one another as well as with the timing of a natural growth and decline cycle of phytoplankton bloom?
3. How do marine bacteria and their enzymes influence the sea-air transfer of humic-like substances, one of the most complex classes of organics in seawater?
4. How does the aggregation of humic substances in seawater affect their fluorescence intensities?
5. Do marine bacteria remain active after sea-air transfer and how is their metabolic activity in SSA influenced by ejection at different stages of a phytoplankton bloom?

1.7 Synopsis of Thesis

The work described in this thesis utilizes a combination of state-of-the-art aerosol generation methods and measurement techniques to uncover new insights into the transfer of organic molecules and microbes from seawater to SSA. Chapter 2 discusses the application and comparison of two widely used fluorescence techniques for the characterization of SSA: EEM spectroscopy and a WIBS. Specifically, the fluorescence signature from the perspective of both bulk aerosol, full spectra and single-particle, integrated intensities was characterized. Chapter 3

discusses the transfer of different classes of organic molecules from seawater to sea spray using EEM spectroscopy. This chapter also discusses how the timing of ejection for these different classes compares to their corresponding seawater trends, the other classes of molecules, and the growth and decline cycle of a phytoplankton bloom. Chapter 4 focuses specifically on the sea-air transfer of HULIS from several phytoplankton blooms and how this transfer is influenced by ocean microbiology and microbial enzymatic activity. Chapter 5 examines the reliability of EEM spectroscopy as a tool to measure HULIS relative abundance despite aggregation processes that may affect HULIS fluorescence. Finally, Chapter 6 discusses the sea-air transfer of metabolically active marine microbes using a unique combination of the RedoxSensor Green dye with 3 different techniques: EEM spectroscopy, flow cytometry, and laser scanning confocal microscopy. By investigating the sea-air transfer of organic matter and microbes, this thesis helps to elucidate the ocean's role in impacting atmospheric chemistry and climate.

1.8 Acknowledgements

Francesca Malfatti is acknowledged for assisting in the editing of this chapter.

1.9 References

Azam, F., T. Fenchel, J. G. Field, J. S. Gray, L. A. Meyer-Reil and F. Thingstad. The ecological role of water-column microbes in the sea. *Marine Ecology Progress Series*. **1983**, *10*(3): 257-263.

Bertram, T. H., R. E. Cochran, V. H. Grassian and E. A. Stone. Sea spray aerosol chemical composition: elemental and molecular mimics for laboratory studies of heterogeneous and multiphase reactions. *Chemical Society Reviews*. **2018**, *47*(7): 2374-2400.

Cavalli, F., M. C. Facchini, S. Decesari, M. Mircea, L. Emblico, S. Fuzzi, D. Ceburnis, Y. J. Yoon, C. D. O'Dowd, J. P. Putaud and A. Dell'Acqua. Advances in characterization of

size-resolved organic matter in marine aerosol over the North Atlantic. *Journal of Geophysical Research-Atmospheres*. **2004**, *109*(D24).

Chen, Q. C., Y. Miyazaki, K. Kawamura, K. Matsumoto, S. Coburn, R. Volkamer, Y. Iwamoto, S. Kagami, Y. G. Deng, S. Ogawa, S. Ramasamy, S. Kato, A. Ida, Y. Kajii and M. Mochida. Characterization of chromophoric water-soluble organic matter in urban, forest, and marine aerosols by HR-ToF-AMS analysis and excitation emission matrix spectroscopy. *Environmental Science & Technology*. **2016**, *50*(19): 10351-10360.

Ciuraru, R., L. Fine, M. van Pinxteren, B. D'Anna, H. Herrmann and C. George. Photosensitized production of functionalized and unsaturated organic compounds at the air-sea interface. *Scientific Reports*. **2015**, *5*.

Coble, P. G. Characterization of marine and terrestrial DOM in seawater using excitation emission matrix spectroscopy. *Marine Chemistry*. **1996**, *51*(4): 325-346.

Cochran, R. E., T. Jayarathne, E. A. Stone and V. H. Grassian. Selectivity across the interface: a test of surface activity in the composition of organic-enriched aerosols from bubble bursting. *Journal of Physical Chemistry Letters*. **2016**, *7*(9): 1692-1696.

Cochran, R. E., O. Laskina, J. V. Trueblood, A. D. Estillore, H. S. Morris, T. Jayarathne, C. M. Sultana, C. Lee, P. Lin, J. Laskin, A. Laskin, J. A. Dowling, Z. Qin, C. D. Cappa, T. H. Bertram, A. V. Tivanski, E. A. Stone, K. A. Prather and V. H. Grassian. Molecular diversity of sea spray aerosol particles: impact of ocean biology on particle composition and hygroscopicity. *Chem*. **2017**, *2*(5): 655-667.

Crawford, I., M. W. Gallagher, K. N. Bower, T. W. Choularton, M. J. Flynn, S. Ruske, C. Listowski, N. Brough, T. Lachlan-Cope, Z. L. Fleming, V. E. Foot and W. R. Stanley. Real-time detection of airborne fluorescent bioparticles in Antarctica. *Atmospheric Chemistry and Physics*. **2017**, *17*(23): 14291-14307.

Cunliffe, M., A. Engel, S. Frka, B. Gasparovic, C. Guitart, J. C. Murrell, M. Salter, C. Stolle, R. Upstill-Goddard and O. Wurl. Sea surface microlayers: a unified physicochemical and biological perspective of the air-ocean interface. *Progress in Oceanography*. **2013**, *109*: 104-116.

Despres, V. R., J. A. Huffman, S. M. Burrows, C. Hoose, A. S. Safatov, G. Buryak, J. Frohlich-Nowoisky, W. Elbert, M. O. Andreae, U. Poschl and R. Jaenicke. Primary biological aerosol particles in the atmosphere: a review. *Tellus Series B-Chemical and Physical Meteorology*. **2012**, *64*.

Determann, S., J. M. Lobbes, R. Reuter and J. Rullkotter. Ultraviolet fluorescence excitation and emission spectroscopy of marine algae and bacteria. *Marine Chemistry*. **1998**, *62*(1-2): 137-156.

Facchini, M. C., M. Rinaldi, S. Decesari, C. Carbone, E. Finessi, M. Mircea, S. Fuzzi, D. Ceburnis, R. Flanagan, E. D. Nilsson, G. de Leeuw, M. Martino, J. Woeltjen and C. D. O'Dowd. Primary submicron marine aerosol dominated by insoluble organic colloids and aggregates. *Geophysical Research Letters*. **2008**, *35*(17).

Fahlgren, C., A. Hagstrom, D. Nilsson and U. L. Zweifel. Annual variations in the diversity, viability, and origin of airborne bacteria. *Applied and Environmental Microbiology*. **2010**, *76*(9): 3015-3025.

Falkowski, P. and D. A. Kiefer. Chlorophyll-a fluorescence in phytoplankton - relationship to photosynthesis and biomass. *Journal of Plankton Research*. **1985**, *7*(5): 715-731.

Gabey, A. M., M. W. Gallagher, J. Whitehead, J. R. Dorsey, P. H. Kaye and W. R. Stanley. Measurements and comparison of primary biological aerosol above and below a tropical forest canopy using a dual channel fluorescence spectrometer. *Atmospheric Chemistry and Physics*. **2010**, *10*(10): 4453-4466.

Gantt, B. and N. Meskhidze. The physical and chemical characteristics of marine primary organic aerosol: a review. *Atmospheric Chemistry and Physics*. **2013**, *13*(8): 3979-3996.

Gledhill, M. and K. N. Buck. The organic complexation of iron in the marine environment: a review. *Frontiers in Microbiology*. **2012**, *3*.

Graber, E. R. and Y. Rudich. Atmospheric HULIS: how humic-like are they? A comprehensive and critical review. *Atmospheric Chemistry and Physics*. **2006**, *6*: 729-753.

Hasenecz, E. S., T. Jayarathne, M. A. Pendergraft, M. V. Santander, K. J. Mayer, J. Sauer, C. Lee, W. S. Gibson, S. M. Kruse, F. Malfatti, K. A. Prather and E. A. Stone. Marine bacteria affect saccharide enrichment in sea spray aerosol during a phytoplankton bloom. *ACS Earth and Space Chemistry*. **2020**, *4*(9): 1638-1649.

Haywood, J. M., V. Ramaswamy and B. J. Soden. Tropospheric aerosol climate forcing in clear-sky satellite observations over the oceans. *Science*. **1999**, *283*(5406): 1299-1303.

Hernandez, M., A. E. Perring, K. McCabe, G. Kok, G. Granger and D. Baumgardner. Chamber catalogues of optical and fluorescent signatures distinguish bioaerosol classes. *Atmospheric Measurement Techniques*. **2016**, *9*(7): 3283-3292.

Hessen, D. O. and L. J. Tranvik (1998). Aquatic humic substances: ecology and biogeochemistry. Berlin; New York, Springer.

IPCC (2013). Climate Change 2013: the physical science basis. Contribution of Working Group I to the fifth assessment report of the Intergovernmental Panel on Climate Change. Cambridge, United Kingdom and New York, NY, USA, Cambridge University Press.

Ishii, S. K. L. and T. H. Boyer. Behavior of reoccurring PARAFAC components in fluorescent dissolved organic matter in natural and engineered systems: a critical review. *Environmental Science & Technology*. **2012**, *46*(4): 2006-2017.

Jaffe, R., K. M. Cawley and Y. Yamashita. Applications of excitation emission matrix fluorescence with parallel factor analysis (EEM-PARAFAC) in assessing environmental dynamics of natural dissolved organic matter (DOM) in aquatic environments: a review. *Advances in the Physicochemical Characterization of Dissolved Organic Matter: Impact on Natural and Engineered Systems*. **2014**, *1160*: 27.

Jayarathne, T., C. M. Sultana, C. Lee, F. Malfatti, J. L. Cox, M. A. Pendergraft, K. A. Moore, F. Azam, A. V. Tivanski, C. D. Cappa, T. H. Bertram, V. H. Grassian, K. A. Prather and E. A. Stone. Enrichment of saccharides and divalent cations in sea spray aerosol during two phytoplankton blooms. *Environmental Science & Technology*. **2016**, *50*(21): 11511-11520.

Kaye, P. H., W. R. Stanley, E. Hirst, E. V. Foot, K. L. Baxter and S. J. Barrington. Single particle multichannel bio-aerosol fluorescence sensor. *Optics Express*. **2005**, *13*(10): 3583-3593.

Klein, A. M., B. J. M. Bohannan, D. A. Jaffe, D. A. Levin and J. L. Green. Molecular evidence for metabolically active bacteria in the atmosphere. *Frontiers in Microbiology*. **2016**, *7*.

Kuniyal, J. C. and R. P. Guleria. The current state of aerosol-radiation interactions: A mini review. *Journal of Aerosol Science*. **2019**, *130*: 45-54.

Laglera, L. M. and C. M. G. van den Berg. Evidence for geochemical control of iron by humic substances in seawater. *Limnology and Oceanography*. **2009**, *54*(2): 610-619.

Lakowicz, J. R. (2006). Principles of fluorescence spectroscopy. New York, Springer.

Leck, C. and E. K. Bigg. Biogenic particles in the surface microlayer and overlaying atmosphere in the central Arctic Ocean during summer. *Tellus Series B-Chemical and Physical Meteorology*. **2005**, *57*(4): 305-316.

Lee, C., C. M. Sultana, D. B. Collins, M. V. Santander, J. L. Axson, F. Malfatti, G. C. Cornwell, J. R. Grandquist, G. B. Deane, M. D. Stokes, F. Azam, V. H. Grassian and K. A. Prather. Advancing model systems for fundamental laboratory studies of sea spray aerosol using the microbial loop. *J Phys Chem A*. **2015**, *119*(33): 8860-8870.

Lewis, E. R. and S. E. Schwartz (2004). Sea salt aerosol production : mechanisms, methods, measurements and models : a critical review. Washington, DC, American Geophysical Union.

Malfatti, F., C. Lee, T. Tinta, M. A. Pendergraft, M. Celussi, Y. Y. Zhou, C. M. Sultana, A. Rotter, J. L. Axson, D. B. Collins, M. V. Santander, A. L. A. Morales, L. I. Aluwihare, N. Riemer, V. H. Grassian, F. Azam and K. A. Prather. Detection of active microbial enzymes in nascent sea spray aerosol: implications for atmospheric chemistry and climate. *Environmental Science & Technology Letters*. **2019**, *6*(3): 171-177.

McCluskey, C. S., T. C. J. Hill, F. Malfatti, C. M. Sultana, C. Lee, M. V. Santander, C. M. Beall, K. A. Moore, G. C. Cornwell, D. B. Collins, K. A. Prather, T. Jayarathne, E. A. Stone, F. Azam, S. M. Kreidenweis and P. J. DeMott. A dynamic link between ice nucleating particles released in nascent sea spray aerosol and oceanic biological activity during two mesocosm experiments. *Journal of the Atmospheric Sciences*. **2017**, *74*(1): 151-166.

Mccoy, D. T., S. M. Burrows, R. Wood, D. P. Grosvenor, S. M. Elliott, P. L. Ma, P. J. Rasch and D. L. Hartmann. Natural aerosols explain seasonal and spatial patterns of Southern Ocean cloud albedo. *Science Advances*. **2015**, *1*(6).

Michaud, J. M., L. R. Thompson, D. Kaul, J. L. Espinoza, R. A. Richter, Z. Z. Xu, C. Lee, K. M. Pham, C. M. Beall, F. Malfatti, F. Azam, R. Knight, M. D. Burkart, C. L. Dupont and K. A. Prather. Taxon-specific aerosolization of bacteria and viruses in an experimental ocean-atmosphere mesocosm. *Nature Communications*. **2018**, *9*.

Mostofa, K. M. G. (2013). Photobiogeochemistry of organic matter: principles and practices in water environments. Heidelberg ; New York, Springer.

Murphy, K. R., C. A. Stedmon, D. Graeber and R. Bro. Fluorescence spectroscopy and multi-way techniques. PARAFAC. *Analytical Methods*. **2013**, *5*(23): 6557.

Nebbioso, A. and A. Piccolo. Molecular characterization of dissolved organic matter (DOM): a critical review. *Analytical and Bioanalytical Chemistry*. **2013**, *405*(1): 109-124.

O'Dowd, C., D. Ceburnis, J. Ovadnevaite, J. Bialek, D. B. Stengel, M. Zacharias, U. Nitschke, S. Connan, M. Rinaldi, S. Fuzzi, S. Decesari, M. C. Facchini, S. Marullo, R. Santoleri, A. Dell'Anno, C. Corinaldesi, M. Tangherlini and R. Danovaro. Connecting marine productivity to sea-spray via nanoscale biological processes: Phytoplankton Dance or Death Disco? *Sci Rep*. **2015**, *5*: 14883.

Parlanti, E., K. Worz, L. Geoffroy and M. Lamotte. Dissolved organic matter fluorescence spectroscopy as a tool to estimate biological activity in a coastal zone submitted to anthropogenic inputs. *Organic Geochemistry*. **2000**, *31*(12): 1765-1781.

Patterson, J. P., D. B. Collins, J. M. Michaud, J. L. Axson, C. M. Sultana, T. Moser, A. C. Dommer, J. Conner, V. H. Grassian, M. D. Stokes, G. B. Deane, J. E. Evans, M. D. Burkart, K. A. Prather and N. C. Gianneschi. Sea spray aerosol structure and composition using cryogenic transmission electron microscopy. *Acs Central Science*. **2016**, *2*(1): 40-47.

Pohlker, C., J. A. Huffman and U. Poschl. Autofluorescence of atmospheric bioaerosols – fluorescent biomolecules and potential interferences. *Atmospheric Measurement Techniques*. **2012**, *5*(1): 37-71.

Pouneva, I. D. Effect of humic substances on the growth of microalgal cultures. *Russian Journal of Plant Physiology*. **2005**, *52*(3): 410-413.

Prather, K. A., T. H. Bertram, V. H. Grassian, G. B. Deane, M. D. Stokes, P. J. DeMott, L. I. Aluwihare, B. P. Palenik, F. Azam, J. H. Seinfeld, R. C. Moffet, M. J. Molina, C. D. Cappa, F. M. Geiger, G. C. Roberts, L. M. Russell, A. P. Ault, J. Baltrusaitis, D. B. Collins, C. E. Corrigan, L. A. Cuadra-Rodriguez, C. J. Ebben, S. D. Forestieri, T. L. Guasco, S. P. Hersey, M. J. Kim, W. F. Lambert, R. L. Modini, W. Mui, B. E. Pedler, M. J. Ruppel, O. S. Ryder, N. G. Schoepp, R. C. Sullivan and D. F. Zhao. Bringing the ocean into the laboratory to probe the chemical complexity of sea spray aerosol. *Proceedings of the National Academy of Sciences of the United States of America*. **2013**, *110*(19): 7550-7555.

Quinn, P. K., T. S. Bates, K. S. Schulz, D. J. Coffman, A. A. Frossard, L. M. Russell, W. C. Keene and D. J. Kieber. Contribution of sea surface carbon pool to organic matter enrichment in sea spray aerosol. *Nature Geoscience*. **2014**, *7*(3): 228-232.

Randles, C. A., L. M. Russell and V. Ramaswamy. Hygroscopic and optical properties of organic sea salt aerosol and consequences for climate forcing. *Geophysical Research Letters*. **2004**, *31*(16).

Rinaldi, M., S. Fuzzi, S. Decesari, S. Marullo, R. Santoleri, A. Provenzale, J. von Hardenberg, D. Ceburnis, A. Vaishya, C. D. O'Dowd and M. C. Facchini. Is chlorophyll-a the best surrogate for organic matter enrichment in submicron primary marine aerosol? *Journal of Geophysical Research: Atmospheres*. **2013**, *118*(10): 4964-4973.

Santander, M. V., B. A. Mitts, M. A. Pendergraft, J. Dinasquet, C. Lee, A. N. Moore, L. B. Cancelada, K. A. Kimble, F. Malfatti and K. A. Prather. Tandem fluorescence measurements of organic matter and bacteria released in sea spray aerosols. *Environmental Science & Technology*. **2021**, *55*(8): 5171-5179.

Santl-Temkiv, T., B. Sikoparija, T. Maki, F. Carotenuto, P. Amato, M. S. Yao, C. E. Morris, R. Schnell, R. Jaenicke, C. Pohlker, P. J. DeMott, T. C. J. Hill and J. A. Huffman. Bioaerosol field measurements: challenges and perspectives in outdoor studies. *Aerosol Science and Technology*. **2019**.

Savage, N. J., C. E. Krentz, T. Konemann, T. T. Han, G. Mainelis, C. Pohlker and J. A. Huffman. Systematic characterization and fluorescence threshold strategies for the wideband integrated bioaerosol sensor (WIBS) using size-resolved biological and interfering particles. *Atmospheric Measurement Techniques*. **2017**, *10*(11): 4279-4302.

Seinfeld, J. H. and S. N. Pandis (2006). Atmospheric chemistry and physics : from air pollution to climate change. Hoboken, N.J., J. Wiley.

Shimotori, K., Y. Omori and T. Hama. Bacterial production of marine humic-like fluorescent dissolved organic matter and its biogeochemical importance. *Aquatic Microbial Ecology*. **2009**, *58*(1): 55-66.

Shimotori, K., K. Watanabe and T. Hama. Fluorescence characteristics of humic-like fluorescent dissolved organic matter produced by various taxa of marine bacteria. *Aquatic Microbial Ecology*. **2012**, *65*(3): 249-260.

Shrestha, M., M. Luo, Y. M. Li, B. Xiang, W. Xiong and V. H. Grassian. Let there be light: stability of palmitic acid monolayers at the air/salt water interface in the presence and absence of simulated solar light and a photosensitizer. *Chemical Science*. **2018**, *9*(26): 5716-5723.

Smets, W., S. Moretti, S. Denys and S. Lebeer. Airborne bacteria in the atmosphere: Presence, purpose, and potential. *Atmospheric Environment*. **2016**, *139*: 214-221.

Stokes, M. D., G. Deane, D. B. Collins, C. Cappa, T. Bertram, A. Dommer, S. Schill, S. Forestieri and M. Survilo. A miniature Marine Aerosol Reference Tank (miniMART) as a compact breaking wave analogue. *Atmospheric Measurement Techniques*. **2016**, *9*(9): 4257-4267.

Stokes, M. D., G. B. Deane, K. Prather, T. H. Bertram, M. J. Ruppel, O. S. Ryder, J. M. Brady and D. Zhao. A marine aerosol reference tank system as a breaking wave analogue for the production of foam and sea-spray aerosols. *Atmospheric Measurement Techniques*. **2013**, *6*(4): 1085-1094.

Sun, J. M. and P. A. Ariya. Atmospheric organic and bio-aerosols as cloud condensation nuclei (CCN): A review. *Atmospheric Environment*. **2006**, *40*(5): 795-820.

Toprak, E. and M. Schnaiter. Fluorescent biological aerosol particles measured with the Waveband Integrated Bioaerosol Sensor WIBS-4: laboratory tests combined with a one year field study. *Atmospheric Chemistry and Physics*. **2013**, *13*(1): 225-243.

Tsui, W. G. and V. F. McNeill. Modeling secondary organic aerosol production from photosensitized humic-like substances (HULIS). *Environmental Science & Technology Letters*. **2018**, *5*(5): 255-259.

Vignati, E., M. C. Facchini, M. Rinaldi, C. Scannell, D. Ceburnis, J. Sciare, M. Kanakidou, S. Myriokefalitakis, F. Dentener and C. D. O'Dowd. Global scale emission and distribution of sea-spray aerosol: Sea-salt and organic enrichment. *Atmospheric Environment*. **2010**, *44*(5): 670-677.

Vrana, D. and J. Votruba. Influence of soluble humic substances on the growth of algae and blue-green algae. *Folia Microbiologica*. **1995**, *40*(2): 207-208.

Wang, X. F., C. M. Sultana, J. Trueblood, T. C. J. Hill, F. Malfatti, C. Lee, O. Laskina, K. A. Moore, C. M. Beall, C. S. McCluskey, G. C. Cornwell, Y. Y. Zhou, J. L. Cox, M. A. Pendergraft, M. V. Santander, T. H. Bertram, C. D. Cappa, F. Azam, P. J. DeMott, V. H.

Grassian and K. A. Prather. Microbial control of sea spray aerosol composition: a tale of two blooms. *ACS Central Science*. **2015**, *1*(3): 124-131.

Wang, X. K., R. Gemayel, N. Hayeck, S. Perrier, N. Charbonnel, C. H. Xu, H. Chen, C. Zhu, L. W. Zhang, L. Wang, S. A. Nizkorodov, X. M. Wang, Z. Wang, T. Wang, A. Mellouki, M. Riva, J. M. Chen and C. George. Atmospheric photosensitization: a new pathway for sulfate formation. *Environmental Science & Technology*. **2020**, *54*(6): 3114-3120.

Yu, J. L., K. Xiao, W. C. Xue, Y. X. Shen, J. H. Tan, S. Liang, Y. F. Wang and X. Huang. Excitation-emission matrix (EEM) fluorescence spectroscopy for characterization of organic matter in membrane bioreactors: principles, methods and applications. *Frontiers of Environmental Science & Engineering*. **2020**, *14*(2).

Zhang, Y. L., M. A. van Dijk, M. L. Liu, G. W. Zhu and B. Q. Qin. The contribution of phytoplankton degradation to chromophoric dissolved organic matter (CDOM) in eutrophic shallow lakes: Field and experimental evidence. *Water Research*. **2009**, *43*(18): 4685-4697.

Zhang, Y. L., Y. Yin, L. Q. Feng, G. W. Zhu, Z. Q. Shi, X. H. Liu and Y. Z. Zhang. Characterizing chromophoric dissolved organic matter in Lake Tianmuhu and its catchment basin using excitation-emission matrix fluorescence and parallel factor analysis. *Water Res*. **2011**, *45*(16): 5110-5122.

Chapter 2. Tandem Fluorescence Measurements of Organic Matter and Bacteria Released in Sea Spray Aerosols

2.1 Synopsis

Biological aerosols, typically identified through their fluorescence properties, strongly influence clouds and climate. Sea spray aerosols (SSA) are a major source of biological aerosols, but detection in the atmosphere is challenging due to potential interference from other sources. Here, the fluorescence signature of isolated SSA, produced using laboratory-based aerosol generation methods, was analyzed and compared with two commonly used fluorescence techniques: excitation-emission matrix spectroscopy (EEMS) and the Wideband Integrated Bioaerosol Sensor (WIBS). A range of dynamic biological ocean scenarios were tested to compare EEMS and WIBS analyses of SSA. Both techniques revealed similar trends in SSA fluorescence intensity in response to changes in ocean microbiology, demonstrating the potential to use the WIBS to measure fluorescent aerosols alongside EEMS bulk solution measurements. Together, these instruments revealed a unique fluorescence signature of isolated, nascent SSA and, for the first time, a size segregated emission of fluorescent species in SSA. Additionally, the fluorescence signature of aerosolized marine bacterial isolates was characterized and showed similar fluorescence peaks to those of SSA, suggesting that bacteria are a contributor to SSA fluorescence. Through investigation of isolated SSA, this study provides a reference for future identification of marine biological aerosols in a complex atmosphere.

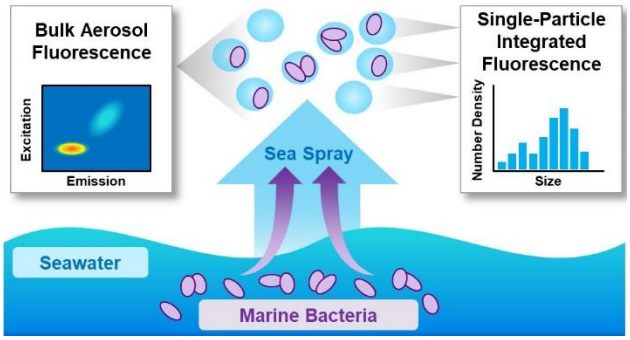

Illustration 2.1. Illustration broadly summarizing the purpose and experimental design combining fluorescence techniques to study SSA.

2.2 Introduction

Biological aerosols, or bioaerosols, are particles that include organisms, biological fragments, excretions, or dispersal units [*Frohlich-Nowoisky et al., 2016*]. These particles are ubiquitous in the atmosphere and can have profound effects on clouds and climate by acting as cloud condensation nuclei and ice nuclei in clouds [*Frohlich-Nowoisky et al., 2016*]. Therefore, there is a strong interest to identify bioaerosols and understand their atmospheric dynamics. A widely used method for bioaerosol identification is fluorescence spectroscopy, which exploits the intrinsically fluorescent biomolecules found in these aerosols [*Pohlker et al., 2012*]. However, aerosols in the atmosphere are often externally mixed populations from different sources, making it a challenge to separate particle types based on fluorescence alone. Thus, it is necessary to characterize the fluorescence of isolated particle sources to disentangle the impact of different bioaerosols in the atmosphere.

The oceans have been shown to be a major source of bioaerosols, via sea spray aerosols (SSA) particles [*Despres et al., 2012; Frohlich-Nowoisky et al., 2016*]. SSA particles are produced when bubbles, entrained by breaking waves, burst at the sea surface. SSA composition can vary depending on the biological state of the ocean [*Prather et al., 2013; Rinaldi et al.,*

2013; Wang et al., 2015]. Previous studies have shown that SSA particles contain bacteria, cell fragments, viruses, enzymes, and other biomolecules that can influence the climate and relevant cloud properties [*Patterson et al., 2016; Malfatti et al., 2019*]. Despite the potential for marine bioaerosols to play a major role in climate, very few studies have used fluorescence as a tool to identify bioaerosols released during nascent SSA production [*Toprak and Schnaiter, 2013; Kasparian et al., 2017; Yue et al., 2019*]. This is, in part, due to the difficulty of using fluorescence to study SSA in the real atmosphere without a basic understanding of the fluorescence signature of SSA.

Here, the fluorescence characterization for isolated, lab-generated SSA is reported. Two common fluorescence methods were used to characterize SSA: excitation-emission matrix spectroscopy (EEMS) and a Wideband Integrated Bioaerosol Sensor (WIBS). EEMS has been widely used to characterize organic matter in a variety of aqueous environments including seawater [*Zhang et al., 2011; Mostofa, 2013; Nebbioso and Piccolo, 2013*]. EEMS has the advantage of taking direct, full-spectrum fluorescence measurements of aqueous samples and can be used to investigate offline, bulk aerosol chemistry. The WIBS collects online, single-particle fluorescence measurements at lower resolution and has been increasingly used to investigate the dynamics of atmospheric bioaerosols in both the laboratory and the field [*Gabey et al., 2010; Toprak et al., 2013; Hernandez et al., 2016; Crawford et al., 2017; Savage et al., 2017*]. However, no studies have used the WIBS to directly measure isolated, nascent SSA in a laboratory setting. In the present study, single-particle and bulk aerosol fluorescence were used to evaluate realistic SSA and determine how SSA fluorescence changes under dynamic ocean biological conditions (e.g. during a phytoplankton bloom). Additionally, these techniques were used to characterize the contribution of marine bacteria to SSA fluorescence through controlled

experiments involving isolated marine bacteria and abiotic seawater. This study provides a framework for using a fluorescence approach to investigate how temporal changes in biological species affect SSA released into the environment.

2.3 Methods

2.3.1. Aerosol Generation and Experiment Design

SSA particles were generated using three different methods: a wave channel located at the Scripps Institution of Oceanography [*Prather et al., 2013; Wang et al., 2015*], a Marine Aerosol Reference Tank (MART) [*Stokes et al., 2013; Lee et al., 2015*], or a miniature Marine Aerosol Reference Tank (miniMART) [*Stokes et al., 2016*]. Each of these aerosol generation methods is an isolated system, without the influence of non-biological fluorescent particles from terrestrial or anthropogenic sources. Additionally, each of these methods produces aerosol size distributions and chemical compositions which mimic that of a breaking ocean wave [*Collins et al., 2014; Stokes et al., 2016*]. The three experimental methods also differed in biological activity in the seawater: 1. Seawater without a phytoplankton bloom; 2. Seawater with Guillard's nutrient medium added to generate a phytoplankton bloom with natural marine microbial communities [*Guillard and Ryther, 1962*]; and 3. Control scenarios consisting of either abiotic seawater or cultured marine bacterial strains in a phosphate- buffered saline solution (4x PBS). Details of the three experiments are provided in Table 2.1 as well as the Supporting Information.

Table 2.1. Layout of the three experimental setups used in this study.

Experiment Number	Bulk Solution	Additions	Aerosol Generation	Fluorescence Measurements
Experiment 1	Seawater	None	Wave channel	EEMS bulk solution, EEMS & WIBS aerosol
Experiment 2	Seawater	F/100 nutrients[a], sodium silicate	MART	EEMS bulk solution, EEMS & WIBS aerosol
Experiment 3a	Seawater & filtered, autoclaved seawater	F/2 nutrients[a]	miniMART	EEMS bulk solution & WIBS aerosol
Experiment 3b	4xPBS with bacterial isolates	None	miniMART	EEMS bulk solution & WIBS aerosol

[a] Final concentration of Guillard's growth medium. A final concentration of F/2 is defined by Guillard & Ryther (1962), therefore, a concentration of F/100 is a 50x dilution.

2.3.2. Aerosol and Seawater Sample Collection

Aerosol samples were measured in real time with the WIBS and collected into a liquid solution for EEMS measurements. Prior to detection with the WIBS, aerosols were dried using in-line silica diffusion driers to maintain a relative humidity of <20% throughout all experiments. As a result of drying and partial quenching of the fluorophores, it is possible that a fraction of fluorescent particles was below the fluorescence threshold. While channel 1 may not be affected due to the strong emission of tryptophan, humic-like substances can show decreased emission when in a powder state [*Pohlker et al., 2012*]. However, SSA particles have been shown to be semisolid below the efflorescence point [*Lee et al., 2020*], therefore, drying should not have a significant effect on the observed trends.

For EEMS analysis of the bulk aerosol, collection involved a liquid spot sampler (Aerosol Devices Inc., 110A), which uses a water condensation growth tube to collect particles

directly into a liquid medium with high efficiency [*Fernandez et al., 2014*]. Aerosols passing through the spot sampler were collected in ultrapure water. Although collection into ultrapure water could potentially change the fluorescence intensity due to bacterial lysis and subsequent solvent exposure, these changes would be slight, due to the lack of new tryptophan formation/breakdown. Additionally, any changes would be consistent throughout the course of these experiments. SSA particles were collected for experiments 1 and 2 at a flow rate of 1.5 liters per minute (LPM) for 1 hour on the MART or overnight (12 hours) on the wave channel. No aerosols were collected for EEMS analysis for experiment 3 (miniMART).

Seawater collection for EEMS analysis was performed for each experiment. For all experiments, seawater samples were collected into either 15 mL or 50 mL sterile, polypropylene tubes. Seawater samples were collected during aerosol generation for Experiment 2 and either prior to, or immediately after, aerosol generation for the other experiments. Excitation-emission matrices (EEMs) were generally measured within 20 minutes of collection.

2.3.3. Bacterial Isolate Culture Preparation

Three different marine-relevant bacterial isolates were chosen due to their presence in the coastal waters off of Scripps Pier: AltSIO, ATW7, and BBFL7 [*Bidle and Azam, 2001; Pedler et al., 2014*]. All isolates were originally derived from the Pacific Ocean off the Scripps Pier in La Jolla, California and isolated by the Azam laboratory at the Scripps Institution of Oceanography. For this experiment, bacterial isolates were streaked out from a frozen glycerol stock onto ZoBell medium. After 24 hours, colonies were picked and grown in liquid ZoBell medium at room temperature on a shaker (130 rpm). The next day, the cultures were harvested through 5 minutes of centrifugation at 9000 g and washed with PBS to remove the supernatant (spent medium).

Optical density was measured at 600 nm in order to have a 1:1:1 (AltSIO:ATW7:BBFL7) ratio of the three cultures in the inoculum with a concentration of $1x10^9$ cells/mL. The final concentration of bacterial cells in the miniMART was ~$1.6x10^5$ cells/mL, which is on the order of known bacterial concentrations in the ocean, especially in oligotrophic regions [*Azam et al., 1983*].

2.3.4. Fluorescence Measurements

WIBS: Online, single-particle fluorescence measurements were taken using a Wideband Integrated Bioaerosol Sensor (Droplet Measurement Technologies, WIBS-NEO). The WIBS operation has been described previously in detail [*Gabey et al., 2010*]. Briefly, the WIBS utilizes two xenon lamps with bandpass filters to generate two excitation wavelengths at 280 nm (Xe1) and 370 nm (Xe2). These excitation wavelengths are intended to target the fluorescence excitation of the amino acid tryptophan and the biological cofactor nicotinamide adenine dinucleotide (NADH), respectively [*Kaye et al., 2005*]. The WIBS collects the fluorescence emission from a particle using two photomultiplier tubes (PMTs) with bandpass filters from 310-400 nm (FL1) and from 420 – 650 nm (FL2). This arrangement creates three main combinations of fluorescence excitation and emission "channels," with different target molecules. These channels are labeled here as channel 1 (Xe1/FL1; Ex/Em = 280 nm/310-400 nm; targeting tryptophan), channel 2 (Xe1/FL2; 280 nm/420-650 nm; targeting riboflavin), and channel 3 (Xe2/FL2; 370nm/420-650 nm, targeting NADH). We focus primarily on channels 1 and 3, as these channels coincide with the EEMs peaks representing the fluorescence from protein-like and humic-like substances (HULIS), respectively. Additionally, we exclude channel 2 from most of

our discussion due to the potential cross-sensitivity of this channel with the other two channels, as reported previously [*Gabey et al., 2011; Toprak et al., 2013*].

A forced trigger sampling period, where the sample flow is off and the xenon lamps are fired, was performed at the start of each day to provide a blank for the fluorescent particle detection. Particles are deemed fluorescent if they exceed a minimum threshold:

$$E_{Threshold_i} = 3\sigma_i + \bar{E}_i \quad [1]$$

where $\bar{E}_i$ is the mean background fluorescence from the forced trigger data and σ_i is the standard deviation of the background for each fluorescence channel (FL_i), as described in previous studies [*Toprak et al., 2013*]. The fluorescence values for particles detected by the WIBS were then subtracted by the forced trigger thresholds for each individual channel. The WIBS-NEO has greater dynamic range compared to previous models, which prevents saturation of the detector for highly fluorescent particles [*Forde et al., 2019*]. The intensity values reported are in arbitrary units, however, the mean SSA intensity values were converted to mass equivalents of tryptophan (channel 1) and quinine (channel 2&3) based on a similar calibration to that defined by Robinson et al. (Figure 2.6) [*Robinson et al., 2017*].

The WIBS uses a 635 nm continuous-wave laser to detect, size, and determine the shape of single particles. Optical diameter measurements, from 0.5 µm to 50 µm, are based on detection of side-scattered light with the FL2 PMT. Analysis of forward-scattered light on a quadrant PMT determines the asymmetry factor (AF) for each particle. The AF is a measure of the shape of a particle, with an AF <10-15 indicative of nearly spherical particles, an AF of 15-30 for aspherical particles, and an AF >30 for rod or fiber shaped particles [*Kaye et al., 2007; Crawford et al., 2017*]. The single-particle optical diameter, measured with the WIBS, was used

to calculate the size distribution of fluorescent particles in each channel. Polystyrene latex spheres were used to verify the accuracy of the WIBS optical diameter measurements. For the size distribution measurements, size bins were divided into 32 bins per decade of optical diameter. Particle counts are displayed as the number concentration of fluorescent particles per liter of air divided by the logarithm of the bin width (dN/dlogDp). In addition to the forced trigger fluorescence threshold, a size threshold was applied to all particles measured with the WIBS. Particles with optical diameters less than D_p = 0.8 µm were excluded from these analyses because of previously reported inaccuracies in the fluorescence detector sensitivity and counting efficiency of smaller particles [*Gabey et al., 2011; Crawford et al., 2017*]. For bacterial isolate size distributions, a fluorescence cutoff of 2.5 standard deviations above the mean background PBS fluorescence in channel 1 was applied to eliminate most PBS particles.

EEMS: Offline, bulk fluorescence excitation-emission matrices (EEMs) of seawater and SSA collected with the liquid spot sampler were measured with an Aqualog spectrophotometer (Horiba Scientific, extended range). Collection periods of at least 1 hour on a MART at 1.5 LPM or approximately 12 hours at 1.5 LPM on the wave channel were used to obtain an adequate fluorescence signal from the protein-like region and often sufficient signal for the HULIS region, depending on seawater biology and chemistry. No processing of seawater samples was necessary to acquire fluorescence signals. Excitation wavelengths ranged from 230-500 nm while the emission collection bands ranged from 250-800 nm, both in ~5 nm increments. Background spectra acquired using ultrapure water or PBS solution were subtracted from all EEMs. EEMs were then corrected for inner filter effects based on the absorbance spectra measured simultaneously. Rayleigh scattering (1st and 2nd order) was removed from all spectra. EEMs were normalized to the area of the Raman scattering peak of water at 350 nm excitation to

convert fluorescence intensities to Raman Units (R.U.) [*Lawaetz and Stedmon, 2009; Murphy, 2011*]. A comparison between the EEM spectrum and the WIBS channels is highlighted in Figure 2.7.

2.4. Results

Three different experiments, with varying biological complexity and activity, were studied in order to compare the fluorescence measurements of EEMS and the WIBS. Experiment 1 used a wave channel and fresh seawater to replicate SSA production of the natural microbial community in coastal seawater with low phytoplankton biomass. Experiment 2 involved a MART for aerosolization of seawater induced with a phytoplankton bloom, typical of realistic bloom conditions with high biomass. Experiment 3 was used as a control of two different scenarios involving a miniMART: abiotic seawater, and a pure bacterial system in a salt solution.

2.4.1. Experiment 1: Bulk Aerosol and Single-Particle Fluorescence of Nascent SSA

EEMs for seawater showed fluorescence in regions that are commonly detected for marine systems (Figure 2.1a) [*Coble, 1996; Mostofa, 2013*]. Specifically, three fluorescence regions were present, representing three different classes of organic molecules. Fluorescence in the region at excitation/emission wavelengths 400-440 nm/680-690 nm is indicative of chlorophyll-a [*Mostofa, 2013*]. Fluorescence at excitation/emission wavelengths <235 nm and 275-280 nm/330-350 nm is attributed to protein-like substances and typically indicates fluorescence from the amino acid tryptophan. In this study, the 275-280 nm excitation was used as an indicator for protein-like fluorescence because of the excitation bounds of the EEMs. Components that emit in this region can range from bacteria cells to viruses to proteinaceous gels [*Determann et al.,*

1998; Lakowicz, 2006; Mostofa, 2013]. EEM features near 260 nm or 360 nm/450-455 nm and at 325 nm/410 nm are indicative of HULIS, complex mixtures of organic molecules produced during the breakdown of organisms and larger biomolecules [*Coble, 1996; Hessen and Tranvik, 1998; Mostofa, 2013*].

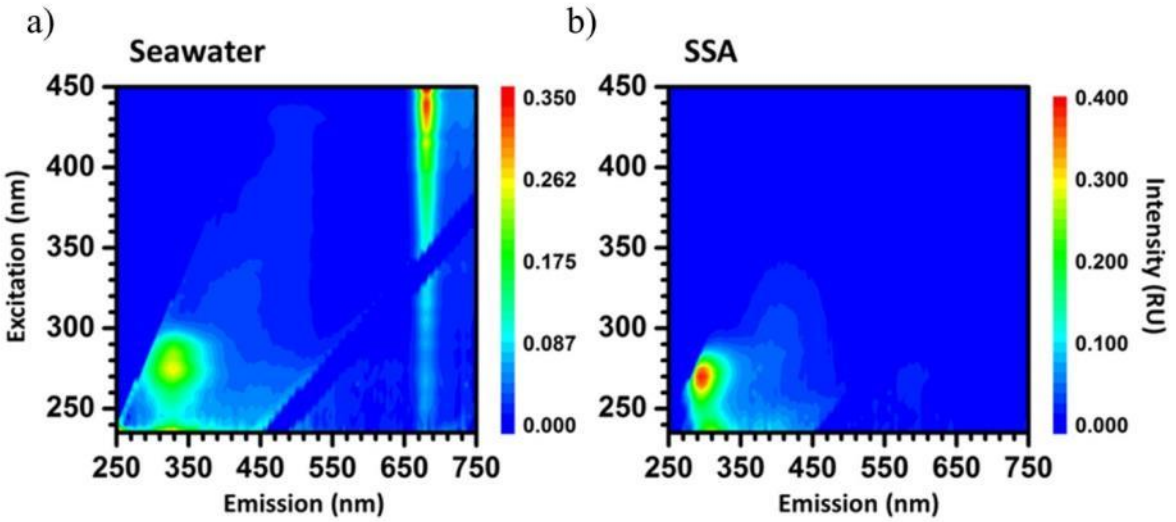

c)	Channel 1 (280 nm/310-400 nm)	Channel 2 (280 nm/420-650 nm)	Channel 3 (370 nm/420-650 nm)
Intensity (a.u.)	1.245e5 ± 5.368e5	2.491e4 ± 6.560e4	3.608e4 ± 1.045e5
Diameter (μm)	2.19 ± 1.01	2.03 ± 0.93	1.63 ± 0.816
AF (a.u.)	6.23 ± 3.25	6.10 ± 3.14	5.57 ± 2.79

Figure 2.1. Selected EEMs for a) seawater and b) nascent SSA collected from the wave channel. c) WIBS measurements of the mean fluorescence intensity, optical diameter, and asymmetry factor (AF) for each fluorescence channel (excitation/emission) for the SSA generated by the wave channel.

EEMs for SSA collected from the wave channel showed different fluorescence signatures than those in seawater, indicating chemical species are selectively transferred into SSA (Figure 2.1b). In contrast to seawater, SSA did not show chlorophyll-a signatures suggesting that larger

phytoplankton species are not efficiently transferred. While both seawater and SSA EEMs showed protein-like and humic-like signatures, SSA EEMs were primarily dominated by protein-like fluorescence with a smaller contribution from HULIS. The ratio of the protein-like peak (Ex: 275 nm/Em: 330 nm) to the humic-like peak (Ex: 360 nm/Em: 450 nm) was evaluated for both samples. The protein-to-humic intensity ratio for seawater was 12.87 whereas the ratio for SSA was 15.63, confirming the increased contribution of protein-like fluorescence in SSA. Additionally, the SSA EEMs showed a shift in the protein-like emission spectra when compared to the protein-like fluorescence in seawater. While seawater showed fluorescence primarily from tryptophan, with an emission peak close to 350 nm, SSA showed a major peak in the emission spectra closer to 300 nm, indicative of fluorescence from the amino acid tyrosine. Tyrosine fluorescence suggests the presence of marine gels or exopolymeric substances in SSA [*Liu et al., 2017*]. The tyrosine peak lies outside the range of wavelengths detected by the WIBS (310-400 nm), thus some portion of SSA fluorescence was not captured using this analytical method. However, the protein peak in SSA extended to longer wavelengths, suggesting tryptophan fluorescence was also present and therefore detectable with the WIBS.

Across seven days of sampling nascent SSA particles generated from the wave channel, the WIBS measured over 100,000 individual fluorescent particles each day. The fluorescent fraction in this low biomass scenario represented 0.87% ± 0.09% of all particles measured with optical diameters greater than D_p = 0.8 µm. The fluorescent fraction measured was relatively low compared to ambient measurements which range from 1.9% to upwards of 40%, but are often influenced by terrestrial bioaerosols [*Crawford et al., 2017; Fennelly et al., 2018*]. In order to define a distinct fluorescence signature for isolated SSA, mean fluorescence intensities of the different fluorescence channels were calculated from all sampling days combined (Figure 2.1c).

Additionally, the channel-specific mean AF and diameter were calculated for fluorescent SSA particles. Particles across all three channels had low AF (~6), with channel 3 particles showing the lowest AF. These low AFs demonstrate that most of the fluorescent particles detected were spherical or spheroidal in shape. The mean diameter of SSA measured in channel 1 were, in general, larger than those in channel 3, indicating different chemical species are transferred into different particle sizes.

The mean daily size distributions of SSA particles generated by the wave channel were measured with the WIBS and separated based on the fluorescence channels (Figure 2.2). The size distributions measured with the WIBS showed a bimodal distribution for channel 1, with a peak optical diameter around D_p = 2.6 μm and a second mode near D_p = 1 μm. The larger-sized mode is suggestive of proteinaceous molecules ejected in supermicron-sized aerosols. Bacteria, which contain a high protein content, have been observed in coarse mode aerosols measured in nascent SSA and off coastal regions [*Shaffer and Lighthart, 1997; Rastelli et al., 2017*]. Previous WIBS studies show that bacteria have dominant fluorescence emission in channel 1 due to the amino acid tryptophan [*Hernandez et al., 2016; Savage et al., 2017*]. Additionally, a fraction of particles that fluoresced in channel 1 also fluoresced in channel 3 (ca. 7% of all channel 1 particles). The particles that fluoresced in both channels 1 and 3 showed a size distribution resembling the main mode for channel 1 fluorescent particles, slightly shifted to larger sizes (Figure 2.8). The size distribution and fluorescence signature of the particles that fluoresced in both channels 1 and 3 suggest that these particles may be metabolically active bacteria, with enhanced NADH. Furthermore, bacteria bound to gels and transparent exopolymeric particles have been observed in this size range [*Mari and Kiorboe, 1996; Aller et al., 2005*]. Bound

bacteria are often larger and enzymatically active which may explain the shift to larger sizes for particles that fluoresce in both channels 1&3 [*Smith et al., 1992*].

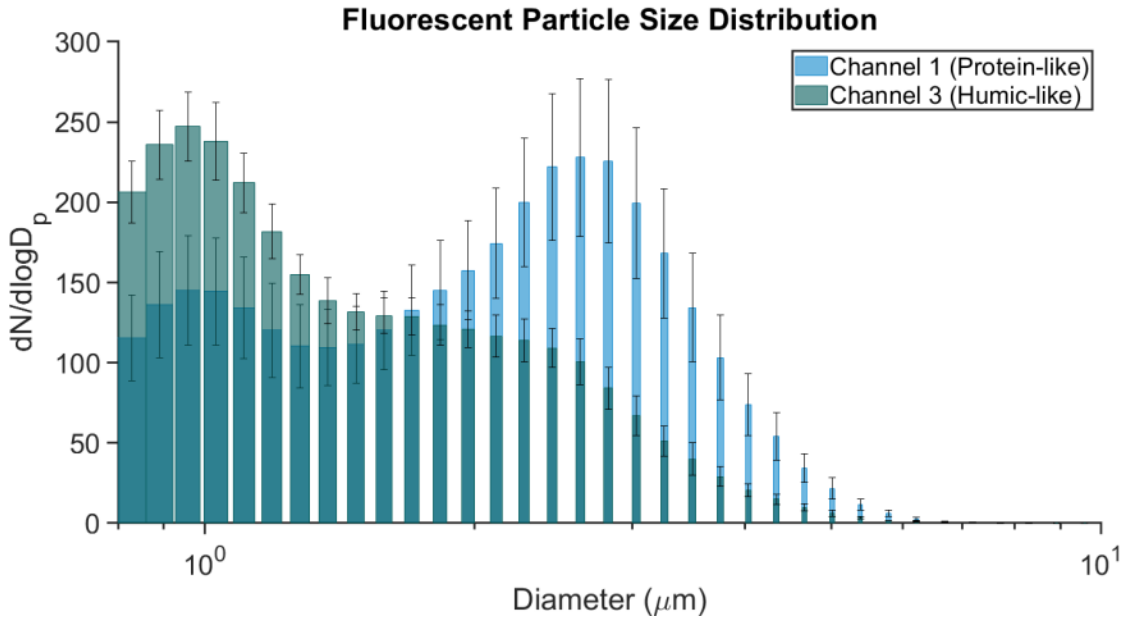

Figure 2.2. SSA size distributions separated by fluorescence channels measured with the WIBS. Channel 1 (protein-like) is in blue with channel 3 (humic-like) overlaid in green. Both size distributions shown are the daily mean particle counts (#/L) normalized to the bin widths and the error bars represent one standard deviation from the mean.

For particles fluorescing in the WIBS channel 3, a peak in the size distribution was observed near D_p = 1 µm with a tail extending into the larger sizes (Figure 2.2). In an ambient setting, fluorescence in this channel is often associated with pollen and fungal spores. However, in this study of isolated, nascent SSA, fluorescence in this channel was likely indicative of HULIS, as shown in previous work by Savage et al. [*Savage et al., 2017*]. Measurements on the molecular weight of marine-based HULIS show it typically consists of small molecules, with 90% of the measured HULIS mass falling below 5 kDa [*Grzybowski, 1995*]. HULIS, by nature, is part of dissolved organic matter in the ocean and is therefore expected to be released across particles of all sizes [*Benner et al., 1992*]. The shape of the total particle size distribution (combined fluorescent and non-fluorescent), measured for SSA generated by the wave channel,

was similar to that of channel 3 (Figure 2.9). This similarity further suggests that the channel 3 measurements by the WIBS are indicative of dissolved HULIS in the SSA.

2.4.2. Experiment 2: Changes in Fluorescence Signatures During a Phytoplankton Bloom

SSA fluorescence was measured with both the WIBS and EEMS throughout an induced phytoplankton bloom to investigate the effect of a changing marine biological state on SSA. The microbial dynamics were measured throughout the course of the phytoplankton bloom (Figure 2.10). The experiment occurred over nine days with *in vivo* chlorophyll-a fluorescence indicating a peak in phytoplankton growth on the third day, followed by senescence for the remainder of the experiment. Heterotrophic bacteria concentrations peaked on the fifth day and declined afterwards. Virus concentrations tracked the heterotrophic bacteria concentrations and increased after the peak in the phytoplankton bloom (Figure 2.10).

WIBS measurements of the SSA fluorescence intensity corresponded with SSA EEMs throughout the phytoplankton bloom (Figure 2.3). WIBS channel 1 (protein-like) showed a general decrease in fluorescence intensity over time. The decreasing fluorescence trend was also observed for the SSA EEMs upon integrating over the same wavelengths of WIBS channel 1. The trends in WIBS channel 1 and EEMs protein-like region revealed a disconnect between the fluorescence observed in SSA and the fluorescence in seawater over the course of the bloom (Figure 2.3). However, when the WIBS channel 3 measurements were compared to the corresponding seawater HULIS-region fluorescence measured with EEMS, the SSA mean fluorescence intensity generally agreed with that in the seawater (Figure 2.11). The difference in enrichment for HULIS and protein-like species into the aerosol indicates a chemical-specific

transfer. More studies are required to determine which factors affect the selective transfer of fluorescent species from seawater to SSA. Nevertheless, the similarity between the WIBS and EEMS measurements of SSA over time reveals that single-particle fluorescence, in combination with seawater analysis, can provide unique insights on SSA composition throughout a wide range of ocean biological conditions.

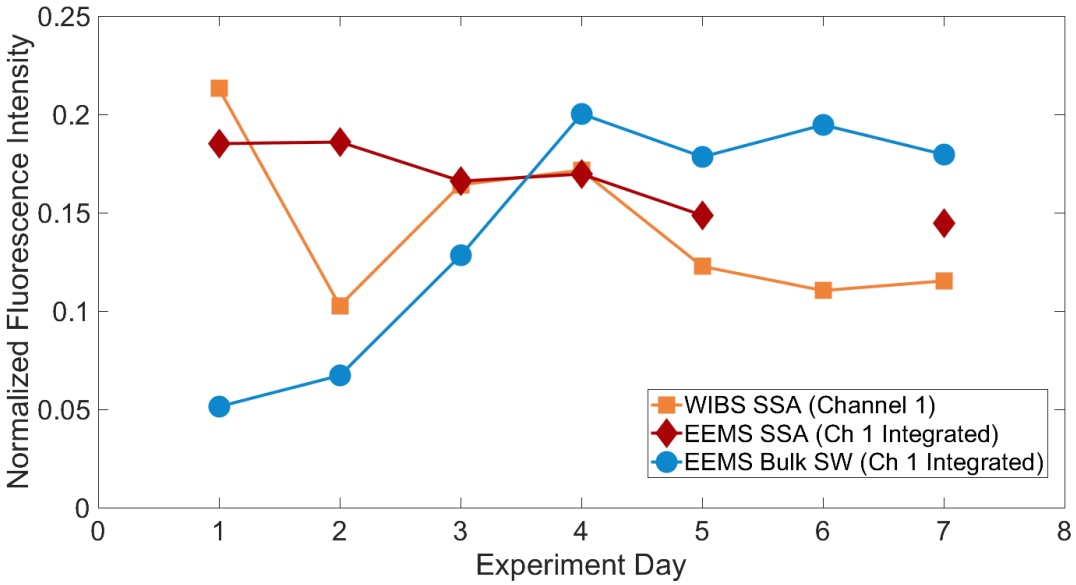

Figure 2.3. WIBS fluorescence channel 1 (protein-like) graphed over time during a phytoplankton bloom. EEM emission integrated over the same wavelengths measured by the WIBS shown over time for both bulk seawater (Bulk SW) and SSA over the course of a phytoplankton bloom. All values are normalized to the sum of intensities for each measurement across all the days of the experiment.

2.4.3. Experiment 3: Characterizing the Fluorescence of Abiotic Seawater and Bacterial Isolates

In order to probe the contribution of marine bacteria to SSA fluorescence, the WIBS and EEMS were used to measure fluorescence under two controlled scenarios: 1) natural seawater vs. filtered, autoclaved seawater (FASW) and 2) marine bacterial isolates in a salt solution. As mentioned previously, seawater used for the FASW experiment was taken from a separate

phytoplankton bloom experiment and the bacterial isolates experiment was run with a PBS medium to minimize background fluorescence.

To better understand the underlying fluorescence signature of SSA, changes in both seawater and SSA fluorescence were measured with EEMS and the WIBS before and after sterilization of the seawater. The FASW EEMs showed an increase in the humic-like fluorescence intensity compared to natural seawater EEMs, suggesting an enhanced production of HULIS during the autoclaving process (Figure 2.4a) [*Andersson et al., 2019*]. The enhanced production of HULIS or a potential change in the selectivity, leading to aerosol enrichment, might explain the increase in the WIBS channel 3 size distribution for FASW SSA (Figure 2.4b). Additionally, WIBS measurements on the FASW SSA showed a decrease in the D_p = 2-3 µm sized mode in the channel 1 fluorescence size distribution compared to the natural SSA (Figure 2.4d), suggesting a lack of large, protein-containing particulates in the FASW SSA. The decrease in the WIBS channel 1 size distribution was not as significant as the diminishment in EEMs protein-like feature (Figure 2.4c), likely because the fluorescent material (reduced but still detected by EEMS) was detected by the WIBS and contributed to the fluorescent size distribution. However, the trends of both instruments further suggest that marine microbes are contributing to the large size mode observed in the WIBS channel 1 size distribution measured for SSA.

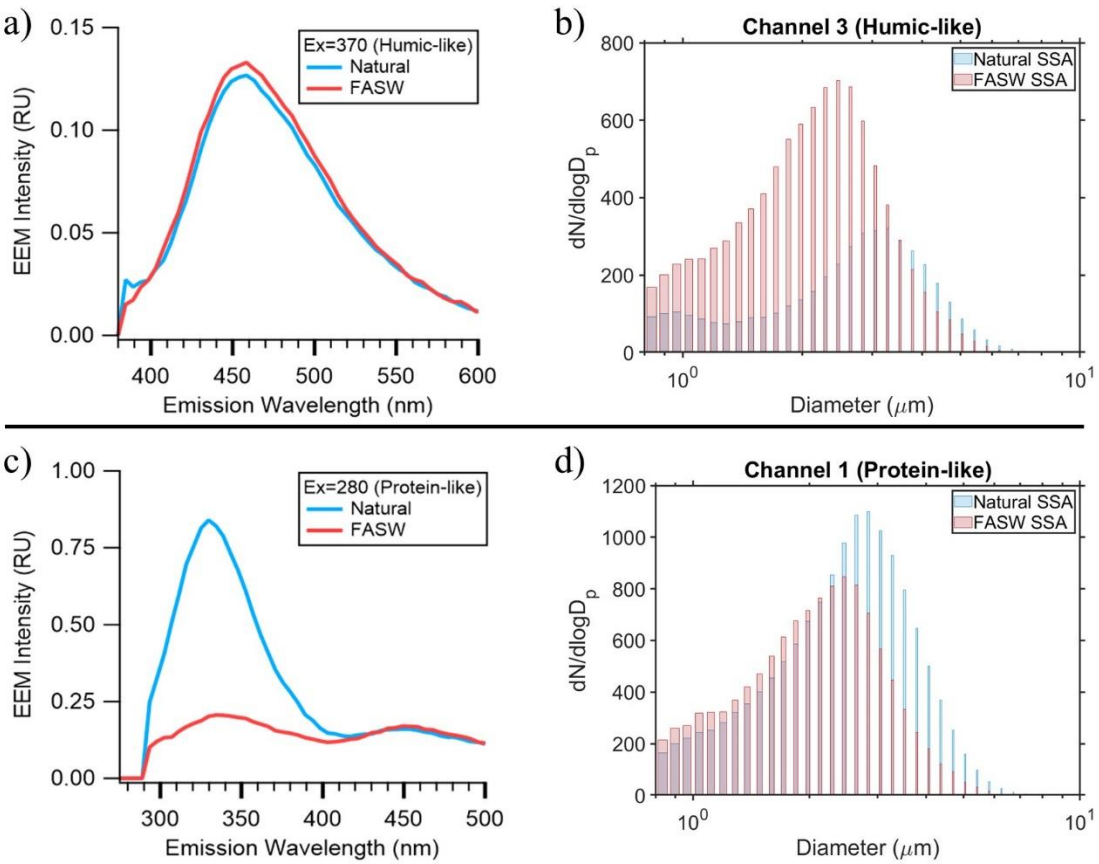

Figure 2.4. Emission spectra from the EEMs of the natural seawater and FASW corresponding to the excitation wavelengths for (a) WIBS channel 3 and (c) WIBS channel 1. Fluorescence size distributions of SSA before and after filtering and autoclaving for (b) WIBS channel 3 (d) WIBS channel 1.

To further elucidate the contribution of marine bacteria to SSA fluorescence, the bulk and aerosol fluorescence signatures were characterized for a solution containing three marine bacterial isolates (AltSIO, ATW7, and BBFL7) (Figure 2.5). The bacterial EEMs showed high fluorescence in the protein region, with no noticeable humic-like fluorescence above the background 4x PBS (Figure 2.5a). This spectrum shared similar characteristics to previously measured EEMs of marine bacteria [*Determann et al., 1998*]. The three individual bacteria were also analyzed separately using EEMS and showed similar spectra with fluorescence predominantly in the protein region and negligible fluorescence in the HULIS region (Figure

2.12). This result indicates that the fluorescence signature of the marine bacterial solution containing all three bacteria was not dominated by one species. The tryptophan-like fluorescence regions from marine bacterial EEMs were also present in seawater and SSA EEMs, suggesting that bacteria are a component in SSA fluorescence.

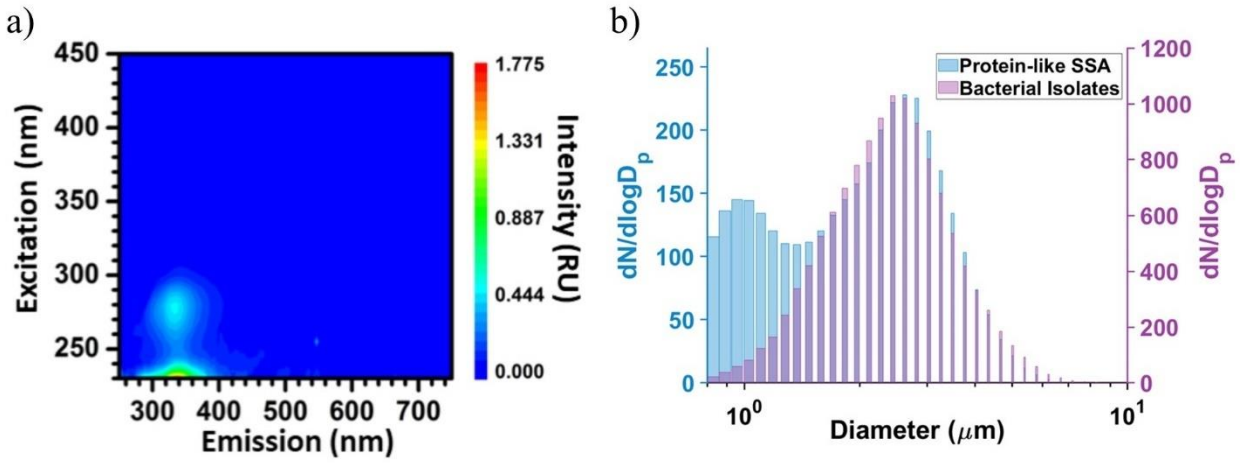

Figure 2.5. Fluorescence of the bacterial isolate mixture measured by a) EEMS (adjusted to the blank EEM of the 4xPBS solution). b) WIBS channel 1 fluorescence size distribution of the bacterial isolates that fluoresced above the PBS background (purple), overlaid on the mean channel 1 size distribution of the wave channel SSA (blue).

The WIBS fluorescence of the bacteria aerosolized with a miniMART showed similar signatures to those detected by EEMS. The bacterial isolates showed an increased mean fluorescence intensity in channel 1 compared to the 4xPBS medium (Figure 2.13). These results were similar to previous WIBS studies, which found that terrestrial bacterial cultures fluoresce strongly in channel 1 [*Hernandez et al., 2016*]. Moreover, the increase in mean fluorescence intensity was not seen in the other two channels measured by the WIBS. The WIBS fluorescence signature for aerosolized marine bacteria paralleled the EEMs of the bacteria in solution, further highlighting the capability of single-particle fluorescence for SSA characterization.

WIBS channel 1 size distribution for the aerosolized bacterial isolates was generated in the same manner to those generated for the wave channel. The background-corrected, fluorescent particle size distribution showed that the bacterial isolates were ejected into predominantly larger particles with the peak of the distribution near D_p = 2.4 μm (Figure 2.5b). The mode of the size distribution of the bacterial isolates was resemblant of the protein-like, nascent SSA measured from the wave channel, indicating that the particles detected in the wave channel likely included bacteria (Figure 2.5b). The slight differences in the size distributions between the seawater and the bacterial isolates might be explained by the proteinaceous constituents in chemically-complex seawater compared to the 4xPBS and the formation of proteinaceous aggregates in natural SSA [*Aller et al., 2005*]. While further work is necessary to fully elucidate the contribution of marine bacteria in SSA and their transport pathways, it is clear that marine bacteria can be ejected into the atmosphere via SSA particles and detected using fluorescence techniques.

2.4.4. Implications

When evaluating which fluorescence technique is appropriate for a specific measurement, multiple factors should be considered. Due to the additional steps necessary in measuring SSA using EEMS, such as impinging the aerosols into a bulk medium, this instrument is better suited for measurements of bulk seawater. However, the WIBS is a useful instrument for characterizing real-time changes in single-particle SSA and shows comparable trends to fluorescence measured with EEMS. Therefore, WIBS aerosol measurements, in tandem with EEMS analysis of bulk solutions, can provide a thorough investigation of fluorescent particle production. Possible modifications to the optics of the WIBS for improved characterization of SSA may involve

extending the fluorescence emission collection of channel 1 to include the major peak of tyrosine fluorescence, shown to be significant in the SSA EEMs spectra.

SSA particles represent one of the most abundant natural aerosols in the atmosphere [*Gantt and Meskhidze, 2013*], but only during the past decade have their role as primary biological aerosols been a major focus of investigation. The unique ability of bioaerosols to affect clouds and climate becomes especially important in remote marine locations where SSA particles can dominate as cloud condensation nuclei or ice nuclei [*Andreae and Rosenfeld, 2008; Burrows et al., 2013; Frohlich-Nowoisky et al., 2016; Vergara-Temprado et al., 2017*]. With growing interest in the atmospheric dynamics of bioaerosols, uncovering the role of SSA has become increasingly critical to our understanding of how bioaerosols influence climate. Our investigations on isolated systems provide a basis for the fluorescence signature of SSA to help unravel the complex trends observed in the atmosphere and move towards identification of marine bioaerosols in the natural environment.

2.5 Acknowledgments

The authors would like to thank the National Science Foundation and the Center for Aerosol Impacts on the Chemistry of the Environment (CAICE), a Center for Chemical Innovation (CHE-1801971) for funding this project. We would also like to thank Kathryn J. Mayer and Mike R. Alves for their thoughtful contributions and edits to this manuscript. All data supporting the conclusions are publicly available at: https://doi.org/10.6075/J0XK8D31

Chapter 2 is reproduced with permission from the American Chemical Society: Santander, M.V., Mitts, B.A., Pendergraft, M.A., Dinasquet, J., Lee, C., Moore, A.N., Cancelada, L.B., Kimble, K.A., Malfatti, F., Prather, K.A., “Tandem fluorescence measurements

of organic matter and bacteria released in sea spray aerosols", *Environmental Science & Technology*, 55 (8), 5171-5179, 2021. The dissertation author and B.A.M. were co-primary investigators and co-first authors of this paper. The dissertation author was the primary experimenter for studies involving EEMS, primary analyst and figure generator for all EEMS datasets, and lead writer of sections describing EEMS methods and results. B.A.M. was the primary experimenter for studies involving the WIBS, primary analyst and figure generator for all WIBS datasets, and lead writer of sections describing WIBS methods and results. The dissertation author and B.A.M. contributed equally to drafting the introduction, synopsis/abstract, and implications sections of the manuscript, and to revisions of all sections.

2.6 Supporting Information

2.6.1. Experimental Designs

Experiment 1. A wave channel was used to produce SSA from natural seawater [*Prather et al., 2013; Wang et al., 2015*]. The wave channel contained 13,000 L of natural seawater taken from Ellen Browning Scripps Memorial Pier (Scripps Pier; 32-52'00" N, 117-15'21" W). During this experiment, a phytoplankton bloom was not induced; therefore the seawater contained the natural microbial community in different growth stages and in a state of low biomass. SSA were produced by paddle-generated waves breaking on an artificial beach, and were measured continuously using the WIBS. SSA were collected for EEMS analysis for one 12-hour time period using an aerosol-to-liquid collection method.

Experiment 2. A Marine Aerosol Reference Tank (MART) was used to generate SSA over the course of a phytoplankton bloom [*Stokes et al., 2013; Lee et al., 2015*]. A large outdoor tank (2200L) was filled with seawater from Scripps Pier and used to supply seawater to the

MART. A phytoplankton bloom was induced in order to investigate the role of ocean microbiology on SSA composition and represent a system with high biomass. To initiate the phytoplankton bloom, Guillard's F/2 medium, diluted to F/100, and sodium silicate were added to the outdoor tank of seawater [*Guillard et al., 1962*]. Each day, 120 L of tank water was transferred to the MART, where aerosol generation occurred via a periodic plunging waterfall. After sample collection, the seawater was cycled back into the outdoor tank to allow the phytoplankton to continue growing. The SSA generated by the MART were measured by the WIBS in one- to two-hour intervals each day. Simultaneously, SSA were collected for approximately 1 hour each day for EEMs analysis. Seawater was also collected daily for EEMs analysis prior to SSA collection. The EEMS intensities for Experiment 2 were compared to the WIBS intensities by normalizing to the sum of intensities for each method across all the sampled days of the phytoplankton bloom. This normalization allowed for a comparison between the relative trends in intensity measured using both instruments.

Experiment 3. To elucidate the role of microbes on SSA fluorescence, two control scenarios were investigated using a miniMART, which uses a water-wheel (mill) to produce a periodic plunging waterfall and generate aerosols [*Stokes et al., 2016*]. In the first scenario, seawater fluorescence was compared before and after filtration and autoclaving. Seawater collected off Scripps Pier was spiked with Guillard's F/2 medium, to induce a mesocosm phytoplankton bloom in a 19 L carboy. During the senescence phase of the bloom, 12 days after spiking the seawater with nutrients, 7 L of water was added to the miniMART for aerosolization and sampling. The remaining seawater from the carboy was filtered using a 0.2 μm filter and then autoclaved for sterilization. After sampling the fresh seawater, the miniMART was drained,

cleaned with 70% ethanol, rinsed with milliQ water, and filled with the filtered, autoclaved seawater for SSA generation.

The second scenario involved the aerosolization of bacterial isolates added to a 4x phosphate-buffered saline solution. Three marine bacterial isolates were used to investigate the fluorescence signature of aerosolized bacteria without the influence of background seawater fluorescence. The bacterial strains were in the same physiological state of exponential growth upon addition to the miniMART.

2.6.2. Enumeration of Heterotrophic Bacteria and Viruses

The seawater samples were fixed with a solution of glutaraldehyde at 0.05% final concentration and stored at -80°C after flash freezing [*Noble and Fuhrman, 1998*]. Heterotrophic bacteria and virus counts were obtained using flow-cytometry at The Scripps Research Institute (TSRI) Flow Core Facility with a BIO-RAD, ZE5 Cell Analyzer. Samples for heterotrophic bacteria were diluted (1:10) in 1xTE buffer (pH 8) and stained with SYBR Green I (1:100 dilution of the commercial stock) at room temperature for 10 minutes in the dark. Viruses were diluted (1:50) in 1xTE buffer and stained (at a 1:50 dilution of the commercial SYBR Green I stock) in the dark for 10 minutes at 80°C [*Gasol and Del Giorgio, 2000*]. Heterotrophic bacteria and virus populations were discriminated based on their signature in the fluorescence (488 nm laser, green fluorescence) versus side-scatter specific cytograms. Signals in the blank samples were subtracted from the sample signals.

2.6.3. Calibration of WIBS Intensities

To compare the SSA mean intensities detected by the WIBS to other WIBS instruments, we applied a calibration similar to that described by Robinson et al. [*Robinson et al., 2017*]. This method compares WIBS fluorescence intensity to the equivalent mass of fluorophore atomized from a standard solution. Tryptophan was used as the fluorophore for channel 1 with ammonium sulfate as a non-fluorescent filler for particle generation. Quinine was used to calibrate channels 2 and 3. For the first standard solution, 0.0212 g of tryptophan and 0.9157 g of ammonium sulfate were added to 150 mL of milliQ water (tryptophan mass percent = 2.26%). For the quinine solution, 0.865 g of quinine were added to 150 mL of milliQ water (quinine mass percent = 100%). Particles were generated with a custom atomizer using particle-free air produced from a zero air generator (Sabio, Model 1001). The particles were dried using silica diffusion driers to an RH <21% before entering the WIBS. Dried particles were assumed to have the same fluorophore mass percent to that in the bulk standard solution. The particle population was a polydisperse distribution, sized using the WIBS. Particles were divided into 5 nm size bins from 0.8 μm to 3 μm and the average particle optical diameter for each size bin was calculated. Assuming the particles were spheres, the particle volume was calculated for each size bin and converted to mass using the particle density: 1.77 g/cm3 for tryptophan particles (assuming ammonium sulfate density) and 1.36 g/cm3 for quinine particles (value provided by supplier).

A log-log linear relationship was observed between the calculated fluorophore mass and the measured WIBS intensity. Regressions were calculated for the first 150 size bins due to higher particle counts in this range. The R2 values for the regressions of the three channels were: 0.928, 0.84, and 0.831 for channels 1-3, respectively. Both quinine calibrations showed a deviation from the fitted line at the higher mass values (Figure 2.6b,c), which was also observed

in the calibration by Robinson et al. and previously accounted for by assuming an excitation penetration depth of 90 nm [*Robinson et al., 2017*]. However, in this study, when a shell penetration depth was assumed, only a slight increase in the R2 value was observed for both quinine regressions. Therefore, the deviation in the fit at higher quinine concentrations was ascribed to the lower particle counts in these size bins. Using the calculated regression fits, the mean values from the SSA generated by the wave channel were converted to the equivalent fluorophore mass (Figure 2.6a-c). The mean intensity ± the standard deviation for nascent SSA in channel 1 was equivalent to 2.331 ± 34.596 fg of tryptophan and for channels 2 and 3 were equivalent to 0.0537 ± 0.400 and 0.116 ± 1.050 fg of quinine, respectively (Figure 2d). As a note, the measured intensities for the SSA samples are blank-subtracted. In order to determine the measured limits of detection (LOD), the calibration curves were generated without subtracting out the blank from the fluorescence values. Based on the forced trigger thresholds for this experiment and the calibration curves without the blank subtracted, the LOD for WIBS channel 1 was equivalent to 1.88 fg of tryptophan and the LOD for channels 2 & 3 were equivalent to 0.0216 fg of quinine and 0.103 fg of quinine, respectively.

2.6.4. Supporting Information Figures

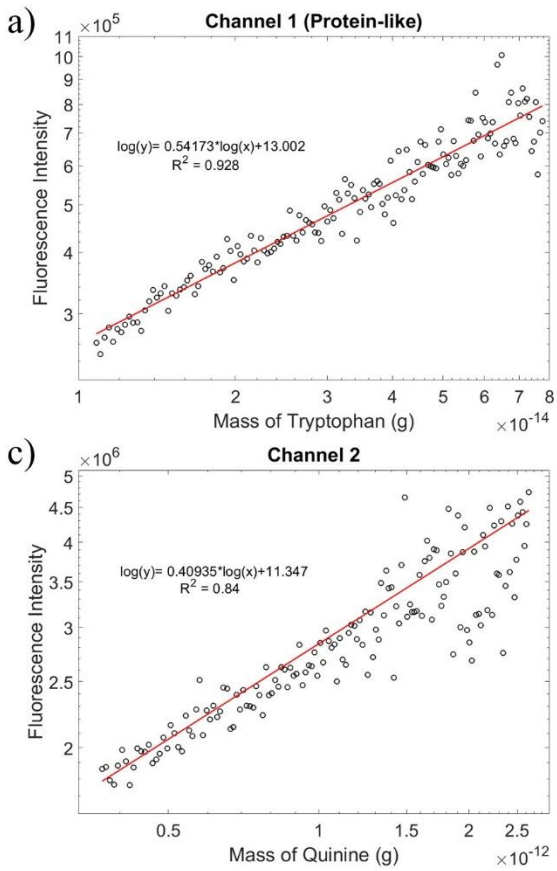

d)

WIBS Channels	Equivalent Fluorophore Mass
Channel 1 (280 nm/310-400 nm)	2.331 ± 34.596 femtograms of tryptophan
Channel 2 (280 nm/420-650 nm)	0.0537 ± 0.400 femtograms of quinine
Channel 3 (370 nm/420-650 nm)	0.116 ± 1.050 femtograms of quinine

Figure 2.6. WIBS calibration regressions comparing fluorophore mass to the WIBS fluorescence intensity for a) channel 1, b) channel 3, c) channel 2. d) Conversion of the WIBS mean fluorescence intensities to the fluorophore equivalent masses for SSA generated by the wave channel.

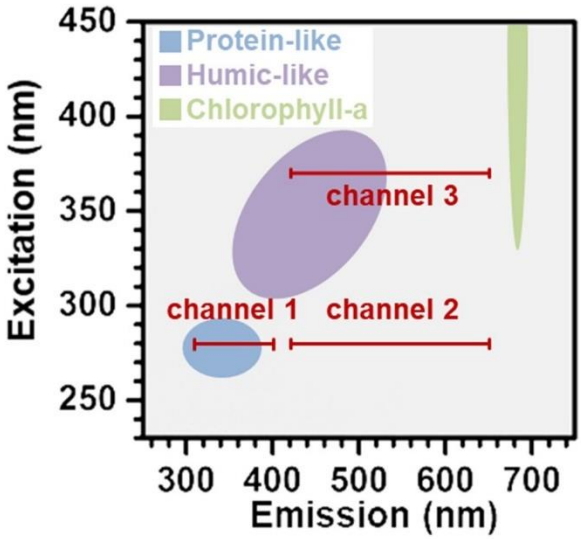

Figure 2.7. Overlay of the WIBS channels compared to an excitation emission matrix. Also labeled are the different fluorescence regions associated with seawater and sea spray aerosols.

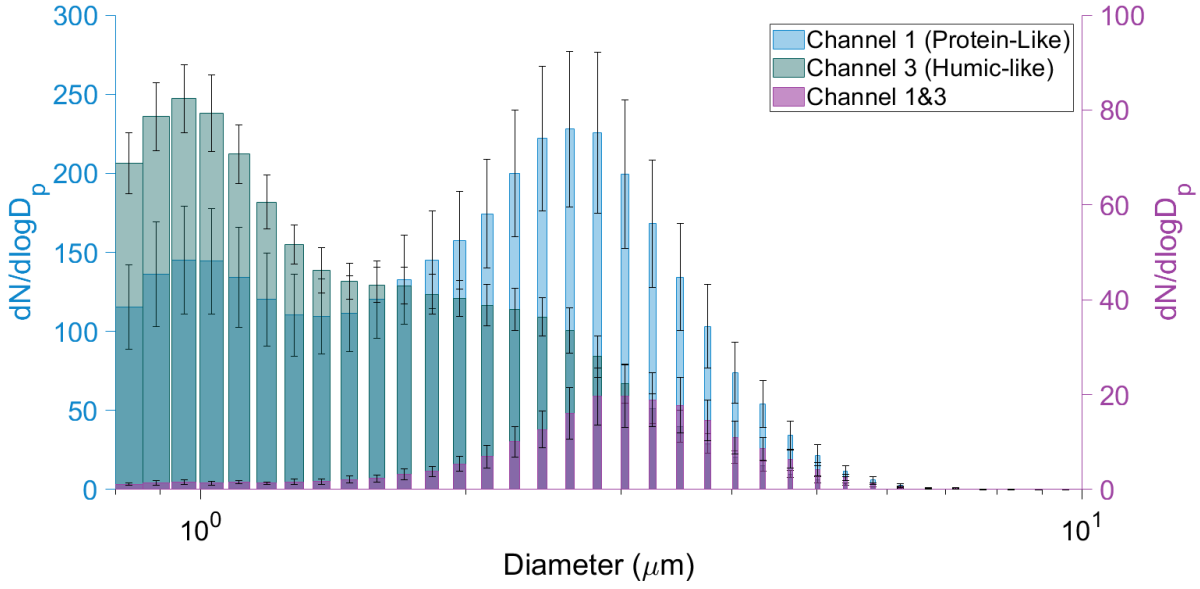

Figure 2.8. SSA size distributions separated by fluorescence channels measured with the WIBS. Channel 1 (protein-like) is in blue, channel 3 (humic-like) overlaid in green, and particles which fluoresced in both channels 1&3 are overlaid in purple. The size distributions shown are the daily mean particle counts (#/L) normalized to the bin widths and the error bars represent one standard deviation from the mean.

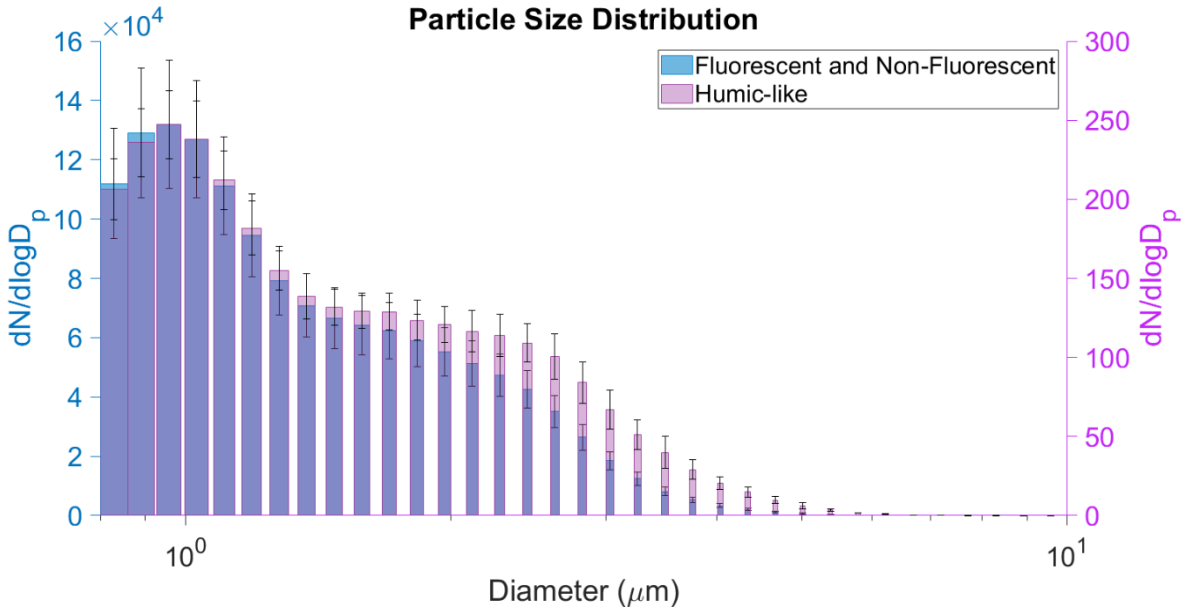

Figure 2.9. Particle size distribution of the SSA generated by the wave channel. Shown are the mean daily size distributions for total particles (fluorescent and non-fluorescent) (blue) as well as humic-like particles (pink). Averages along with standard deviations are derived from the seven days of sampling SSA from the wave channel.

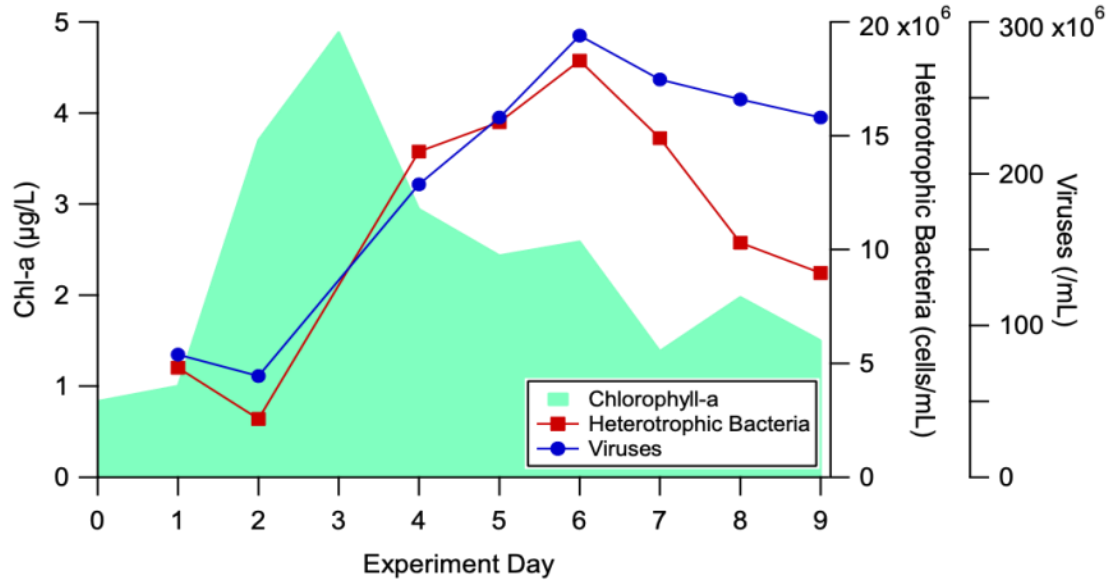

Figure 2.10. Microbial changes in the mesocosm phytoplankton bloom experiment. Chlorophyll-a (green area), heterotrophic bacteria (red squares), and viruses (blue circles) concentrations are measured over time.

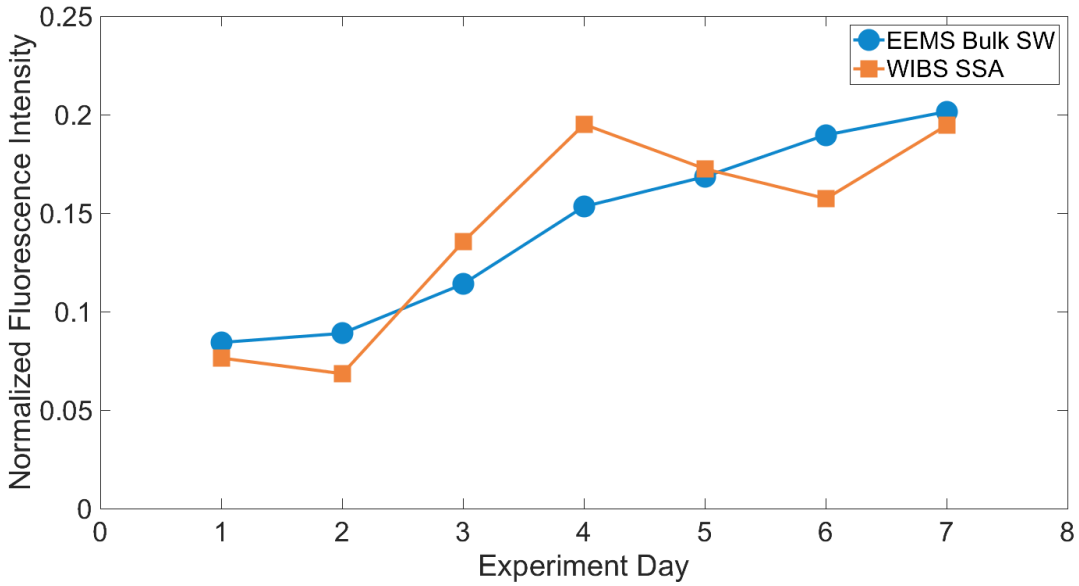

Figure 2.11. WIBS SSA mean intensity values for channel 3 (orange squares) compared to the EEMs mean intensity for the bulk seawater corresponding to the excitation and emission wavelengths of the WIBS channel 3 (blue cicrles). Experiment days refer to the day of the phytoplankton bloom experiment.

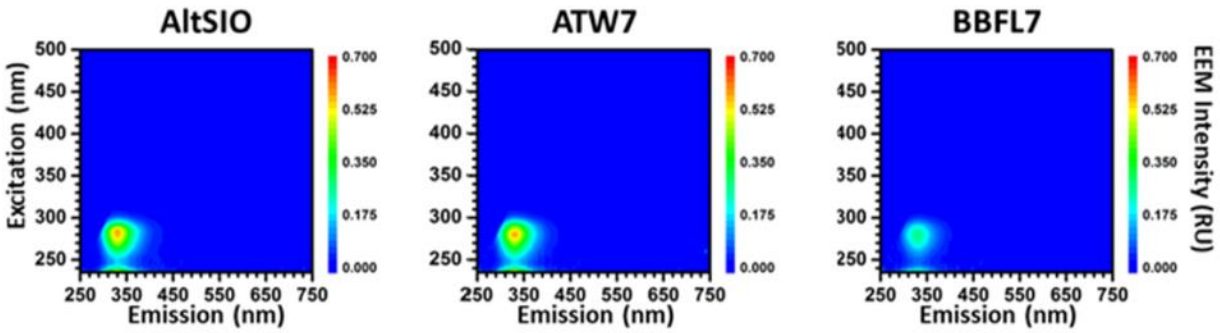

Figure 2.12. Selected EEMs for three different bacterial isolates: AltSIO, ATW7, and BBFL7.

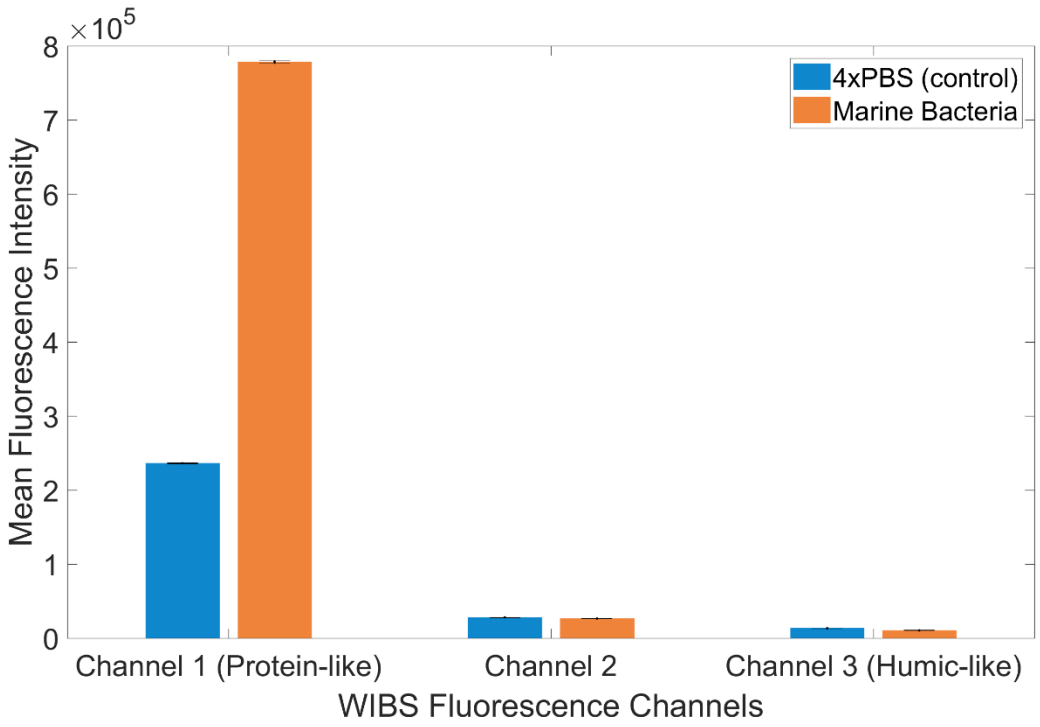

Figure 2.13. WIBS mean fluorescence intensity across each channel for the marine bacterial isolates compared to the 4xPBS solution (background). Error bars shown represent the standard error for each measurement.

2.7 References

Aller, J. Y., M. R. Kuznetsova, C. J. Jahns and P. F. Kemp. The sea surface microlayer as a source of viral and bacterial enrichment in marine aerosols. *Journal of Aerosol Science*. **2005**, *36*(5-6): 801-812.

Andersson, M. G. I., N. Catalan, Z. Rahman, L. J. Tranvik and E. S. Lindstrom. Effects of sterilization on dissolved organic carbon (DOC) composition and bacterial utilization of DOC from lakes. *Aquatic Microbial Ecology*. **2019**, *82*(2): 199-208.

Andreae, M. O. and D. Rosenfeld. Aerosol-cloud-precipitation interactions. Part 1. The nature and sources of cloud-active aerosols. *Earth-Science Reviews*. **2008**, *89*(1-2): 13-41.

Azam, F., T. Fenchel, J. G. Field, J. S. Gray, L. A. Meyer-Reil and F. Thingstad. The Ecological Role of Water-Column Microbes in the Sea. *Marine Ecology Progress Series*. **1983**, *10*(3): 257-263.

Benner, R., J. D. Pakulski, M. Mccarthy, J. I. Hedges and P. G. Hatcher. Bulk Chemical Characteristics of Dissolved Organic-Matter in the Ocean. *Science*. **1992**, *255*(5051): 1561-1564.

Bidle, K. D. and F. Azam. Bacterial control of silicon regeneration from diatom detritus: Significance of bacterial ectohydrolases and species identity. *Limnology and Oceanography*. **2001**, *46*(7): 1606-1623.

Burrows, S. M., C. Hoose, U. Poeschl and M. G. Lawrence. Ice nuclei in marine air: biogenic particles or dust? *Atmospheric Chemistry and Physics*. **2013**, *13*(1): 245-267.

Coble, P. G. Characterization of marine and terrestrial DOM in seawater using excitation emission matrix spectroscopy. *Marine Chemistry*. **1996**, *51*(4): 325-346.

Collins, D. B., D. F. Zhao, M. J. Ruppel, O. Laskina, J. R. Grandquist, R. L. Modini, M. D. Stokes, L. M. Russell, T. H. Bertram, V. H. Grassian, G. B. Deane and K. A. Prather. Direct aerosol chemical composition measurements to evaluate the physicochemical differences between controlled sea spray aerosol generation schemes. *Atmospheric Measurement Techniques*. **2014**, *7*(11): 3667-3683.

Crawford, I., M. W. Gallagher, K. N. Bower, T. W. Choularton, M. J. Flynn, S. Ruske, C. Listowski, N. Brough, T. Lachlan-Cope, Z. L. Fleming, V. E. Foot and W. R. Stanley. Real-time detection of airborne fluorescent bioparticles in Antarctica. *Atmospheric Chemistry and Physics*. **2017**, *17*(23): 14291-14307.

Despres, V. R., J. A. Huffman, S. M. Burrows, C. Hoose, A. S. Safatov, G. Buryak, J. Frohlich-Nowoisky, W. Elbert, M. O. Andreae, U. Poschl and R. Jaenicke. Primary biological aerosol particles in the atmosphere: a review. *Tellus Series B-Chemical and Physical Meteorology*. **2012**, *64*.

Determann, S., J. M. Lobbes, R. Reuter and J. Rullkotter. Ultraviolet fluorescence excitation and emission spectroscopy of marine algae and bacteria. *Marine Chemistry*. **1998**, *62*(1-2): 137-156.

Fennelly, M. J., G. Sewell, M. B. Prentice, D. J. O'Connor and J. R. Sodeau. Review: The Use of Real-Time Fluorescence Instrumentation to Monitor Ambient Primary Biological Aerosol Particles (PBAP). *Atmosphere*. **2018**, *9*(1).

Fernandez, A. E., G. S. Lewis and S. V. Hering. Design and Laboratory Evaluation of a Sequential Spot Sampler for Time-Resolved Measurement of Airborne Particle Composition. *Aerosol Science and Technology*. **2014**, *48*(6): 655-663.

Forde, E., M. Gallagher, M. Walker, V. Foot, A. Attwood, G. Granger, R. Sarda-Esteve, W. Stanley, P. Kaye and D. Topping. Intercomparison of Multiple UV-LIF Spectrometers Using the Aerosol Challenge Simulator. *Atmosphere*. **2019**, *10*(12).

Frohlich-Nowoisky, J., C. J. Kampf, B. Weber, J. A. Huffman, C. Pohlker, M. O. Andreae, N. Lang-Yona, S. M. Burrows, S. S. Gunthe, W. Elbert, H. Su, P. Hoor, E. Thines, T. Hoffmann, V. R. Despres and U. Poschl. Bioaerosols in the Earth system: Climate, health, and ecosystem interactions. *Atmospheric Research*. **2016**, *182*: 346-376.

Gabey, A. M., M. W. Gallagher, J. Whitehead, J. R. Dorsey, P. H. Kaye and W. R. Stanley. Measurements and comparison of primary biological aerosol above and below a tropical forest canopy using a dual channel fluorescence spectrometer. *Atmospheric Chemistry and Physics*. **2010**, *10*(10): 4453-4466.

Gabey, A. M., W. R. Stanley, M. W. Gallagher and P. H. Kaye. The fluorescence properties of aerosol larger than 0.8 mu m in urban and tropical rainforest locations. *Atmospheric Chemistry and Physics*. **2011**, *11*(11): 5491-5504.

Gantt, B. and N. Meskhidze. The physical and chemical characteristics of marine primary organic aerosol: a review. *Atmospheric Chemistry and Physics*. **2013**, *13*(8): 3979-3996.

Gasol, J. M. and P. A. Del Giorgio. Using flow cytometry for counting natural planktonic bacteria and understanding the structure of planktonic bacterial communities. *Scientia Marina*. **2000**, *64*(2): 197-224.

Grzybowski, W. Selected properties of different molecular size fractions of humic substances isolated from surface Baltic water in the Gdańsk Deep area. *Oceanologia*. **1995**, *38*(1): 33-47.

Guillard, R. R. and J. H. Ryther. Studies of Marine Planktonic Diatoms .1. Cyclotella Nana Hustedt, and Detonula Confervacea (Cleve) Gran. *Canadian Journal of Microbiology*. **1962**, *8*(2): 229.

Hernandez, M., A. E. Perring, K. McCabe, G. Kok, G. Granger and D. Baumgardner. Chamber catalogues of optical and fluorescent signatures distinguish bioaerosol classes. *Atmospheric Measurement Techniques*. **2016**, *9*(7): 3283-3292.

Hessen, D. O. and L. J. Tranvik (1998). Aquatic humic substances: ecology and biogeochemistry. Berlin; New York, Springer.

Kasparian, J., C. Hassler, B. Ibelings, N. Berti, S. Bigorre, V. Djambazova, E. Gascon-Diez, G. Giuliani, R. Houlmann, D. Kiselev, P. de Laborie, A. D. Le, T. Magouroux, T. Neri, D. Palomino, S. Pfandler, N. Ray, G. Sousa, D. Staedler, F. Tettamanti, J. P. Wolf and M. Beniston. Assessing the Dynamics of Organic Aerosols over the North Atlantic Ocean. *Scientific Reports*. **2017**, *7*.

Kaye, P. H., K. Aptowicz, R. K. Chang, V. Foot and G. Videen. Angularly resolved elastic scattering from airborne particles - Potential for characterizing, classifying, and identifying individual aerosol particles. *Optics of Biological Particles*. **2007**, *238*: 31-+.

Kaye, P. H., W. R. Stanley, E. Hirst, E. V. Foot, K. L. Baxter and S. J. Barrington. Single particle multichannel bio-aerosol fluorescence sensor. *Optics Express*. **2005**, *13*(10): 3583-3593.

Lakowicz, J. R. (2006). Principles of fluorescence spectroscopy. New York, Springer.

Lawaetz, A. J. and C. A. Stedmon. Fluorescence Intensity Calibration Using the Raman Scatter Peak of Water. *Applied Spectroscopy*. **2009**, *63*(8): 936-940.

Lee, C., C. M. Sultana, D. B. Collins, M. V. Santander, J. L. Axson, F. Malfatti, G. C. Cornwell, J. R. Grandquist, G. B. Deane, M. D. Stokes, F. Azam, V. H. Grassian and K. A. Prather. Advancing Model Systems for Fundamental Laboratory Studies of Sea Spray Aerosol Using the Microbial Loop. *J Phys Chem A*. **2015**, *119*(33): 8860-8870.

Lee, H. D., H. S. Morris, O. Laskina, C. M. Sultana, C. Lee, T. Jayarathne, J. L. Cox, X. F. Wang, E. S. Hasenecz, P. J. DeMott, T. H. Bertram, C. D. Cappa, E. A. Stone, K. A. Prather, V. H. Grassian and A. V. Tivanski. Organic Enrichment, Physical Phase State, and Surface Tension Depression of Nascent Core-Shell Sea Spray Aerosols during Two Phytoplankton Blooms. *ACS Earth and Space Chemistry*. **2020**, *4*(4): 650-660.

Liu, L. Z., Q. Huang, Y. L. Zhang, B. Q. Qin and G. W. Zhu. Excitation-emission matrix fluorescence and parallel factor analyses of the effects of N and P nutrients on the

extracellular polymeric substances of Microcystis aeruginosa. *Limnologica*. **2017**, *63*: 18-26.

Malfatti, F., C. Lee, T. Tinta, M. A. Pendergraft, M. Celussi, Y. Y. Zhou, C. M. Sultana, A. Rotter, J. L. Axson, D. B. Collins, M. V. Santander, A. L. A. Morales, L. I. Aluwihare, N. Riemer, V. H. Grassian, F. Azam and K. A. Prather. Detection of Active Microbial Enzymes in Nascent Sea Spray Aerosol: Implications for Atmospheric Chemistry and Climate. *Environmental Science & Technology Letters*. **2019**, *6*(3): 171-177.

Mari, X. and T. Kiorboe. Abundance, size distribution and bacterial colonization of transparent exopolymeric particles (TEP) during spring in the Kattegat. *Journal of Plankton Research*. **1996**, *18*(6): 969-986.

Mostofa, K. M. G. (2013). Photobiogeochemistry of organic matter: principles and practices in water environments. Heidelberg ; New York, Springer.

Murphy, K. R. A Note on Determining the Extent of the Water Raman Peak in Fluorescence Spectroscopy. *Applied Spectroscopy*. **2011**, *65*(2): 233-236.

Nebbioso, A. and A. Piccolo. Molecular characterization of dissolved organic matter (DOM): a critical review. *Analytical and Bioanalytical Chemistry*. **2013**, *405*(1): 109-124.

Noble, R. T. and J. A. Fuhrman. Use of SYBR Green I for rapid epifluorescence counts of marine viruses and bacteria. *Aquatic Microbial Ecology*. **1998**, *14*(2): 113-118.

Patterson, J. P., D. B. Collins, J. M. Michaud, J. L. Axson, C. M. Sultana, T. Moser, A. C. Dommer, J. Conner, V. H. Grassian, M. D. Stokes, G. B. Deane, J. E. Evans, M. D. Burkart, K. A. Prather and N. C. Gianneschi. Sea Spray Aerosol Structure and Composition Using Cryogenic Transmission Electron Microscopy. *ACS Central Science*. **2016**, *2*(1): 40-47.

Pedler, B. E., L. I. Aluwihare and F. Azam. Single bacterial strain capable of significant contribution to carbon cycling in the surface ocean. *Proceedings of the National Academy of Sciences of the United States of America*. **2014**, *111*(20): 7202-7207.

Pohlker, C., J. A. Huffman and U. Poschl. Autofluorescence of atmospheric bioaerosols – fluorescent biomolecules and potential interferences. *Atmospheric Measurement Techniques*. **2012**, *5*(1): 37-71.

Prather, K. A., T. H. Bertram, V. H. Grassian, G. B. Deane, M. D. Stokes, P. J. DeMott, L. I. Aluwihare, B. P. Palenik, F. Azam, J. H. Seinfeld, R. C. Moffet, M. J. Molina, C. D. Cappa, F. M. Geiger, G. C. Roberts, L. M. Russell, A. P. Ault, J. Baltrusaitis, D. B. Collins, C. E. Corrigan, L. A. Cuadra-Rodriguez, C. J. Ebben, S. D. Forestieri, T. L. Guasco, S. P. Hersey, M. J. Kim, W. F. Lambert, R. L. Modini, W. Mui, B. E. Pedler, M. J. Ruppel, O. S. Ryder, N. G. Schoepp, R. C. Sullivan and D. F. Zhao. Bringing the ocean into the laboratory to probe the chemical complexity of sea spray aerosol. *Proceedings of the National Academy of Sciences of the United States of America*. **2013**, *110*(19): 7550-7555.

Rastelli, E., C. Corinaldesi, A. Dell'Anno, M. Lo Martire, S. Greco, M. C. Facchini, M. Rinaldi, C. O'Dowd, D. Ceburnis and R. Danovaro. Transfer of labile organic matter and microbes from the ocean surface to the marine aerosol: an experimental approach. *Scientific Reports*. **2017**, *7*.

Rinaldi, M., S. Fuzzi, S. Decesari, S. Marullo, R. Santoleri, A. Provenzale, J. von Hardenberg, D. Ceburnis, A. Vaishya, C. D. O'Dowd and M. C. Facchini. Is chlorophyll-a the best surrogate for organic matter enrichment in submicron primary marine aerosol? *Journal of Geophysical Research: Atmospheres*. **2013**, *118*(10): 4964-4973.

Robinson, E. S., R. S. Gao, J. P. Schwarz, D. W. Fahey and A. E. Perring. Fluorescence calibration method for single-particle aerosol fluorescence instruments. *Atmospheric Measurement Techniques*. **2017**, *10*(5): 1755-1768.

Savage, N. J., C. E. Krentz, T. Konemann, T. T. Han, G. Mainelis, C. Pohlker and J. A. Huffman. Systematic characterization and fluorescence threshold strategies for the wideband integrated bioaerosol sensor (WIBS) using size-resolved biological and interfering particles. *Atmospheric Measurement Techniques*. **2017**, *10*(11): 4279-4302.

Shaffer, B. T. and B. Lighthart. Survey of culturable airborne bacteria at four diverse locations in Oregon: Urban, rural, forest, and coastal. *Microbial Ecology*. **1997**, *34*(3): 167-177.

Smith, D. C., M. Simon, A. L. Alldredge and F. Azam. Intense Hydrolytic Enzyme Activity on Marine Aggregates and Implications for Rapid Particle Dissolution. *Nature*. **1992**, *359*(6391): 139-142.

Stokes, M. D., G. Deane, D. B. Collins, C. Cappa, T. Bertram, A. Dommer, S. Schill, S. Forestieri and M. Survilo. A miniature Marine Aerosol Reference Tank (miniMART) as a compact breaking wave analogue. *Atmospheric Measurement Techniques*. **2016**, *9*(9): 4257-4267.

Stokes, M. D., G. B. Deane, K. Prather, T. H. Bertram, M. J. Ruppel, O. S. Ryder, J. M. Brady and D. Zhao. A Marine Aerosol Reference Tank system as a breaking wave analogue for the production of foam and sea-spray aerosols. *Atmospheric Measurement Techniques*. **2013**, *6*(4): 1085-1094.

Toprak, E. and M. Schnaiter. Fluorescent biological aerosol particles measured with the Waveband Integrated Bioaerosol Sensor WIBS-4: laboratory tests combined with a one year field study. *Atmospheric Chemistry and Physics*. **2013**, *13*(1): 225-243.

Vergara-Temprado, J., B. J. Murray, T. W. Wilson, D. O'Sullivan, J. Browse, K. J. Pringle, K. Ardon-Dryer, A. K. Bertram, S. M. Burrows, D. Ceburnis, P. J. DeMott, R. H. Mason, C. D. O'Dowd, M. Rinaldi and K. S. Carslaw. Contribution of feldspar and marine organic aerosols to global ice nucleating particle concentrations. *Atmospheric Chemistry and Physics*. **2017**, *17*(5): 3637-3658.

Wang, X. F., C. M. Sultana, J. Trueblood, T. C. J. Hill, F. Malfatti, C. Lee, O. Laskina, K. A. Moore, C. M. Beall, C. S. McCluskey, G. C. Cornwell, Y. Y. Zhou, J. L. Cox, M. A. Pendergraft, M. V. Santander, T. H. Bertram, C. D. Cappa, F. Azam, P. J. DeMott, V. H. Grassian and K. A. Prather. Microbial Control of Sea Spray Aerosol Composition: A Tale of Two Blooms. *ACS Central Science*. **2015**, *1*(3): 124-131.

Yue, S. Y., L. J. Ren, T. L. Song, L. J. Li, Q. R. Xie, W. J. Li, M. J. Kang, W. Y. Zhao, L. F. Wei, H. Ren, Y. L. Sun, Z. F. Wang, R. M. Ellam, C. Q. Liu, K. Kawamura and P. Q. Fu. Abundance and Diurnal Trends of Fluorescent Bioaerosols in the Troposphere over Mt. Tai, China, in Spring. *Journal of Geophysical Research-Atmospheres*. **2019**, *124*(7): 4158-4173.

Zhang, Y. L., Y. Yin, L. Q. Feng, G. W. Zhu, Z. Q. Shi, X. H. Liu and Y. Z. Zhang. Characterizing chromophoric dissolved organic matter in Lake Tianmuhu and its catchment basin using excitation-emission matrix fluorescence and parallel factor analysis. *Water Res*. **2011**, *45*(16): 5110-5122.

Chapter 3. Factors Controlling the Transfer of Biogenic Organic Species from Seawater to Sea Spray Aerosol

3.1 Synopsis

Ocean waves transfer sea spray aerosol (SSA) to the atmosphere, and these SSA particles can be enriched in organic matter relative to salts compared to seawater ratios. A fundamental understanding of the factors controlling the transfer of biogenic organic matter from the ocean to the atmosphere remains elusive. Field studies that focus on understanding the connection between organic species in seawater and SSA are complicated by the numerous processes and sources affecting the composition of aerosols in the marine environment. Here, an isolated ocean-atmosphere system enables direct measurements of the sea-air transfer of different classes of biogenic organic matter over the course of two phytoplankton blooms. By measuring excitation-emission matrices of bulk seawater, the sea surface microlayer, and SSA, we investigate time series of the transfer of fluorescent species including chlorophyll-a, protein-like substances, and humic-like substances. Herein, we show the emergence of different molecular classes in SSA at specific times over the course of a phytoplankton bloom, suggesting that SSA chemical composition changes over time in response to changing ocean biological conditions. We compare the temporal behaviors for the transfer of each component, and discuss the factors contributing to differences in transfer between phases.

3.2 Introduction

Breaking waves in the ocean produce sea spray aerosols (SSA), and the ocean represents a dominant source of atmospheric aerosols [*Seinfeld and Pandis, 2006; de Leeuw et al., 2011; Gantt and Meskhidze, 2013; Patterson et al., 2016*]. SSA particles are comprised of a complex array of biogenic species, including intact microbes, which control the physicochemical properties of SSA and thus affect their atmospheric behavior [*Gantt et al., 2013*]. In recent decades, significant effort has been aimed at trying to establish a link between the composition of SSA and the biological state of the ocean [*Gaston et al., 2011; Prather et al., 2013; O'Dowd et al., 2015; Ceburnis et al., 2016; Leck and Bigg, 2017*], specifically related to phytoplankton growth [*O'Dowd et al., 2004; Bigg and Leck, 2008; Schmitt-Kopplin et al., 2012; Rinaldi et al., 2013; Miyazaki et al., 2020*] and the microbial loop [*Azam et al., 1983; Lee et al., 2015; O'Dowd et al., 2015; Wang et al., 2015*].

In addition to biological processes, physical and chemical processes play a complex role in affecting the composition of the atmosphere. Physical factors such as changes in SSA flux or the physical size of molecules and particles in seawater determine the efficiency of sea-air transfer of organic matter [*Alpert et al., 2015; Collins et al., 2016*]. Previous studies have suggested that increased dissolved organic carbon (DOC) concentrations or increased surface activity of the chemical species of interest enhance the transfer process [*Burrows et al., 2014; Lee et al., 2015; Cochran et al., 2016; Rastelli et al., 2017*]. Many hydrophobic biogenic species have been shown to be enriched in the sea-surface microlayer (SSML) [*Blanchard, 1964; Oppo et al., 1999; Aller et al., 2005; Engel et al., 2017*], the uppermost layer (1-1000 μm) on top of the ocean that serves as a critical environmental interface [*Liss and Duce, 1997; Cunliffe et al., 2013*]. However, observed associations between specific classes of organic molecules,

phytoplankton growth, and seawater-SSML-SSA transfer have been inconsistent between multiple studies.

Here, we investigate the physical and chemical mechanisms controlling the sea-air transfer of organic species in SSA by probing the composition of collected bulk seawater, SSML, and SSA samples with excitation-emission matrix (EEM) spectroscopy in combination with parallel factor analysis (PARAFAC) [*Coble, 1996; Hessen and Tranvik, 1998; Mostofa, 2013*]. EEM spectroscopy is an extension of fluorescence spectroscopy that has been increasingly used to characterize organic matter in a variety of aquatic systems, including seawater [*Zhang et al., 2011; Mostofa, 2013; Nebbioso and Piccolo, 2013*]. Using EEMs for chemical characterization allows for direct, rapid measurements [*Zhang et al., 2011*] and minimizes the possibility of artifacts created by sample storage or harsh processing conditions. Three sets of biologically diverse fluorophores are monitored: (1) chlorophyll-a, which is an indicator for phytoplankton biomass; (2) protein-like substances; and (3) humic-like substances (HULIS) [*Coble, 1996; Hessen et al., 1998; Mostofa, 2013*]. Additionally, we use PARAFAC analysis to separate EEMs into a set of individual fluorescent components [*Stedmon and Bro, 2008; Mostofa, 2013; Murphy et al., 2013; Nebbioso et al., 2013*]. Changes in fluorescence signatures over time are used to provide insight into the factors affecting the transfer of biogenic organic species from the ocean to the atmosphere.

3.3 Methods

3.3.1 Phytoplankton Bloom Experiments

Two phytoplankton blooms were induced in an indoor tank. The first phytoplankton bloom experiment (MART A) was conducted in January 2014 and lasted 17 days, while the

second experiment (MART B) took place in April 2014 and lasted 26 days. Both microcosm experiments were induced using methods described previously [*Lee et al., 2015*]. In these experiments, 60 L of seawater from the Scripps Institution of Oceanography pier was filtered using a 50 μm mesh screen to remove debris and zooplankton that graze on phytoplankton (Sefar Nitex 03−100/32) and placed into a Marine Aerosol Reference Tank (MART) [*Stokes et al., 2013*]. Seawater conditions at the time of sampling are included in the Supplemental Information (**Table 3.2**). Seawater was spiked with Guillard's F medium (diluted by a factor of 2) to induce a phytoplankton bloom [*Guillard and Ryther, 1962*]. Two fluorescent tubes (Full Spectrum Solutions, model 205457; T8 format, color temperature 5700 K, 2950 lumens) were attached to the sides of the MART to promote the growth of phytoplankton [*Brown and Richards, 1968*]. The low light levels relative to solar conditions [*Lee et al., 2015*], the absence of UV radiation, and the relatively short lifetime of SSA in the MART (minutes) [*Stokes et al., 2013*] makes it unlikely that photochemistry would cause differences between the SSA and seawater (bulk, or SSML). Similar lighting for both tanks also rules out photochemical change as an origin for any differences between MART A and MART B microcosms. The progress of the phytoplankton bloom was monitored daily by measuring *in vivo* chlorophyll-a fluorescence using a handheld fluorimeter (Turner Designs, Aquafluor). The handheld fluorimeter measures the fluorescence at 395 nm excitation and ≥660 nm emission.

3.3.2 Generation of Aerosols and Sample Collection

The MART uses a periodic plunging waterfall to generate aerosols, a method that has been described previously [*Stokes et al., 2013; Lee et al., 2015*]. The MART consists of an isolated system that allows for the study of SSA without the influence of aerosol particles from

other non-marine sources. While physical processes such as wind are not reproduced in the MART system, the MART plunging waterfall has been shown to produce a bubble size distribution that is similar to the bubble size distribution observed in the ocean. Thus, the MART produces SSA size distributions that mimic the size distributions of nascent SSA over the ocean, allowing us to solely focus on the particles produced during the bubble bursting process. Aerosol generation occurred for two hours followed by two hours of no particle generation or seawater mixing. Aerosols were collected daily using glass impingers (Chemglass, CG-1820, 0.2 μm D_p lower cutoff at 1 LPM) loaded with 20 mL of ultrapure (Type 1) water. The airflow through the impingers was 1 LPM for 2 hours. The impingers were cleaned daily by heating to 500 °C for 7 hours. In MART B, three impingers were used in parallel to collect SSA.

All bulk seawater and SSML samples were collected in vials that were previously cleaned with an acid-rinse using 0.1 N HCl followed by multiple rinses of ultrapure water, and then heating at 500 °C for 7 hours. Bulk seawater samples were collected daily from a spigot located on the side of the MART. SSML samples were collected using the glass plate method once every two days to prevent excessive depletion of the microlayer [*Cunliffe et al., 2013*]. The SSML was collected in between wave-breaking periods. During this time, the MART waterfall is turned off and no bubbles are produced. SSML collection occurs ~10-15 minutes after waterfall and bubble production stops. Previous studies report that the SSML re-establishes itself within seconds [*Engel et al., 2017*] and is thus established prior to sample collection. Organic and biological material scavenged and brought to the surface during the prior wave-breaking periods remains at the surface and is collected via the glass plate method. The glass plate was cleaned directly before and after each collection by rinsing with 1 N HCl, followed by an ethanol rinse, and multiple rinses using ultrapure water.

To examine the roles of phytoplankton and bacteria, both bulk seawater and SSML were filtered using a microanalysis vacuum filter setup (EMD Millipore Corp, Cat. Num. XA5002501) and hand pump (Fisher Scientific, Part Num. 1367811E). Samples were first analyzed without filtering, and then filtered sequentially (both size filters used were 25 mm polycarbonate Isopore Membrane filter) with a 2.0 μm filter (EMD Millipore Corp, GTTP02500) to remove large phytoplankton [*Salonen, 1974*] and again with a 0.2 μm filter (EMD Millipore Corp, TTTP02500) to remove bacteria, allowing viruses and dissolved organic carbon (DOC) to pass through [*Morán et al., 1999*]. EEMs were obtained after each filtration. All glassware used during filtration (including the stainless steel mesh support screen) was rinsed with ultrapure water and cleaned by heating to 500 °C for 7 hours after use. Polycarbonate filters were sterilized using 1 N HCl and rinsed with ultrapure water.

3.3.3 Excitation-Emission Matrices and Parallel Factor Analysis

EEMs were obtained for all samples using a spectrofluorometer (Horiba Scientific, Aqualog with extended range). Three aliquots were taken from each of the three impingers, and an EEM was measured for each sample (total of nine EEMs per day for SSA phase). Excitation wavelengths ranged from 235-450 nm. Emission ranged from 250-800 nm. For the second half of the MART A experiment, EEM measurements were performed using a standard Aqualog spectrofluorometer covering an emission wavelength range of 250-620 nm. A background spectrum acquired with ultrapure water was subtracted from all EEMs. EEMs were corrected for inner-filter effects based on absorbance spectra measured simultaneously. Rayleigh scatter (1^{st} and 2^{nd} order) was removed in the analysis using an interpolation method [*Bahram et al., 2006*]. EEMs were also normalized to the area of the Raman Scattering peak of water at 350nm

excitation to convert fluorescence intensities to Raman Units (R.U.) [*Lawaetz and Stedmon, 2009; Murphy, 2011*]. The EEMs converted to R.U. were incorporated into the PARAFAC models. EEMs included in figures were smoothed with a Savitzky-Golay filter (4^{th} order, 15-point for MART A, 4^{th} order, 9-point for MART B to prevent distorting the narrower chlorophyll-a peak) [*Press, 1992*]. The smoothing of EEMs was not done prior to PARAFAC modeling or any other data analysis. All error bars shown, unless otherwise noted, represent the standard deviation of the mean (N=9) for the 9 SSA measurements.

PARAFAC modeling for each of the two MARTs was carried out using the DOMFluor toolbox in MATLAB (The MathWorks, Inc.) [*Stedmon et al., 2008; Murphy et al., 2013*]. The PARAFAC model for MART A consisted of 274 EEMs, while the MART B PARAFAC model used 451 EEMs. Both PARAFAC models' datasets consisted of EEMs for all phases (bulk seawater, SSML, and SSA). In order to model the complete MART A dataset, which contains EEMs from two spectrofluorometers with different emission wavelength ranges and increments, the dataset EEMs were cut and linearly interpolated to give emission wavelengths that ranged from 250 to 600 in 2 nm increments. For both MART A and MART B, a PARAFAC model was validated using split-half validation as well as random initialization analysis to ensure that the model generated was not a local minimum but a least squares result [*Murphy et al., 2013*].

3.4 Results & Discussion

3.4.1 Phytoplankton Blooms in Two Laboratory-based Mesocosms

Two phytoplankton microcosm studies were carried out to study sea-air transfer that occurs as a function of bloom conditions. The two microcosm experiments were conducted in the MART and are referred to as MART A (seawater collected and experiment conducted in Jan.

2014) and MART B (collected/conducted in April, 2014). Seawater used in the MART A and MART B microcosm experiments had different initial chlorophyll-a levels (1.33 mg/m^3 for MART A; 4.49 mg/m^3 for MART B), and the same nutrient amounts were added to both MARTs (see Methods) to induce phytoplankton blooms.

The progression of the phytoplankton bloom was monitored daily via *in vivo* chlorophyll-a fluorescence using a hand-held fluorometer (**Figure 3.1a, 3.1e**). Based on these *in vivo* chlorophyll-a measurements, each bloom was categorized into three stages: (1) growth, which lasted 8-9 days for both blooms, (2) peak, which lasted for 3-4 days after the growth stage, and (3) decline, which persisted after the peak for 5 days in MART A and 14 days in MART B. We note that a second growth phase with lower chlorophyll-a levels developed in both microcosms. Although both MART microcosms were induced using the same nutrient additions, MART B reached a higher (~3×) chlorophyll-a concentration at the peak of the bloom (**Figure 3.1a, 3.1e**). We investigate temporal changes in the transfer of different biogenic species transfer to SSA through these growth and death processes.

3.4.2 Assignment of Fluorescence Bands and Parallel Factor Analysis

In both phytoplankton bloom experiments, fluorescence was observed within EEM regions commonly detected in natural marine systems (**Figure 3.1b-c, 3.1f-g**) [*Coble, 1996; Mostofa, 2013*]. The EEM fluorescence regions fall into three main classes: chlorophyll-a, protein-like substances, and HULIS. An example EEM depicting the three main fluorescence regions is included in the Supplemental Information (**Figure 3.7**). The chlorophyll-a peak appeared at excitation/emission wavelengths of (400-440 nm) / (680-690 nm), while the HULIS peaks appeared at (260 or 360 nm) / (450-455 nm) and at (325 nm) / (410 nm) [*Coble, 1996;*

Hessen et al., 1998; Mostofa, 2013; Rosario-Ortiz and Korak, 2017]. The peaks for protein-like substances were further divided into two regions: a tryptophan-like region at (<235 and 275-280 nm) / (330-350 nm) and a tyrosine-like region at (<235 and 275 nm) / (295-310 nm) for tyrosine-like species) [*Coble, 1996; Mostofa, 2013*].

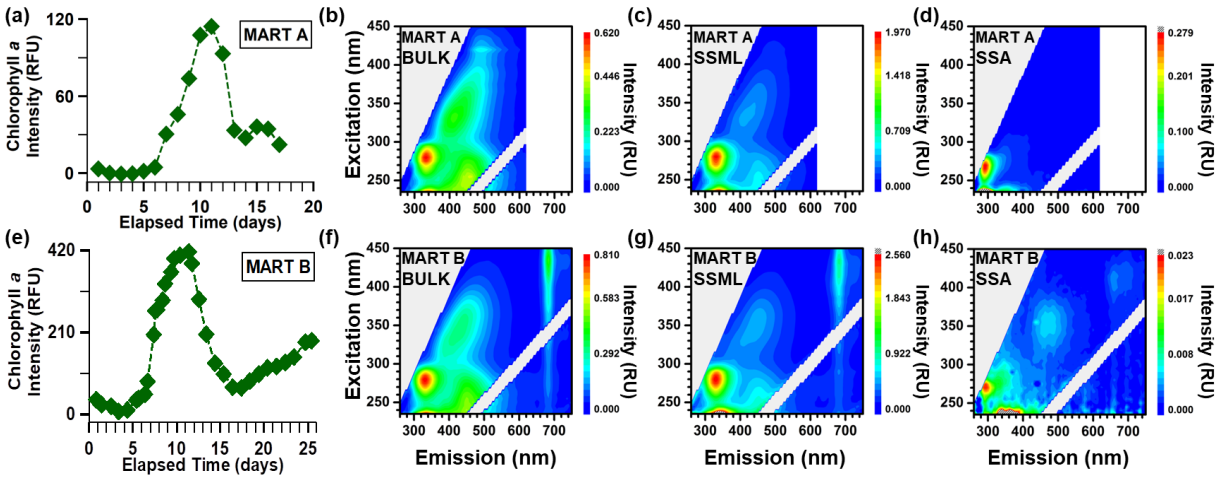

Figure 3.1. Chlorophyll-a time traces (a, e) and selected fluorescence excitation-emission matrices (EEMs) (b-d, f-h) for phytoplankton bloom experiments in MART A (top) and MART B (bottom). All EEMs shown are for unfiltered samples measured during the bloom decline stage (Day 17 for MART A, Day 15 for MART B). The EEMs shown are bulk seawater (b, f), sea-surface microlayer (SSML) (c, g), and sea spray aerosol (SSA) (d, h). Dark gray regions (in UV excitation region of g, h) indicate amplitudes that exceed the given scale.

PARAFAC analysis was performed on the entire EEM dataset from each MART to distinguish the individual fluorophore contributions (**Figure 3.2, Table 3.1**). Six components were found in MART A, and four components were found in MART B. PARAFAC components were associated with chromophores as follows: A1, A4, and B1 (tryptophan-like); A5 (tyrosine-like); B3 (chlorophyll-a); A2, A3, A6, B2, B4 (HULIS). Components A4, A5, and A6 only appeared in MART A (**Table 3.1**). Although a tyrosine-like feature (A5) was evident in the SSA EEMs for MART B, a tyrosine component was excluded from the PARAFAC model due to the

small amplitude relative to other protein-like features and the number of SSA spectra within the dataset. Using the online OpenFluor spectral database [*Murphy et al., 2014*], all compounds identified here using a PARAFAC model were spectrally similar to components found in multiple marine environments [*Kowalczuk et al., 2010; Yamashita et al., 2010; Jørgensen et al., 2011*].

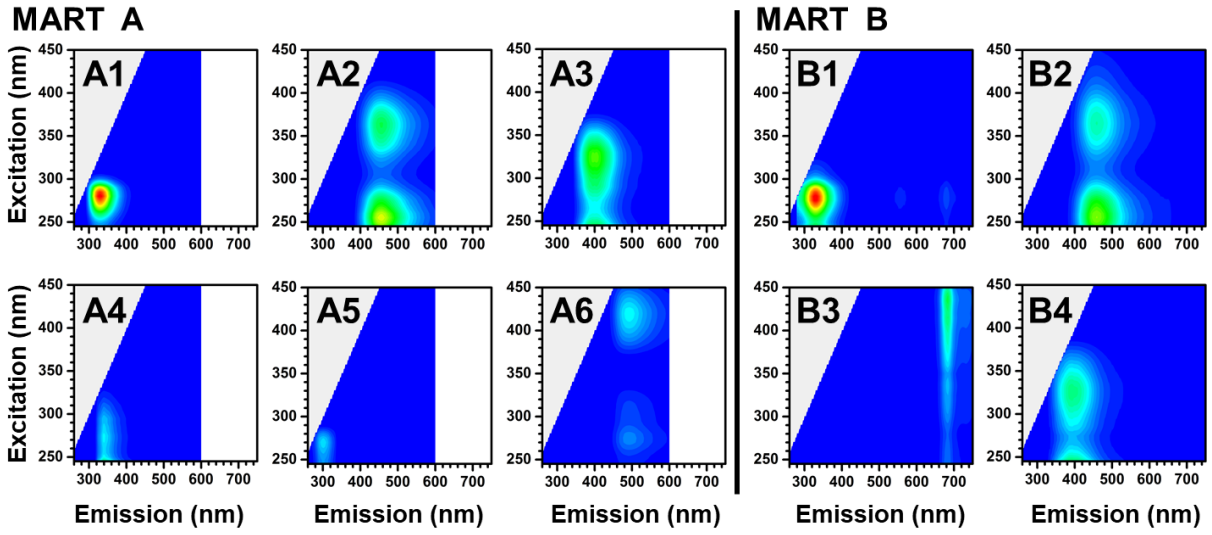

Figure 3.2. Representative components determined from PARAFAC analysis for MART A (A1-6, on left) and MART B (B1-4, on right). The components A1-6 have the same color scale as in Figure 3.1b; the amplitudes are from PARAFAC decomposition of the EEM in that panel (MART A bulk seawater on day 17). Similarly, components B1-4 have the same color scale as in Figure 3.1f, and the amplitudes result from decomposition of the EEM for MART B bulk seawater sample on day 15.

Within a single phase (bulk seawater, SSML or SSA), the fluorescence intensities of each component varied over time (**Figure 3.8, Figure 3.9**). It is important to note that we only compared the magnitude of fluorescence intensities within a single phase because of the different sampling methods used for bulk seawater, SSML and SSA. Thus, we focused on *temporal changes* in fluorescence intensity between phases. Moreover, we focused primarily on the temporal trends in MART B, which contained a more comprehensive SSA dataset. In the

following sections, we describe how the fluorescence signals of chlorophyll-a, protein-like substances, and HULIS changed over the course of the phytoplankton bloom and discuss how these changes are associated with different factors influencing sea-air transfer.

3.4.3 Chlorophyll-a in Bulk Seawater, SSML, and SSA

Chlorophyll-a fluorescence, observed in MART B EEMs, appeared in all phases (bulk seawater, SSML, and SSA) (**Figure 3.1f-h**). To study the transfer of phytoplankton and bacteria cells to SSA, we examined chlorophyll-a fluorescence in 3 different seawater size fractions: unfiltered seawater, 2.0 μm-filtered seawater, and 0.2 μm-filtered (**Figure 3.3**). The 2.0 μm-filter removes large phytoplankton and retains bacteria and dissolved organics, while the 0.2 μm-filter removes bacteria and retains dissolved organics in the seawater. Chlorophyll-a concentrations in bulk seawater and SSML showed distinct temporal trends for each of these size fractions. In the unfiltered bulk seawater, the temporal trend in chlorophyll-a for EEMs in MART B tracked the growth and decline of phytoplankton, similar to the hand-held fluorometer (**Figure 3.1e**). After filtering bulk seawater with a 2.0 μm filter to remove large phytoplankton, chlorophyll-a was still present in bulk seawater (**Figure 3.3**) but showed no growth or decay over days 5-15. The presence of chlorophyll-a after 2.0 μm-filtration is indicative of either the presence of chlorophyll-containing cell fragments and organelles or the presence of cyanobacteria, specifically *Prochlorococcus*, which is the most abundant photosynthetic organism in the ocean [*Partensky et al., 1999*]. Additionally, chlorophyll-a fluorescence was completely removed after filtering bulk seawater and SSML with a 0.2 μm filter (not pictured), which indicates that freely dissolved chlorophyll-a was not present.

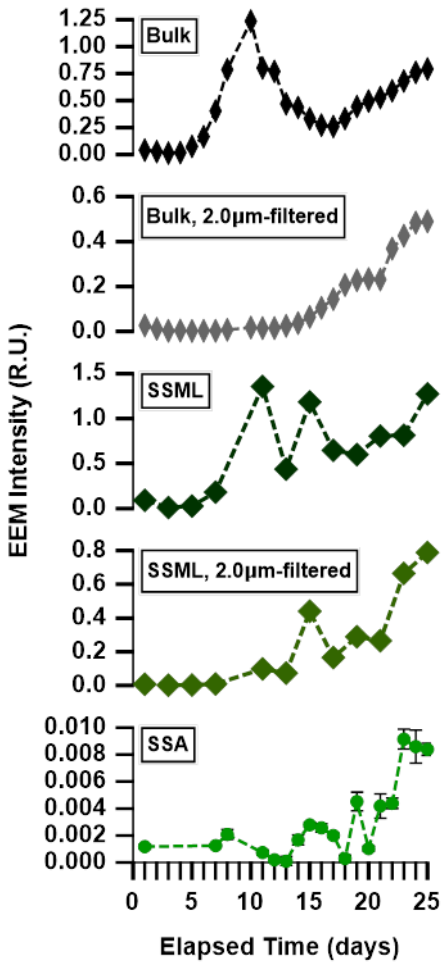

Figure 3.3. Temporal trends in chlorophyll-a signal from MART B for (top to bottom): unfiltered bulk seawater, bulk seawater after 2.0 µm filtration, unfiltered SSML, SSML after 2.0 µm filtration, and SSA. The signals are quantified in Raman units (R.U., see Methods).

The SSA EEMs indicate that the chlorophyll-a increased gradually through the second growth stage, similar to the trends found for the 2.0 µm-filtered bulk seawater and SSML (**Figure 3.3**). The fluorescence trends for the SSA correlate with the trends for 2.0 µm-filtered SSML ($r^2 = 0.86$, $p < 0.01$). The correlation between chlorophyll-a signals of SSA and 2.0-µm filtered bulk seawater is only slightly lower ($r^2 = 0.76$, $p < 0.01$). Therefore, we conclude that the chlorophyll-a in SSA originates from material residing in the 0.2 – 2.0 micron size range (either in the bulk seawater or SSML), and thus is most sensitive to the transfer of organelles and small

cells such as bacteria [*Salonen, 1974; Kuroiwa et al., 1981; Liberton et al., 2011*]. In other words, the transfer of chlorophyll-a from seawater to SSA is likely dominated by cyanobacteria or by cell fragments produced by microbial degradation of whole phytoplankton cells.

3.4.4 Protein-like EEMS Components

In MART A and MART B, the protein-like regions, either tryptophan- or tyrosine-like features, or both, were observed in the EEMs of all phases of the blooms (**Figure 3.1b-d, 3.1f-h**). Previous studies have shown that the tryptophan-like and tyrosine-like fluorescence signals can be linked to a variety of proteinaceous components, including cell or cell fragments, exopolymeric substances, soluble amino acids/peptides/proteins, and other indolic and phenolic compounds [*Determann et al., 1998; Lakowicz, 2006; Mostofa, 2013; Rosario-Ortiz et al., 2017*]. EEMS of unfiltered bulk seawater and SSML in MART A and B produced tryptophan-like emission signals at ~330 nm that overwhelmed the tyrosine-like emission signals at ~300 nm (**Figure 3.1**). This trend is expected because EEMs for these phases are similar to signals in the protein region reported previously for marine microorganisms [*Determann et al., 1998*], and tryptophan is generally the strongest emitter from proteins and microbes upon 280 nm excitation[*Determann et al., 1998; Lakowicz, 2006*].

In both MART A and B, the bulk seawater and SSML EEMs showed the greatest tryptophan-like fluorescence intensity either at the peak or the decline stage of the bloom, consistent with the growth of microbes during a phytoplankton bloom (**Figure 3.4, Figure 3.10**) [*Miyazaki et al., 2018*]. A more surprising trend emerges when examining the protein-like signals in SSA. In contrast to seawater, protein-like fluorescence in SSA for MART B was most intense before the peak of the phytoplankton bloom and decreased over the course of the bloom

(**Figure 3.4**). Additionally, EEMs of SSA for both MART A and B primarily showed tyrosine-like fluorescence signal with less contribution from tryptophan-like fluorescence that was dominant in the bulk seawater and SSML phases (**Figure 3.4, Figure 3.10**).

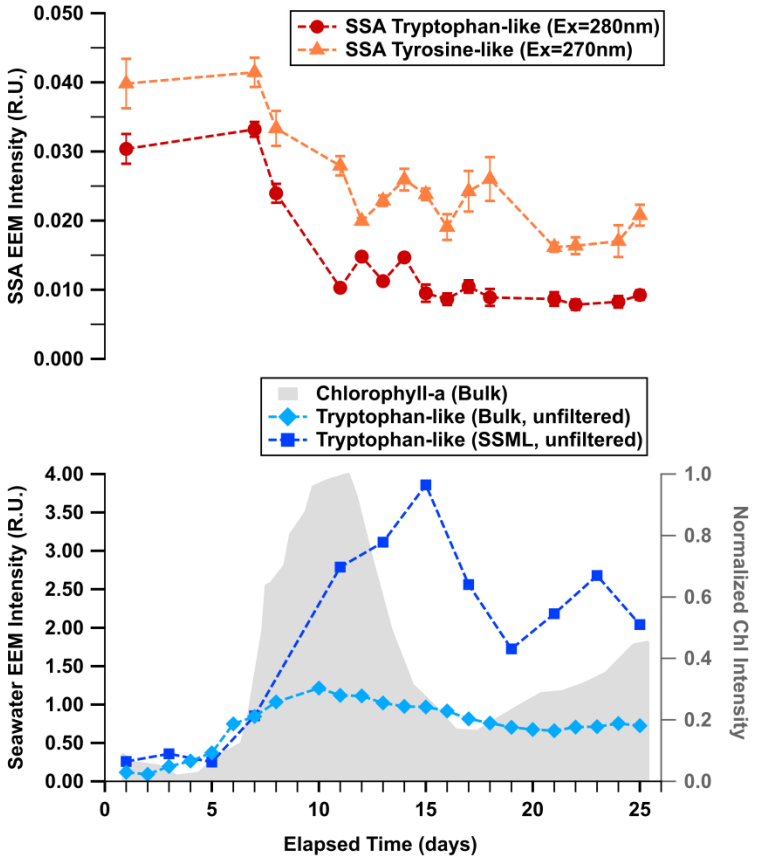

Figure 3.4. Fluorescence intensity temporal trends in MART B for chlorophyll-a in unfiltered bulk seawater (grey), tryptophan-like substances in bulk seawater and SSML (blue), tryptophan-like substances in SSA (Ex= 280 nm; red circles), and tyrosine-like substances in SSA (Ex= 270 nm; triangles). Error bars represent the standard deviation of the mean (N=9; see Methods).

The overall decrease in protein-like signal over time and enhanced tyrosine signal in SSA suggests that the principal sources of protein-like fluorescence in the aerosol phase differ from those in bulk seawater/SSML phases [*Kuznetsova et al., 2005*]. The seawater EEMs showed mainly tryptophan-like fluorescence. As mentioned previously, tryptophan is the dominant fluorophore for microorganisms including bacteria [*Determann et al., 1998*]. Bacteria are

abundant in seawater, even under non-bloom conditions [*Whitman et al., 1998*]. Previous studies have observed bacteria in isolated SSA [*Patterson et al., 2016*] and a similar peak in microbial signatures in SSA prior to phytoplankton bloom growth [*Sultana et al., 2017*].

While the tryptophan-like fluorescence in the bulk seawater and SSML could be attributed to bacteria, the enhanced tyrosine-like fluorescence could be attributed to soluble exudates or extracellular polymeric substances (EPS). EPS makes up a significant fraction of dissolved organic matter in seawater [*Verdugo et al., 2004; Decho and Gutierrez, 2017*]. Previous work has shown that tyrosine can dominate EEMs of soluble EPS in some conditions [*Liu et al., 2017*]. Thus, we suggest that while bacteria cells are transferred to SSA, sea-air transfer is dominated by soluble exudates. In this scenario, the decrease in protein-like signal in SSA could be due to the colonization of bacteria with particulate matter in seawater, which has been shown to occur in seawater after a phytoplankton bloom [*Riemann et al., 2000*], and/or less efficient transfer of soluble exudates/EPS as particles in seawater become stickier and increase in size over the course of a bloom [*Kuznetsova et al., 2005; Orellana et al., 2011; Decho et al., 2017; Miyazaki et al., 2018*].

3.4.5 Transfer of Humic-like Substances from Seawater to SSA

HULIS peaks were present in bulk seawater and SSML for both blooms (**Figure 3.1b-c, 3.1f-h**). EEMs of bulk seawater in the MART A experiment had an additional HULIS band at 420 nm excitation / 490 nm emission (**Figure 3.1b**). The same humic-like peaks present in seawater of MART A were also present in the EEMs of the corresponding SSA (while not apparent in **Figure 3.1d**, these peaks appear on a magnified scale, **Figure 3.8**), while only the 360 nm excitation HULIS peak was present in the SSA EEMs for MART B.

Temporal trends for HULIS fluorescence in the SSML of MART B showed a large increase roughly coincident with the chlorophyll-a growth, followed by a leveling off as the bloom progresses and declines (**Figure 3.5, squares**). In this same MART, bulk seawater showed an initial rise in HULIS fluorescence coincident with that of the SSML, then a gradual increase after the bloom peak (**Figure 3.5, diamonds**). In contrast to seawater, the HULIS fluorescence of the SSA (**Figure 3.5, circles)** reached its maximum *after* the peak in chlorophyll-a in bulk seawater, and eventually decreased to initial levels. The MART A microcosm showed similarly contrasting trends for HULIS fluorescence of the SSML and SSA phases. Separate from the temporal trends, we note a slight (~20 nm) redshift in the fluorescence spectra from the start of the bloom to the peak stage, followed by a return to the original wavelength late in the bloom (**Figure 3.11**).

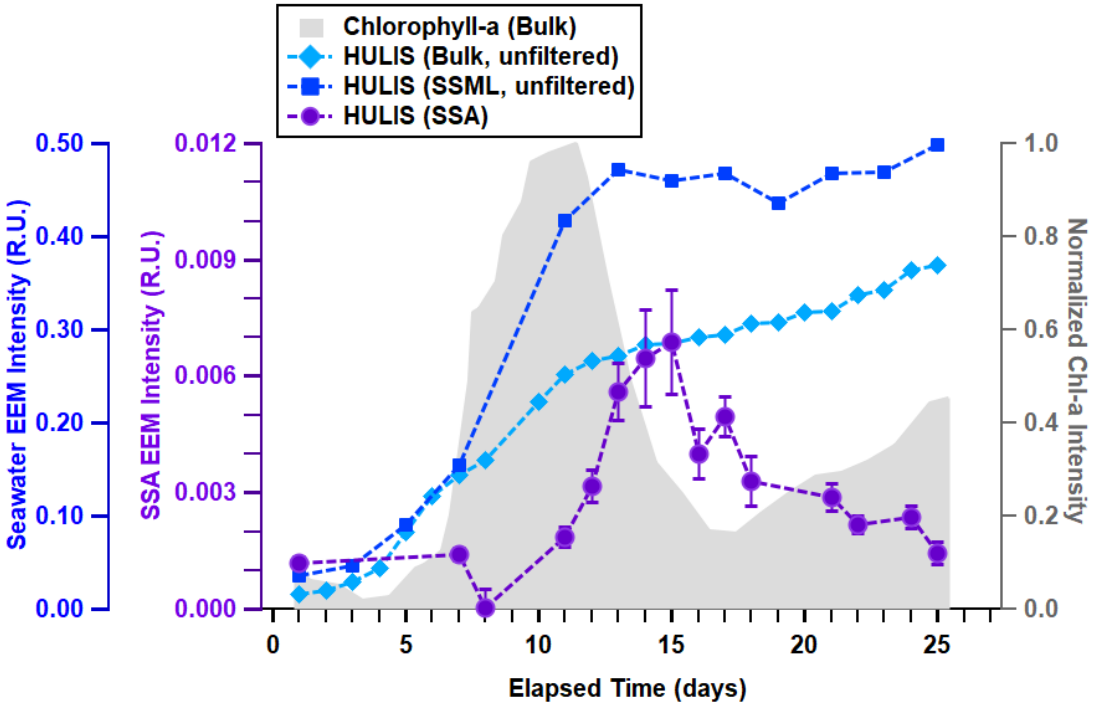

Figure 3.5. Temporal trends in fluorescence intensity of chlorophyll-a in unfiltered bulk seawater (grey shading), HULIS in unfiltered bulk seawater and SSML (Ex/Em=360 nm/450 nm; blue diamonds and squares, respectively), and SSA (Ex/Em=360 nm/472 nm; purple circles). Error bars represent the standard deviation of the mean (N=9; see Methods).

The delay in the increase of SSA HULIS fluorescence has not been reported previously. This delay is a clear indication that phytoplankton in bulk seawater are not direct drivers of HULIS transfer from the ocean to the atmosphere. Additionally, this lag between the peaks in chlorophyll-a and SSA HULIS in SSA is consistent with the increase in bacteria concentrations typically observed in seawater after the peak of a phytoplankton bloom [*Ogawa et al., 2001; Jiao et al., 2010; Lee et al., 2015; O'Dowd et al., 2015; Wang et al., 2015*]. Bacterial degradation is vital for HULIS production and HULIS chemical composition [*Rashid, 1985; Hessen et al., 1998*]. This connection with bacteria suggests, as previous studies have shown, that microbial interactions play a critical role in the enrichment of organic matter, particularly HULIS, in SSA [*Lee et al., 2015; O'Dowd et al., 2015; Wang et al., 2015*].

The decline in SSA HULIS emission despite the increase or plateau in bulk seawater and SSML, respectively, can be explained by changes in the chemical nature of the HULIS. The spectral changes in SSML HULIS (~20 nm redshift), which nearly coincided with the increase and subsequent decrease of HULIS fluorescence in the SSA, suggest that bacteria induce changes in HULIS chemical composition over the course of a bloom [*Miano et al., 1990; Chen et al., 2003*]. For example, there may be a shift to a more surface-active form of HULIS, which would impact the efficiency of HULIS transfer from sea surface to SSA. While further chemical and size characterization studies are required to identify the mechanism for HULIS transfer, these findings clearly demonstrate that the HULIS concentration in seawater alone does not correlate with the transfer and peak HULIS concentration in SSA.

3.4.6 Implications for Sea-to-Air Transfer of Organic Matter

Identifying the factors that control the release of biomolecules and microbes from the ocean to the atmosphere is critical because these biogenic organic species have different influences on clouds, climate, weather, and atmospheric chemistry [*Sun and Ariya, 2006; Orellana et al., 2011; McCluskey et al., 2017; Santl-Temkiv et al., 2019*]. For example, microbes identified using protein fluorescence are likely contributors to ice formation in clouds [*McCluskey et al., 2017; Santl-Temkiv et al., 2019*], while humic-like substances have been linked to cloud nucleation and atmospheric photochemistry, such as the production of reactive gases like nitrous acid in the atmosphere [*Stemmler et al., 2006; Slade et al., 2017*]. Here, we used a lab-controlled microcosm in conjunction with rapid analysis via EEM spectroscopy to monitor changes and probe connections in the bulk seawater, SSML, and SSA. While previous studies have attempted to correlate SSA organic enrichment with parameters such as SSA particle flux or seawater DOC concentrations, we found no links between changes in fluorescent signatures and SSA particle flux (number, surface area, or volume) or DOC concentrations (**Figure 3.12**) [*Alpert et al., 2015; Collins et al., 2016*]. Instead, our study reveals three major findings regarding sea-air transfer of organic matter:

First, none of the classes of organics investigated (chlorophyll-a, protein-like substances, and HULIS) showed a dependence on the growth of phytoplankton as indicated by chlorophyll-a in the bulk seawater. This suggests that phytoplankton are not producing the majority of the fluorescent organic matter that is directly transferred to SSA. Instead, phytoplankton likely play a key role in producing the organic precursors to those species that ultimately become transferred to SSA. This also suggests that microbial degradation controls the transfer of organic matter, breaking down constituents into the appropriate size range and proper chemical properties for

efficient sea-air transfer [*Lee et al., 2015; O'Dowd et al., 2015; Wang et al., 2015; Ceburnis et al., 2016; Rastelli et al., 2017*].

Second, we show that the peaks in SSA of different organic species do not correspond to peaks for these same species in bulk seawater or the SSML. Thus, this study reveals that factors beyond bulk seawater and SSML concentrations control the concentrations of biogenic species in SSA in the atmosphere. Previous studies have shown selective transfer occurs, for example due to enhanced surface adsorption [*Cochran et al., 2016*] or microbe cell membrane chemistry [*Michaud et al., 2018*]. This study suggests that processes that can alter the size and chemical properties of biogenic organic matter play an important role in controlling sea-air transfer.

Finally, transfer of the three different organic classes studied here occurred at different points during the bloom, suggesting different factors controlled the release of each species (**Figure 3.6**). The transfer of each class was likely affected by different physical, biological, and chemical factors that depend on microbial conversion processes to modify size and chemical properties [*Wang et al., 2015*]. Chlorophyll-a transfer requires the *breakdown* of cells into cell fragments and organelles (**Figure 3.6**) [*Kuroiwa et al., 1981; Liberton et al., 2011*]. The transfer of protein-like substances is reduced by *colonization* of particulate matter by bacteria likely linked to the formation of "sticky" exudates (**Figure 3.6**). The transfer of HULIS depends on *chemical* changes induced by bacteria (**Figure 3.6**). The transfer of these classes into SSA at different times clearly shows that while SSA can be enriched with organic species, the specific types of organic molecules in SSA change over time, which will lead to different chemical and climate-relevant properties such as water uptake, cloud formation, and ice nucleation.

By isolating the ocean and atmosphere during a bloom, these studies are the first to begin unraveling the mechanisms by which ocean-derived biological species in seawater are

transferred into SSA. Future experiments will be performed to probe how changes in seawater particulate size distributions, colonization, marine gel production, and other ocean processes affect the transfer of dissolved and particulate organic matter from the ocean to the atmosphere. The ultimate goal will be to better understand the factors controlling the biogeochemical cycling of organic species between the ocean and atmosphere.

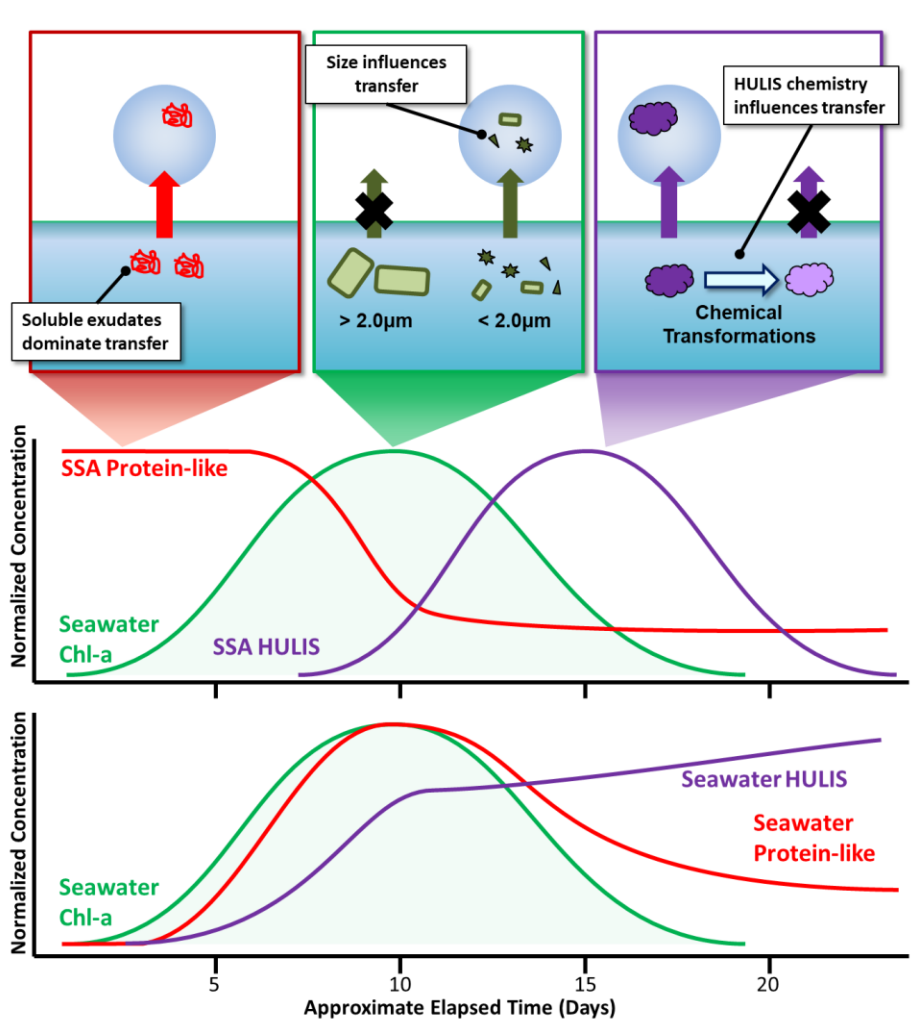

Figure 3.6. Summary of EEM chromophores (chlorophyll-a, humic substances, and protein-like) and factors that are likely to have an influence on transfer to aerosol particles. Approximate concentrations are normalized to their respective maxima.

3.5 Acknowledgments

This study was funded through the National Science Foundation Center for Aerosol Impacts on the Chemistry of the Environment (NSF CAICE), a Center for Chemical Innovation (CHE-1801971). The authors would like to thank Lihini Aluwihare, Wilson Mendoza, Grant Deane, Farooq Azam, Judy Kim, and Rebecca Simpson for valuable feedback and discussions. The datasets generated during and/or analyzed during the current study are available at: https://doi.org/10.6075/J0NC5ZQ1.

Chapter 3 is reproduced with permission from Scientific Reports: Santander, M.V., Schiffer, J.M., Lee, C., Axson, J.L., Tauber, M.J., Prather, K.A., "Factors controlling the transfer of biogenic organic species from seawater to sea spray aerosol", Scientific Reports, 12 (1), 3580, 2022. The dissertation author was the primary investigator and author of this paper. M.V.S., M.J.T. and K.A.P. designed the experiments. M.V.S., C.L., J.L.A. performed the experiments. M.V.S. and J. M. S. analyzed the data. M.V.S., J.M.S., M.J.T. and K.A.P. wrote the paper.

3.6 Supporting Information

3.6.1 Supporting Information Figures

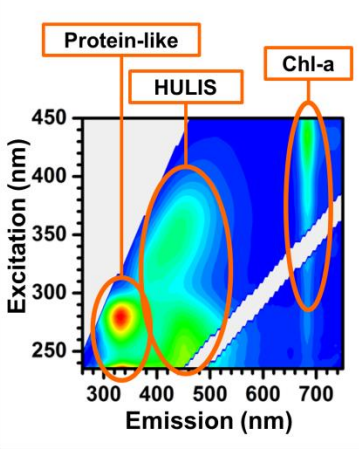

Figure 3.7. Example EEM depicting the locations of seawater fluorophore regions

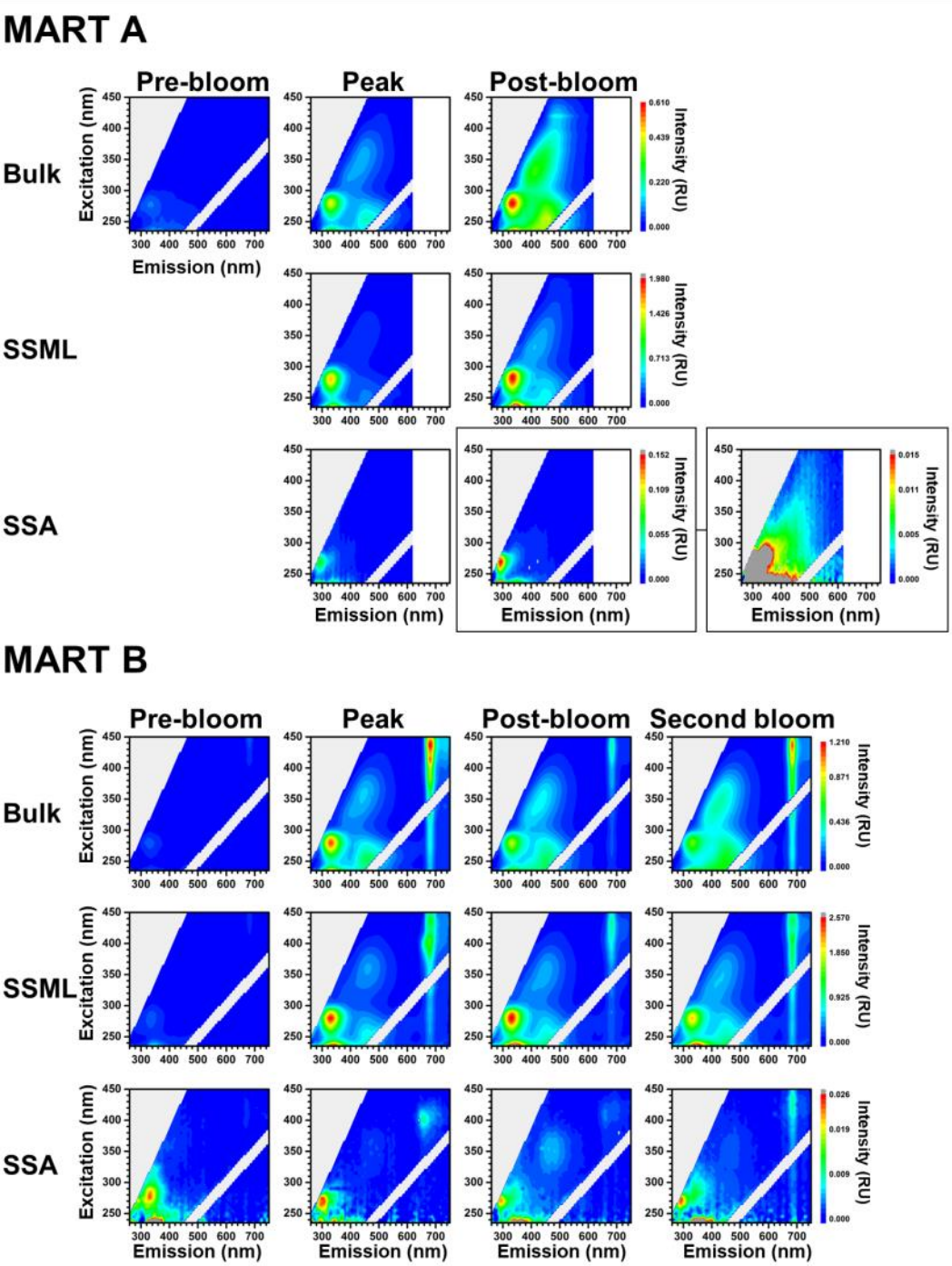

Figure 3.8. Selected EEMs for bulk seawater, SSML, and SSA at different stages for MART A and MART B mesocosms. The EEM for MART A post-bloom SSA is shown with two different scales to show the presence of the humic-like fluorescence bands.

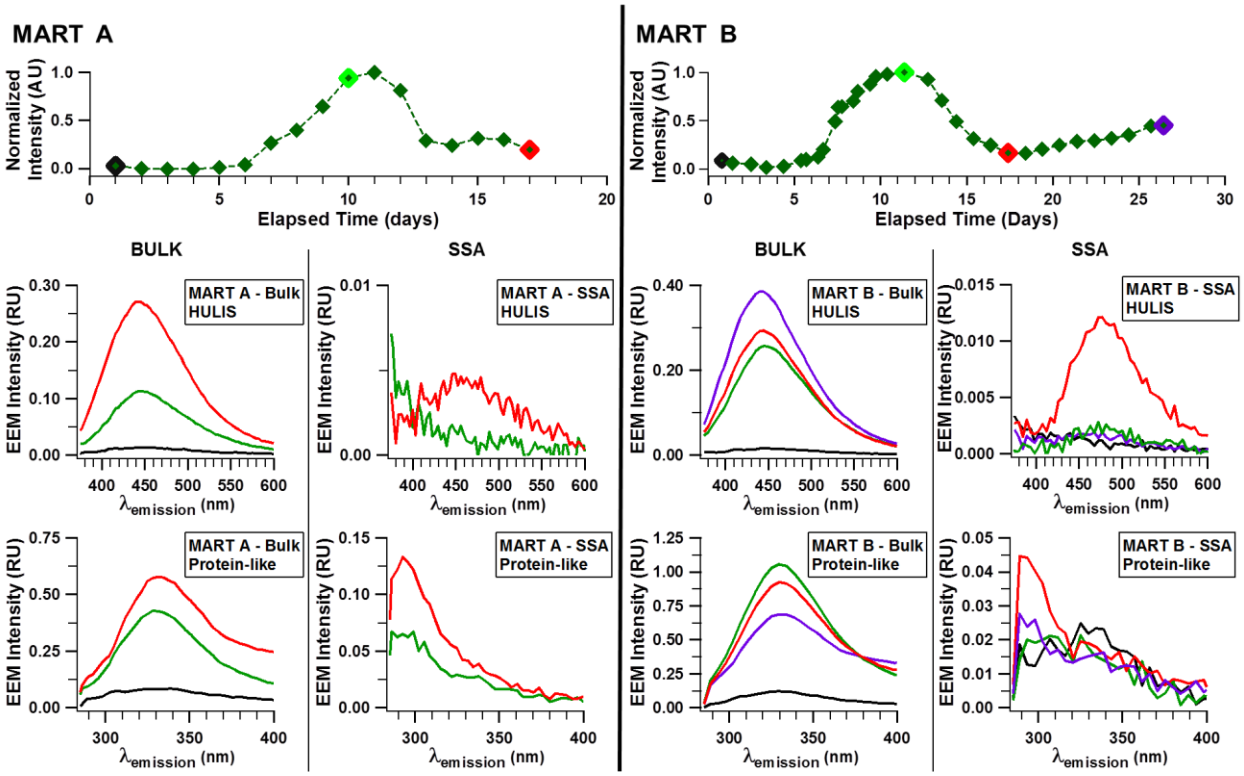

Figure 3.9. MART A and MART B chlorophyll-a temporal trends (top) and select emission spectra for bulk seawater and SSA. Panels labeled "HULIS" or "Protein-like" were excited with 360 nm or 275 nm light, respectively. Colors correspond to different stages: pre-bloom (black), bloom peak (green), post-bloom (red), and second bloom (purple).

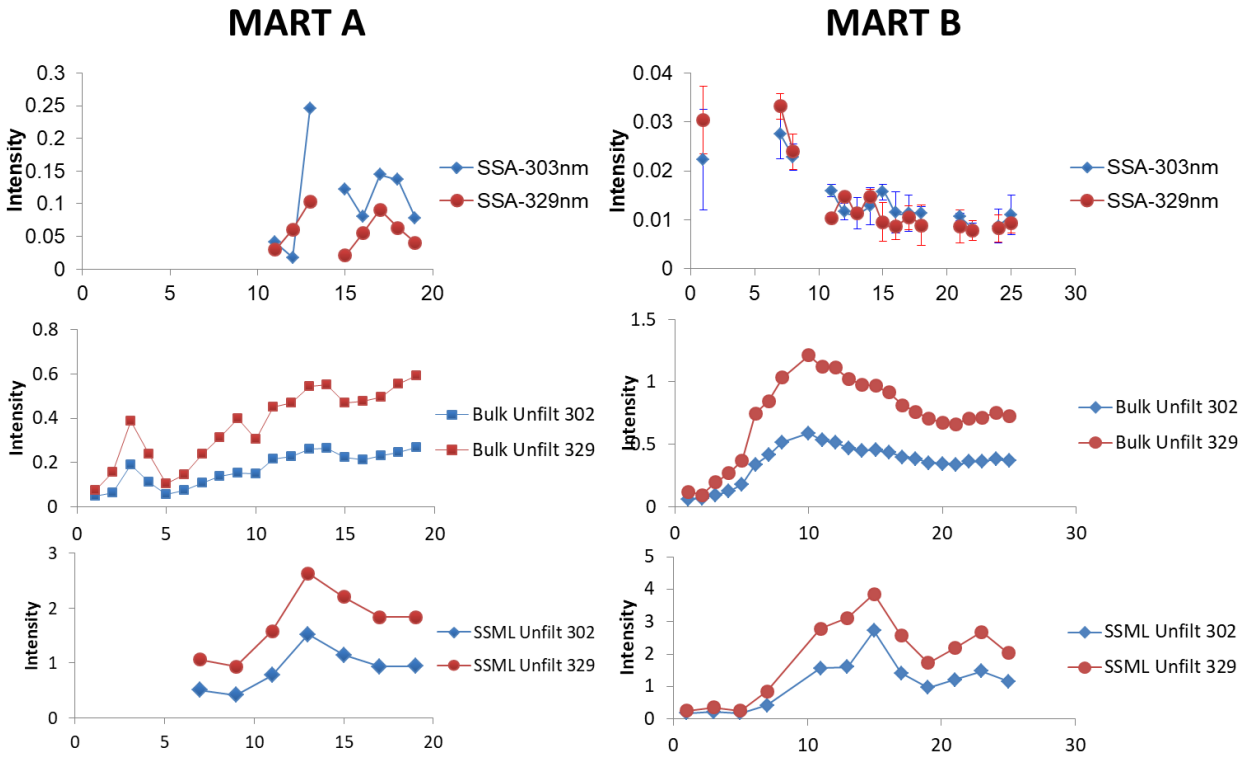

Figure 3.10. Trends in the EEMs amplitudes, at wavelength positions that report on the tyrosine-like component (Ex/Em = 280 nm / 303 or 305 nm) and tryptophan-like component (Ex/Em = 280 nm / 329nm). The amplitudes (intensity) are taken directly from the EEMs, and are not from PARAFAC analysis. The first row shows trends in the SSA phase. MART A samples were collected only once. MART B samples were collected three times, and error bars show one standard deviation. The gaps in data reflect samples with unusually high or low fluorescence relative to the other samples and are excluded as outliers. The second and third rows show trends for the unfiltered bulk and SSML

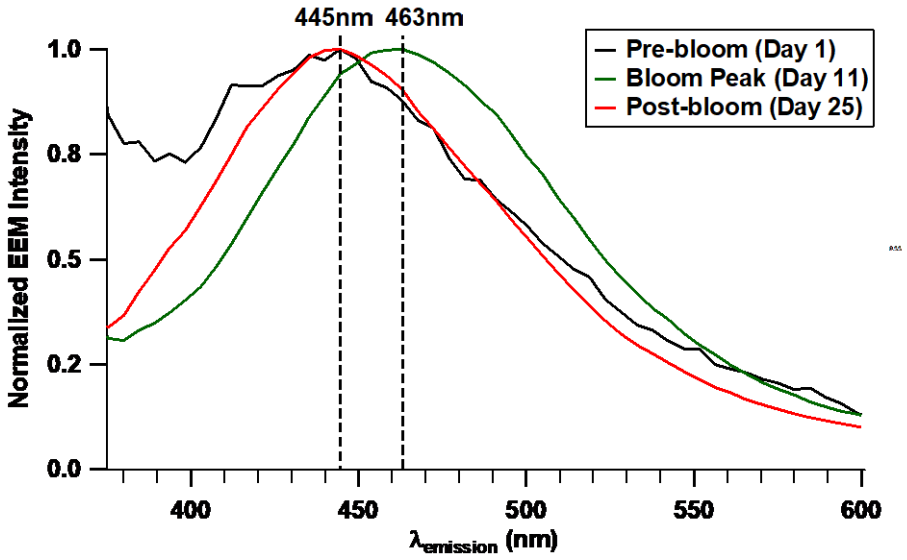

Figure 3.11. Emission spectra for SSML samples of MART B, excited at 360 nm to probe the HULIS component.

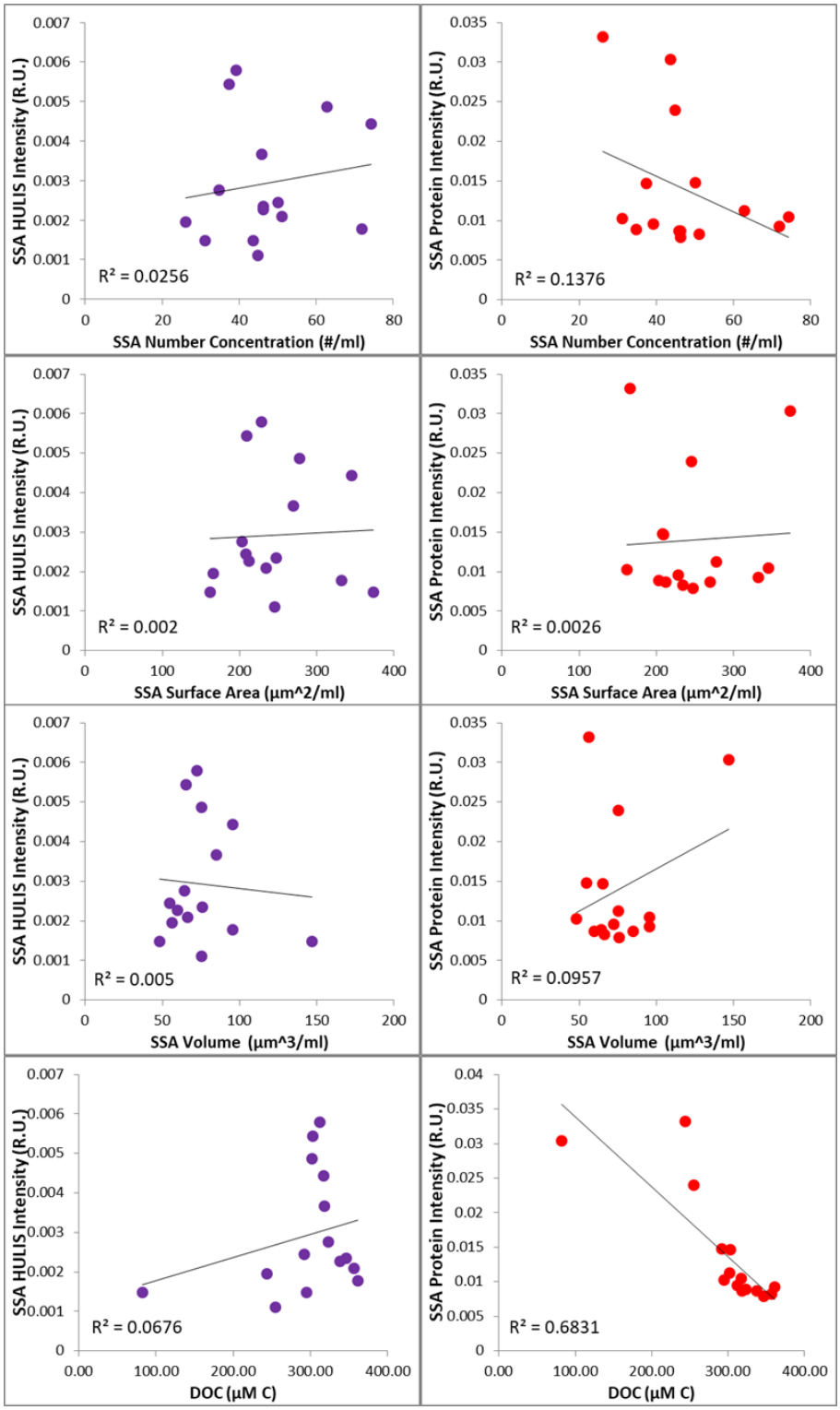

Figure 3.12. Relationships of HULIS (left) and protein-like substances (right) versus SSA particle number, surface area, and volume concentrations, and DOC.

3.6.2 Supporting Information Tables

Table 3.1. Excitation and emission maxima for each of the PARAFAC components identified for MART A and MART B

Component	*Ex (nm)*	*Em (nm)*	*Description*
MART A			
A1	280	330	Tryptophan-like
A2	255, 365	453	Humic
A3	325	396	Humic
A4	<245, 275	340	Tryptophan-like
A5	270	302	Tyrosine-like
A6	275, 420	492	Humic
MART B			
B1	280	330	Protein-like, tryptophan-like
B2	255, 365	460	Humic
B3	435	684	Chlorophyll *a*
B4	<245, 325	394	Humic

Table 3.2. Seawater collection times and conditions for MART A and B

Date	*Chlorophyll-a (mg m^{-3})*	*Water Temp. (^{o}C)*	*Pressure (dbar)*	*Salinity (PSU)*	*MART*
1/15/2014 20:00	1.33	15.30	4.83	33.54	A
4/11/2014 12:00	4.49	14.34	3.51	33.43	B

3.7 References

Aller, J. Y., M. R. Kuznetsova, C. J. Jahns and P. F. Kemp. The sea surface microlayer as a source of viral and bacterial enrichment in marine aerosols. *Journal of Aerosol Science*. **2005**, *36*(5-6): 801-812.

Alpert, P. A., W. P. Kilthau, D. W. Bothe, J. C. Radway, J. Y. Aller and D. A. Knopf. The influence of marine microbial activities on aerosol production: a laboratory mesocosm study. *Journal of Geophysical Research-Atmospheres*. **2015**, *120*(17): 8841-8860.

Azam, F., T. Fenchel, J. G. Field, J. S. Gray, L. A. Meyer-Reil and F. Thingstad. The ecological role of water-column microbes in the sea. *Marine Ecology Progress Series*. **1983**, *10*(3): 257-263.

Bahram, M., R. Bro, C. Stedmon and A. Afkhami. Handling of Rayleigh and Raman scatter for PARAFAC modeling of fluorescence data using interpolation. *Journal of Chemometrics*. **2006**, *20*(3-4): 99-105.

Bigg, E. K. and C. Leck. The composition of fragments of bubbles bursting at the ocean surface. *Journal of Geophysical Research*. **2008**, *113*(D11).

Blanchard, D. C. Sea-to-air transport of surface active material. *Science*. **1964**, *146*(3642): 396-397.

Brown, T. E. and F. L. Richards. Effect of growth environment on physiology of algae - light intensity. *Journal of Phycology*. **1968**, *4*(1): 38.

Burrows, S. M., O. Ogunro, A. A. Frossard, L. M. Russell, P. J. Rasch and S. M. Elliott. A physically based framework for modeling the organic fractionation of sea spray aerosol from bubble film Langmuir equilibria. *Atmospheric Chemistry and Physics*. **2014**, *14*(24): 13601-13629.

Ceburnis, D., A. Masalaite, J. Ovadnevaite, A. Garbaras, V. Remeikis, W. Maenhaut, M. Claeys, J. Sciare, D. Baisnee and C. D. O'Dowd. Stable isotopes measurements reveal dual carbon pools contributing to organic matter enrichment in marine aerosol. *Scientific Reports*. **2016**, *6*.

Chen, J., E. J. LeBoef, S. Dai and B. H. Gu. Fluorescence spectroscopic studies of natural organic matter fractions. *Chemosphere*. **2003**, *50*(5): 639-647.

Coble, P. G. Characterization of marine and terrestrial DOM in seawater using excitation emission matrix spectroscopy. *Marine Chemistry*. **1996**, *51*(4): 325-346.

Cochran, R. E., T. Jayarathne, E. A. Stone and V. H. Grassian. Selectivity across the interface: a test of surface activity in the composition of organic-enriched aerosols from bubble bursting. *Journal of Physical Chemistry Letters*. **2016**, *7*(9): 1692-1696.

Collins, D. B., T. H. Bertram, C. M. Sultana, C. Lee, J. L. Axson and K. A. Prather. Phytoplankton blooms weakly influence the cloud forming ability of sea spray aerosol. *Geophysical Research Letters*. **2016**, *43*(18): 9975-9983.

Cunliffe, M., A. Engel, S. Frka, B. Gasparovic, C. Guitart, J. C. Murrell, M. Salter, C. Stolle, R. Upstill-Goddard and O. Wurl. Sea surface microlayers: a unified physicochemical and biological perspective of the air-ocean interface. *Progress in Oceanography*. **2013**, *109*: 104-116.

de Leeuw, G., E. L. Andreas, M. D. Anguelova, C. W. Fairall, E. R. Lewis, C. O'Dowd, M. Schulz and S. E. Schwartz. Production flux of sea spray aerosol. *Reviews of Geophysics*. **2011**, *49*(2).

Decho, A. W. and T. Gutierrez. Microbial extracellular polymeric substances (EPSs) in ocean systems. *Frontiers in Microbiology*. **2017**, *8*(922).

Determann, S., J. M. Lobbes, R. Reuter and J. Rullkotter. Ultraviolet fluorescence excitation and emission spectroscopy of marine algae and bacteria. *Marine Chemistry*. **1998**, *62*(1-2): 137-156.

Engel, A., H. W. Bange, M. Cunliffe, S. M. Burrows, G. Friedrichs, L. Galgani, H. Herrmann, N. Hertkorn, M. Johnson, P. S. Liss, P. K. Quinn, M. Schartau, A. Soloviev, C. Stolle, R. C. Upstill-Goddard, M. van Pinxteren and B. Zäncker. The ocean's vital skin: toward an integrated understanding of the sea surface microlayer. *Frontiers in Marine Science*. **2017**, *4*(165).

Gantt, B. and N. Meskhidze. The physical and chemical characteristics of marine primary organic aerosol: a review. *Atmospheric Chemistry and Physics*. **2013**, *13*(8): 3979-3996.

Gaston, C. J., H. Furutani, S. A. Guazzotti, K. R. Coffee, T. S. Bates, P. K. Quinn, L. I. Aluwihare, B. G. Mitchell and K. A. Prather. Unique ocean-derived particles serve as a proxy for changes in ocean chemistry. *Journal of Geophysical Research*. **2011**, *116*(D18).

Guillard, R. R. and J. H. Ryther. Studies of marine planktonic diatoms .1. Cyclotella nana Hustedt, and Detonula confervacea (Cleve) Gran. *Canadian Journal of Microbiology*. **1962**, *8*(2): 229.

Hessen, D. O. and L. J. Tranvik (1998). Aquatic humic substances: ecology and biogeochemistry. Berlin; New York, Springer.

Jiao, N., G. J. Herndl, D. A. Hansell, R. Benner, G. Kattner, S. W. Wilhelm, D. L. Kirchman, M. G. Weinbauer, T. Luo, F. Chen and F. Azam. Microbial production of recalcitrant dissolved organic matter: long-term carbon storage in the global ocean. *Nat Rev Micro*. **2010**, *8*(8): 593-599.

Jørgensen, L., C. A. Stedmon, T. Kragh, S. Markager, M. Middelboe and M. Søndergaard. Global trends in the fluorescence characteristics and distribution of marine dissolved organic matter. *Marine Chemistry*. **2011**, *126*(1-4): 139-148.

Kowalczuk, P., W. J. Cooper, M. J. Durako, A. E. Kahn, M. Gonsior and H. Young. Characterization of dissolved organic matter fluorescence in the South Atlantic Bight with use of PARAFAC model: relationships between fluorescence and its components, absorption coefficients and organic carbon concentrations. *Marine Chemistry*. **2010**, *118*(1-2): 22-36.

Kuroiwa, T., T. Suzuki, K. Ogawa and S. Kawano. The chloroplast nucleus - distribution, number, size, and shape, and a model for the multiplication of the chloroplast genome during chloroplast development. *Plant and Cell Physiology*. **1981**, *22*(3): 381-396.

Kuznetsova, M., C. Lee and J. Aller. Characterization of the proteinaceous matter in marine aerosols. *Marine Chemistry*. **2005**, *96*(3-4): 359-377.

Lakowicz, J. R. (2006). Principles of fluorescence spectroscopy. New York, Springer.

Lawaetz, A. J. and C. A. Stedmon. Fluorescence intensity calibration using the raman scatter peak of water. *Applied Spectroscopy*. **2009**, *63*(8): 936-940.

Leck, C. and K. E. Bigg. Comparison of sources and nature of the tropical aerosol with the summer high Arctic aerosol. *Tellus B: Chemical and Physical Meteorology*. **2017**, *60*(1): 118-126.

Lee, C., C. M. Sultana, D. B. Collins, M. V. Santander, J. L. Axson, F. Malfatti, G. C. Cornwell, J. R. Grandquist, G. B. Deane, M. D. Stokes, F. Azam, V. H. Grassian and K. A. Prather. Advancing model systems for fundamental laboratory studies of sea spray aerosol using the microbial loop. *J Phys Chem A*. **2015**, *119*(33): 8860-8870.

Liberton, M., J. R. Austin, 2nd, R. H. Berg and H. B. Pakrasi. Insights into the complex 3-D architecture of thylakoid membranes in unicellular cyanobacterium Cyanothece sp. ATCC 51142. *Plant Signal Behav*. **2011**, *6*(4): 566-569.

Liss, P. S. and R. A. Duce (1997). The sea surface and global change. Cambridge ; New York, Cambridge University Press.

Liu, L. Z., Q. Huang, Y. L. Zhang, B. Q. Qin and G. W. Zhu. Excitation-emission matrix fluorescence and parallel factor analyses of the effects of N and P nutrients on the extracellular polymeric substances of Microcystis aeruginosa. *Limnologica*. **2017**, *63*: 18-26.

McCluskey, C. S., T. C. J. Hill, F. Malfatti, C. M. Sultana, C. Lee, M. V. Santander, C. M. Beall, K. A. Moore, G. C. Cornwell, D. B. Collins, K. A. Prather, T. Jayarathne, E. A. Stone, F. Azam, S. M. Kreidenweis and P. J. DeMott. A dynamic link between ice nucleating particles released in nascent sea spray aerosol and oceanic biological activity during two mesocosm experiments. *Journal of the Atmospheric Sciences*. **2017**, *74*(1): 151-166.

Miano, T., G. Sposito and J. P. Martin. Fluorescence spectroscopy of model humic acid-type polymers. *Geoderma*. **1990**, *47*(3-4): 349-359.

Michaud, J. M., L. R. Thompson, D. Kaul, J. L. Espinoza, R. A. Richter, Z. Z. Xu, C. Lee, K. M. Pham, C. M. Beall, F. Malfatti, F. Azam, R. Knight, M. D. Burkart, C. L. Dupont and K. A. Prather. Taxon-specific aerosolization of bacteria and viruses in an experimental ocean-atmosphere mesocosm. *Nature Communications*. **2018**, *9*.

Miyazaki, Y., K. Suzuki, E. Tachibana, Y. Yamashita, A. Muller, K. Kawana and J. Nishioka. New index of organic mass enrichment in sea spray aerosols linked with senescent status in marine phytoplankton. *Scientific Reports*. **2020**, *10*(1).

Miyazaki, Y., Y. Yamashita, K. Kawana, E. Tachibana, S. Kagami, M. Mochida, K. Suzuki and J. Nishioka. Chemical transfer of dissolved organic matter from surface seawater to sea spray water-soluble organic aerosol in the marine atmosphere. *Scientific Reports*. **2018**, *8*.

Morán, X. A. G., J. M. Gasol, L. Arin and M. Estrada. A comparison between glass fiber and membrane filters for the estimation of phytoplankton POC and DOC production. *Marine Ecology Progress Series*. **1999**, *187*: 31-41.

Mostofa, K. M. G. (2013). Photobiogeochemistry of organic matter: principles and practices in water environments. Heidelberg ; New York, Springer.

Murphy, K. R. A note on determining the extent of the water raman peak in fluorescence spectroscopy. *Applied Spectroscopy*. **2011**, *65*(2): 233-236.

Murphy, K. R., C. A. Stedmon, D. Graeber and R. Bro. Fluorescence spectroscopy and multi-way techniques. PARAFAC. *Analytical Methods*. **2013**, *5*(23): 6557.

Murphy, K. R., C. A. Stedmon, P. Wenig and R. Bro. OpenFluor- an online spectral library of auto-fluorescence by organic compounds in the environment. *Analytical Methods*. **2014**, *6*(3): 658-661.

Nebbioso, A. and A. Piccolo. Molecular characterization of dissolved organic matter (DOM): a critical review. *Analytical and Bioanalytical Chemistry*. **2013**, *405*(1): 109-124.

O'Dowd, C., D. Ceburnis, J. Ovadnevaite, J. Bialek, D. B. Stengel, M. Zacharias, U. Nitschke, S. Connan, M. Rinaldi, S. Fuzzi, S. Decesari, M. C. Facchini, S. Marullo, R. Santoleri, A. Dell'Anno, C. Corinaldesi, M. Tangherlini and R. Danovaro. Connecting marine productivity to sea-spray via nanoscale biological processes: phytoplankton dance or death disco? *Sci Rep*. **2015**, *5*: 14883.

O'Dowd, C. D., M. C. Facchini, F. Cavalli, D. Ceburnis, M. Mircea, S. Decesari, S. Fuzzi, Y. J. Yoon and J. P. Putaud. Biogenically driven organic contribution to marine aerosol. *Nature*. **2004**, *431*(7009): 676-680.

Ogawa, H., Y. Amagai, I. Koike, K. Kaiser and R. Benner. Production of refractory dissolved organic matter by bacteria. *Science*. **2001**, *292*(5518): 917-920.

Oppo, C., S. Bellandi, N. D. Innocenti, A. M. Stortini, G. Loglio, E. Schiavuta and R. Cini. Surfactant components of marine organic matter as agents for biogeochemical fractionation and pollutant transport via marine aerosols. *Marine Chemistry*. **1999**, *63*(3-4): 235-253.

Orellana, M. V., P. A. Matrai, C. Leck, C. D. Rauschenberg, A. M. Lee and E. Coz. Marine microgels as a source of cloud condensation nuclei in the high Arctic. *Proceedings of the National Academy of Sciences of the United States of America*. **2011**, *108*(33): 13612-13617.

Partensky, F., W. R. Hess and D. Vaulot. Prochlorococcus, a marine photosynthetic prokaryote of global significance. *Microbiology and Molecular Biology Reviews*. **1999**, *63*(1): 106.

Patterson, J. P., D. B. Collins, J. M. Michaud, J. L. Axson, C. M. Sultana, T. Moser, A. C. Dommer, J. Conner, V. H. Grassian, M. D. Stokes, G. B. Deane, J. E. Evans, M. D. Burkart, K. A. Prather and N. C. Gianneschi. Sea spray aerosol structure and composition using cryogenic transmission electron microscopy. *Acs Central Science*. **2016**, *2*(1): 40-47.

Prather, K. A., T. H. Bertram, V. H. Grassian, G. B. Deane, M. D. Stokes, P. J. DeMott, L. I. Aluwihare, B. P. Palenik, F. Azam, J. H. Seinfeld, R. C. Moffet, M. J. Molina, C. D. Cappa, F. M. Geiger, G. C. Roberts, L. M. Russell, A. P. Ault, J. Baltrusaitis, D. B. Collins, C. E. Corrigan, L. A. Cuadra-Rodriguez, C. J. Ebben, S. D. Forestieri, T. L. Guasco, S. P. Hersey, M. J. Kim, W. F. Lambert, R. L. Modini, W. Mui, B. E. Pedler, M. J. Ruppel, O. S. Ryder, N. G. Schoepp, R. C. Sullivan and D. F. Zhao. Bringing the ocean into the laboratory to probe the chemical complexity of sea spray aerosol. *Proceedings of the National Academy of Sciences of the United States of America*. **2013**, *110*(19): 7550-7555.

Press, W. H. (1992). Numerical recipes in C : the art of scientific computing. Cambridge ; New York, Cambridge University Press.

Rashid, M. A. (1985). Geochemistry of marine humic compounds. New York, Springer-Verlag.

Rastelli, E., C. Corinaldesi, A. Dell'Anno, M. Lo Martire, S. Greco, M. C. Facchini, M. Rinaldi, C. O'Dowd, D. Ceburnis and R. Danovaro. Transfer of labile organic matter and microbes from the ocean surface to the marine aerosol: an experimental approach. *Scientific Reports*. **2017**, *7*.

Riemann, L., G. F. Steward and F. Azam. Dynamics of bacterial community composition and activity during a mesocosm diatom bloom. *Appl Environ Microbiol*. **2000**, *66*(2): 578-587.

Rinaldi, M., S. Fuzzi, S. Decesari, S. Marullo, R. Santoleri, A. Provenzale, J. von Hardenberg, D. Ceburnis, A. Vaishya, C. D. O'Dowd and M. C. Facchini. Is chlorophyll-a the best

surrogate for organic matter enrichment in submicron primary marine aerosol? *Journal of Geophysical Research: Atmospheres*. **2013**, *118*(10): 4964-4973.

Rosario-Ortiz, F. L. and J. A. Korak. Oversimplification of dissolved organic matter fluorescence analysis: potential pitfalls of current methods. *Environmental Science & Technology*. **2017**, *51*(2): 759-761.

Salonen, K. Effectiveness of cellulose ester and perforated polycarbonate membrane filters in separating bacteria and phytoplankton. *Annales Botanici Fennici*. **1974**, *11*(2): 133-135.

Santl-Temkiv, T., B. Sikoparija, T. Maki, F. Carotenuto, P. Amato, M. S. Yao, C. E. Morris, R. Schnell, R. Jaenicke, C. Pohlker, P. J. DeMott, T. C. J. Hill and J. A. Huffman. Bioaerosol field measurements: challenges and perspectives in outdoor studies. *Aerosol Science and Technology*. **2019**.

Schmitt-Kopplin, P., G. Liger-Belair, B. P. Koch, R. Flerus, G. Kattner, M. Harir, B. Kanawati, M. Lucio, D. Tziotis, N. Hertkorn and I. Gebefügi. Dissolved organic matter in sea spray: a transfer study from marine surface water to aerosols. *Biogeosciences*. **2012**, *9*(4): 1571-1582.

Seinfeld, J. H. and S. N. Pandis (2006). Atmospheric chemistry and physics: from air pollution to climate change. Hoboken, N.J., J. Wiley.

Slade, J. H., M. Shiraiwa, A. Arangio, H. Su, U. Poschl, J. Wang and D. A. Knopf. Cloud droplet activation through oxidation of organic aerosol influenced by temperature and particle phase state. *Geophysical Research Letters*. **2017**, *44*(3): 1583-1591.

Stedmon, C. A. and R. Bro. Characterizing dissolved organic matter fluorescence with parallel factor analysis: a tutorial. *Limnology and Oceanography: Methods*. **2008**, *6*: 572-579.

Stemmler, K., M. Ammann, C. Donders, J. Kleffmann and C. George. Photosensitized reduction of nitrogen dioxide on humic acid as a source of nitrous acid. *Nature*. **2006**, *440*(7081): 195-198.

Stokes, M. D., G. B. Deane, K. Prather, T. H. Bertram, M. J. Ruppel, O. S. Ryder, J. M. Brady and D. Zhao. A marine aerosol reference tank system as a breaking wave analogue for the production of foam and sea-spray aerosols. *Atmospheric Measurement Techniques*. **2013**, *6*(4): 1085-1094.

Sultana, C. M., H. Al-Mashat and K. A. Prather. Expanding single particle mass spectrometer analyses for the identification of microbe signatures in sea spray aerosol. *Analytical Chemistry*. **2017**, *89*(19): 10162-10170.

Sun, J. M. and P. A. Ariya. Atmospheric organic and bio-aerosols as cloud condensation nuclei (CCN): A review. *Atmospheric Environment*. **2006**, *40*(5): 795-820.

Verdugo, P., A. L. Alldredge, F. Azam, D. L. Kirchman, U. Passow and P. H. Santschi. The oceanic gel phase: a bridge in the DOM-POM continuum. *Marine Chemistry*. **2004**, *92*(1-4): 67-85.

Wang, X. F., C. M. Sultana, J. Trueblood, T. C. J. Hill, F. Malfatti, C. Lee, O. Laskina, K. A. Moore, C. M. Beall, C. S. McCluskey, G. C. Cornwell, Y. Y. Zhou, J. L. Cox, M. A. Pendergraft, M. V. Santander, T. H. Bertram, C. D. Cappa, F. Azam, P. J. DeMott, V. H. Grassian and K. A. Prather. Microbial control of sea spray aerosol composition: a tale of two blooms. *ACS Central Science*. **2015**, *1*(3): 124-131.

Whitman, W. B., D. C. Coleman and W. J. Wiebe. Prokaryotes: The unseen majority. *Proceedings of the National Academy of Sciences of the United States of America*. **1998**, *95*(12): 6578-6583.

Yamashita, Y., A. Panton, C. Mahaffey and R. Jaffé. Assessing the spatial and temporal variability of dissolved organic matter in Liverpool Bay using excitation–emission matrix fluorescence and parallel factor analysis. *Ocean Dynamics*. **2010**, *61*(5): 569-579.

Zhang, Y. L., Y. Yin, L. Q. Feng, G. W. Zhu, Z. Q. Shi, X. H. Liu and Y. Z. Zhang. Characterizing chromophoric dissolved organic matter in Lake Tianmuhu and its catchment basin using excitation-emission matrix fluorescence and parallel factor analysis. *Water Res*. **2011**, *45*(16): 5110-5122.

Chapter 4. Bacterial Control of Marine Humic-like Substance Production, Composition, Size, and Transfer to Sea Spray Aerosols During Phytoplankton Blooms

4.1 Synopsis

Humic-like substances (HULIS) are present in every environmental reservoir, including the ocean and the atmosphere. Ocean-derived HULIS can be transferred to the atmosphere in the form of sea spray aerosols (SSA). Little information exists on the factors controlling this transfer process or how HULIS alters SSA physicochemical properties, cloud-forming ability, and atmospheric reactions. Here, using excitation-emission matrix spectroscopy and isolated ocean-atmosphere systems, we investigated how ocean biology affects HULIS sea-to-air transfer during multiple phytoplankton bloom experiments. We posit that bacterial enzymatic activity on phytoplankton-derived organic matter control HULIS size, production, and chemical composition. We found that shifts in the HULIS fluorescence emission spectra reveal changes in HULIS chemical composition induced by bacteria. High bacterial enzymatic activity on the proteinaceous, lipid, and phosphorus-rich organic pools enhanced HULIS production and its transfer to SSA. HULIS consistently accumulated across all experiments. The majority of HULIS was smaller than 0.2 μm or 50 kDa. Our results suggest that enzymatic-processing bacteria transform the composition of HULIS in seawater, degrading dissolved organic matter into diverse chemical structures that are more efficiently transferred to the atmosphere in SSA.

4.2 Introduction

Humic-like substances (HULIS) are ubiquitous in all natural environments including the soil, oceans, and the atmosphere.[*Rashid, 1985; Hessen and Tranvik, 1998; Graber and Rudich, 2006*] They consist of a complex mixture of organic molecules that are generated during the breakdown of dead organisms and larger biomolecules [*Rashid, 1985; Hessen et al., 1998*]. HULIS in aerosol particles [*Graber et al., 2006*] influence cloud formation and lifetime and atmospheric composition [*Stemmler et al., 2007; Borgatta and Navea, 2015; Slade et al., 2017; Chen et al., 2021*]. It has been postulated that the ocean is the main source of atmospheric HULIS in sea spray aerosols (SSA) generated by breaking waves [*Cavalli et al., 2004; Graber et al., 2006*]. Many studies investigating the sea-air transfer of organic matter have recognized that marine microbes, specifically interactions between phytoplankton production and bacterial enzymatic activities, play a critical role in controlling SSA chemistry [*Prather et al., 2013; Lee et al., 2015; O'Dowd et al., 2015; Wang et al., 2015; Malfatti et al., 2019; Freney et al., 2021*]. However, controlled studies of the chemical and biological factors that control the production, chemical composition, and size of HULIS and their transfer to SSA have yet to be probed.

In this study, we used excitation emission matrix (EEM) spectroscopy to characterize marine-derived HULIS and investigate the mechanisms that regulate the transfer of HULIS from seawater to SSA [*Mostofa, 2013; Murphy et al., 2013; Nebbioso and Piccolo, 2013*]. EEM spectroscopy acquires fluorescence emission spectra at multiple excitation wavelengths, which are concatenated to form a single excitation-emission matrix. EEMs allow for rapid, direct measurements of the fluorescent organic matter in seawater without requiring sample storage or preprocessing. By concatenating multiple excitation wavelengths, EEMs can characterize multiple classes of fluorophores within each sample, including protein-like substances and

chlorophyll in seawater [*Parlanti et al., 2000; Coble, 2007; Mostofa, 2013*]. This study focuses solely on HULIS fluorescence in seawater and SSA. Previous studies have identified HULIS by a broad fluorescence peak with an excitation wavelength of 360 nm and emission wavelengths ranging from 430-470 nm [*Pohlker et al., 2012; Lee et al., 2015*]. By monitoring this peak over time, changes in HULIS concentrations and chemical composition can be investigated in seawater and SSA.

Here we hypothesize that bacterial enzymes alter the production, chemical composition, and size of HULIS, and that these changes increase the efficiency of HULIS transfer from the ocean to the atmosphere in SSA. We performed experiments to disentangle the impact of phytoplankton, bacteria, and bacterial enzymes on HULIS composition and transfer. Controlled phytoplankton bloom experiments allowed for the investigation of HULIS properties under phytoplankton and bacterial growth cycles of varying bloom intensities. Perturbation experiments, where marine bacterial isolates were added, help clarify the role of bacteria and their enzymes on HULIS composition. Specifically, we examined the impact of proteases (cleavage site leucine), lipases (cleavage site oleate), and alkaline phosphatases (cleavage site phosphate), which have been shown to be relevant for sea-air transfer of organic matter [*Malfatti et al., 2019*]. We then probed the impact of these enzymes on seawater HULIS properties, and how this affects HULIS transfer from seawater to SSA. While studies have shown that phytoplankton blooms affect seawater and SSA chemistry [*Prather et al., 2013; Lee et al., 2015; Wang et al., 2015*], this study goes beyond phytoplankton and provides new insights into the links between bacterial enzyme activity and HULIS production, physicochemical properties and sea-air transfer.

4.3 Methods

4.3.1 Phytoplankton Bloom Experiments

Seventeen phytoplankton bloom experiments were conducted using natural seawater. Seawater collected from the Ellen Browning Scripps Memorial Pier (32-52'00" N, 117-15’21" W) was filtered using an acid washed 50 μm mesh screen (Sefar Nitex 03−100/32) to remove zooplankton, a grazer of phytoplankton. In the experiments discussed here, three mesocosm conditions were employed; seawater was 1) placed directly into a 120 L Marine Aerosol Reference Tank (MART) [*Stokes et al., 2013*], 2) placed into a 3000 L outdoor tank to allow phytoplankton abundance to increase, followed by aerosolization in a MART [*Trueblood et al., 2019*], or 3), in a 30,000 L waveflume at Scripps Institution of Oceanography (**TABLE 4.1, S1**). In the seven experiments labeled as Exp1-7, HULIS was sampled in the bulk seawater (total and size fractionated) and in the SSA (**TABLE 4.1**). Exp1, or the Investigation into Marine PArticle Chemistry and Transfer Science (IMPACTS) campaign, was conducted in the waveflume is Exp1 [*Wang et al., 2015*], while Exp3-7 used the MART for SSA generation. In the ten experiments labeled as S01-S10, total HULIS was sampled only in the bulk seawater (**SI TABLE 4.2**). Methods used for phytoplankton mesocosm experiments in both the waveflume and the MARTs have been described previously [*Lee et al., 2015; Wang et al., 2015*]. Briefly, the seawater was spiked with Guillard’s F/2 algae nutrient medium [*Guillard and Ryther, 1962*] (concentrations ranging from F/100 to F/2) to induce a phytoplankton bloom and then incubated with fluorescent lights (Full Spectrum Solutions, model 205457; T8 format, color temperature 5700 K, 2950 lumens) [*Brown and Richards, 1968*]. Experiments carried out in the outdoor tank used sunlight rather than fluorescent lights for incubation. The growth and decline of phytoplankton were monitored daily using an Aquafluor handheld fluorometer (Turner Designs,

Aquafluor) to measure *in vivo* chlorophyll-a fluorescence (excitation at 395 nm and emission ≥660 nm).

Table 4.1. List of the experiments probing the dynamics of HULIS. Experiments designated as Exp1-7 are experiments where EEMs were collected for both bulk seawater and SSA. HB = heterotrophic bacterial abundances, V = viral abundances, DOC = dissolved organic carbon, and CHL = *in vivo* or extracted chlorophyll; Imp = impingers, Spot = Spot sampler

NAME	YEAR	Tank System	SSA Generator	System Volume (L)	SSA Collection	DURATION (days)	CHL (µg/L)	Bulk Seawater Measurements				
								CHL	HB	V	DOC	Enzyme Activity
Exp1	2014	Wave-flume	Wave-flume	30000	Imp	37	5.76	X	X	X	X	X
Exp2	2019	Wave-flume	Wave-flume	30000	Spot	21	18.70	X	X	X	X	X
Exp3	2018	Outdoor Tank/ MART	MART	100	Spot	9	12.65	X	X	X	X	X
Exp4	2018	Outdoor Tank/ MART	MART	100	Spot	9	11.41	X	X	X	X	X
Exp5	2014	MART	MART	100	Imp	26	39.08	X	--	--	X	--
Exp6	2014	MART	MART	100	Imp	19	13.10	X	--	--	X	--
Exp7	2019	Outdoor Tank/ MART	MART	100	Spot	9	1.90	X	X	X	--	--

For Exp4, marine bacteria isolates were introduced into the MART after the peak of the phytoplankton bloom. Three different marine-relevant bacteria isolates were used: *Alteromonas macleodii* (AltSIO), *Pseudoalteromonas sp.* (ATW7), and *Flavobacteria sp.* (BBFL7). These three strains were chosen due to their high protease activities that, in previous studies, were found to be effective in the dissolution of particulate silica present in diatom frustule [*Bidle and Azam, 2001*]. AltSIO was also added due to its ability to break down dissolved organic carbon [*Pedler et al., 2014*]. These three "local" species were originally isolated from the Pacific Ocean off of the Ellen Browning Scripps Memorial Pier. The bacterial isolates were prepared by growing colonies on solid ZoBell medium from the frozen stock culture for 24 hours. Colonies were then transferred to liquid ZoBell medium at room temperature and grown on a shaker at 130 rpm for approximately 24 hours. Liquid cultures were harvested by spinning at 9000 g for 5 minutes, followed by a wash with 0.2 µm filtered and sterilized seawater to remove the supernatant (spent medium). Optical density measured at 600 nm was checked in order to have 1:1:1 (AltSIO:ATW7:BBFL7) ratio of the isolates in the inoculum that was $1x10^9$ cells/L.

4.3.2 Aerosol Generation and Aerosol Sample Collection

SSA was generated using two aerosol generation approaches: the Marine Aerosol Reference Tank (MART) [*Stokes et al., 2013; Trueblood et al., 2019; Santander et al., 2022*] and breaking waves in the waveflume at SIO [*Wang et al., 2015*]. Briefly, the MART uses a periodic plunging waterfall to generate bubble plumes that burst to form SSA. By creating an isolated system for studying SSA, the MART prevents the inclusion of atmospheric aerosols from non-marine sources. The MART has been shown to produce SSA size distributions that are similar to the size distributions measured of nascent SSA in field studies [*Stokes et al., 2013*].

For experiments in the 3000 L outdoor tank, 100 L of seawater was transferred daily from the outdoor tank to the MARTs and then transferred back to the outdoor tank the following day after refilling the MARTs with a fresh batch of seawater from the outdoor tank [*Trueblood et al., 2019*]. The SIO waveflume is a 33 meter long sealed glass channel that uses a moving paddle to create a wave that breaks on an artificial beach, generating SSA [*Stokes et al., 2013*]. Similar to the MART, the waveflume is an isolated system that removes non-marine aerosols.

Aerosols were collected using one of two different methods (see details in **TABLE 4.1**). Aerosols were collected using glass impingers (Chemglass, CG-1820, 0.2 μm D_p lower cutoff at 1 LPM) containing 20 mL of ultrapure (Type 1) water. The airflow through the impingers was set at 1 LPM for 2 hours for MART experiments and 6 hours for waveflume experiments. Alternatively, aerosols were collected daily using two liquid spot samplers (Aerosol Devices, LSS110A), which use a condensation growth tube to collect particles [*Fernandez et al., 2014*], in a size range of 5 nm to >10 μm, into a 0.7 mL liquid vial filled with ultrapure (Type 1) water. The airflow through the spot samplers was 1.5 LPM over the 1 hour collection period. The samples from the two liquid spot samplers were then combined and diluted to 1.5 mL before measuring with EEM spectroscopy.

4.3.3 Bulk Seawater Collection, DOC, and Microbiology Analysis

Bulk seawater samples were collected and analyzed for EEMs, dissolved organic carbon (DOC) concentrations, heterotrophic bacteria and virus concentrations, and enzyme activity. All bulk seawater samples were collected in glass vials prepared for total organic carbon (TOC) analysis. Briefly, vials were cleaned with an acetone rinse followed by several ultrapure water rinses followed by an acid wash with 0.1 N HCL and multiple ultrapure water rinses, then heated

at 500 °C for 7 hours. Bulk samples were collected daily from a spigot located on the side of the MART or syphoned out of the waveflume. DOC samples were prepped by filtering seawater with a combusted 0.7 µm glass fiber filter (Whatman GF/F, Z242489) and acidifying to pH 2 with ~2 drops of trace metal-free concentrated 12 M HCl. Samples were stored in the dark at room temperature. DOC was analyzed by using the high-temperature combustion method (Shimadzu Instruments) [*Alvarez-Salgado and Miller, 1998*].

Heterotrophic bacteria and virus concentrations for all experiments were obtained either by epifluorescence microscopy or flow cytometry. All water samples for microbial abundance were preserved using 10% electron microscopy grade glutaraldehyde and then incubated at 4 °C for 10 minutes followed by flash freezing in liquid nitrogen and then storing at -80 °C. Samples were analyzed with an epifluorescence microscope (Keyence BZ-X700, final magnification 100x after staining) with SYBR Green I (Life Technologies, S-7563) following the Noble and Furhman protocol for bacteria and viruses [*Noble and Fuhrman, 1998*]. Samples analyzed via flow cytometry (BIO-RAD, ZE5 Cell Analyzer, at The Scripps Research Institute (TSRI) Flow Core Facility) for heterotrophic bacteria were first diluted (1:10) in 1×TE buffer (pH 8), then were stained with SYBR Green I at RT for 10 minutes (at a 10:4 dilution of the commercial stock) in the dark [*Gasol and Del Giorgio, 2000*]. For viruses, samples were diluted (1:50) in 1×TE buffer (pH 8) and stained with SYBR Green I at 80 °C for 10 minutes in the dark (at a 5×10^{-5} dilution of the commercial stock). Heterotrophic bacteria and virus populations were discriminated based on their signature in the FL1 (488 nm laser, green fluorescence) vs. side scattering (SSC) specific cytograms [*Marie et al., 1997; Brussaard, 2004*].

Bacterial enzymatic activities (protease, lipase and alkaline phosphatase) were measured using the fluorogenic substrate method [*Hoppe, 1983*]. Briefly, fluorogenic substrates: L-leucine-

7-amido-4-methyl-coumarin (Sigma, L2145), 4-methyl-umbelliferyl oleate (Sigma, 75164), 4-methyl-umbelliferyl-phosphate (Sigma, M8883) were added to the sample at 20 μM final concentrations (in Exp1, Exp3, and Exp4). Fluorescence was measured once immediately after the addition of the fluorogenic substrates, incubated in the dark for 45 minutes, and measured again. Fluorescence was measured using 355 nm excitation and 460 nm emission by a multimode reader (SynergyTM H1, BioTek) on 96-well microliter plates. The fluorescence signal results from the cleavage of free fluorophores (4-methylumbelliferone (MUF) and 7-amido-4-methylcoumarin (AMC)) from the substrate and is directly proportional to the hydrolysis rate and thus the bacterial enzymatic activity. Standard curves were generated for each measurement to relate fluorescence intensity to fluorophore concentration.

Bulk seawater samples were size-fractionated (see **TABLE 4.1**). Seawater was filtered by 0.2 μm filter either with a microanalysis vacuum filter setup (EMD Millipore Corp, Cat. Num. XA5002501) with hand pump (Fisher Scientific, Part Num. 1367811E) and a 0.2 μm polycarbonate filter (EMD Millipore Corp, GTTP02500), or by syringe filtration (BD, 309604; Pall Acrodisc, PN4602). For Exp3 and Exp4, samples were then sequentially filtered via centrifuge filtration using a 50 kDa centrifuge filter (Amicon Ultra 2 mL, UFC205024) and centrifuging at 4000 g for 15 minutes (Eppendorf, 5810, Rotor A-4-44). All filtration glassware was cleaned by rinsing with ultrapure water and heating to 500 °C for 7 hours. Syringe filters and centrifuge filters were cleaned with several ultrapure water filtrations prior to use.

4.3.4 Excitation-Emission Matrix Spectroscopy

EEMs were obtained for all bulk seawater and SSA samples using a spectrofluorometer (Horiba Scientific, Aqualog with extended range). Excitation wavelengths ranged from 235-450

nm. Emission wavelengths ranged from 250-800 nm. A background spectrum was acquired with ultrapure water and subtracted from all EEMs. EEMs were corrected for inner-filter effects based on absorbance spectra measured simultaneously. Rayleigh scatter (1^{st} and 2^{nd} order) was removed. EEMs were also normalized to the area of the Raman Scattering peak of water at 350 nm excitation to convert fluorescence intensities to Raman Units (R.U.) [*Lawaetz and Stedmon, 2009; Murphy, 2011*]. The abundance of HULIS is presented as the fluorescence intensity of the HULIS peak at wavelengths of 360 nm excitation and 450 nm emission unless otherwise specified.

4.4 Results and Discussion

4.4.1 Seawater HULIS Correlate with DOC and Display a Narrow Size Range

Phytoplankton bloom experiments were carried out to investigate differences in HULIS production over a wide range of biological conditions and different bloom densities. The progression of the phytoplankton blooms were monitored using *in vivo* chlorophyll-a fluorescence, which is used as a proxy for phytoplankton biomass (**Figure 4.1**). Each bloom experiment showed similar behavior in terms of a chlorophyll-a increase followed by a decrease over several days, with the exception of Exp7, which showed minimal change in chlorophyll-a levels, representing a non-bloom scenario. Notably, the chlorophyll-a data for Exp1 produced two maxima, indicative of two sequential phytoplankton bloom cycles. All blooms showed very different bloom densities (indicated by chlorophyll-a), with maximum values ranging from 1.90 µg/L (during Exp7) to 39.08 µg/L (in Exp5). The heterotrophic bacteria and virus concentrations peaked approximately 3 days after chlorophyll-a in most experiments (**Figure 4.1**), with the

exception of Exp7. This staggered progression is consistent with previous phytoplankton bloom experiments [*Lee et al., 2015*].

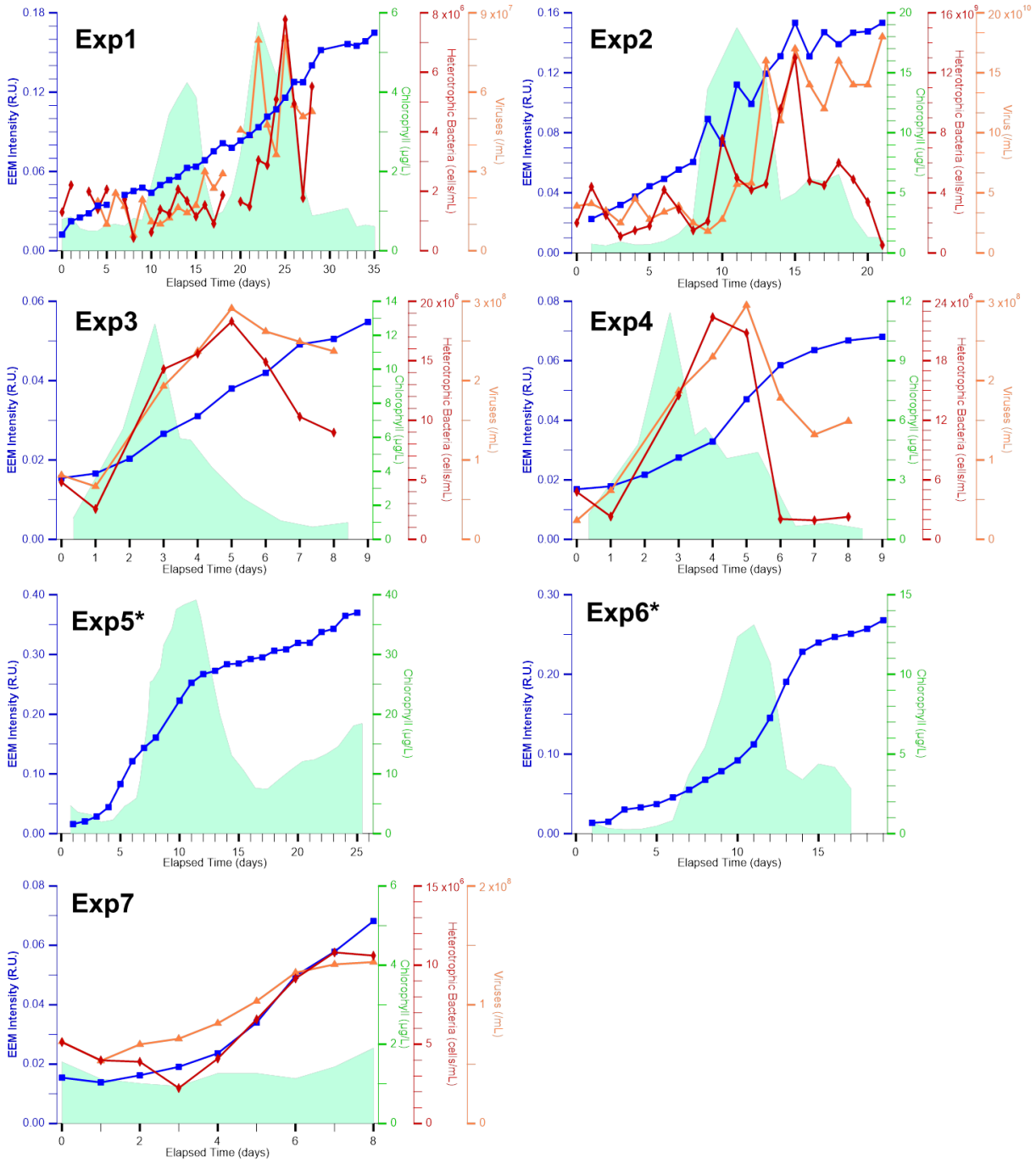

Figure 4.1. Time series for chlorophyll-a, HULIS fluorescence (360 nm excitation, 450 nm emission), heterotrophic bacteria concentrations and virus concentrations in bulk seawater during phytoplankton blooms in 7 experiments. Asterisks (*) indicate no measurements for bacterial and viral abundance.

Nutrient additions induced phytoplankton blooms which influenced heterotrophic bacteria and virus abundances in the seawater. EEMs of seawater HULIS reflect the enhanced biological activity. In all cases, the intensity of the HULIS fluorescence peak measured by EEMs increased over time, indicating steady production and accumulation of HULIS in seawater (**Figure 4.1**). Even for Exp1 and Exp7, which exhibited distinctive bloom dynamics, accumulation of HULIS occurred over time. Despite the wide range in phytoplankton bloom densities, HULIS accumulation was not correlated with maxima in *in vivo* chlorophyll, suggesting phytoplankton abundance is not singularly responsible for HULIS production in seawater. (**Figure 4.9**). Therefore, a combination of both phytoplankton and bacteria were responsible for the increased HULIS concentration.

In all experiments, temporal changes in bulk seawater HULIS EEM intensity correlated with DOC (**Figure 4.2**, Spearman's ρ ranges from 0.79 to 0.98). This correlation suggests that 1) the organic molecules that make up the DOC pool contribute to HULIS and 2) HULIS fluorescence intensity reflects DOC concentrations in the ocean. We speculate that the degree of recalcitrance of the DOC is reflected in the HULIS intensity. From the analysis of the EEM vs DOC slopes across the entire dataset, we distinguish 3 families of slope steepness: Exp1-like; Exp2-3-4-like and Exp5-6-like (**Figure 4.3**). Moreover, we propose that the slope steepness is related to the extent of the chemical modification caused by bacterial enzymatic activities on the DOC pool that influences its recalcitrance (or lability). Higher enzymatic activities were measured in Exp2-3-4 than in family Exp1, suggesting that during Exp2-3-4, the DOC pools were processed more intensively thus depleting the labile compounds faster and creating more recalcitrant molecules that had a stronger HULIS signal intensity (**Figure 4.10**).

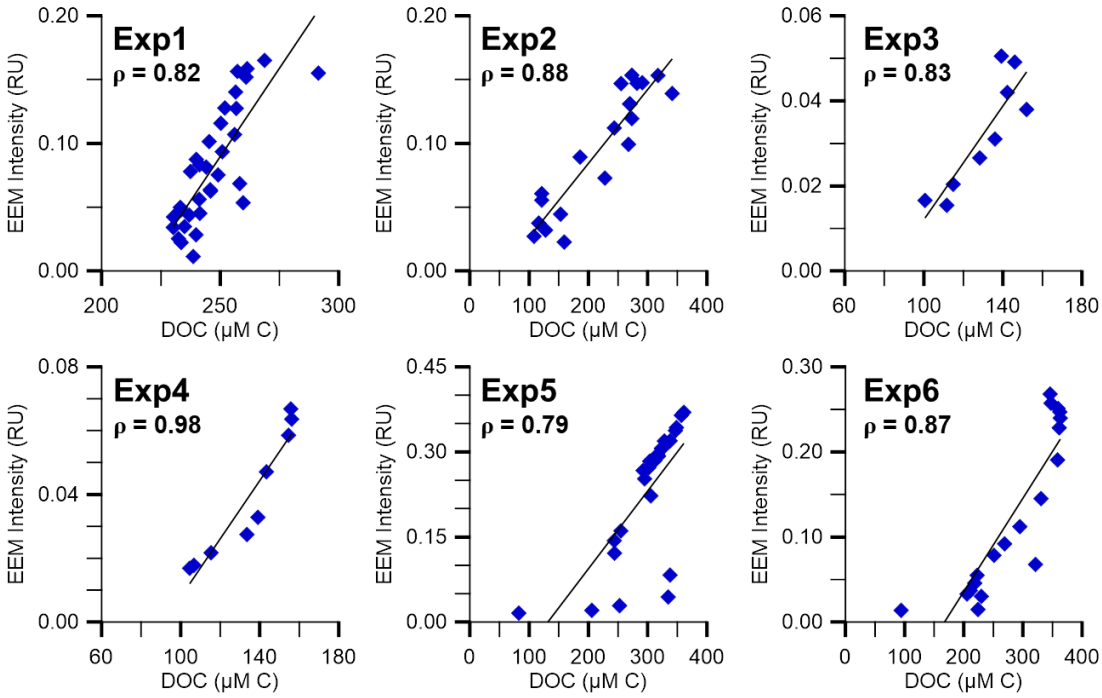

Figure 4.2. Correlations between HULIS EEM intensity (360 nm excitation, 450 nm emission) and DOC concentrations in bulk seawater for multiple phytoplankton bloom experiments (except for Exp7 where DOC was not sampled). Spearman's correlation coefficient, ρ, listed for each experiment.

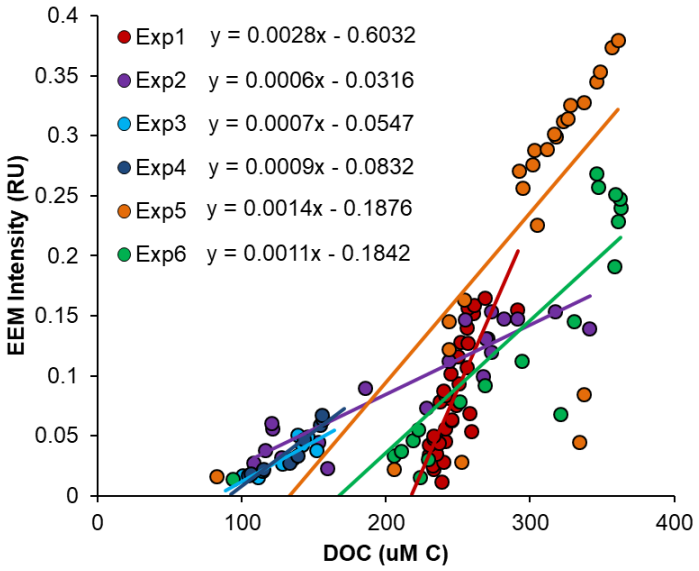

Figure 4.3. EEM vs DOC for all experiments (with points and slopes color coded for each experiment), except for Exp7 where DOC was not sampled.

To identify size-dependent changes in HULIS concentrations, seawater samples were sequentially filtered (**Figure 4.4**). The majority of the HULIS EEM signal (> 80%) was in the smallest size fraction (<50 kDa or <0.2 µm), even in experiments with large bloom intensities and high DOC concentrations. While previous studies have also shown the majority of HULIS to be in the smallest size fractions [*Grzybowski, 1995*], this study shows that this size-dependence holds throughout a phytoplankton bloom cycle. This result confirms that the HULIS fluorescent signal does not originate from the bacteria or viruses themselves. The retention of HULIS fluorescence after filtration supports the hypothesis that HULIS in SSA is largely derived from the dissolved fraction of organic matter in the DOC pool.

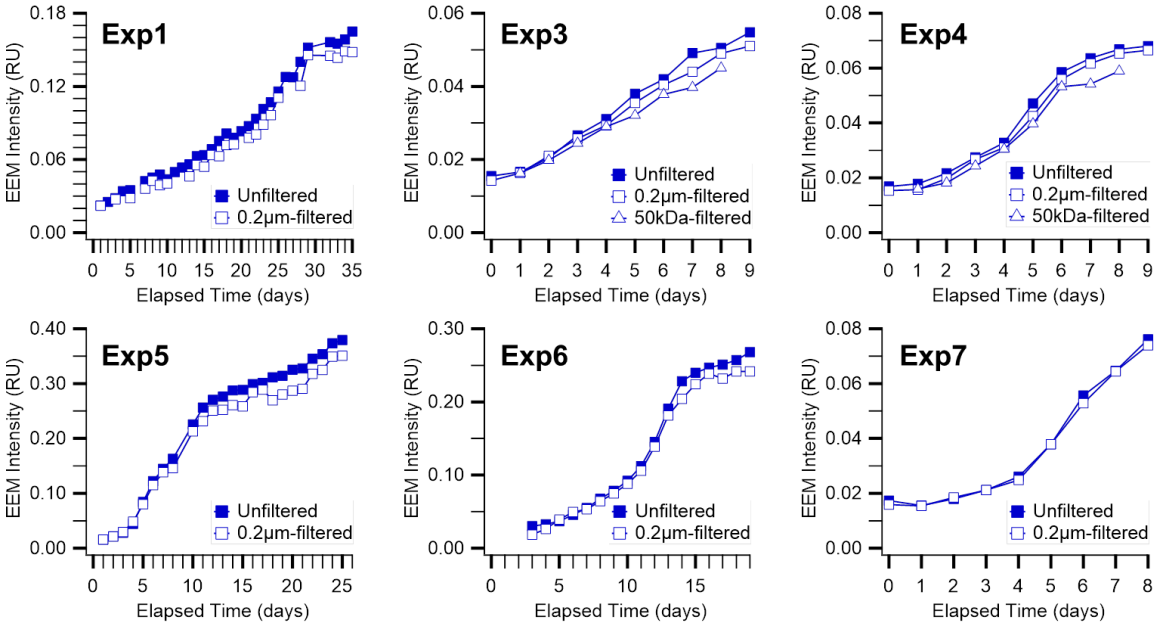

Figure 4.4. Size fractionation of HULIS in seawater: HULIS EEM intensity (360 nm excitation, 450 nm emission) before and after initial and subsequent filtrations

4.4.2 Microbial Activities Affect HULIS Production and Chemistry

In order to further probe the roles of bacteria and their enzymes on HULIS production and chemical composition, EEMs were collected from phytoplankton bloom experiments with and without the addition of specific marine bacteria isolates to enhance enzyme activity (Exp3 and Exp4, respectively). The enzyme activities for proteases, lipases, and alkaline phosphatases, important for sea-air transfer, were also monitored over time. While Exp3 and Exp4 began with the same seawater, Exp4 showed enhanced HULIS production after the addition of bacteria isolates compared to Exp3, which did not have bacteria isolates added (**Figure 4.5, Day 4-9**). Enzyme activity data showed that the added bacterial strains resulted in high alkaline phosphatase activity (**Figure 4.5**), thus leading to a significant change in phosphorous-rich compounds in seawater. These findings support the hypothesis that bacterial enzyme activity enhances the production of HULIS in the seawater by acting on phytoplankton exudates and detritus.

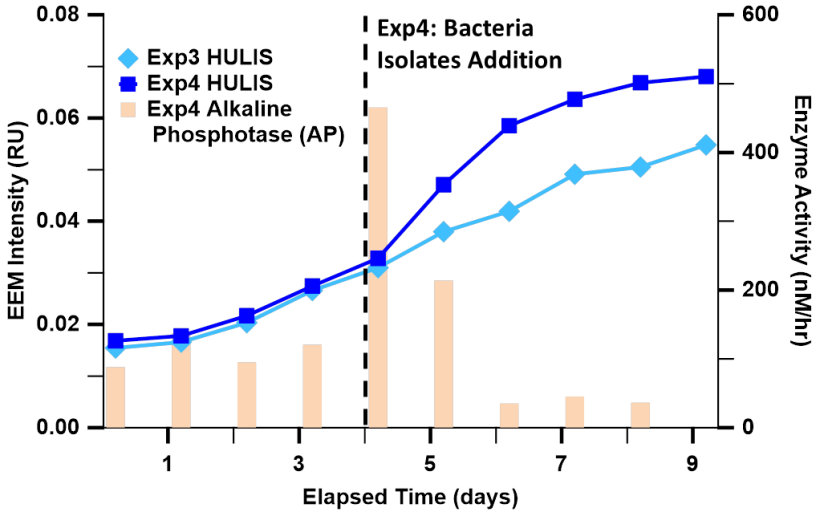

Figure 4.5. HULIS fluorescence (360 nm excitation, 450 nm emission) over time during Exp3 and Exp4 with alkaline phosphatase activity over time during Exp4. Marine bacteria isolates added to MART in Exp4 on day 4.

Following HULIS concentration findings in seawater, we investigated links between bacterial enzyme activity and HULIS chemical composition by comparing enzyme activities to shifts in the wavelength where the maximum of the HULIS emission occurred (**Figure 4.6**). Shifts in the wavelength at maximum HULIS emission are associated with changes in HULIS chemical composition [*Miano et al., 1990; Chen et al., 2003*]. In Exp1, we observed a small shift in the HULIS emission maximum for filtered bulk seawater from 426 nm near the beginning of the experiment to 450 nm leading into the first phytoplankton bloom peak. The HULIS emission maximum during the second bloom showed an even smaller shift compared to the first bloom, likely due to the formation of already-processed, recalcitrant material that is resistant to further enzymatic breakdown. A shift was also observed in Exp2 during the last 5 days of the experiment. In Exp3 and Exp4, the maximum of the HULIS EEM signal shifted from 445 nm at the beginning of the bloom to 455 nm near the peak of the bloom, followed by a shift back to 445 nm several days later (**Figure 4.5**). These shifts indicated that the HULIS chemical composition changed over the course of a phytoplankton bloom.

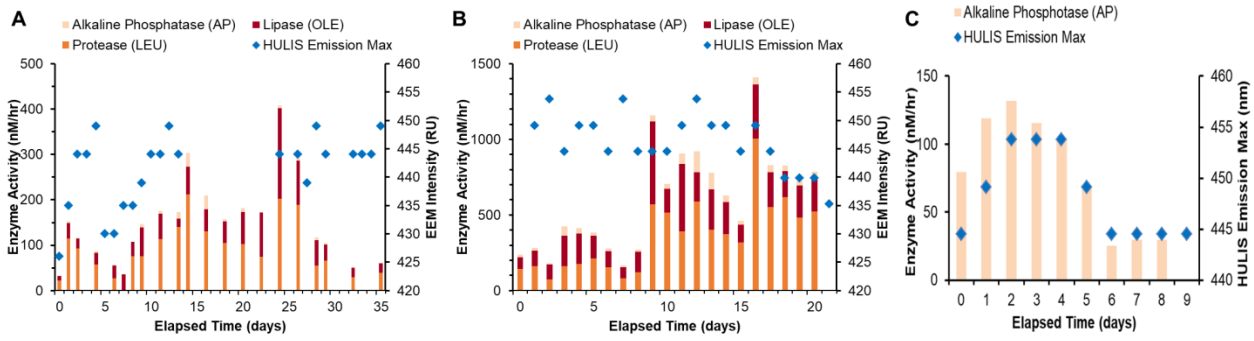

Figure 4.6. Enzyme activities along with the wavelength for HULIS emission maximum in the bulk seawater during Exp1 (A) and Exp2 (B) for protease and lipase activity and during Exp3 (C) for alkaline phosphatase.

Comparing the enzyme activities with the shifts in fluorescence emission suggests that bacteria drive the changes in HULIS chemical composition. These shifts in the wavelength at maximum HULIS emission were contemporaneous with the changes in enzymatic activities (**Figure 4.6**). In Exp1 and Exp2, changes in HULIS chemistry were driven by proteases and lipases, while in Exp3 and Exp4, HULIS chemistry were driven by bacterial alkaline phosphatases (**Figure 4.6b, Figure 4.11**). The correspondence between enzyme activity and HULIS chemistry supports the hypothesis that bacterial activity directly shapes HULIS composition in the seawater. These changes likely impact the efficiency of air-sea transfer.

4.4.3 HULIS Transfer from the Ocean to the Atmosphere

We show that the enzymatic activities of bacteria play a primary role in HULIS production and changes in HULIS chemical composition in seawater. To assess how these seawater changes impact the sea-air transfer of HULIS, SSA collected during Exp1-Exp7 was analyzed for changes in HULIS concentrations over the course of phytoplankton blooms. The "transmission factor" (defined here as the ratio of the maximum HULIS intensity in bulk seawater to the maximum HULIS intensity in SSA) is approximately 1000-fold (with a range of 0.055-0.37:1.1-6.8 $x10^{-5}$) and is comparable across experiments. As mentioned previously, bulk seawater EEMs consistently showed an increase in HULIS over the course of a phytoplankton bloom. For SSA, however, despite the steady accumulation of HULIS in bulk seawater, HULIS enrichment in SSA did not follow the same trend. In contrast, SSA HULIS concentrations rose and fell at certain times during a bloom, rather than increased steadily as observed in seawater (**Figure 4.7, Figure 4.11**).

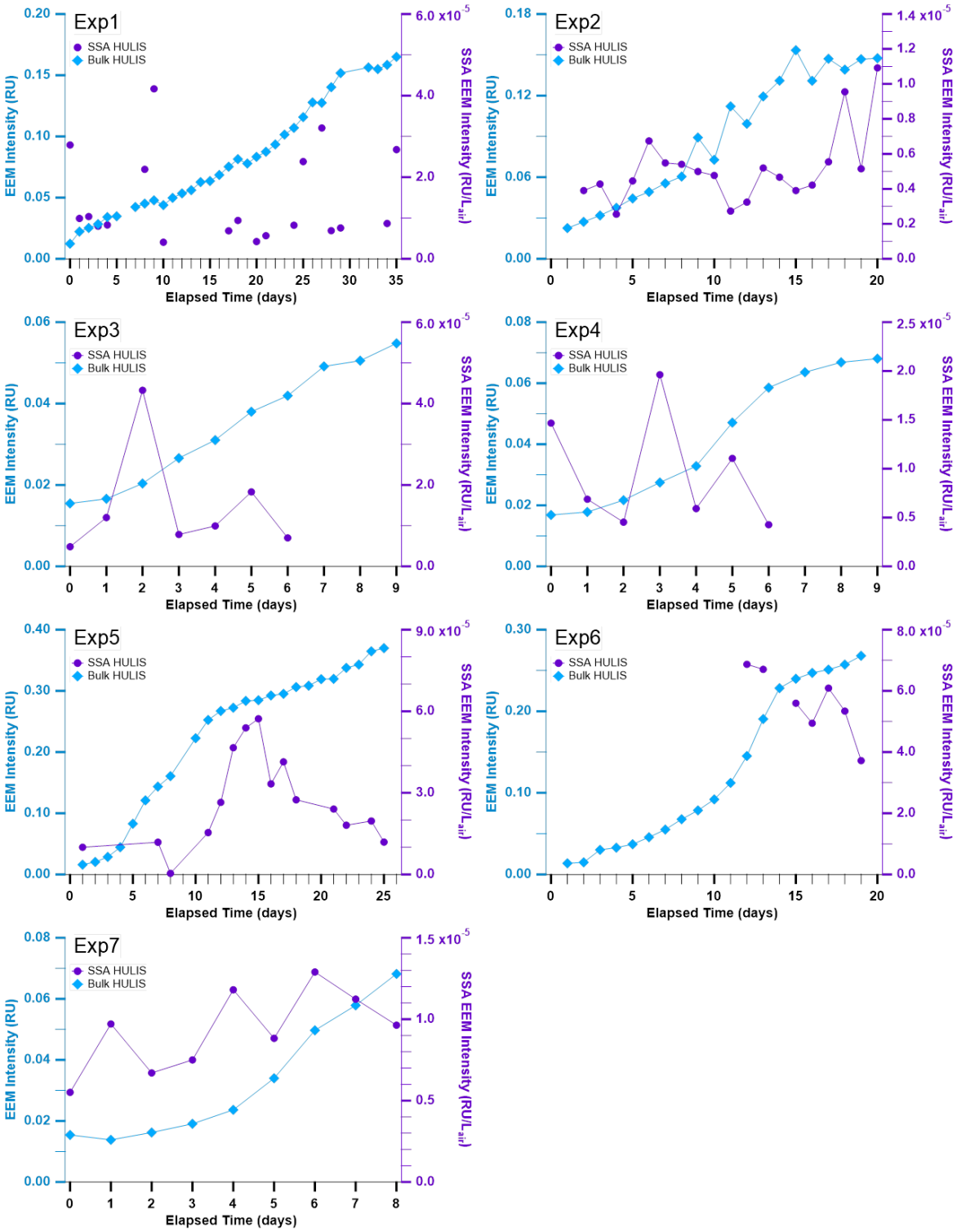

Figure 4.7. HULIS EEM intensity in seawater (blue) and SSA (purple) over the course of various induced phytoplankton bloom experiments.

Comparing HULIS in SSA with enzymatic activity data suggests that certain enzymes drive the transfer of HULIS from seawater to SSA (**Figure 4.8, Figure 4.12, Figure 4.13**). During Exp1 and Exp2, higher concentrations of HULIS were observed in SSA during periods of high protease and lipase activity (**Figure 4.8**). The co-occurrence between elevated HULIS concentrations and high enzyme activity is also consistent for Exp3 and Exp4, which showed more SSA HULIS during high alkaline phosphatase activity (**Figure 4.8**). Moreover, the increase in SSA HULIS and high enzyme activity coincide with changes in HULIS chemical composition, as indicated by the shifts in the emission spectra. Thus, the combination of high enzyme activities, the shifts in HULIS chemical composition, and HULIS in SSA supports the hypothesis that enzyme activity regulates HULIS sea-air transfer by transforming HULIS chemical composition to diverse structures that allows for more efficient transfer. Alternatively high enzyme activities at the sea surface could influence the interface properties and thus the ability to release HULIS in SSA. Microbial activity plays a central role in transforming seawater composition [*Wang et al., 2015*], leading to the transfer of HULIS from bulk seawater to SSA.

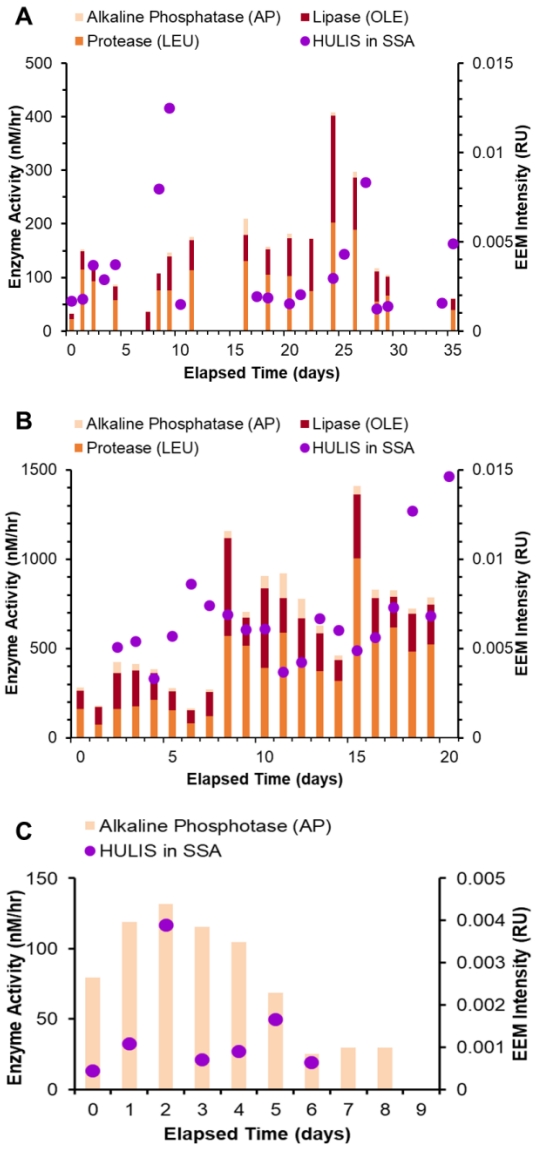

Figure 4.8. HULIS fluorescence intensity in SSA (circles) and enzyme activity (bars) in the bulk seawater during Exp1 (A), Exp2 (B) and Exp3 (C). For Exp1, only HULIS in SSA data within one day of enzyme measurements and vice versa are plotted.

4.5 Conclusion

Previous laboratory experiments have shown that HULIS concentrations in bulk seawater are different from concentrations in SSA, suggesting other factors besides seawater abundance control atmospheric HULIS concentrations [*Santander et al., 2022*]. Thus a better understanding of how different marine microbes control the transfer process is needed. Microbial enzymatic

activity has been found to play a major role in affecting the sea-air transfer of organic matter in SSA as well as their climate properties [*Wang et al., 2015; Jayarathne et al., 2016; McCluskey et al., 2017*]. This study aims to elucidate the biological factors controlling the dynamics of HULIS and transfer from the ocean to the atmosphere under a range of ocean microbiological conditions.

Here, the influence of marine bacteria on HULIS size, production, and chemical composition were investigated to elucidate the effects that influence sea-air transfer. Regarding HULIS size over the course of each phytoplankton bloom, seawater HULIS concentration consistently increased over the course of the bloom and correlated with DOC; however, throughout the entire bloom progression, the vast majority of HULIS existed in the smallest seawater size fraction (<50 kDa). For HULIS production, perturbation experiments with marine bacteria isolates additions revealed that bacteria and their enzymes enhanced the production and increased concentrations of HULIS. Finally, shifts in the HULIS emission spectra coincided with high enzyme activities, suggesting that marine bacteria induce changes in HULIS chemical composition through enzymatic activity.

In this study, we hypothesized that bacteria drive changes in HULIS size, production, and chemical composition, and that these changes induced by bacteria enhance the transfer of HULIS to SSA. In the quest to elucidate the impact of enzymes on HULIS sea-air transfer, we note that changes in SSA HULIS did not correlate with chlorophyll-a, DOC, heterotrophic bacteria, or virus concentrations. Our findings reveal that the changes in HULIS chemical composition, induced by bacterial enzymes, are the major drivers for the sea-air transfer of HULIS. While bacteria do play a role in affecting HULIS size and production, these factors appear to be less vital for sea-air transfer than the induced changes in chemical composition. Thus, we provide evidence that bacterial enzymatic activities drive changes in seawater chemistry, which then

directly impact SSA chemical composition. This study emphasizes the complex role that marine microbiology, specifically bacterial enzymatic activity, plays in SSA formation and composition.

4.6 Acknowledgments

The authors would like to thank Julie Dinasquet and Rebecca Simpson for valuable discussion and feedback. This work was funded by the National Science Foundation Center for Aerosol Impacts on the Chemistry of the Environment (NSF-CAICE), a Center for Chemical Innovation (CHE-1801971). All data supporting the conclusions in this study are publicly available at: https://doi.org/10.6075/J0S46S4J.

Chapter 4 has been submitted to Journal of Geophysical Research: Atmospheres: Santander, M.V.,* Malfatti, F.,* Pendergraft, M.A., Morris, C., Kimble, K.A., Mitts, B.A., Wang, X., Mayer, K.J., Sauer, J.S., Lee, C.L., Prather, K.A., "Bacterial control of marine humic-like substance production, composition, size, and transfer to sea spray aerosols during phytoplankton blooms." The dissertation author was the co-primary investigator and co-author of this paper. Authors with * contributed equally. M.V.S., F.M., and K.A.P. designed the experiments. F.M., M.P., C.M., K.A.K. performed enzyme activity measurements, all coauthor participated in the experiments, M.V.S. and F.M. analyzed the data and wrote the paper.

4.7 Supporting Information

4.7.1 Supporting Information Figures

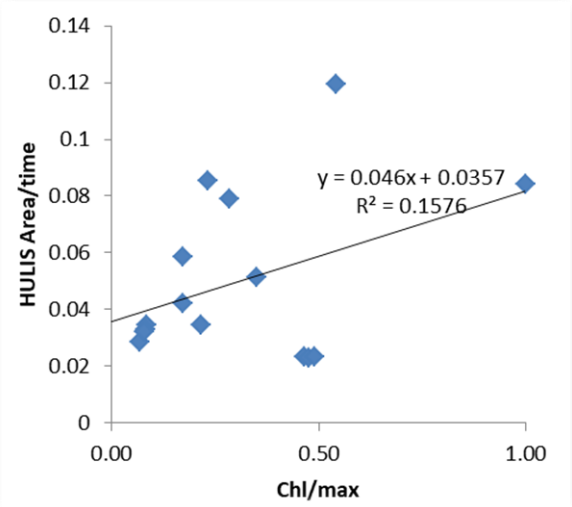

Figure 4.9. Correlation plot of HULIS EEM intensity (normalized by duration of the phytoplankton bloom experiment) vs *in vivo* chlorophyll a (normalized to maximum value of all experiments)

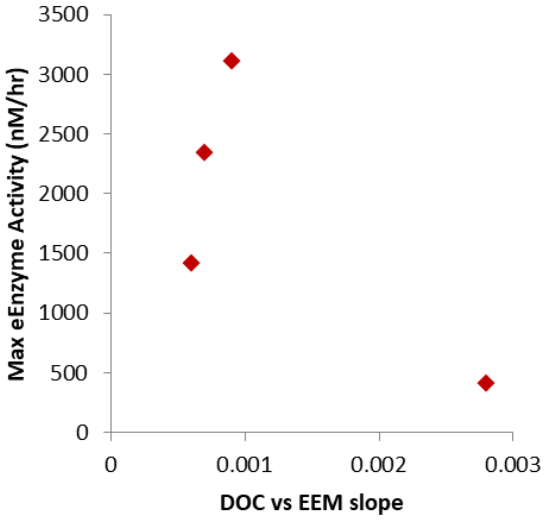

Figure 4.10. Maximum enzyme activity vs the slope of the line generated from the DOC vs HULIS EEM intensity correlation plots.

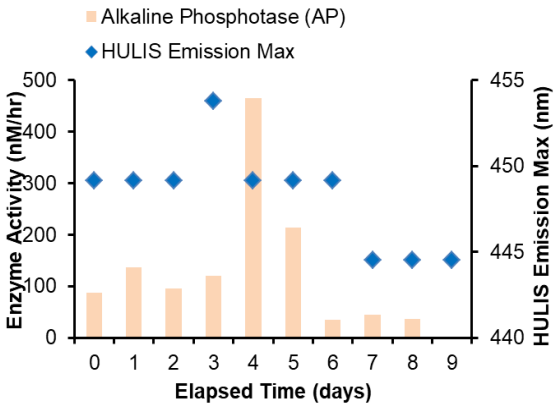

Figure 4.11. Enzyme activities along with the wavelength for HULIS emission maximum during Exp4 for alkaline phosphatase

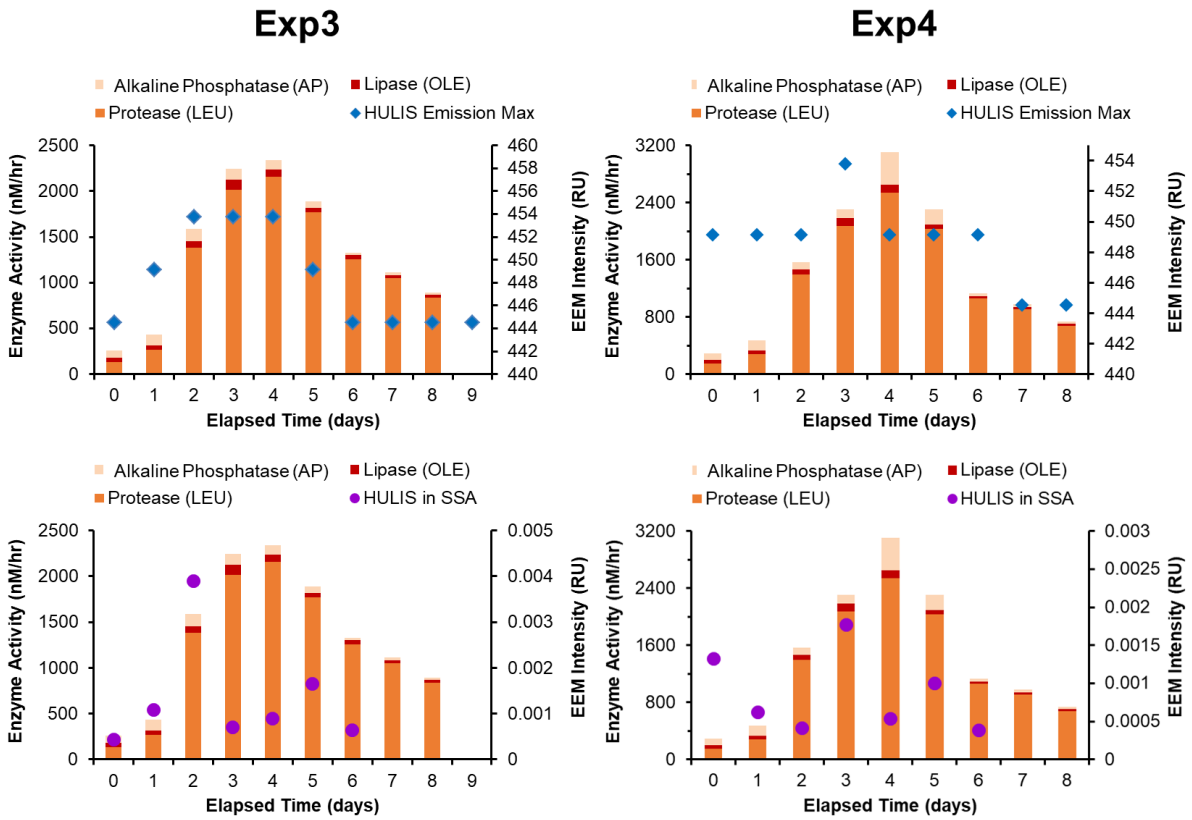

Figure 4.12. HULIS emission maximum wavelengths (top) and HULIS intensity in SSA (bottom) for Exp3 and Ep4 alongside combined protease, lipase, and alkaline phosphatase activities.

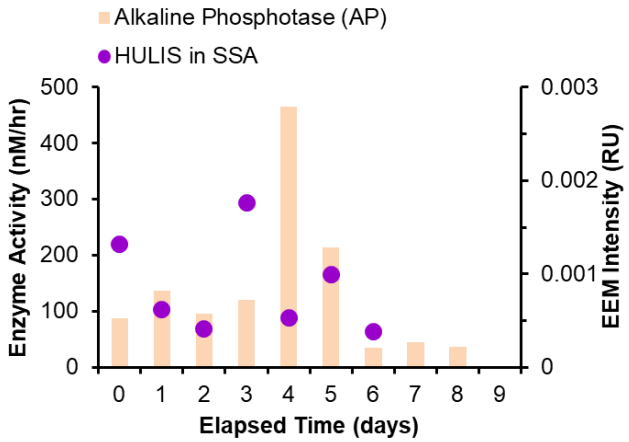

Figure 4.13 HULIS fluorescence intensity in SSA (circles) and enzyme activity (bars) in the bulk seawater during 4.

4.7.2 Supporting Information Tables

Table 4.2. List of additional experiments probing the dynamics of HULIS in seawater. HB = heterotrophic bacterial abundances, V = viral abundances, DOC = dissolved organic carbon, and CHL = *in vivo* or extracted chlorophyll

NAME	YEAR	SEASON	Tank System	System Volume (L)	Experiment Duration (days)	CHL MAX (µg/L)	Bulk Seawater Measurements			
							in vivo chl	HB	V	DOC
S01	2016	Summer	Outdoor Tank	2400	9	23.93	X	X	X	X
S02	2016	Summer	Outdoor Tank	2400	9	7.00	X	X	X	X
S03	2016	Summer	Outdoor Tank	2400	8	4.37	X	X	X	--
S04	2016	Summer	Outdoor Tank	2400	8	8.57	X	X	X	--
S05	2018	Summer	Outdoor Tank/MART	2400	7	11.28	X	X	X	X
S06	2018	Summer	Outdoor Tank/MART	2400	7	11.53	X	X	X	X
S07	2018	Summer	Outdoor Tank/MART	2400	7	11.89	X	X	X	X
S08	2018	Summer	Outdoor Tank/MART	2400	12	2.26	X	X	X	X
S09	2018	Summer	Outdoor Tank/MART	2400	12	2.20	X	X	X	X
S10	2018	Summer	Outdoor Tank/MART	2400	12	2.18	X	X	X	X

4.8 References

Alvarez-Salgado, X. A. and A. E. J. Miller. Simultaneous determination of dissolved organic carbon and total dissolved nitrogen in seawater by high temperature catalytic oxidation: conditions for precise shipboard measurements. *Marine Chemistry*. **1998**, *62*(3-4): 325-333.

Bidle, K. D. and F. Azam. Bacterial control of silicon regeneration from diatom detritus: Significance of bacterial ectohydrolases and species identity. *Limnology and Oceanography*. **2001**, *46*(7): 1606-1623.

Borgatta, J. and J. G. Navea. Fate of aqueous iron leached from tropospheric aerosols during atmospheric acidic processing: a study of the effect of humic-like substances. *Air Pollution Xxiii*. **2015**, *198*: 155-166.

Brown, T. E. and F. L. Richards. Effect of growth environment on physiology of algae - light intensity. *Journal of Phycology*. **1968**, *4*(1): 38.

Brussaard, C. P. D. Optimization of procedures for counting viruses by flow cytometry. *Applied and Environmental Microbiology*. **2004**, *70*(3): 1506-1513.

Cavalli, F., M. C. Facchini, S. Decesari, M. Mircea, L. Emblico, S. Fuzzi, D. Ceburnis, Y. J. Yoon, C. D. O'Dowd, J. P. Putaud and A. Dell'Acqua. Advances in characterization of size-resolved organic matter in marine aerosol over the North Atlantic. *Journal of Geophysical Research-Atmospheres*. **2004**, *109*(D24).

Chen, J., E. J. LeBoef, S. Dai and B. H. Gu. Fluorescence spectroscopic studies of natural organic matter fractions. *Chemosphere*. **2003**, *50*(5): 639-647.

Chen, J., Z. J. Wu, X. Zhao, Y. J. Wang, J. C. Chen, Y. T. Qiu, T. M. Zong, H. X. Chen, B. B. Wang, P. Lin, W. Liu, S. Guo, M. S. Yao, L. M. Zeng, H. Wex, X. Liu, M. Hu and S. M. Li. Atmospheric humic-like substances (HULIS) act as ice active entities. *Geophysical Research Letters*. **2021**, *48*(14).

Coble, P. G. Marine optical biogeochemistry: the chemistry of ocean color. *Chemical Reviews*. **2007**, *107*(2): 402-418.

Fernandez, A. E., G. S. Lewis and S. V. Hering. Design and laboratory evaluation of a sequential spot sampler for time-resolved measurement of airborne particle composition. *Aerosol Science and Technology*. **2014**, *48*(6): 655-663.

Freney, E., K. Sellegri, A. Nicosia, L. R. Williams, M. Rinaldi, J. T. Trueblood, A. S. H. Prévôt, M. Thyssen, G. Grégori, N. Haëntjens, J. Dinasquet, I. Obernosterer, F. Van Wambeke, A. Engel, B. Zäncker, K. Desboeufs, E. Asmi, H. Timonen and C. Guieu. Mediterranean nascent sea spray organic aerosol and relationships with seawater biogeochemistry. *Atmos. Chem. Phys.* **2021**, *21*(13): 10625-10641.

Gasol, J. M. and P. A. Del Giorgio. Using flow cytometry for counting natural planktonic bacteria and understanding the structure of planktonic bacterial communities. *Scientia Marina*. **2000**, *64*(2): 197-224.

Graber, E. R. and Y. Rudich. Atmospheric HULIS: how humic-like are they? A comprehensive and critical review. *Atmospheric Chemistry and Physics*. **2006**, *6*: 729-753.

Grzybowski, W. Selected properties of different molecular size fractions of humic substances isolated from surface Baltic water in the Gdańsk Deep area. *Oceanologia*. **1995**, *38*(1): 33-47.

Guillard, R. R. and J. H. Ryther. Studies of marine planktonic diatoms .1. Cyclotella nana Hustedt, and Detonula confervacea (Cleve) Gran. *Canadian Journal of Microbiology*. **1962**, *8*(2): 229.

Hessen, D. O. and L. J. Tranvik (1998). Aquatic humic substances: ecology and biogeochemistry. Berlin; New York, Springer.

Hoppe, H. G. Significance of exoenzymatic activities in the ecology of brackish water - measurements by means of methylumbelliferyl-substrates. *Marine Ecology Progress Series*. **1983**, *11*(3): 299-308.

Jayarathne, T., C. M. Sultana, C. Lee, F. Malfatti, J. L. Cox, M. A. Pendergraft, K. A. Moore, F. Azam, A. V. Tivanski, C. D. Cappa, T. H. Bertram, V. H. Grassian, K. A. Prather and E. A. Stone. Enrichment of saccharides and divalent cations in sea spray aerosol during two phytoplankton blooms. *Environmental Science & Technology*. **2016**, *50*(21): 11511-11520.

Lawaetz, A. J. and C. A. Stedmon. Fluorescence intensity calibration using the raman scatter peak of water. *Applied Spectroscopy*. **2009**, *63*(8): 936-940.

Lee, C., C. M. Sultana, D. B. Collins, M. V. Santander, J. L. Axson, F. Malfatti, G. C. Cornwell, J. R. Grandquist, G. B. Deane, M. D. Stokes, F. Azam, V. H. Grassian and K. A. Prather.

Advancing model systems for fundamental laboratory studies of sea spray aerosol using the microbial loop. *J Phys Chem A*. **2015**, *119*(33): 8860-8870.

Malfatti, F., C. Lee, T. Tinta, M. A. Pendergraft, M. Celussi, Y. Y. Zhou, C. M. Sultana, A. Rotter, J. L. Axson, D. B. Collins, M. V. Santander, A. L. A. Morales, L. I. Aluwihare, N. Riemer, V. H. Grassian, F. Azam and K. A. Prather. Detection of active microbial enzymes in nascent sea spray aerosol: implications for atmospheric chemistry and climate. *Environmental Science & Technology Letters*. **2019**, *6*(3): 171-177.

Marie, D., F. Partensky, S. Jacquet and D. Vaulot. Enumeration and cell cycle analysis of natural populations of marine picoplankton by flow cytometry using the nucleic acid stain SYBR Green I. *Applied and Environmental Microbiology*. **1997**, *63*(1): 186-193.

McCluskey, C. S., T. C. J. Hill, F. Malfatti, C. M. Sultana, C. Lee, M. V. Santander, C. M. Beall, K. A. Moore, G. C. Cornwell, D. B. Collins, K. A. Prather, T. Jayarathne, E. A. Stone, F. Azam, S. M. Kreidenweis and P. J. DeMott. A dynamic link between ice nucleating particles released in nascent sea spray aerosol and oceanic biological activity during two mesocosm experiments. *Journal of the Atmospheric Sciences*. **2017**, *74*(1): 151-166.

Miano, T., G. Sposito and J. P. Martin. Fluorescence spectroscopy of model humic acid-type polymers. *Geoderma*. **1990**, *47*(3-4): 349-359.

Mostofa, K. M. G. (2013). Photobiogeochemistry of organic matter: principles and practices in water environments. Heidelberg ; New York, Springer.

Murphy, K. R. A note on determining the extent of the water raman peak in fluorescence spectroscopy. *Applied Spectroscopy*. **2011**, *65*(2): 233-236.

Murphy, K. R., C. A. Stedmon, D. Graeber and R. Bro. Fluorescence spectroscopy and multi-way techniques. PARAFAC. *Analytical Methods*. **2013**, *5*(23): 6557.

Nebbioso, A. and A. Piccolo. Molecular characterization of dissolved organic matter (DOM): a critical review. *Analytical and Bioanalytical Chemistry*. **2013**, *405*(1): 109-124.

Noble, R. T. and J. A. Fuhrman. Use of SYBR Green I for rapid epifluorescence counts of marine viruses and bacteria. *Aquatic Microbial Ecology*. **1998**, *14*(2): 113-118.

O'Dowd, C., D. Ceburnis, J. Ovadnevaite, J. Bialek, D. B. Stengel, M. Zacharias, U. Nitschke, S. Connan, M. Rinaldi, S. Fuzzi, S. Decesari, M. C. Facchini, S. Marullo, R. Santoleri, A.

Dell'Anno, C. Corinaldesi, M. Tangherlini and R. Danovaro. Connecting marine productivity to sea-spray via nanoscale biological processes: phytoplankton dance or death disco? *Sci Rep*. **2015**, *5*: 14883.

Parlanti, E., K. Worz, L. Geoffroy and M. Lamotte. Dissolved organic matter fluorescence spectroscopy as a tool to estimate biological activity in a coastal zone submitted to anthropogenic inputs. *Organic Geochemistry*. **2000**, *31*(12): 1765-1781.

Pedler, B. E., L. I. Aluwihare and F. Azam. Single bacterial strain capable of significant contribution to carbon cycling in the surface ocean. *Proceedings of the National Academy of Sciences of the United States of America*. **2014**, *111*(20): 7202-7207.

Pohlker, C., J. A. Huffman and U. Poschl. Autofluorescence of atmospheric bioaerosols – fluorescent biomolecules and potential interferences. *Atmospheric Measurement Techniques*. **2012**, *5*(1): 37-71.

Prather, K. A., T. H. Bertram, V. H. Grassian, G. B. Deane, M. D. Stokes, P. J. DeMott, L. I. Aluwihare, B. P. Palenik, F. Azam, J. H. Seinfeld, R. C. Moffet, M. J. Molina, C. D. Cappa, F. M. Geiger, G. C. Roberts, L. M. Russell, A. P. Ault, J. Baltrusaitis, D. B. Collins, C. E. Corrigan, L. A. Cuadra-Rodriguez, C. J. Ebben, S. D. Forestieri, T. L. Guasco, S. P. Hersey, M. J. Kim, W. F. Lambert, R. L. Modini, W. Mui, B. E. Pedler, M. J. Ruppel, O. S. Ryder, N. G. Schoepp, R. C. Sullivan and D. Zhao. Bringing the ocean into the laboratory to probe the chemical complexity of sea spray aerosol. *Proceedings of the National Academy of Sciences of the United States of America*. **2013**, *110*(19): 7550-7555.

Rashid, M. A. (1985). Geochemistry of marine humic compounds. New York, Springer-Verlag.

Santander, M. V., J. M. Schiffer, C. Lee, J. L. Axson, M. J. Tauber and K. A. Prather. Factors controlling the transfer of biogenic organic species from seawater to sea spray aerosol. *Scientific Reports*. **2022**, *12*(1): 3580.

Slade, J. H., M. Shiraiwa, A. Arangio, H. Su, U. Poschl, J. Wang and D. A. Knopf. Cloud droplet activation through oxidation of organic aerosol influenced by temperature and particle phase state. *Geophysical Research Letters*. **2017**, *44*(3): 1583-1591.

Stemmler, K., M. Ndour, Y. Elshorbany, J. Kleffmann, B. D'Anna, C. George, B. Bohn and M. Ammann. Light induced conversion of nitrogen dioxide into nitrous acid on submicron humic acid aerosol. *Atmospheric Chemistry and Physics*. **2007**, *7*(16): 4237-4248.

Stokes, M. D., G. B. Deane, K. Prather, T. H. Bertram, M. J. Ruppel, O. S. Ryder, J. M. Brady and D. Zhao. A marine aerosol reference tank system as a breaking wave analogue for the production of foam and sea-spray aerosols. *Atmospheric Measurement Techniques*. **2013**, *6*(4): 1085-1094.

Trueblood, J. V., X. Wang, V. W. Or, M. R. Alves, M. V. Santander, K. A. Prather and V. H. Grassian. The old and the new: aging of sea spray aerosol and formation of secondary marine aerosol through OH oxidation reactions. *ACS Earth and Space Chemistry*. **2019**, *3*(10): 2307-2314.

Wang, X. F., C. M. Sultana, J. Trueblood, T. C. J. Hill, F. Malfatti, C. Lee, O. Laskina, K. A. Moore, C. M. Beall, C. S. McCluskey, G. C. Cornwell, Y. Y. Zhou, J. L. Cox, M. A. Pendergraft, M. V. Santander, T. H. Bertram, C. D. Cappa, F. Azam, P. J. DeMott, V. H. Grassian and K. A. Prather. Microbial control of sea spray aerosol composition: a tale of two blooms. *ACS Central Science*. **2015**, *1*(3): 124-131.

Chapter 5. Assessing Aggregation as a Potential Artifact Impacting the Fluorescence Intensity of Humic Substances in Seawater

5.1 Synopsis

Humic substances are ubiquitous in the environment and play an important role in carbon cycling. They are frequently characterized by measured fluorescence using excitation-emission matrices (EEMs). Humic substances are also known to aggregate in the marine environment which can potentially quench and reduce the fluorescence signal, presenting a challenge to study changes in relative abundance. This potential artifact has not been fully explored for marine humic substances. Here, we investigate spontaneous and calcium-induced aggregation of a commercial humic acid as well as humic substances in seawater using nanoparticle tracking analysis (NTA) and EEM spectroscopy. We show that changes in seawater particle size distributions do not correspond to changes in fluorescence intensity for both spontaneous and calcium-induced aggregation, which indicates that changes in fluorescence signals of humic substances can serve as a robust measurement of relative concentrations that are unaffected by aggregation. These findings are also supported by monitoring fluorescence and particle size distributions over the course of a larger-scaled phytoplankton bloom experiment. Further structural studies using EDTA suggests that the shielding of fluorescent moieties due to ion-mediated aggregation plays a critical role in preventing aggregation-caused quenching for marine humic substances. This study allows for an improved understanding of ocean humic substances,

providing evidence that fluorescence serves as a reliable indicator for humic substance relative abundance in seawater even under differing levels of aggregation.

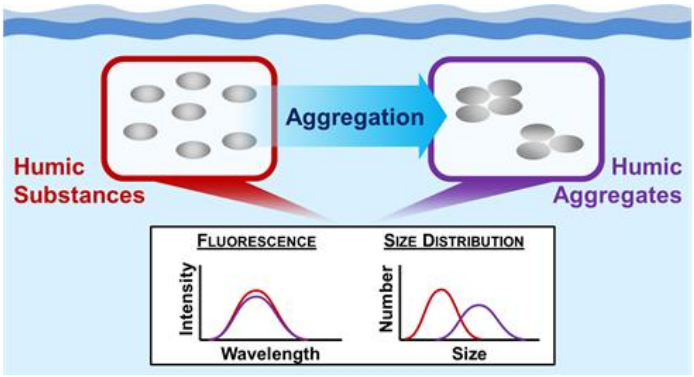

Illustration 5.1. Illustration broadly summarizing the purpose and experimental design investigating aggregation as a potential artifact impacting humic substance fluorescence intensity

5.2 Introduction

Humic substances encompass operationally-defined humic and fulvic acids. They were originally defined as sub-fractions of organic matter in soils, or derived from aquatic plants, with specific properties: colored and polar materials, which could be protonated at low pH (containing acidic functional groups) [*Thurman and Malcolm, 1981; Rashid, 1985; Hessen and Tranvik, 1998; Lehmann and Kleber, 2015*]. These fractions of organic matter are identified as humic substances based on the method used to isolate them from aquatic environments (e.g. Aiken, Thurman and Malcolm) or based on their optical properties. Although structurally complex, humic substances have been linked to degraded lignin components in terrestrial environments, and condensed lipids and other biomolecules in marine environments [*Malcolm, 1990; Kieber et al., 1997*]. Chemical signatures for humic substances (often referred to as humic-like substances or HULIS) have also been identified in the atmosphere. Atmospheric HULIS has been suggested to play major roles as photosensitizers and cloud seeds [*Graber and Rudich, 2006; Shrestha et al., 2018; Tsui and McNeill, 2018; Wang et al., 2020*]. The prevalence of humic substances in

soil, aquatic systems, and the atmosphere shows that they play an important role in the cycling of carbon throughout the environment [*Rashid, 1985; Hessen et al., 1998; Gerke, 2018; Win et al., 2018*].

The dynamics of humic substances are often investigated using fluorescence spectroscopy, specifically excitation-emission matrix (EEM) spectroscopy [*Mostofa, 2013; Murphy et al., 2013; Nebbioso and Piccolo, 2013*]. In EEM spectroscopy, fluorescence emission spectra at multiple excitation wavelengths are concatenated into a single excitation vs. emission map, providing a wider scope of the fluorophores within a sample. EEM spectroscopy is a widely used technique to characterize dissolved organic matter (DOM) in a variety of aquatic systems [*Zhang et al., 2011; Mostofa, 2013; Murphy et al., 2013; Nebbioso et al., 2013; Cao et al., 2016*] and allows for direct, rapid measurements, which minimizes potential artifacts from sample storage or preprocessing. Thus, EEM spectroscopy is ideal for natural aqueous samples such as seawater, which can contain multiple fluorophores.

One potential issue that arises when using EEMs to assess changes in humic substance abundance is aggregation. Organic matter in the ocean is known to form aggregates and large marine polymer gels [*Chin et al., 1998; Verdugo et al., 2004*]. Humic substances have been shown to spontaneously aggregate over the course of hours in artificial solutions at pH 7.5 and at low ionic strength [*Baalousha et al., 2006*]. In the presence of divalent cations such as calcium ions, humic substances can aggregate on timescales as short as minutes [*Palmer and von Wandruszka, 2001; Baalousha et al., 2006; Kloster et al., 2013*]. Moreover, during periods of high biological activity (e.g., during a phytoplankton bloom), humic substance concentrations can be elevated, promoting aggregation [*Lee et al., 2015*]. While the fluorescence of some chromophores is unaffected, or even enhanced, by aggregation, other chromophores will undergo

aggregation-caused quenching, in which aggregates exhibit enhanced pi-pi stacking interactions, decreasing their fluorescence intensity [*Lakowicz, 2006; Chen et al., 2019*]. This phenomenon is especially notable under high concentrations [*Lakowicz, 2006*]. Thus, while humic substances are known to aggregate, many studies, even across different fields, relate changes in humic substance fluorescence intensity to changes in abundance based on the assumption that processes such as aggregation do not alter fluorescence intensity [*Bieroza et al., 2010; Wei et al., 2016; Wang et al., 2017; Yamin et al., 2017; Arai et al., 2018; Kwon et al., 2018*]. Because this assumption has not been fully explored for marine systems, the production or breakdown of humic substances has remained a challenge to study.

Here, we investigate the reliability of fluorescence spectroscopy for direct measurements of the relative concentrations of humic substance in the presence of aggregation processes. Specifically, we track the changes in particle size distributions and corresponding fluorescence in several different solutions: commercial humic acid solutions, seawater, and seawater with high biological activity (several days after the peak of a phytoplankton bloom), before and after spontaneous and calcium-induced aggregation. Furthermore, we examine how fluorescence intensity changes after the addition of ethylenediamine-tetra-acetic acid (EDTA), which is commonly used to separate cations from complexing material [*Chin et al., 1998*]. In each of these scenarios, we probe the hypothesis that fluorescence of humic substances is not quenched after undergoing aggregation with calcium ions or after using EDTA to remove calcium-induced aggregation. Additionally, by monitoring the changes in fluorescence and particle size distributions over the course of a phytoplankton bloom, we explore the hypothesis that changes in the particle size distribution are unrelated to changes in the humic substance fluorescence intensity in seawater.

Numerous studies have linked humic substances in marine systems to several broad fluorescence regions in EEMs [*Coble, 1996; Parlanti et al., 2000; Coble, 2007; Mostofa, 2013*]. More specifically, previous studies have designated three fluorescence regions for humic substances: a peak with excitation/emission wavelengths at (360 nm) / (450 nm), at (260 nm) / (450 nm), and at (325 nm) / (410 nm) [*Coble, 1996; Hessen et al., 1998; Mostofa, 2013*]. Seawater EEMs also commonly show fluorescence at two additional regions corresponding to protein-like substances and chlorophyll-a with excitation/emission wavelengths at (275-280 and <235 nm) / (330-350 nm) and (400-440 nm) / (680-690 nm), respectively [*Coble, 1996; Parlanti et al., 2000*]. These two peaks lie outside the humic-like regions and are excluded in this study. Commercial humic acid, in contrast to seawater humic substances, shows a different fluorescence signature with a broad excitation spectrum that peaks at 250 nm and extends to >400 nm, and an emission peak at approximately 435 nm. Here, we primarily focus on the peak in seawater at 360 nm excitation to probe changes in fluorescence intensity.

By investigating the changes in humic substance fluorescence under various aggregation states, we assess if aggregation impacts the ability to quantify the amount of humic substances in the marine environment.

5.3 Materials and Methods

Multiple phytoplankton bloom mesocosm experiments were conducted to investigate the temporal changes in seawater particle size distributions and fluorescence. Details of the phytoplankton blooms have been described previously [*Lee et al., 2015; Trueblood et al., 2019*]. Briefly, blooms were carried out in a 2400 L outdoor tank. Seawater was obtained from the Ellen Browning Scripps Memorial Pier (Scripps Pier, 32-52'00" N, 117-15’21" W) and filtered using a

50 μm mesh screen (Sefar Nitex 03−100/32) to reduce zooplankton that graze on phytoplankton. A phytoplankton bloom was induced by spiking the seawater with Guillard's F algae nutrient medium [*Guillard and Ryther, 1962*] diluted by a factor of 100. Progression of the phytoplankton bloom was monitored using a handheld fluorometer (Turner Designs, Aquafluor) to measure *in vivo* chlorophyll fluorescence.

For aggregation studies, humic acid solutions were made with humic acid sodium salt (CAS 68131-04-4) purchased from Sigma Aldrich. Artificial seawater used as a solvent for humic acid solutions was made from reef salt (Brightwell Aquatics, NeoMarine Salt Mix). Real seawater was collected directly from the Scripps Pier. A phytoplankton bloom in a 4 L flask was induced by amending seawater with Guillard's F medium (diluted by a factor of 2) [*Guillard et al., 1962*] and incubating under fluorescent lights (Full Spectrum Solutions, model 205457; T8 format, color temperature 5700 K, 2950 lumens). Calcium chloride solutions were made from calcium chloride salts (CAS 10043-52-4) purchased from Sigma Aldrich. The calcium chloride solution was used to induce aggregation by adding a drop of solution (0.043M $CaCl_2$) directly to the sample in the cuvette. The addition of a drop of this $CaCl_2$ solution to the cuvette results in a 10% increase in Ca^{2+} concentration from the artificial seawater. EDTA experiments were performed by dissolving disodium EDTA (Macron Fine Chemicals, CAS 6381-92-6) in ultrapure water and adding a drop of solution (>0.05M EDTA) to the sample in the cuvette (similar to calcium chloride addition).

EEMs were measured using an Aqualog Fluorometer (Horiba Scientific, Aqualog with extended range). EEMs were scanned from 230-450 nm excitation and 240-820 nm emission. In the Aqualog software, EEMs were automatically blank-subtracted (using ultrapure water as a blank), corrected for inner filter effects, and Rayleigh masked (1^{st} and 2^{nd} order). EEM spectra

were converted to Raman Units (RU) by normalizing to the area under the Raman peak of ultrapure water with 1 nm increments at 350 nm excitation [*Lawaetz and Stedmon, 2009; Murphy, 2011*]. The area under the Raman peak was determined using the FDOMcorr toolbox in MATLAB [*Stedmon and Bro, 2008; Murphy et al., 2013*]. To quantify humic substance fluorescence, the maximum fluorescence at 360 nm excitation/450 nm emission was used (**Figure 5.3**).

Size distributions for particles in solution (both humic acid solutions and seawater) were obtained by using a Multi-sizing Advanced Nanoparticle Tracking Analysis instrument (MANTA Instruments Inc., ViewSizer 3000). The optimal size range for MANTA includes particles in the size range of about 10-1000 nm, which is ideal for investigating changes in the size of humic substances [*Palmer et al., 2001; Baalousha et al., 2006*]. Data were obtained by recording 50 or 100 movies for each sample. From each movie, the MANTA instrument software counted and calculated the size for each particle tracked. Particle size distributions and particle concentrations were initially obtained for particles in 1 nm bin sizes. Particle counts were then re-binned using larger bins, with increasing increment sizes, and are reported as PSD (particle size distribution) in units of counts/ml/nm, where the counts in each bin were normalized to the bin size.

5.4 Results and Discussion

5.4.1 Spontaneous Aggregation of a Commercial Humic Acid Solution

To identify how spontaneous aggregation of humic substances affects humic substance fluorescence intensity, EEMs for solutions of humic acid in artificial seawater at multiple concentrations ranging from 0.05 mg/L to 10.5 mg/L were measured before and after letting the

solutions sit in the dark for a day. The maximum fluorescence intensities (at 360 nm excitation) were measured for a range of concentrations of commercial humic acid (**Figure 5.1**). The fluorescence intensity of humic acid in solution increased linearly with concentration. More notably, the fluorescence intensities of all solutions, and therefore the linearity, were maintained after measuring the solutions again after 24 hours, which suggests that either spontaneous aggregation is not occurring or that the fluorescence intensities do not change as a result of spontaneous aggregation. The latter result would suggest that humic substance fluorescence is a robust measurement across a wide range of humic substance concentrations.

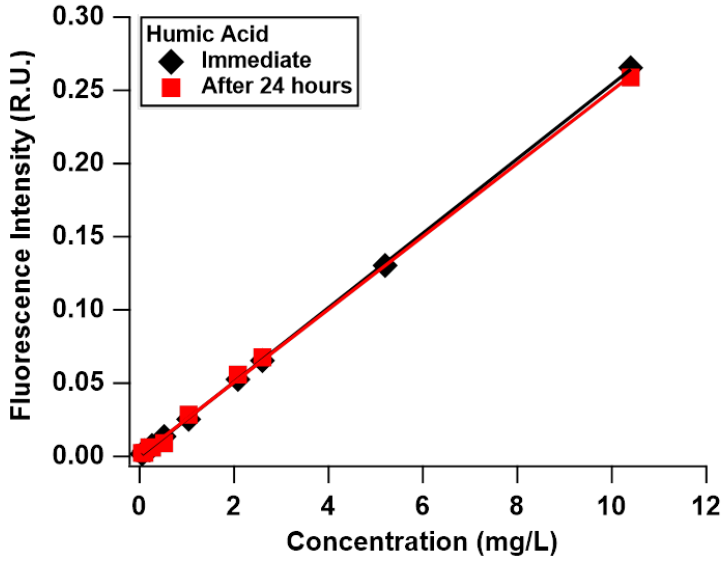

Figure 5.1. Fluorescence intensity (360 nm excitation) for different concentrations of a commercial humic acid taken immediately (black) and after letting the solution spontaneously aggregate for 1 day (red).

To determine whether spontaneous aggregation was occurring, the humic acid solution with the highest concentration was measured for particle size distribution changes. Size distributions (**Figure 5.6**) showed that after sitting for >24 hours, aggregation occurred as indicated by a shift to larger particle sizes (with the mode of the distribution increasing from approximately 530 nm to 650 nm). This is consistent with studies reporting that spontaneous

aggregation over hours occurs in humic acid solutions with varying salt concentrations [*Chin et al., 1998; Baalousha et al., 2006; Kloster et al., 2013*]. Although spontaneous aggregation occurred, it did not change fluorescence intensity. Thus, these results provide evidence supporting the hypothesis that aggregation does not affect fluorescence and that fluorescence is a robust measurement that can reliably detect relative changes in humic substance abundance.

5.4.2 Aggregation of Humic Acid Solutions and Seawater Induced with Calcium Ions

The effect of aggregation on humic acid fluorescence was further probed by spiking solutions with a drop of $CaCl_2$ solution to induce aggregation (**Figure 5.2**). Aggregation in solutions spiked with calcium ion (Ca^{2+}) has been previously shown to occur within a couple minutes [*Kloster et al., 2013*]. At the $CaCl_2$ concentration used, a single drop added directly to the sample in the cuvette resulted in a 10% increase in Ca^{2+} concentration from the artificial seawater. The process of adding a drop of a solution for a small change in ion concentration was ideal for minimizing the effects of sample dilution and changes in ionic strength, which would potentially affect fluorescence intensity [*Baalousha et al., 2006*]. To ensure that the Ca^{2+} solution was indeed inducing aggregation, size distributions for a humic acid solution were measured before and 2 minutes after Ca^{2+} addition (**Figure 5.2a**). After the addition of Ca^{2+}, there was a clear change in the size distribution with a decrease in particles less than 100nm and a peak appearing at larger sizes of ~200-400 nm in diameter.

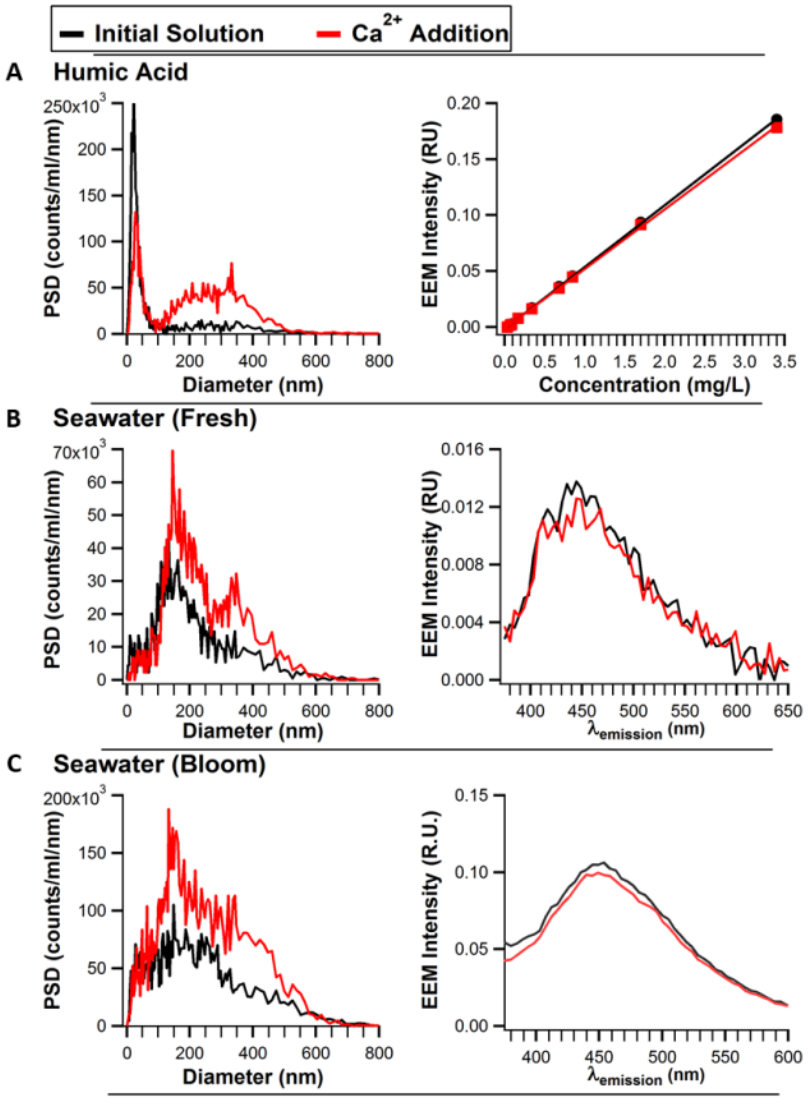

Figure 5.2. Dissolved particle size distributions (PSD, left) and fluorescence (right, 360 nm excitation) before (black) and after (red) induced aggregation with Ca^{2+} for solutions of (a) a commercial humic acid dissolved in artificial seawater, (b) seawater, and (c) seawater after the peak of a phytoplankton bloom.

EEMs of humic acid solutions at concentrations similar to those used for the 24-hour spontaneous aggregation experiments were measured before and immediately after the addition of calcium cations (**Figure 5.2, right**). Even though a clear change in the size distribution was observed after calcium addition, no corresponding changes occurred in the fluorescence spectra. As shown before, fluorescence intensities for humic acid increased linearly with concentration.

With the addition of calcium, the fluorescence intensities showed very little decrease as a result of aggregation, with a decrease of less than 4% of the initial fluorescence intensity at the highest concentration studied and smaller percent decreases at lower concentrations. The lack of decrease in fluorescence intensity agrees with the shielding of fluorescent moieties due to cation-binding (with Ca^{2+}), which has been suggested previously [*Engebretson and Vonwandruszka, 1994*]. Thus, binding to calcium ions likely orients the humic substance molecules such that pi-pi stacking is inefficient and fluorescence does not decrease.

The same trends are evident for induced aggregation of naturally-occurring humic substances in real seawater (**Figure 5.2b**) and seawater after an induced phytoplankton bloom (**Figure 5.2c**). Seawater after an induced phytoplankton bloom contained a much higher concentration of dissolved organic matter, including humic substances, which resulted in a 10x increase in the fluorescence intensity (**Figure 5.2b, 5.2c**). Despite differences in organic matter abundance, both fresh seawater and bloom-induced seawater showed similar behavior after inducing aggregation with Ca^{2+} ions. The particle size distributions before and 2 minutes after Ca^{2+} addition showed an increase in particles approximately 200 nm in diameter, as well as a growth in larger particles in the size range of 300-400 nm, suggesting that aggregation had been induced. Size distributions were also obtained for seawater without Ca^{2+} addition (**Figure 5.7**) and showed that aggregation was not occurring spontaneously during the time frame of the measurements (approximately 1 hour for two successive measurements). Even though both seawater and bloom-induced seawater showed changes in particle size distributions, very small changes in fluorescence intensity were apparent. The change in the fluorescence intensity after Ca^{2+} addition was not found to be statistically significant (seawater: $p=0.29$; seawater bloom: $p=0.11$). The lack of decrease in fluorescence intensity despite induced aggregation further

supports the hypothesis that fluorescence of humic substances in seawater is unaffected by their aggregation.

5.4.3 Seawater Particle Size Distribution and Humic Substance Fluorescence over the Course of an Induced Phytoplankton Bloom

To further explore aggregation under more realistic ocean conditions, two larger-scale phytoplankton bloom experiments were induced in the lab, with EEM and size distributions measured over time as the phytoplankton bloom progressed. Two additional blooms were conducted but with lower PSD time resolution and are thus included in the Supporting Information (**Figure 5.8**). Each bloom showed an increase in the chlorophyll-*a* signal, with a peak reached on the 3rd or 4th day, and a subsequent decrease, indicative of the initial growth and subsequent decline of phytoplankton (**Figure 5.3**). This chlorophyll progression is consistent with previous phytoplankton bloom experiments performed in a similar manner [*Lee et al., 2015; Wang et al., 2015*].

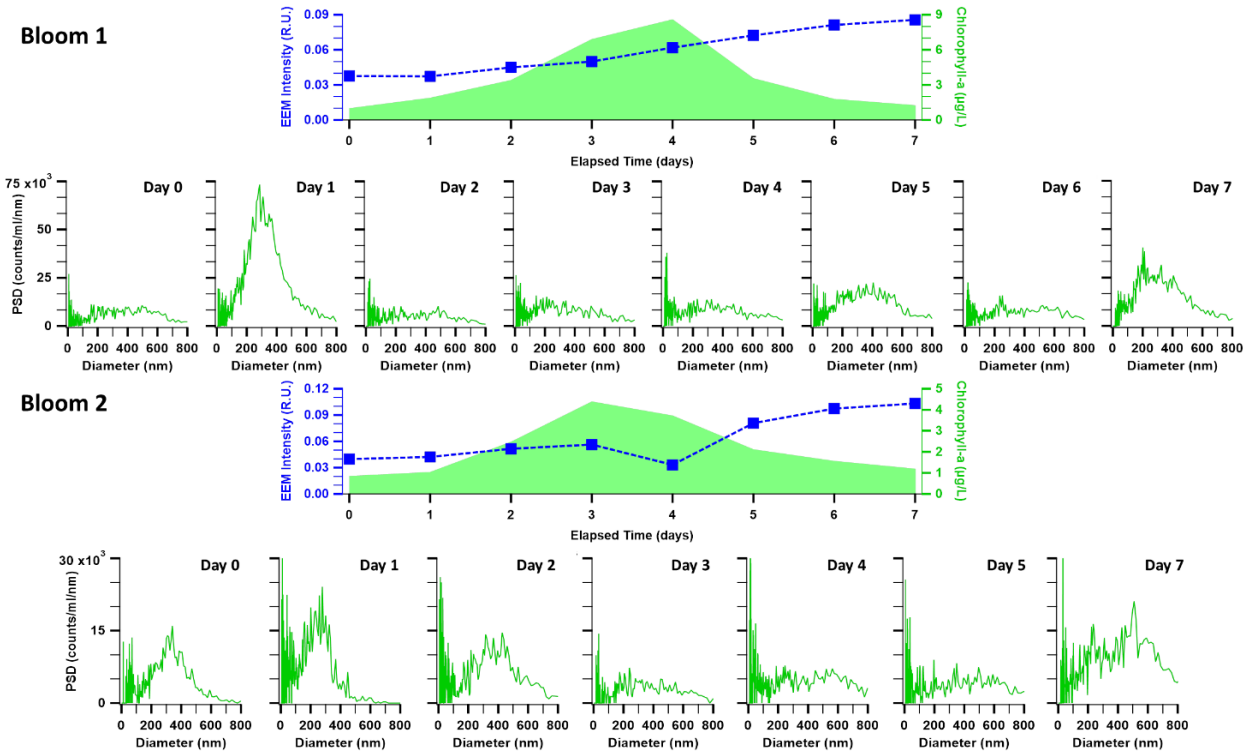

Figure 5.3. Changes in the seawater particle size distribution and humic substance fluorescence (360 nm excitation/450 nm emission) over the course of 2 phytoplankton blooms.

In bulk seawater, the humic substance fluorescence intensity (measured at 360 nm excitation/450 nm emission) continuously increased over time suggesting that fluorescent DOM accumulated over the experiment even as chlorophyll concentrations decreased. Daily changes in the seawater particle size distribution, however, were much more variable (**Figure 5.3**). Previous work looking at size distributions at sizes larger (2-300 µm) than the size range studied here have shown increases in concentration of larger particles over time [*Li and Logan, 1995*]. In contrast to previous work and the gradual increase in fluorescence observed in this study, size distributions showed no continuous shift, but rather dynamic fluctuations across the entire size range measured. These fluctuations were inconsistent across the four different phytoplankton blooms (**Figure 5.3, Figure 5.8**). Coagulation with particles outside the measured size range (>1-2 µm) [*Li et al., 1995*] or interactions with marine microbes [*Biddanda, 1988; Azam et al.,*

1994] could lead to the dynamic size changes observed during a phytoplankton bloom. Despite the large daily fluctuations in size and counts, increases in particle counts suggest based on previous work that the dissolved organic matter is undergoing aggregation [*Chin et al., 1998; Verdugo, 2012; Xu and Guo, 2018*]. However, the continuous increase in humic substance fluorescence over time suggests that their fluorescence is independent of dissolved particle counts or size distributions.

5.4.4 Decreased Fluorescence of Humic Substances with EDTA Addition

In order to further investigate the role of ion-induced aggregation on the fluorescence intensity of marine humic substances, EDTA was added to both commercial humic acid solutions and seawater after the previous Ca^{2+} addition experiments. While the addition of Ca^{2+} promotes aggregation by enhancing cross-linking between organic molecules [*Verdugo, 2012*], EDTA chelates the Ca2+ and so removes these cross-links. Size distributions of EDTA and $CaCl_2$ solutions alone showed that these additions themselves do not contribute to the size distributions (**Figure 5.9**). Particle size distribution measurements for humic acid solutions (~1.3 mg/L humic acid) and seawater after EDTA addition unexpectedly revealed an increase in larger sized particles compared to the original solution, indicative of further aggregation (**Figure 5.4**). In seawater, particle concentrations decreased from the Ca^{2+} addition, but the distribution is shifted to larger sizes (300-500 nm) compared to the original solution, indicating the retention of large aggregates (**Figure 5.4**). For both humic acid solutions and seawater, the humic substance fluorescence intensity substantially decreased after EDTA addition compared to the original solution (**Figure 5.4**).

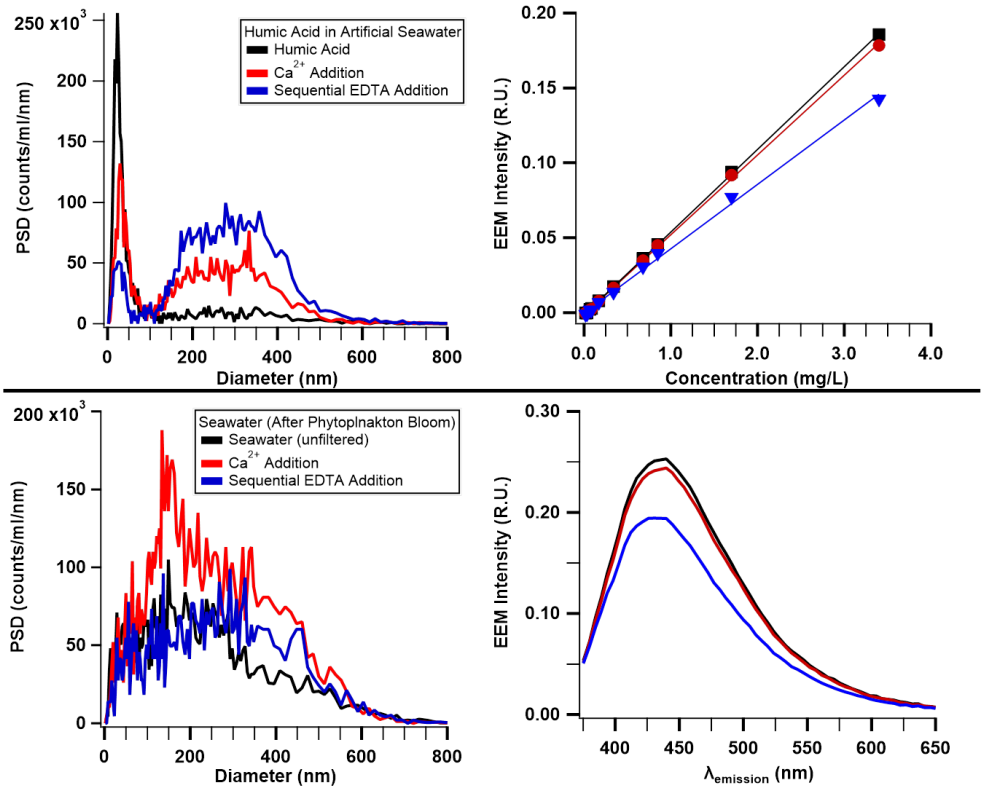

Figure 5.4. Dissolved particle size distributions (left) and fluorescence (right, 360 nm excitation) for a humic acid solution (top) and seawater after a phytoplankton bloom (bottom) with no treatment (black), addition of Ca^{2+} (red), and after EDTA addition (blue)

The particle size distribution changes and the corresponding decrease in fluorescence intensity contrasts with the expected behavior of EDTA [*Chin et al., 1998*] and requires further investigation. Examination of the UV-vis spectra before and after EDTA addition do not suggest the appearance of a metal-EDTA complex that could contribute to enhanced inner filter effects that would absorb fluorescence and decrease the observed intensities (**Figure 5.10**). It is possible that EDTA-induced aggregation is due to incomplete cation chelation by EDTA leading to large humic-EDTA complexes or large humic complexes held together via pi-pi stacking interactions [*Shetty et al., 1996; Amrutha and Jayakannan, 2008*]. In both of the above cases, EDTA would lead to more flexible humic structures, leading to more efficient pi-pi stacking, and thus

decreasing fluorescence. The effect of EDTA suggests that the nature of the aggregation (ion-mediated or not) likely determines the impact on fluorescence intensity.

5.5 Conclusions

In this study, we investigated whether aggregation of humic substances led to changes in the fluorescence intensity of humic substances. We show that in most cases for humic substances in seawater, fluorescence was not affected by aggregation and so was a reliable measure of humic acid concentration. Using both a commercial humic acid and humic substances naturally present in seawater, we show that neither spontaneous aggregation nor calcium-induced aggregation lead to changes in the fluorescence spectra of humic substances. Larger scale phytoplankton bloom experiments also supported the hypothesis that changes in fluorescence are independent of changes in particle counts or size distributions. The lack of decrease in fluorescence intensity after calcium-induced aggregation is likely a result of the shielding of fluorescent moieties due to cation-binding [*Engebretson et al., 1994*]. We also show an unexpected decrease in fluorescence with EDTA addition, which suggests that cation-binding plays a critical role in minimizing possible quenching (**Figure 5.5**).

In the marine environment, humic substances are mostly ion-bound due to high calcium and magnesium concentrations [*Mantoura et al., 1978*]. Thus, in the absence of EDTA, fluorescence remains unaffected by aggregation and is a reliable indicator for changes in humic substance relative abundance in seawater. Future investigations on the nature of organic matter aggregation will further improve the characterization of humic substances and their dynamics in natural environments.

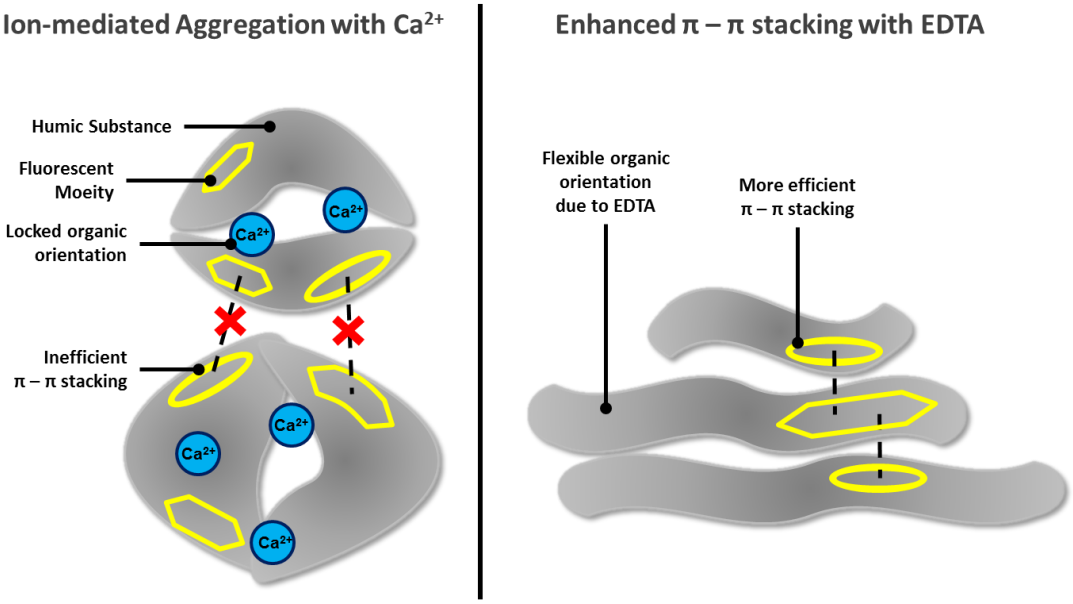

Figure 5.5. Pictorial representation depicting the ion-mediated aggregation that results in minimal changes to fluorescence intensity (left) and the enhanced π–π stacking interactions upon addition of EDTA leading to the quenching of fluorescence (right).

5.6 Acknowledgements

The authors would like to thank Christopher Lee, Linh Ahn Cat, Julie Dinasquet, Charlotte DeWald, Rebecca Simpson, Michael J. Tauber, and Thomas Hill for valuable discussion and feedback. The authors thank the National Science Foundation Center for Aerosol Impacts on the Chemistry of the Environment (NSF-CAICE), a Center for Chemical Innovation (CHE-1801971) for funding. All data supporting the conclusions are publicly available at: https://doi.org/10.6075/J02J6C1V.

Chapter 5 has been submitted to Environmental Science and Technology: Santander, M.V., Wang, X., Aluwihare, L.I., Prather, K.A., "Assessing Aggregation as a Potential Artifact Impacting the Fluorescence Intensity of Humic Substances in Seawater." The dissertation author was the primary investigator and author of this paper. M.V.S., X.W., L.I.A., and K.A.P designed the experiments. M.V.S performed the fluorescence and particle size distribution measurements and wrote the paper.

5.7 Supporting Information Figures

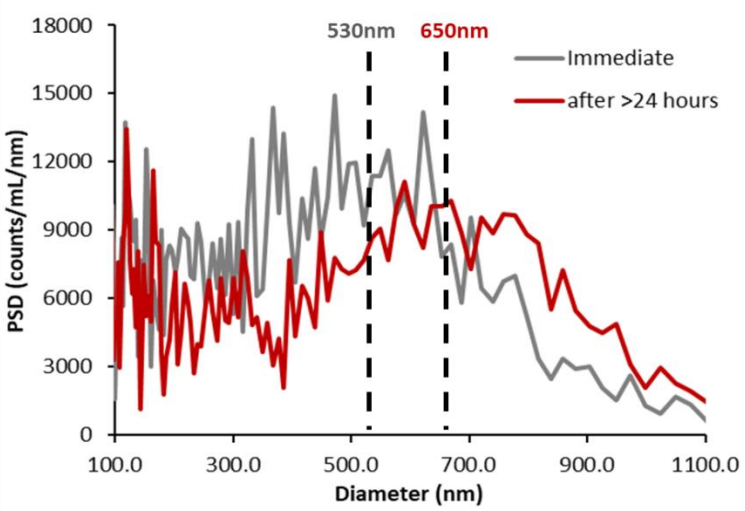

Figure 5.6. Particle size distributions of humic acid in artificial seawater measured immediately (gray) and after letting sit for >24 hours (red). Lines indicate approximate centers of the main distribution size mode for each distribution.

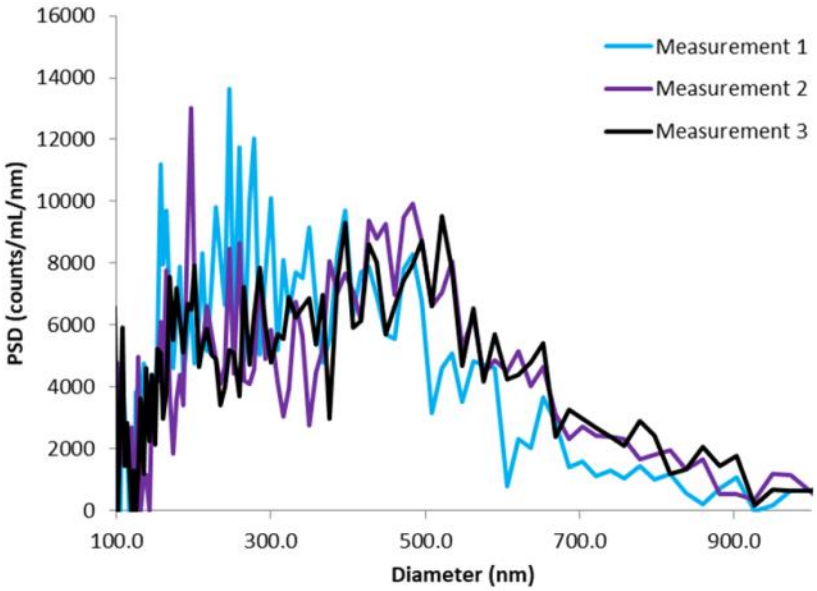

Figure 5.7. Seawater particles size distribution measurements taken sequentially with no additions.

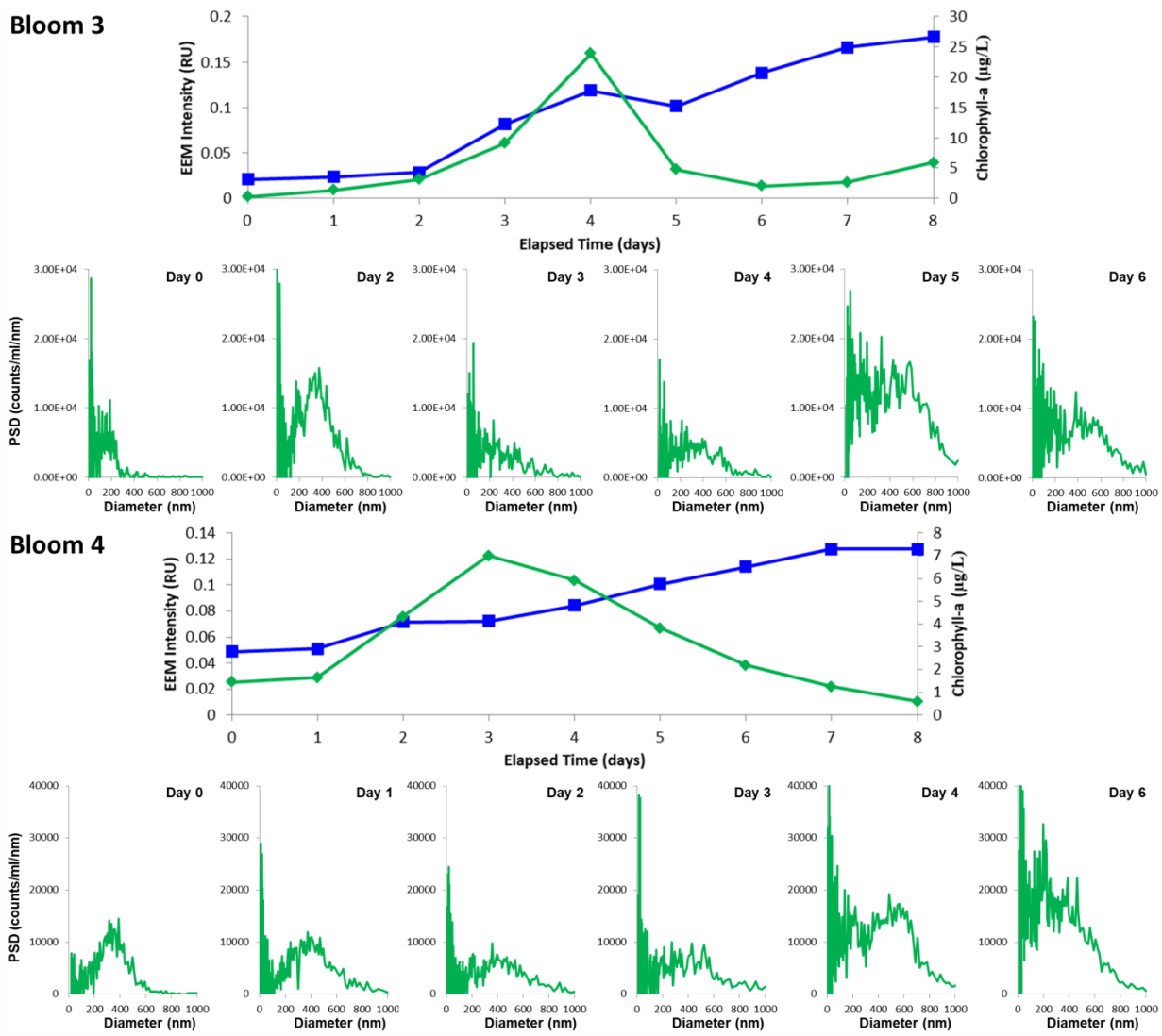

Figure 5.8. Changes in the seawater particle size distribution, humic substance fluorescence (360 nm excitation/450 nm emission, blue squares), and *in vivo* chlorophyll-a concentrations (green diamonds) over the course of 3 phytoplankton bloom experiments.

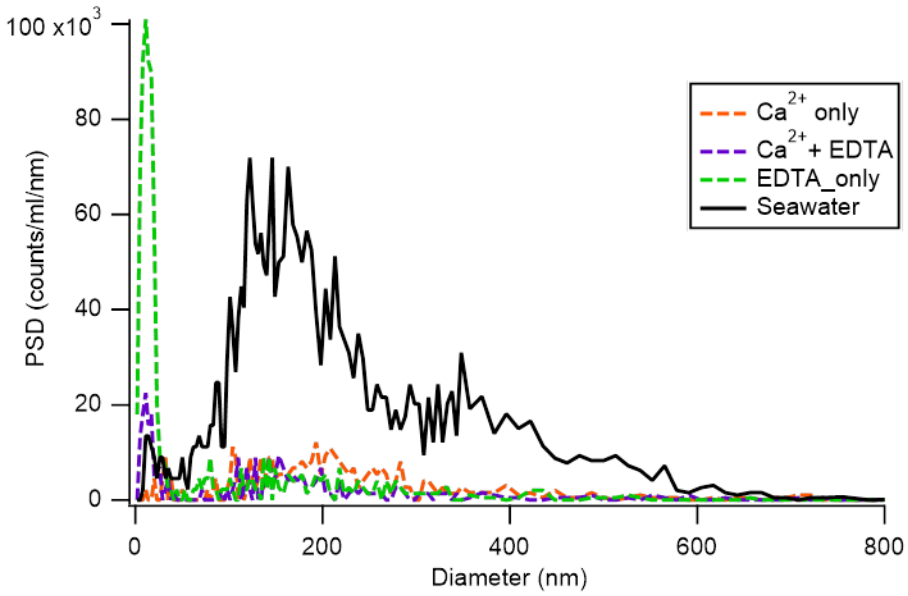

Figure 5.9. Particle size distributions of ultrapure water with calcium ion solution addition only (red), EDTA addition only (green), calcium ion and EDTA additions (purple), and seawater with no additions (black)

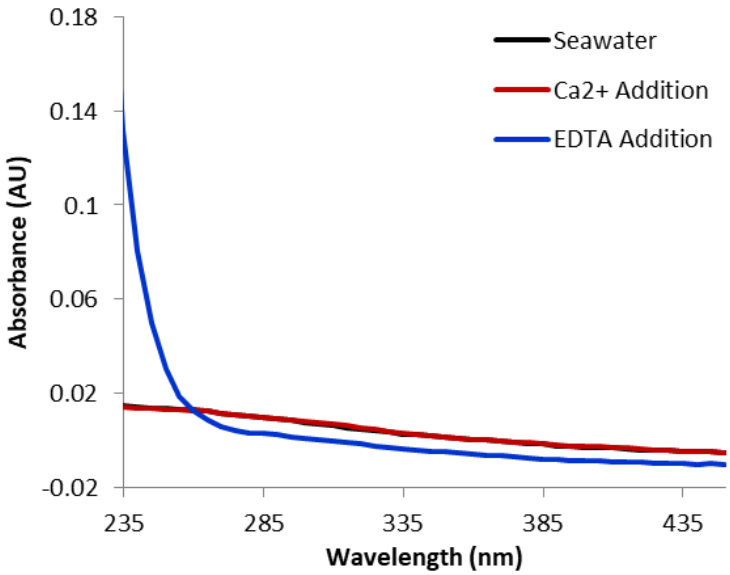

Figure 5.10. UV-vis spectra of seawater before (black) and after addition of calcium ions (red) and EDTA (blue)

5.8 References

Amrutha, S. R. and M. Jayakannan. Probing the pi-stacking induced molecular aggregation in pi-conjugated polymers, oligomers, and their blends of p-phenylenevinylenes. *Journal of Physical Chemistry B*. **2008**, *112*(4): 1119-1129.

Arai, K., S. Wada, K. Shimotori, Y. Omori and T. Hama. Production and degradation of fluorescent dissolved organic matter derived from bacteria. *Journal of Oceanography*. **2018**, *74*(1): 39-52.

Azam, F., D. C. Smith, G. F. Steward and A. Hagstrom. Bacteria - organic matter coupling and its significance for oceanic carbon cycling. *Microbial Ecology*. **1994**, *28*(2): 167-179.

Baalousha, M., M. Motelica-Heino and P. Le Coustumer. Conformation and size of humic substances: effects of major cation concentration and type, pH, salinity, and residence time. *Colloids and Surfaces a-Physicochemical and Engineering Aspects*. **2006**, *272*(1-2): 48-55.

Biddanda, B. A. Microbial aggregation and degradation of phytoplankton-derived detritus in seawater .2. microbial-metabolism. *Marine Ecology Progress Series*. **1988**, *42*(1): 89-95.

Bieroza, M. Z., J. Bridgeman and A. Baker. Fluorescence spectroscopy as a tool for determination of organic matter removal efficiency at water treatment works. *Integrating Water Systems*. **2010**: 467-+.

Cao, F., P. M. Medeiros and W. L. Miller. Optical characterization of dissolved organic matter in the Amazon River plume and the Adjacent Ocean: examining the relative role of mixing, photochemistry, and microbial alterations. *Marine Chemistry*. **2016**, *186*: 178-188.

Chen, Y. C., J. W. Y. Lam, R. T. K. Kwok, B. Liu and B. Z. Tang. Aggregation-induced emission: fundamental understanding and future developments. *Materials Horizons*. **2019**, *6*(3): 428-433.

Chin, W. C., M. V. Orellana and P. Verdugo. Spontaneous assembly of marine dissolved organic matter into polymer gels. *Nature*. **1998**, *391*(6667): 568-572.

Coble, P. G. Characterization of marine and terrestrial DOM in seawater using excitation emission matrix spectroscopy. *Marine Chemistry*. **1996**, *51*(4): 325-346.

Coble, P. G. Marine optical biogeochemistry: the chemistry of ocean color. *Chemical Reviews*. **2007**, *107*(2): 402-418.

Engebretson, R. R. and R. Vonwandruszka. Microorganization in dissolved humic acids. *Environmental Science & Technology*. **1994**, *28*(11): 1934-1941.

Gerke, J. Concepts and misconceptions of humic substances as the stable part of soil organic matter: a review. *Agronomy-Basel*. **2018**, *8*(5).

Graber, E. R. and Y. Rudich. Atmospheric HULIS: how humic-like are they? A comprehensive and critical review. *Atmospheric Chemistry and Physics*. **2006**, *6*: 729-753.

Guillard, R. R. and J. H. Ryther. Studies of marine planktonic diatoms .1. Cyclotella nana Hustedt, and Detonula confervacea (Cleve) Gran. *Canadian Journal of Microbiology*. **1962**, *8*(2): 229.

Hessen, D. O. and L. J. Tranvik (1998). Aquatic humic substances: ecology and biogeochemistry. Berlin; New York, Springer.

Kieber, R. J., L. H. Hydro and P. J. Seaton. Photooxidation of triglycerides and fatty acids in seawater: Implication toward the formation of marine humic substances. *Limnology and Oceanography*. **1997**, *42*(6): 1454-1462.

Kloster, N., M. Brigante, G. Zanini and M. Avena. Aggregation kinetics of humic acids in the presence of calcium ions. *Colloids and Surfaces A: Physicochemical and Engineering Aspects*. **2013**, *427*: 76-82.

Kwon, H. K., G. Kim, W. A. Lim and J. W. Park. In-situ production of humic-like fluorescent dissolved organic matter during Cochlodinium polykrikoides blooms. *Estuarine Coastal and Shelf Science*. **2018**, *203*: 119-126.

Lakowicz, J. R. (2006). Principles of fluorescence spectroscopy. New York, Springer.

Lawaetz, A. J. and C. A. Stedmon. Fluorescence intensity calibration using the raman scatter peak of water. *Applied Spectroscopy*. **2009**, *63*(8): 936-940.

Lee, C., C. M. Sultana, D. B. Collins, M. V. Santander, J. L. Axson, F. Malfatti, G. C. Cornwell, J. R. Grandquist, G. B. Deane, M. D. Stokes, F. Azam, V. H. Grassian and K. A. Prather.

Advancing model systems for fundamental laboratory studies of sea spray aerosol using the microbial loop. *J Phys Chem A*. **2015**, *119*(33): 8860-8870.

Lehmann, J. and M. Kleber. The contentious nature of soil organic matter. *Nature*. **2015**, *528*(7580): 60-68.

Li, X. Y. and B. E. Logan. Size distributions and fractal properties of particles during a simulated phytoplankton bloom in a mesocosm. *Deep-Sea Research Part II-Topical Studies in Oceanography*. **1995**, *42*(1): 125-138.

Malcolm, R. L. The uniqueness of humic substances in each of soil, stream and marine environments. *Analytica Chimica Acta*. **1990**, *232*(1): 19-30.

Mantoura, R. F. C., A. Dickson and J. P. Riley. The complexation of metals with humic materials in natural waters. *Estuarine and Coastal Marine Science*. **1978**, *6*(4): 387-408.

Mostofa, K. M. G. (2013). Photobiogeochemistry of organic matter: principles and practices in water environments. Heidelberg ; New York, Springer.

Murphy, K. R. A note on determining the extent of the water raman peak in fluorescence spectroscopy. *Applied Spectroscopy*. **2011**, *65*(2): 233-236.

Murphy, K. R., C. A. Stedmon, D. Graeber and R. Bro. Fluorescence spectroscopy and multi-way techniques. PARAFAC. *Analytical Methods*. **2013**, *5*(23): 6557.

Nebbioso, A. and A. Piccolo. Molecular characterization of dissolved organic matter (DOM): a critical review. *Analytical and Bioanalytical Chemistry*. **2013**, *405*(1): 109-124.

Palmer, N. E. and R. von Wandruszka. Dynamic light scattering measurements of particle size development in aqueous humic materials. *Fresenius J Anal Chem*. **2001**, *371*(7): 951-954.

Parlanti, E., K. Worz, L. Geoffroy and M. Lamotte. Dissolved organic matter fluorescence spectroscopy as a tool to estimate biological activity in a coastal zone submitted to anthropogenic inputs. *Organic Geochemistry*. **2000**, *31*(12): 1765-1781.

Rashid, M. A. (1985). Geochemistry of marine humic compounds. New York, Springer-Verlag.

Shetty, A. S., J. S. Zhang and J. S. Moore. Aromatic pi-stacking in solution as revealed through the aggregation of phenylacetylene macrocycles. *Journal of the American Chemical Society*. **1996**, *118*(5): 1019-1027.

Shrestha, M., M. Luo, Y. M. Li, B. Xiang, W. Xiong and V. H. Grassian. Let there be light: stability of palmitic acid monolayers at the air/salt water interface in the presence and absence of simulated solar light and a photosensitizer. *Chemical Science*. **2018**, *9*(26): 5716-5723.

Stedmon, C. A. and R. Bro. Characterizing dissolved organic matter fluorescence with parallel factor analysis: a tutorial. *Limnology and Oceanography: Methods*. **2008**, *6*: 572-579.

Thurman, E. M. and R. L. Malcolm. Preparative isolation of aquatic humic substances. *Environmental Science & Technology*. **1981**, *15*(4): 463-466.

Trueblood, J. V., X. Wang, V. W. Or, M. R. Alves, M. V. Santander, K. A. Prather and V. H. Grassian. The old and the new: aging of sea spray aerosol and formation of secondary marine aerosol through OH oxidation reactions. *ACS Earth and Space Chemistry*. **2019**, *3*(10): 2307-2314.

Tsui, W. G. and V. F. McNeill. Modeling secondary organic aerosol production from photosensitized humic-like substances (HULIS). *Environmental Science & Technology Letters*. **2018**, *5*(5): 255-259.

Verdugo, P. Marine microgels. *Ann Rev Mar Sci*. **2012**, *4*: 375-400.

Verdugo, P., A. L. Alldredge, F. Azam, D. L. Kirchman, U. Passow and P. H. Santschi. The oceanic gel phase: a bridge in the DOM-POM continuum. *Marine Chemistry*. **2004**, *92*(1-4): 67-85.

Wang, L., Y. J. Li, Y. Xiong, X. H. Mao, L. Y. Zhang, J. F. Xu, W. B. Tan, J. S. Wang, T. T. Li, B. D. Xi and D. H. Wang. Spectroscopic characterization of dissolved organic matter from sludge solubilization treatment by micro-bubble technologyLei. *Ecological Engineering*. **2017**, *106*: 94-100.

Wang, X. F., C. M. Sultana, J. Trueblood, T. C. J. Hill, F. Malfatti, C. Lee, O. Laskina, K. A. Moore, C. M. Beall, C. S. McCluskey, G. C. Cornwell, Y. Y. Zhou, J. L. Cox, M. A. Pendergraft, M. V. Santander, T. H. Bertram, C. D. Cappa, F. Azam, P. J. DeMott, V. H. Grassian and K. A. Prather. Microbial control of sea spray aerosol composition: a tale of two blooms. *ACS Central Science*. **2015**, *1*(3): 124-131.

Wang, X. K., R. Gemayel, N. Hayeck, S. Perrier, N. Charbonnel, C. H. Xu, H. Chen, C. Zhu, L. W. Zhang, L. Wang, S. A. Nizkorodov, X. M. Wang, Z. Wang, T. Wang, A. Mellouki, M. Riva, J. M. Chen and C. George. Atmospheric photosensitization: a new pathway for sulfate formation. *Environmental Science & Technology*. **2020**, *54*(6): 3114-3120.

Wei, D., H. Dong, N. Wu, H. H. Ngo, W. S. Guo, B. Du and Q. Wei. A fluorescence approach to assess the production of soluble microbial products from aerobic granular sludge under the stress of 2,4-dichlorophenol. *Scientific Reports*. **2016**, *6*.

Win, M. S., Z. Y. Tian, H. Zhao, K. Xiao, J. X. Peng, Y. Shang, M. H. Wu, G. L. Xiu, S. L. Lu, S. Yonemochi and Q. Y. Wang. Atmospheric HULIS and its ability to mediate the reactive oxygen species (ROS): A review. *Journal of Environmental Sciences*. **2018**, *71*: 13-31.

Xu, H. C. and L. D. Guo. Intriguing changes in molecular size and composition of dissolved organic matter induced by microbial degradation and self-assembly. *Water Research*. **2018**, *135*: 187-194.

Yamin, G., M. Borisover, E. Cohen and J. van Rijn. Accumulation of humic-like and proteinaceous dissolved organic matter in zero-discharge aquaculture systems as revealed by fluorescence EEM spectroscopy. *Water Research*. **2017**, *108*: 412-421.

Zhang, Y. L., Y. Yin, L. Q. Feng, G. W. Zhu, Z. Q. Shi, X. H. Liu and Y. Z. Zhang. Characterizing chromophoric dissolved organic matter in Lake Tianmuhu and its catchment basin using excitation-emission matrix fluorescence and parallel factor analysis. *Water Res*. **2011**, *45*(16): 5110-5122.

Chapter 6. Metabolically Active Microbes in Sea Spray Aerosols Cycle Inorganic and Organic Carbon Pools: from Single Cells to Bulk Fluorescence-based Analysis During a Phytoplankton Bloom

6.1 Synopsis

Bacteria are launched into the atmosphere during the production of sea spray aerosols (SSA) from breaking waves. Active bacteria in the air can impact atmospheric chemistry; however, very little is understood about the metabolic activity of these airborne bacteria after ejection into the atmosphere. Here we used *Bac*Light™ RedoxSensor™ Green (RSG), a dye that assays bacterial reductase activity, combined with excitation-emission matrix (EEM) spectroscopy, flow cytometry, and Laser Scanning Confocal Microscopy (LSCM), to test hypotheses on the microbial metabolic activity in SSA during phytoplankton bloom mesocosm experiments. We found that metabolically active microbes were present in SSA and thus had the potential to alter SSA chemistry. Moreover, changes in metabolic activity in SSA corresponded with shifts in the microbial community structure. Finally, microbial activity was positively correlated with dissolved inorganic carbon (DIC) and humic-like substance (HULIS) concentrations, indicating that active bacteria impact both the inorganic and organic carbon pools

in seawater. This study provides insight into how marine bacteria can directly influence the physicochemical and climate-relevant properties of seawater and SSA.

6.2 Introduction

Sea spray aerosols (SSA) are one of the most abundant aerosol types in the atmosphere and play a critical role in influencing clouds and climate [*Gantt and Meskhidze, 2013*]. The SSA impact on climate is dictated by SSA chemical composition [*Gantt et al., 2013; Schill et al., 2015; Bertram et al., 2018*]. Previous studies have shown SSA to contain a wide variety of chemical and biological components including small organic molecules like proteins and lipids, phytoplankton fragments, viruses, and intact bacteria [*Patterson et al., 2016; Leck and Bigg, 2017; Bertram et al., 2018; Malfatti et al., 2019*]. Marine bacteria in SSA have been a major recent focus due to their known potential to influence climate and their potential to impact human health [*Asselman et al., 2019; Cavicchioli et al., 2019*]. Recent work based on DNA extracted from SSA have identified various marine bacteria species that can be ejected into the atmosphere and potential factors that can lead to transfer, such as cell wall composition [*Michaud et al., 2018*]. However, further studies are necessary to better understand their role in the atmosphere after ejection, such as their metabolic activity. Metabolically active microbes can alter SSA chemistry, thus influencing atmospheric chemistry and climate [*Smets et al., 2016*]; however, metabolic activity of microbes in SSA is poorly understood.

Metabolically active microbes in the ocean are vital for keeping marine ecosystems functioning [*Azam and Malfatti, 2007*]. The microbial processing of the organic matter pool allows for the continuous supply of nutrients for other organisms within the trophic food web [*Repeta and Boiteau, 2017*]. The microbial recycling of dissolved carbon is associated with

microbial metabolic activity. Microbial activity can be measured by assessing oxidase and reductase status [*Rodriguez et al., 1992; Sieracki et al., 1999; Proctor and Souza, 2001; Gasol and Aristegui, 2007*]. In a cell, oxidases and reductases are important enzymes for the electron transport chain (*i.e.* respiration) and cellular metabolism [*Falkowski et al., 2008*]. Moreover, improving the resolution limits to observe microbes, thus interrogating individual cells within their microscale environment [*Azam et al., 2007*], has become increasingly important in order to address fundamental questions on who is doing what, when, why and how they change [*Hatzenpichler et al., 2020*].

Recent work on microbial metabolic activity has used the *Bac*Light™ RedoxSensor™ Green (RSG) dye, which targets reductases in the cell [*Kalyuzhnaya et al., 2008; Cologgi et al., 2011; Konopka et al., 2011*]. RSG offers several advantages compared to the other methods because it is less toxic and less taxon specific [*Singer et al., 2017*]. From a microbial perspective, in order to live and thrive, bacteria need to have ATP, the energic metabolic currency and a reduced cellular state within [*Pirt, 1965*]. In other words, RSG dye detects the necessary condition to define life from death. This method has yet to be applied to atmospheric systems from single cell to bulk analysis.

Here we investigated the metabolic activity of marine microbes, defined here as a RSG-positive signal, in seawater and in SSA to unravel the potential role of marine bacteria on SSA chemical transformations. Specifically, we tested the following hypotheses:

1. Metabolically active microbes remain active in SSA after transfer and changes in bulk and SSA activity correlate with shifts in microbial community composition;
2. Microbial activity changes in bulk and SSA are influenced by the progression of the phytoplankton bloom;

3. Metabolically active microbes impact seawater inorganic and organic carbon pools.

To probe metabolic activity, the use of RSG dye is combined with three fluorescence-based techniques: excitation-emission matrix (EEM) spectroscopy, flow cytometry, and Laser Scanning Confocal Microscopy (LSCM). The ability of this approach to study metabolic activity was assessed through the characterization of marine bacteria isolates and SSA collected in isolated microcosm experiments. Using this combination of techniques in a large-scale phytoplankton bloom mesocosm in a wave channel, changes in SSA metabolic activity were monitored and compared to biological changes observed in seawater to identify links between ocean biology and the sea-air transfer of microbes. Furthermore, changes in seawater and SSA metabolic activity were compared to DIC and HULIS in order to uncover the relationships between microbe metabolic activity and seawater inorganic and organic matter composition. By investigating microbial activity in seawater and isolated SSA, we gain insight into the impact of microbes on the chemistry of the real ocean and atmosphere.

6.3 Experimental Method

6.3.1. Phytoplankton Bloom Experiments

Phytoplankton bloom experiments were conducted using natural seawater. Seawater collected from the Ellen Browning Scripps Memorial Pier (32-52'00" N, 117-15’21" W) was initially filtered using an acid-washed 50 μm mesh screen (Sefar Nitex 03−100/32) to remove zooplankton, a grazer of phytoplankton. Experiments focused on temporal changes in metabolic activity were performed during the SeaSCAPE campaign, also known as Sea Spray Chemistry and Particle Evolution campaign, which was conducted in the summer of 2019 [*Sauer et al., 2022*]. We present the data of SeaSCAPE 1 and 3 bloom cycles, here referred to as Experiment-1

and Experiment-2, respectively. In SeaSCAPE, seawater was placed in a 30,000 L wave channel at the Scripps Institution of Oceanography (SIO). Methods for conducting phytoplankton bloom mesocosm experiments using both the MART and the wave channel have been described previously [*Lee et al., 2015; Wang et al., 2015; Sauer et al., 2022*]. In short, the seawater was initially spiked with Guillard's F algae nutrient medium (concentrations ranging from F/100 to F/2) in order to induce a phytoplankton bloom [*Guillard and Ryther, 1962*]. The seawater was incubated with fluorescent lights (Full Spectrum Solutions, model 205457; T8 format, color temperature 5700 K, 2950 lumens) to promote phytoplankton growth [*Brown and Richards, 1968*]. Phytoplankton growth and decline were monitored daily using an Aquafluor handheld fluorometer (Turner Designs, Aquafluor) to measure *in vivo* chlorophyll-a fluorescence. Detailed protocols for biological measurements including microbial community fingerprint via 16S rRNA gene sequencing can be found in Sauer et al. [*Sauer et al., 2022*].

6.3.2. SSA Generation and Aerosol Sample Collection

Two techniques were used to generate aerosols: the Marine Aerosol Reference Tank (MART) [*Stokes et al., 2013; Lee et al., 2015*] and the wave channel at SIO [*Prather et al., 2013; Wang et al., 2015*]. Both techniques have been shown to produce SSA size distributions that mimic the SSA size distribution observed over the ocean [*Stokes et al., 2013; Collins et al., 2014*]. These techniques also have the advantage of producing SSA in an isolated system, which prevents the inclusion of other non-marine aerosols. The MART utilizes a periodic plunging waterfall to create a bubble plume that bursts to produce SSA. The SIO wave channel consists of a 30-meter-long sealed glass channel that uses a moving paddle on one end to create a wave that breaks on an artificial beach, generating SSA.

Aerosols were collected daily using a liquid spot sampler (Aerosol Devices, LSS110A). The spot sampler uses a condensation growth tube to collect particles [*Fernandez et al., 2014*], in a size range of 5 nm to >10 μm. Particles were collected into a 0.7-mL liquid vial filled with filtered autoclaved seawater (FASW) or a 4x phosphate-buffered saline (PBS) solution to simulate seawater salt concentrations with minimal organic matter background fluorescence. The spot sampler collected aerosols at a flow rate of 1.8 LPM for either 1 hour, in the case of Experiment-1, or for approximately 6 hours, for Experiment-2. Samples were diluted with 4x PBS to 1.5 mL prior to measurements.

6.3.3. RSG Staining Protocol

To assess metabolic activity, 1 mL of seawater or SSA samples were incubated for 30 min in the dark at environmental temperature with 10 μL of *Bac*Light™ RedoxSensor™ Green Vitality Kit (B34954, Thermo Fisher, RSG) according to manufacturer guidelines. The fresh samples were analyzed immediately for EEM and LSCM. An RSG aliquot was fixed with EM-grade glutaraldehyde (5% final concentration), flash frozen in liquid nitrogen and then stored at -80 C prior to flow cytometry preparation. Negative control experiments for EEM and flow cytometry used seawater samples incubated with CCCP (1 μM final) prior to RSG addition. BBFL7 was excluded from the CCCP experiments due to low optical density of the BBFL7 culture at the time of measurement.

6.3.4. RSG -Live-Excitation-Emission Matrix Spectroscopy

Fluorescence excitation-emission matrices (EEMs) for all bulk seawater and SSA samples were obtained using an Aqualog spectrofluorometer (Horiba Scientific, Aqualog with

extended range). EEMs were obtained for excitation wavelengths ranging from 235-500 nm and emission wavelengths ranging from 250-800 nm. A background spectrum acquired with ultrapure water was subtracted from all bulk seawater EEMs. SSA EEMs used either FASW or 4x PBS spectrum for background correction, depending on the collection solution used. EEMs were corrected for inner-filter effects based on absorbance spectra measured simultaneously. Rayleigh scatter (1^{st} and 2^{nd} order) in all EEMs was removed. All EEMs were also normalized to the area of the Raman Scattering peak of water at 350 nm excitation to convert fluorescence intensities to Raman Units (R.U.) [*Lawaetz and Stedmon, 2009; Murphy, 2011*].

6.3.5. RSG- In Situ Live- Laser Scanning Confocal Microscopy

After 30 min of incubation in the dark, the RSG-stained seawater samples were immediately imaged at the A1R Nikon LSCM live. Chambered coverslips (300 µL sample) and 60x water immersion objective (Plan Apo VC DIC N2 60x, 0.07 µm/px con 1.8 NA, Nikon) on a temperature controlled stage (at 25 C, temperature of the wave channel experiment) were used for imaging. RSG wavelengths were monitored at 488 nm and 520 nm. DAPI was used as a counterstain (10 µg/mL final solution, 405 nm and 470 nm) and also for natural *in vivo* fluorescence (605 nm and 650 nm). Z stacks were acquired to assess RSG metabolically active microbes *in situ*. LSCM settings (laser power and noise filter) were maintained constant for reproducibility. Image analysis was performed using FIJI software (Schindelin et al., 2012, see SI for detailed protocols) to estimate relative RSG fluorescence following the Samo et al. (2014) protocol [*Schindelin et al., 2012; Samo et al., 2014*].

6.3.6. RSG- Flow Cytometry

Seawater or SSA samples stained and unstained with RSG were analyzed via flow cytometry (BD FACS CANTO II in OGS Italy and BIO-RAD, ZE5 Cell Analyzer, at The Scripps Research Institute (TSRI) Flow Core Facility). For RSG-stained seawater, heterotrophic bacteria were first diluted (1:10) in 1×TE buffer (pH 8), and then run at medium flow. For RSG-stained SSA, undiluted samples were run at medium flow. Samples not stained with RSG were instead stained with SYBR Green I at RT for 10 minutes (at a 10:4 dilution of the commercial stock) in the dark and treated as RSG stained samples [*Gasol and Del Giorgio, 2000*]. Heterotrophic bacteria populations were discriminated based on their signature in the FL1 (488 nm laser, green fluorescence) vs. side scattering (SSC) specific cytograms [*Marie et al., 1997; Brussaard, 2004*].

6.3.7. Bacteria Isolates for Proof of Concept RSG Staining

Four different marine-relevant bacteria isolates, originally derived from the Pacific Ocean off the Scripps pier in La Jolla, were isolated by the Azam laboratory at the Scripps Institution of Oceanography (SIO): a γ-proteobacteria, *Pseudoalteromonas* species, ATW7, a sphingobacteria-flavobacteria, BBFL7, a γ-proteobacteria *Alteromonas*, AltSIO, and a *Vibrio*, SWAT3 [*Bidle and Azam, 2001; Long and Azam, 2001; Pedler et al., 2014*]. ATW7 and BBFL7 were chosen due to their intense proteolytic activities that lead to effective dissolution of particulates [*Bidle et al., 2001*]. AltSIO was chosen as another isolate due to its ability to break down dissolved organic carbon compounds [*Pedler et al., 2014*]. SWAT3 produces light, is motile and produces antibiotics making it an excellent antagonizer [*Long et al., 2001*]. Bacteria isolates were streaked out from frozen cultures onto solid ZoBell medium. After 24 hours, colonies were picked and

grown in liquid ZoBell medium at room temperature on a shaker (130 rpm). The next day, the cultures were harvested by spinning at 9000G for 5 minutes and washed with filtered autoclaved seawater or PBS to remove the supernatant. For experiments using only AltSIO, ATW7, and BBFL7, optical density measured at 600 nm was monitored in order to have 1:1:1 (AltSIO:ATW7:BBFL7) ratio of the cultures in the inoculum that was $1x10^9$ cells/mL. The final concentration of bacterial cells was diluted to 1.6×10^5 cells/mL, which is on the order of known bacterial concentrations in the ocean [*Azam et al., 1983*]. Marine bacteria isolate experiments and SSA RSG protocol development occurred during the 3rd bloom cycle of the BEAST campaign, also known as the Biological Effects on Air-Sea Transfer, which was conducted in the summer of 2018 [*Hasenecz et al., 2020; Santander et al., 2021*]. In BEAST, 2200 L of seawater was placed in a large outdoor tank. Seawater from the tank was transferred daily from the tank to a 120 L Marine Aerosol Reference Tanks for aerosol generation and transferred back to the outdoor tank (see section 6.3.2 above).

6.4 Results and Discussion

In order to investigate metabolic activity in seawater and SSA, a RSG protocol for EEM spectroscopy was first developed using marine bacteria isolates then tested in a more complex scenario during a phytoplankton bloom for SSA application. In a realistic 30,000 L phytoplankton bloom mesocosm in a wave channel, the developed protocol was used to test the hypothesis that metabolically active bacteria could be transferred from bulk seawater to SSA and that active cells correlate with DIC and HULIS concentrations.

6.4.1 EEM Signal Characterization for the Metabolic Activity of Marine Bacteria Isolates

The metabolic activity of three marine-relevant bacteria isolates was investigated in order to assess and optimize the use of RSG to study microbial activity in marine systems. EEM fluorescence signals were observed for each of the three bacteria isolates used (AltSIO, ATW7, and BBFL7), indicating the presence of metabolically active microbes (**Figure 6.1**). In each case, a strong fluorescence signal was observed with maximum excitation at 485 nm and emission at 520 nm in seawater. The three bacteria strains showed different dye fluorescence intensities, with BBFL7 showing the greatest intensity and with ATW7 showing the least, despite the similar cell concentrations and growth phase for all three isolates. Thus, changes in the metabolic activity of individual bacteria populations can influence the observed total metabolic activity indicated by EEMs. Application of RSG to SSA generated from seawater and seawater containing added bacteria isolates showed fluorescence signals in wavelength regions in agreement with those observed for the bacteria isolates alone (**Figure 6.9**). Furthermore, enhanced RSG signal from seawater with added bacteria isolates confirmed that the fluorescence originates from the active bacteria in SSA (**Figure 6.9**).

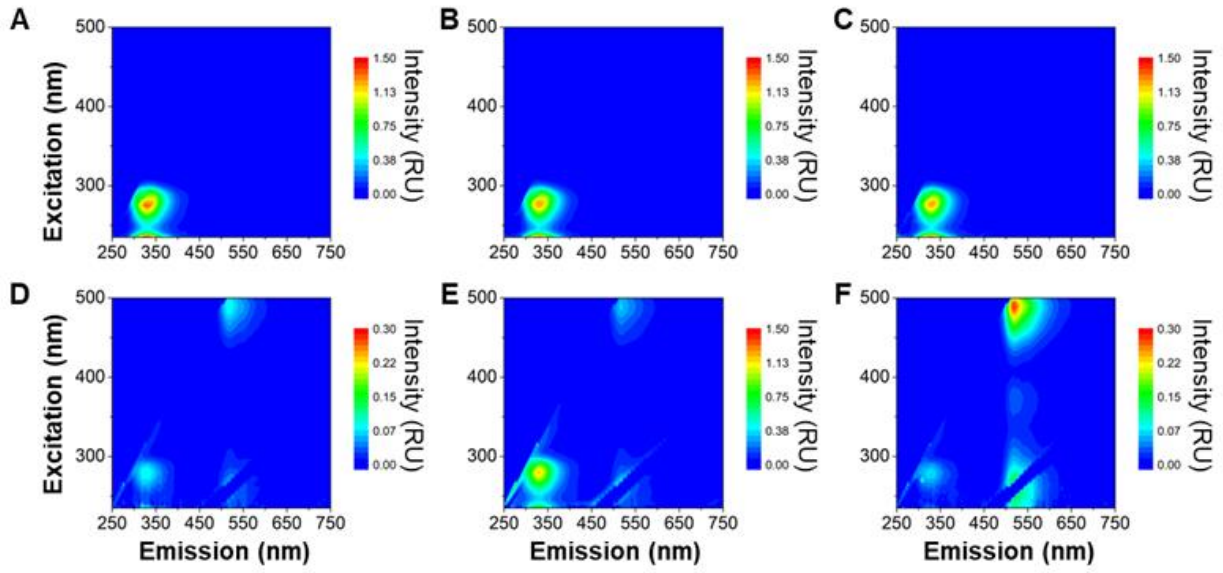

Figure 6.1. Selected EEMs before (top) and after (bottom) addition of RedoxSensor Green for three bacteria isolates: AltSIO (a, d), ATW7 (b, e), and BBFL7 (c, f). AltSIO and BBFL7 solutions after RG addition were diluted (1:10) to prevent saturation of the fluorescence detector.

To further probe the metabolic activity of bacteria isolates, CCCP was used to inhibit cellular respiration and prevent the production of a fluorescence signal from RedoxSensor Green (**Figure 6.2**). For all of the bacteria isolates tested, samples treated with CCCP followed by RSG showed a drastic reduction in dye fluorescence compared to samples treated with dye only and no CCCP. It is evident that the inhibition of cellular respiration leads to the suppression of dye fluorescence, further indicating that the observed fluorescence signal in the EEMs is due to microbial activity.

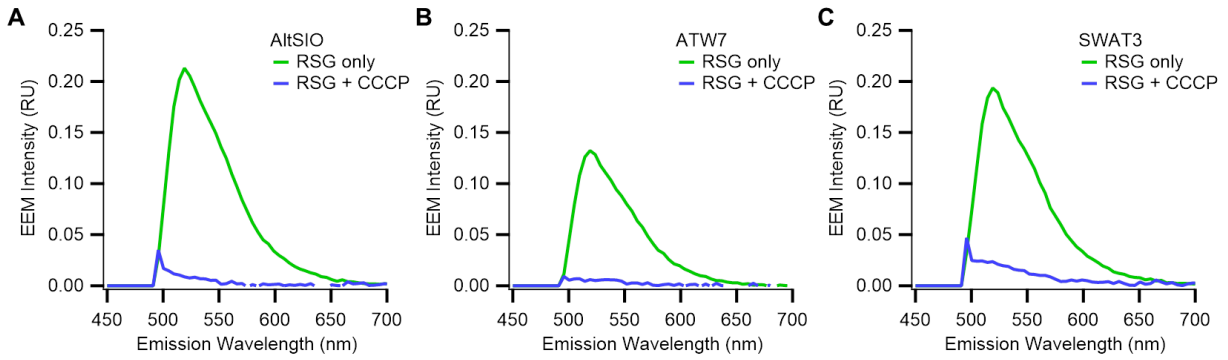

Figure 6.2. Emission spectra (Ex = 485 nm) of three bacteria isolates: a) AltSIO, b) ATW7, and c) SWAT 3, following the addition of RSG (green) and addition of RSG and CCCP (blue) prior to dye incubation.

6.4.2 Metabolic Activity in Seawater and SSA over Time in a Complex Bloom Scenario

To investigate the changes in seawater and SSA metabolic activity over time, RSG fluorescence was monitored over the course of two phytoplankton bloom mesocosm experiments with different bloom densities. In Experiment-1, extracted chlorophyll-a, a proxy for phytoplankton biomass, reached a maximum of 6.56 µg/L, representing a modest bloom. In Experiment-2, extracted chlorophyll-a values reached a maximum of 18.74 µg/L, indicative of a high biomass phytoplankton bloom. The changes in metabolic activity for each experiment and their implications for ocean biogeochemistry and atmospheric chemistry are discussed in the following sections.

6.4.3 Experiment-1: RSG-based Fluorescence for Individual Cell Live Imaging

During Experiment-1, on 7, 8 and 9 of July 2019, seawater samples processed with RSG were imaged live with LSCM (**Figure 6.3**) in order to gain insight into the microscale context of metabolically active microbes living in bulk seawater during a phytoplankton bloom. Using the

intensity image analysis of the LSCM 3D live scans dataset, we identified 3 classes of objects that presented a green fluorescent signal (RSG-positive) categorized based on DAPI, *in vivo* chlorophyll-a fluorescence, and area. These 3 RSG-positive classes are defined as: 1) heterotrophic bacteria (DAPI signal, no *in vivo* chlorophyll-a signal, area: 0.15-3 μm^2), 2) cyanobacteria (DAPI signal, *in vivo* chlorophyll-a signal, area: 0.15-5 μm^2), and 3) the "other" group (no DAPI, no *in vivo* chlorophyll a signal, area < 0.15 μm^2). While we cannot confirm the identity of the "other" class due to the infeasibility of further sampling, we propose that this class may consist of ultramicrobacteria [*Williams et al., 2011*] or cellular debris that exhibited RSG-linked reductase activity. Future experiments using "lysis-challenging" to test for viral production upon metabolically-active bacteria lysis or testing for ultramicrobacteria and cellular debris via size exclusion can elucidate the identity of the "other" class.

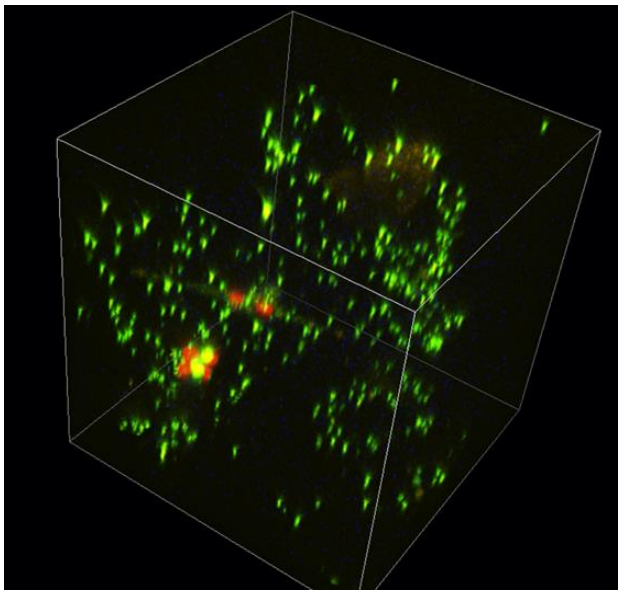

Figure 6.3. LSCM image of microbes stained with RSG.

A grand total of 1525 objects were imaged in live acquisition. Of those, 1280 were heterotrophic bacteria and 211 were Cyanobacteria, specifically *Synechococcus*, which showed

particularly high abundance. Analysis of the total fluorescence per class area (**Figure 6.4A, 6.4B**) and the normalized total fluorescence per area (**Figure 6.4C, 6.4D**) revealed that the highest percentage of metabolically active cells were in the smaller intensity classes, 0-100 and 101-200 μm^2, for both heterotrophic bacteria and Cyanobacteria (**Figure 6.4A** and **6.4B** respectively). Furthermore, the fluorescence intensity normalized per area showed that cells in the 0.26-1.00 μm^2 area range were more active than larger cells (**Figure 6.4C, 6.4D** for heterotrophic bacteria and Cyanobacteria). Furthermore, heterotrophic bacteria showed higher RSG intensity values than Cyanobacteria. Metabolically active cells were also shown to be attached onto detrital aggregates. From the analysis of EEM and microscopy data, we found good agreement with the two methods (**Figure 6.10**).

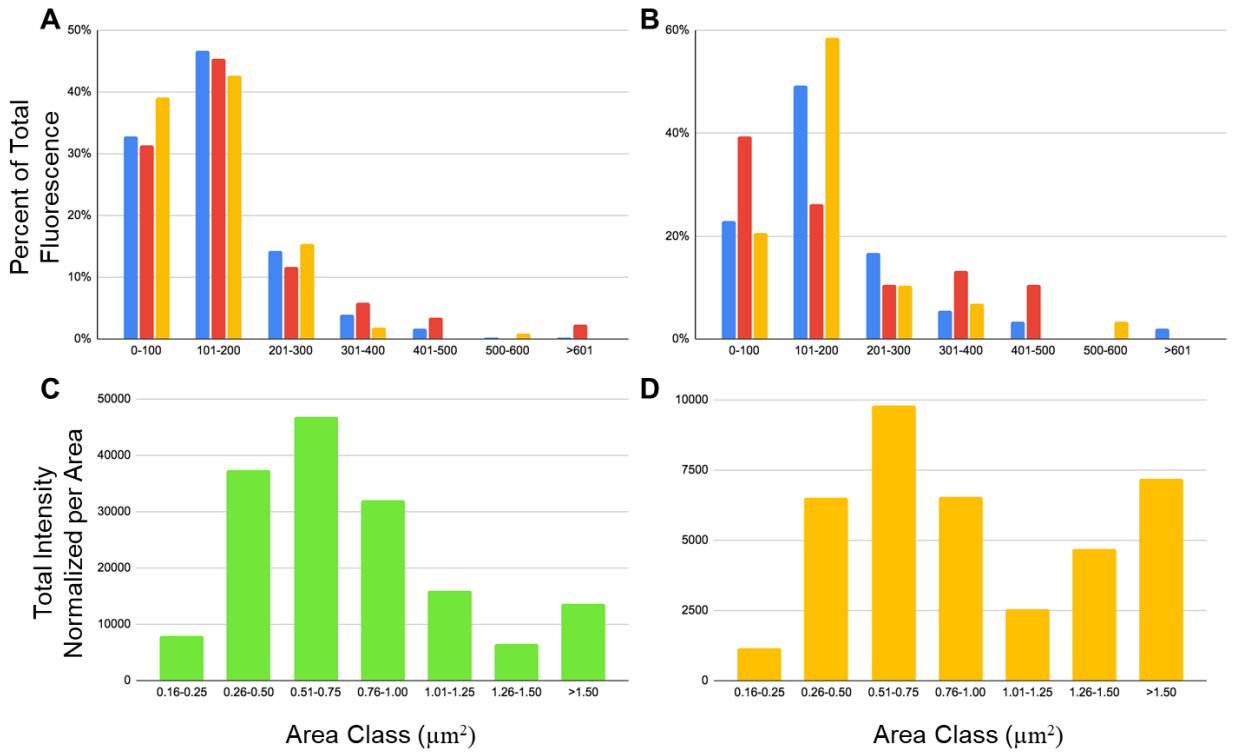

Figure 6.4. RSG individual cell intensity measurements. A, B: Percentage of total fluorescence intensity per area classes. A Heterotrophic bacteria and B Cyanobacteria. C, D: Total fluorescence intensity in relative fluorescence units normalized per area classes C Heterotrophic bacteria and D Cyanobacteria. Blue, July 8th; Red, July 9th; Orange, July 10th.

6.4.4. Experiment-2: RSG-based Fluorescence Methods Indicates Intense Microbial Metabolic Activities over the Course of a Phytoplankton Bloom

In Experiment-2, we monitored the microbial metabolic activity in seawater and SSA over time in order to better understand the coupling between primary producers and microbial consumers. *In vivo* chlorophyll-a values reached a maximum in approximately 11 days, while peak bacteria concentrations occurred in 9-12 days (**Figure 6.11**). The observed pattern for phytoplankton growth and decline was consistent with trends found in previous phytoplankton mesocosm experiments [*Lee et al., 2015; Wang et al., 2015*]. Seawater total metabolic activity over time, as indicated by the RSG fluorescence signal in the EEMs, peaks after 13 days and it was strongly correlated with the heterotrophic bacteria concentrations (**Figure 6.5A**). Moreover, both total metabolic activity and heterotrophic bacteria concentrations correlated with RSG-positive cells, as indicated by concentrations measured with flow cytometry (**Figure 6.5A, Figure 6.12**). These results confirmed that marine bacteria were the main drivers for changes in the observed total metabolic activity in seawater.

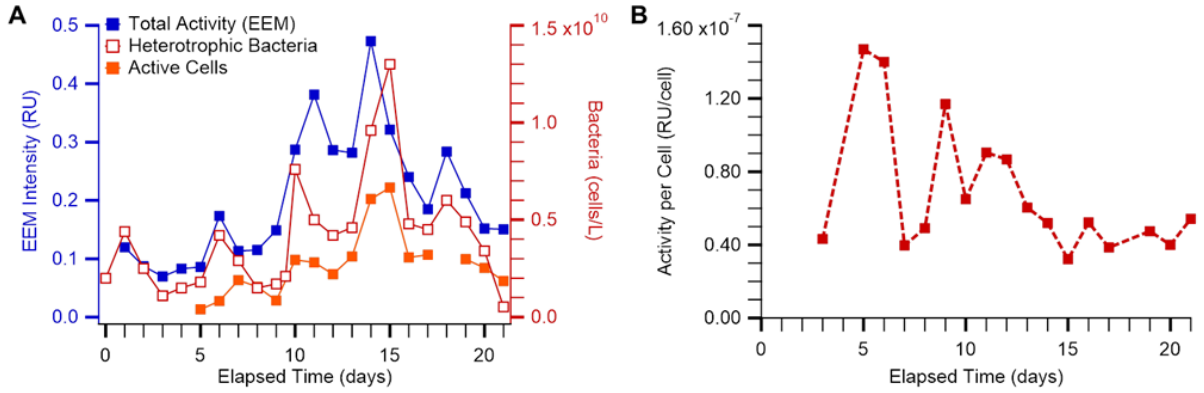

Figure 6.5. Seawater temporal trend of metabolically active cells and total metabolic activity indicated by EEM intensity (a) as well as the approximate activity per cell (b) in seawater during Experiment-2.

Normalizing the EEM intensities to the corresponding metabolically active cell concentrations gave a metric for the activity per cell, thus providing further insight into the changes in metabolic activity in seawater and SSA. In seawater, the total activity, measured by EEM intensity, was greatest after the peak of the phytoplankton bloom (**Figure 5A**). However, the activity per cell was greatest before the peak of the bloom and showed an overall decreasing trend over time (**Figure 5B**). Differences between the total and the per-cell activity could indicate shifts in the metabolic state of different populations of marine microbes, with increasing abundance of less active cells while the per-cell activity was decreasing. Nonetheless, it is clear that microbial activity and activity per cell showed major changes over the course of a bloom. Thus, not only is the diversity of microbial communities important in dictating seawater chemistry, but also critical is their overall activities defined here as the ability to degrade and transform organic compounds.

Examination of the SSA EEMs during Experiment-2 showed the appearance of a fluorescence signal from RSG similar to Experiment-1, again indicative of metabolically active microbes in SSA. Furthermore, analysis of the temporal trend for EEM fluorescence in SSA revealed large changes in the metabolic activity in SSA (**Figure 6.6**). Similar to seawater, the greatest activity in SSA occurred after the peak of the phytoplankton bloom, as indicated by *in vivo* chlorophyll-a fluorescence measurements (**Figure 6.6**). The same trends were also detected when examining the metabolically active cells in SSA. Thus, not only was the metabolic activity in SSA dynamic, but changes were also driven by the biological conditions of the seawater, such as bloom intensity. Increases in the transfer of metabolically active microbes to SSA likely affect the ability of SSA to influence atmospheric chemistry [*Vaitilingom et al., 2013*].

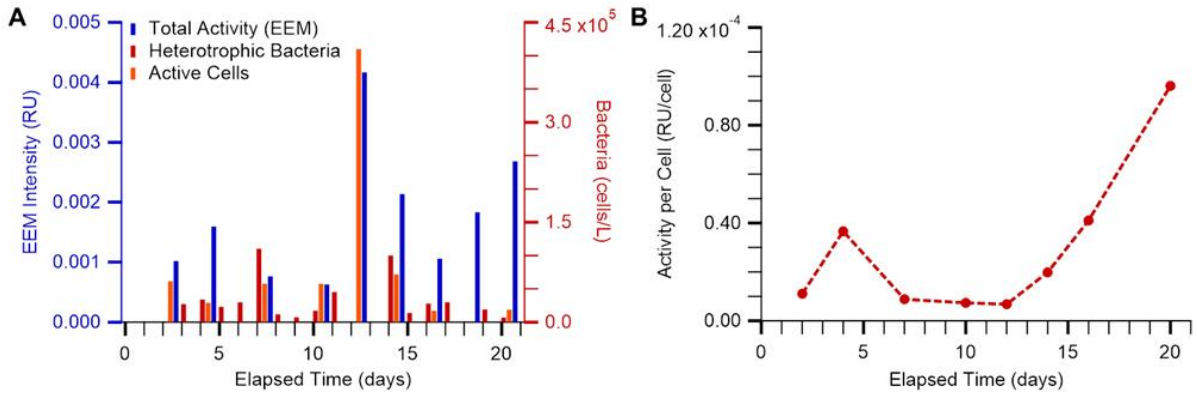

Figure 6.6. SSA temporal trend of metabolically active cells and total metabolic activity indicated by EEM intensity (top) as well as the approximate activity per cell (EEM intensity normalized to active cell concentration) during Experiment-2.

Comparisons between the metabolic activities in each compartment revealed differing trends between the activities per cell in SSA and seawater (**Figure 6.5, Figure 6.6**). In contrast to the decreasing activity per cell observed in the seawater over time, SSA activity per cell appeared to increase over time with the greatest activity per cell occurring at the end of the experiment (**Figure 6.6**). The similarities between seawater and SSA total activity suggest that metabolic activity in SSA was related to seawater phytoplankton bloom dynamics, specifically the growth of metabolically active bacteria. However, differences between seawater and SSA activity per cell suggest that SSA activity was not a result of direct transfer of all bacterial cells from the bulk seawater. Instead, these trends may be due to a shift in the active populations in seawater or the selective transfer of active species to SSA.

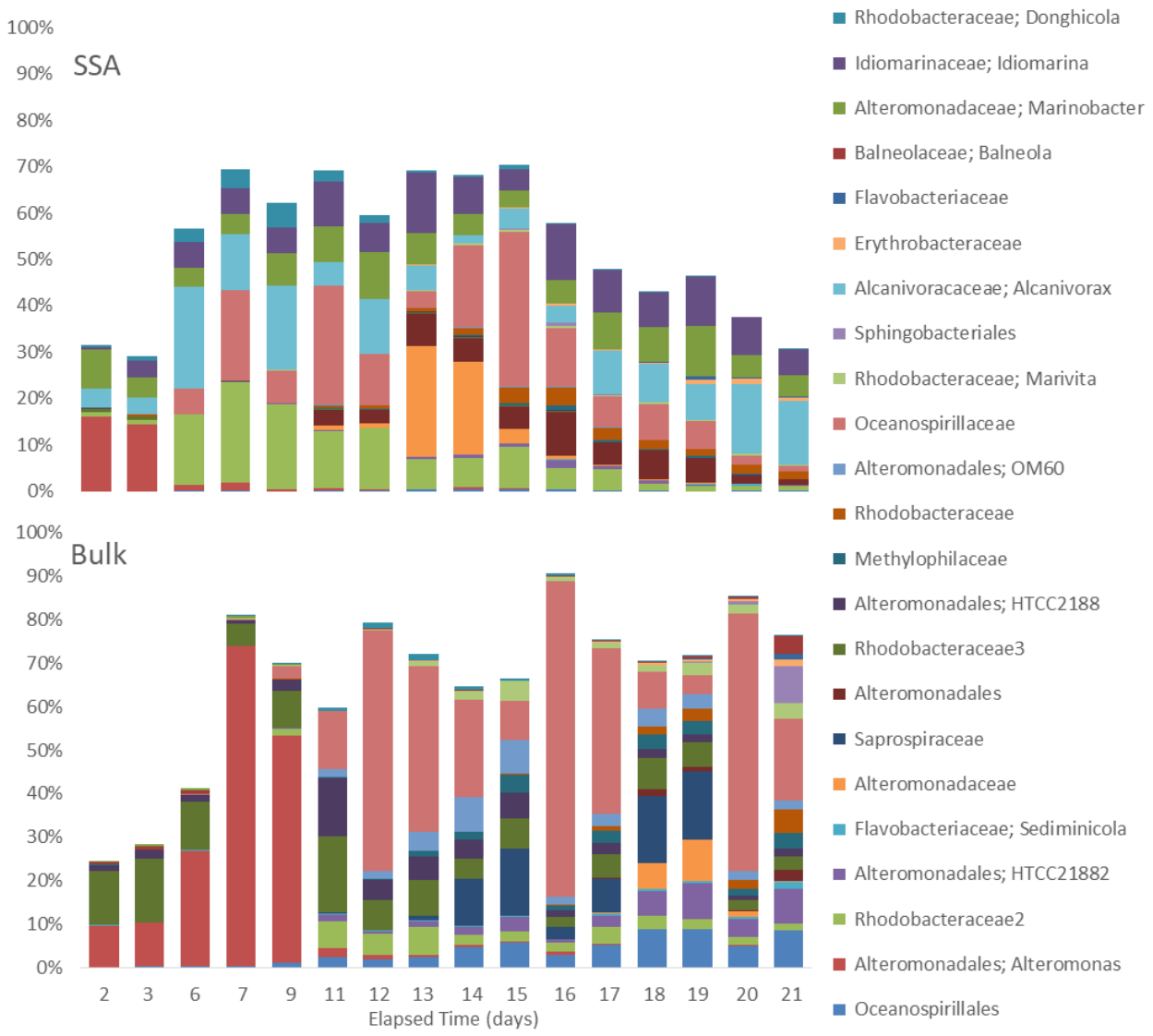

Figure 6.7. SSA and seawater temporal trends of bacterial community structure in Experiment-2/SeaSCAPE 3. Relative abundance of only ASVs representing more than 1% are shown.

Microbial communities in seawater and in SSA were dynamic over the course of the experiment **(Figure 6.7**). Within the experiment, abrupt changes of the community structure were correlated with man-made perturbations (e.g. Day 6 nutrients amendment, Day 9 outdoor tank amendment, Day 13 wall scraping, and Day 16 pump mixing). In terms of metabolically active cells, the outdoor amendment and the wall scraping resulted in a community shift and in

an increase of RSG fluorescent cells in seawater and SSA. From the community fingerprint in seawater, the main players were *Rhodobacteraceae* 2, *Rhodobacteraceae* 3 and *Alteromonadales* HTCC2188 and *Oceanospirillaceae*. In SSA, these perturbations caused an increase in diversity of the taxa that were aerosolized. Wall scraping showed a major effect in RSG fluorescent signals that correlated with the rapid increase of *Alteromonadaceae* and *Alteromonadales*. At the end of the experiment, in seawater the activity per cell (**Figure 6.5**) stayed within a tight range (0.40-0.50 $x10^{-7}$ RU/cell) despite the changes of the microbial players suggesting that the diverse taxa were proportionally equally active. On the other hand, in SSA at the end of the experiment, there were a few players dominating the most abundant taxa (i.e. *Alcanivorax, Marinobacter* and *Idomarina*) that might be responsible for the ramping up of the activity per cell signal (**Figure 6.6**). Thus, SSA metabolic activity may be controlled by specific microbial players that are more effectively transferred to SSA.

6.4.5. Correlations Between Metabolic Activity and Seawater Chemistry

In order to assess the impact of metabolic activity on seawater chemistry and biology, the metabolic activity based on RSG fluorescence was compared with heterotrophic bacteria concentrations, dissolved inorganic carbon (DIC), bacteria production, and HULIS fluorescence (**Figure 6.13, Figure 6.14**). Within the marine biogeochemical carbon cycle, it is known that heterotrophic bacteria are master regulators of the fate of dissolved and particulate organic matter [*Azam et al., 1983*]. Heterotrophic bacteria respire O_2 and produce CO_2 (DIC) while degrading the organic matter and contribute to the formation of recalcitrant organic matter that is slow to degrade, such as HULIS [*Azam et al., 1983; Rashid, 1985; Hessen and Tranvik, 1998*].

Network analysis showed a positive correlation between RSG EEM intensity, metabolically active cell concentrations, and heterotrophic bacteria concentrations in seawater, confirming the hypothesis that marine bacteria are the main drivers for observed marine metabolic activity (**Figure 6.8, Table 6.1, Table 6.2**). A positive correlation between these three metrics and DIC suggests that marine bacterial metabolic activity influences DIC, but additional factors besides bacterial metabolic activity control DIC concentrations in seawater. Heterotrophic bacteria, total activity, and active cell concentrations also showed a positive correlation with HULIS, suggesting that increased activity can lead to enhanced production of recalcitrant material. These associations provided evidence that marine bacteria metabolic activity plays a crucial role in both organic and inorganic carbon transformations in seawater.

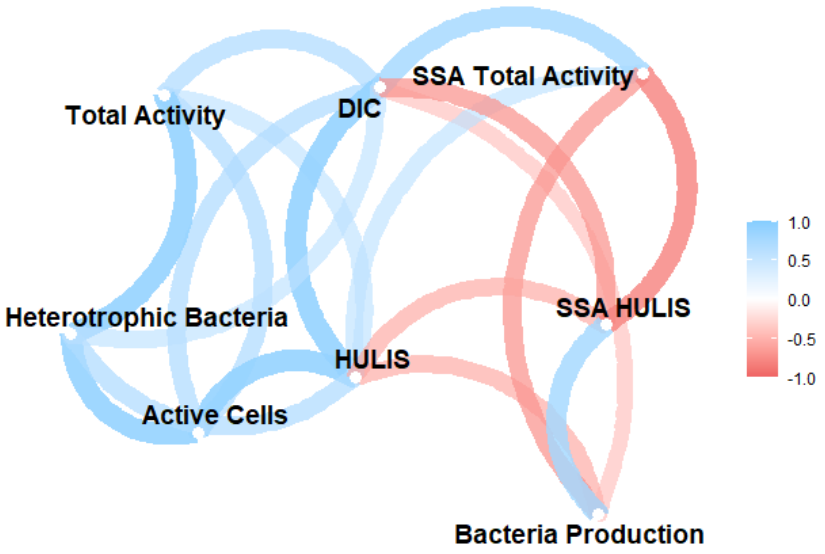

Figure 6.8. Correlation network plot for several seawater and SSA metrics over time in Experiment-2.

6.5 Conclusion

Metabolically active microbes in SSA have the potential to alter aerosol and atmospheric chemistry [*Vaitilingom et al., 2013; Klein et al., 2016; Smets et al., 2016*]. Here we use a novel approach to investigate the metabolic activity in SSA and seawater using a fluorescent dye in combination with EEM spectroscopy, microscopy, and flow cytometry. In addition to metabolically active cell concentrations, this combination of techniques also provides active cell size distributions, total metabolic activity, and an approximate average metabolic activity per cell. This approach allows for improved insights into the dynamics of metabolically active bacteria by probing both single cells and bulk solutions and can be applied in both field and laboratory studies.

The studies of isolated SSA described here reveal that marine microbes that are launched into the atmosphere via SSA remain metabolically active. The retention of microbial metabolic activity after ejection into the atmosphere has major implications for climate and human health. Previous work has shown that enzymes in SSA can directly alter SSA chemistry as well as atmospheric chemistry via coagulation with existing particles [*Malfatti et al., 2019*]. In a similar fashion, metabolically active microbes in SSA can alter atmospheric chemistry via continuous processing of organic matter after ejection from the ocean [*Vaitilingom et al., 2013; Klein et al., 2016*].

By monitoring the metabolic activity over the course of a phytoplankton bloom, these studies show that metabolic activity in both seawater and SSA are dynamic and closely tied to the biological state of the ocean. The greatest changes are observed after the peak of a phytoplankton bloom. Changes in the metabolic activity per cell also occur at different times during a phytoplankton bloom, with declining metabolic activity per cell observed over time in

seawater and increasing activity per cell occurring over time in SSA. These trends in seawater and SSA, along with the microbial community structure temporal trends, suggest that SSA metabolic activity is enhanced due to shifts in the microbe community structure and the selective transfer of active species. Additionally, high metabolic activity correlates with DIC and HULIS, which indicates that active microbes impact both the organic and inorganic pools in seawater. This study emphasizes the critical role that active microbes in the chemistry of the ocean and the atmosphere.

6.6 Acknowledgments

The authors would like to thank the National Science Foundation and the Center for Aerosol Impacts on the Chemistry of the Environment (CAICE), a Center for Chemical Innovation (CHE-1801971) for funding this project.

Chapter 6 is in preparation: Santander, M.V.,* Malfatti, F.,* Pendergraft, M.A., Dinasquet, J., Mayer, K.J., Sauer, J.S., Lee, C.L., Prather, K.A., "Metabolically Active Microbes in Sea Spray Aerosols Cycle Inorganic and Organic Carbon Pools: from Single Cells to Bulk Fluorescence-based Analysis During a Phytoplankton Bloom." The dissertation author was the co-primary investigator and co-author of this paper. Authors denoted with * contributed equally. M.V.S., F.M., and K.A.P. designed the experiments. M.V.S. and F.M. analyzed the data, all coauthor participated in the experiments, M.V.S. and F.M. analyzed the data and wrote the paper.

6.7 Supporting Information

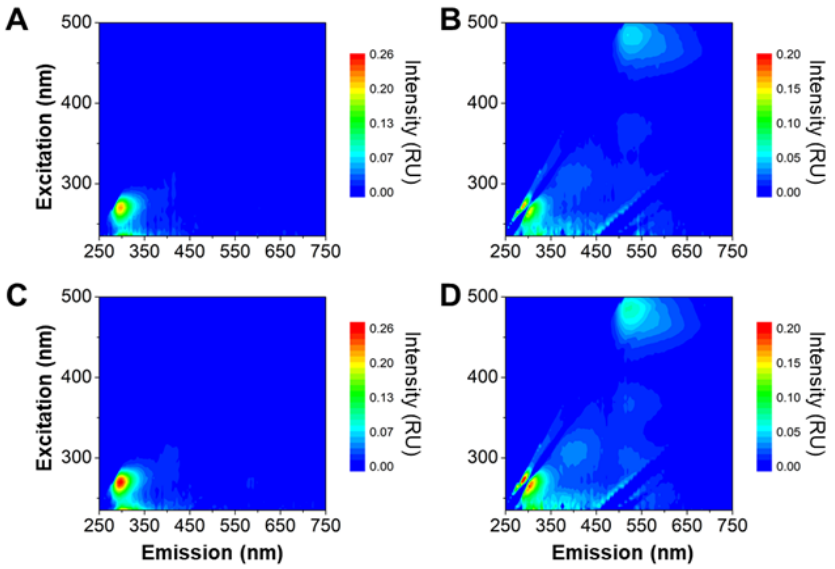

Figure 6.9. Select EEM spectra of SSA generated from two MARTS during the BEAST experiment before (left) and after (right) staining with RG: SSA from a MART with normal phytoplankton bloom progression (a, b) and SSA from a MART after bacteria isolates addition, before and after RSG staining (c, d).

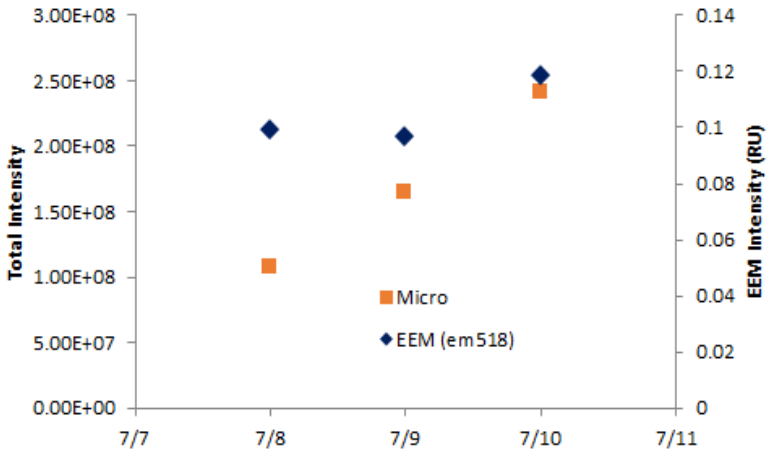

Figure 6.10. Fluorescence intensity over 3 days of Experiment-1 determined by microscopy (orange squares) and EEM (blue diamonds)

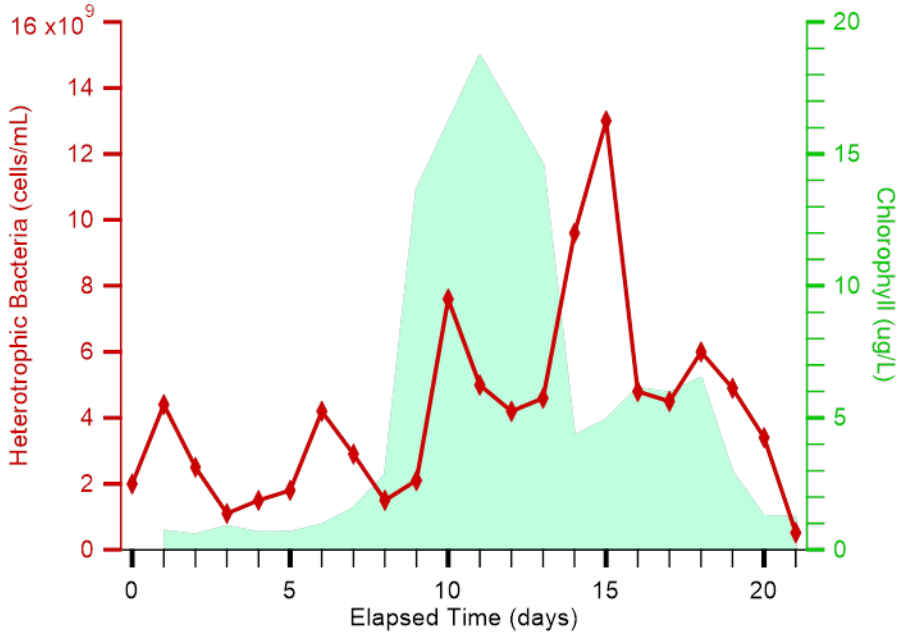

Figure 6.11. Changes in chlorophyll-a and heterotrophic bacteria over time during the Experiment-2 phytoplankton bloom.

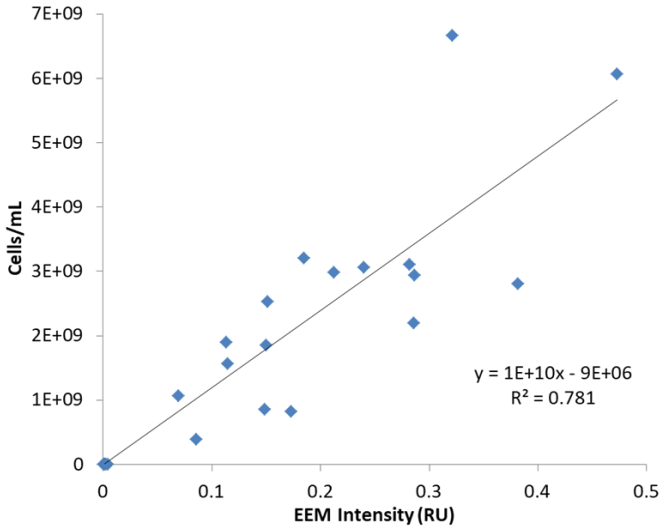

Figure 6.12. Correlation between metabolically active cells and dye EEM intensity (RU), in Experiment-2.

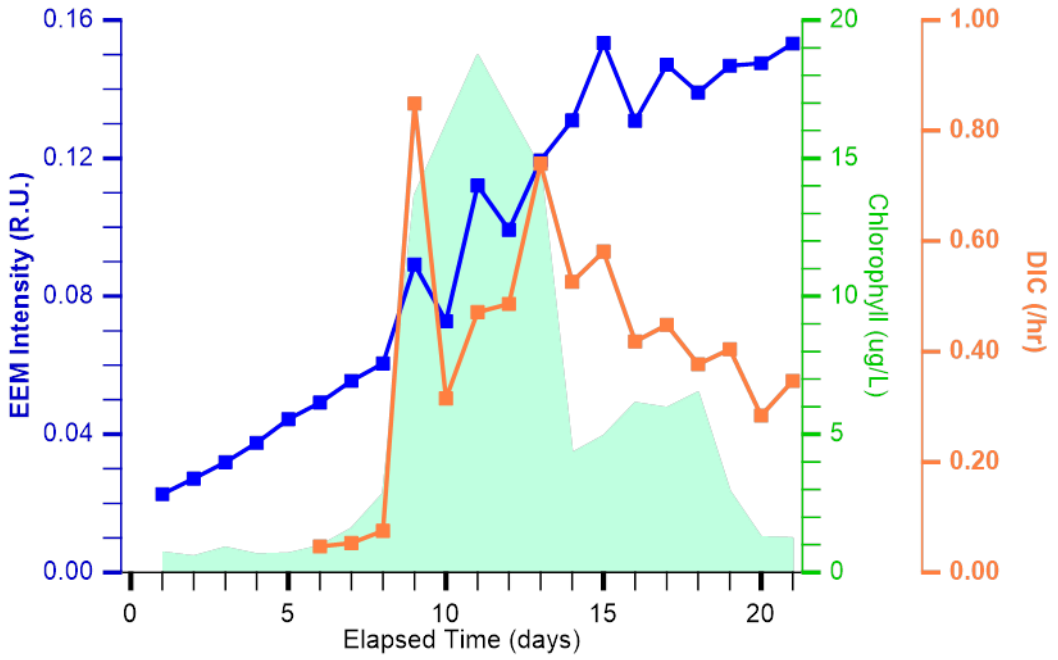

Figure 6.13. Changes in chlorophyll-a, HULIS, and DIC over time during the Experiment-2 phytoplankton bloom.

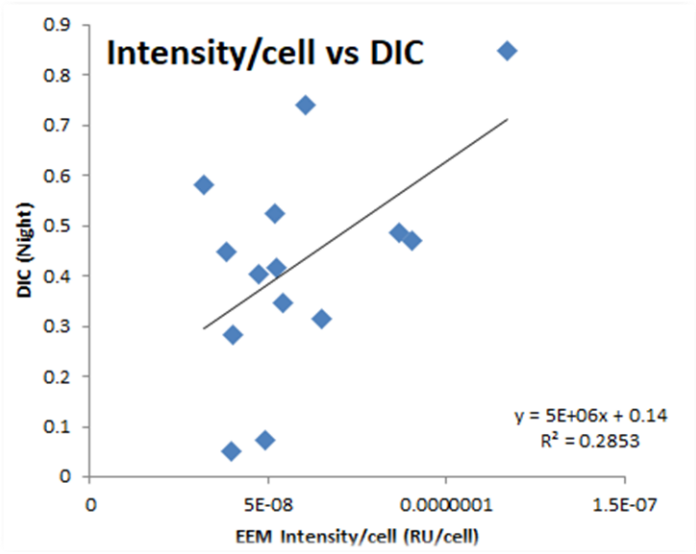

Figure 6.14. Correlation between EEM intensity normalized to flow cytometry cell counts of bulk seawater and DIC concentrations, in Experiment-2.

Table 6.1. Spearman correlation coefficients for seawater and SSA metrics. Coefficients with magnitudes greater than or equal to 0.6 are listed in bold.

	Total Activity	Active Cells	Activity/ cell	HULIS	DIC	Bacteria Production	Hetero-trophic Bacteria	SSA Total Activity	SSA Active Cells	SSA Activity/ cell	SSA HULIS	SSML Bacteria Production
Total Activity	1	**0.7**	0.3	**0.6**	**0.7**	0.2	**0.9**	0.2	0.3	-0.1	-0.2	0.3
Active Cells		1	0	**0.9**	**0.7**	-0.3	**0.9**	0.2	-0.2	**0.6**	-0.3	**0.8**
Activity/cell			1	0.1	0.3	-0.2	0.1	0.3	0.2	**-0.6**	**-0.7**	0.2
HULIS				1	**0.9**	**-0.6**	**0.7**	**0.6**	0.1	0.5	**-0.6**	**0.9**
DIC					1	-0.5	**0.6**	**0.8**	0.5	0.1	**-0.7**	**0.7**
Bacteria Production						1	0.1	**-0.7**	0	-0.4	**0.8**	**-0.8**
Heterotrophic Bacteria							1	0	-0.1	0.3	-0.1	0.5
SSA Total Activity								1	**0.7**	-0.1	**-0.8**	0.5
SSA Active Cells									1	**-0.6**	-0.3	-0.2
SSA Activity/cell										1	0.1	**0.6**
SSA HULIS											1	**-0.7**
SSML Bacteria Production												1

Table 6.2. Calculated t values for correlations between various seawater and SSA metrics.

	Total Activity	Active Cells	Activity per cell	HULIS	DIC	Bacteria Production	Hetero-trophic Bacteria	SSA Total Activity	SSA Active Cells	SSA Activity per cell	SSA HULIS	SSML Bacteria Production
Total Activity	-	3.80	1.22	3.27	3.67	0.79	9.00	0.54	0.77	-0.25	-0.87	1.09
Active Cells		-	0.00	8.00	3.53	-1.09	8.00	0.41	-0.41	1.50	-1.22	4.00
Activity per cell			-	0.39	1.13	-0.71	0.39	0.63	0.41	-1.50	-3.80	0.61
HULIS				-	7.73	-2.90	4.27	1.98	0.25	1.41	-3.18	7.15
DIC					-	-1.83	2.81	2.98	1.15	0.20	-3.67	2.59
Bacteria Production						-	0.39	-2.19	0.00	-0.98	4.99	-4.62
Heterotrophic Bacteria							-	0.00	-0.25	0.77	-0.43	2.08
SSA Total Activity								-	2.40	-0.25	-3.53	1.29
SSA Active Cells									-	-1.84	-0.77	-0.46
SSA Activity per cell										-	0.25	1.68
SSA HULIS											-	-3.25
SSML Bacteria Production												-

6.8 References

Asselman, J., E. Van Acker, M. De Rijcke, L. Tilleman, F. Van Nieuwerburgh, J. Mees, K. A. C. De Schamphelaere and C. R. Janssen. Marine biogenics in sea spray aerosols interact with the mTOR signaling pathway. *Scientific Reports*. **2019**, *9*(1): 675.

Azam, F., T. Fenchel, J. G. Field, J. S. Gray, L. A. Meyer-Reil and F. Thingstad. The ecological role of water-column microbes in the sea. *Marine Ecology Progress Series*. **1983**, *10*(3): 257-263.

Azam, F. and F. Malfatti. Microbial structuring of marine ecosystems. *Nature Reviews Microbiology*. **2007**, *5*(10): 782-791.

Bertram, T. H., R. E. Cochran, V. H. Grassian and E. A. Stone. Sea spray aerosol chemical composition: elemental and molecular mimics for laboratory studies of heterogeneous and multiphase reactions. *Chemical Society Reviews*. **2018**, *47*(7): 2374-2400.

Bidle, K. D. and F. Azam. Bacterial control of silicon regeneration from diatom detritus: Significance of bacterial ectohydrolases and species identity. *Limnology and Oceanography*. **2001**, *46*(7): 1606-1623.

Brown, T. E. and F. L. Richards. Effect of growth environment on physiology of algae - light intensity. *Journal of Phycology*. **1968**, *4*(1): 38.

Brussaard, C. P. D. Optimization of procedures for counting viruses by flow cytometry. *Applied and Environmental Microbiology*. **2004**, *70*(3): 1506-1513.

Cavicchioli, R., W. J. Ripple, K. N. Timmis, F. Azam, L. R. Bakken, M. Baylis, M. J. Behrenfeld, A. Boetius, P. W. Boyd, A. T. Classen, T. W. Crowther, R. Danovaro, C. M. Foreman, J. Huisman, D. A. Hutchins, J. K. Jansson, D. M. Karl, B. Koskella, D. B. Mark Welch, J. B. H. Martiny, M. A. Moran, V. J. Orphan, D. S. Reay, J. V. Remais, V. I. Rich, B. K. Singh, L. Y. Stein, F. J. Stewart, M. B. Sullivan, M. J. H. van Oppen, S. C. Weaver, E. A. Webb and N. S. Webster. Scientists' warning to humanity: microorganisms and climate change. *Nat Rev Microbiol*. **2019**, *17*(9): 569-586.

Collins, D. B., D. F. Zhao, M. J. Ruppel, O. Laskina, J. R. Grandquist, R. L. Modini, M. D. Stokes, L. M. Russell, T. H. Bertram, V. H. Grassian, G. B. Deane and K. A. Prather. Direct aerosol chemical composition measurements to evaluate the physicochemical differences between controlled sea spray aerosol generation schemes. *Atmos. Meas. Tech.* **2014**, *7*(11): 3667-3683.

Cologgi, D. L., S. Lampa-Pastirk, A. M. Speers, S. D. Kelly and G. Reguera. Extracellular reduction of uranium via Geobacter conductive pili as a protective cellular mechanism. *Proceedings of the National Academy of Sciences of the United States of America*. **2011**, *108*(37): 15248-15252.

Falkowski, P. G., T. Fenchel and E. F. Delong. The microbial engines that drive Earth's biogeochemical cycles. *Science*. **2008**, *320*(5879): 1034-1039.

Fernandez, A. E., G. S. Lewis and S. V. Hering. Design and laboratory evaluation of a sequential spot sampler for time-resolved measurement of airborne particle composition. *Aerosol Science and Technology*. **2014**, *48*(6): 655-663.

Gantt, B. and N. Meskhidze. The physical and chemical characteristics of marine primary organic aerosol: a review. *Atmospheric Chemistry and Physics*. **2013**, *13*(8): 3979-3996.

Gasol, J. M. and J. Aristegui. Cytometric evidence reconciling the toxicity and usefulness of CTC as a marker of bacterial activity. *Aquatic Microbial Ecology*. **2007**, *46*(1): 71-83.

Gasol, J. M. and P. A. Del Giorgio. Using flow cytometry for counting natural planktonic bacteria and understanding the structure of planktonic bacterial communities. *Scientia Marina*. **2000**, *64*(2): 197-224.

Guillard, R. R. and J. H. Ryther. Studies of marine planktonic diatoms .1. Cyclotella nana Hustedt, and Detonula confervacea (Cleve) Gran. *Canadian Journal of Microbiology*. **1962**, *8*(2): 229.

Hasenecz, E. S., T. Jayarathne, M. A. Pendergraft, M. V. Santander, K. J. Mayer, J. Sauer, C. Lee, W. S. Gibson, S. M. Kruse, F. Malfatti, K. A. Prather and E. A. Stone. Marine bacteria affect saccharide enrichment in sea spray aerosol during a phytoplankton bloom. *ACS Earth and Space Chemistry*. **2020**, *4*(9): 1638-1649.

Hatzenpichler, R., V. Krukenberg, R. L. Spietz and Z. J. Jay. Next-generation physiology approaches to study microbiome function at single cell level. *Nature Reviews Microbiology*. **2020**, *18*(4): 241-256.

Hessen, D. O. and L. J. Tranvik (1998). Aquatic humic substances: ecology and biogeochemistry. Berlin; New York, Springer.

Kalyuzhnaya, M. G., M. E. Lidstrom and L. Chistoserdova. Real-time detection of actively metabolizing microbes by redox sensing as applied to methylotroph populations in Lake Washington. *Isme Journal*. **2008**, *2*(7): 696-706.

Klein, A. M., B. J. M. Bohannan, D. A. Jaffe, D. A. Levin and J. L. Green. Molecular evidence for metabolically active bacteria in the atmosphere. *Frontiers in Microbiology*. **2016**, *7*.

Konopka, M. C., T. J. Strovas, D. S. Ojala, L. Chistoserdova, M. E. Lidstrom and M. G. Kalyuzhnaya. Respiration response imaging for real-time detection of microbial function at the single-cell level. *Applied and Environmental Microbiology*. **2011**, *77*(1): 67-72.

Lawaetz, A. J. and C. A. Stedmon. Fluorescence intensity calibration using the raman scatter peak of water. *Applied Spectroscopy*. **2009**, *63*(8): 936-940.

Leck, C. and K. E. Bigg. Comparison of sources and nature of the tropical aerosol with the summer high Arctic aerosol. *Tellus B: Chemical and Physical Meteorology*. **2017**, *60*(1): 118-126.

Lee, C., C. M. Sultana, D. B. Collins, M. V. Santander, J. L. Axson, F. Malfatti, G. C. Cornwell, J. R. Grandquist, G. B. Deane, M. D. Stokes, F. Azam, V. H. Grassian and K. A. Prather. Advancing model systems for fundamental laboratory studies of sea spray aerosol using the microbial loop. *J Phys Chem A*. **2015**, *119*(33): 8860-8870.

Long, R. A. and F. Azam. Antagonistic interactions among marine pelagic bacteria. *Applied and Environmental Microbiology*. **2001**, *67*(11): 4975-4983.

Malfatti, F., C. Lee, T. Tinta, M. A. Pendergraft, M. Celussi, Y. Y. Zhou, C. M. Sultana, A. Rotter, J. L. Axson, D. B. Collins, M. V. Santander, A. L. A. Morales, L. I. Aluwihare, N. Riemer, V. H. Grassian, F. Azam and K. A. Prather. Detection of active microbial enzymes in nascent sea spray aerosol: implications for atmospheric chemistry and climate. *Environmental Science & Technology Letters*. **2019**, *6*(3): 171-177.

Marie, D., F. Partensky, S. Jacquet and D. Vaulot. Enumeration and cell cycle analysis of natural populations of marine picoplankton by flow cytometry using the nucleic acid stain SYBR Green I. *Applied and Environmental Microbiology*. **1997**, *63*(1): 186-193.

Michaud, J. M., L. R. Thompson, D. Kaul, J. L. Espinoza, R. A. Richter, Z. Z. Xu, C. Lee, K. M. Pham, C. M. Beall, F. Malfatti, F. Azam, R. Knight, M. D. Burkart, C. L. Dupont and K. A. Prather. Taxon-specific aerosolization of bacteria and viruses in an experimental ocean-atmosphere mesocosm. *Nature Communications*. **2018**, *9*.

Murphy, K. R. A note on determining the extent of the water raman peak in fluorescence spectroscopy. *Applied Spectroscopy*. **2011**, *65*(2): 233-236.

Patterson, J. P., D. B. Collins, J. M. Michaud, J. L. Axson, C. M. Sultana, T. Moser, A. C. Dommer, J. Conner, V. H. Grassian, M. D. Stokes, G. B. Deane, J. E. Evans, M. D. Burkart, K. A. Prather and N. C. Gianneschi. Sea spray aerosol structure and composition using cryogenic transmission electron microscopy. *Acs Central Science*. **2016**, *2*(1): 40-47.

Pedler, B. E., L. I. Aluwihare and F. Azam. Single bacterial strain capable of significant contribution to carbon cycling in the surface ocean. *Proceedings of the National Academy of Sciences of the United States of America*. **2014**, *111*(20): 7202-7207.

Pirt, S. J. The maintenance energy of bacteria in growing cultures. *Proc R Soc Lond B Biol Sci*. **1965**, *163*(991): 224-231.

Prather, K. A., T. H. Bertram, V. H. Grassian, G. B. Deane, M. D. Stokes, P. J. DeMott, L. I. Aluwihare, B. P. Palenik, F. Azam, J. H. Seinfeld, R. C. Moffet, M. J. Molina, C. D. Cappa, F. M. Geiger, G. C. Roberts, L. M. Russell, A. P. Ault, J. Baltrusaitis, D. B. Collins, C. E. Corrigan, L. A. Cuadra-Rodriguez, C. J. Ebben, S. D. Forestieri, T. L. Guasco, S. P. Hersey, M. J. Kim, W. F. Lambert, R. L. Modini, W. Mui, B. E. Pedler, M. J. Ruppel, O. S. Ryder, N. G. Schoepp, R. C. Sullivan and D. F. Zhao. Bringing the ocean into the laboratory to probe the chemical complexity of sea spray aerosol. *Proceedings of the National Academy of Sciences of the United States of America*. **2013**, *110*(19): 7550-7555.

Proctor, L. M. and A. C. Souza. Method for enumeration of 5-cyano-2,3-ditoyl tetrazolium chloride (CTC)-active cells and cell-specific CTC activity of benthic bacteria in riverine, estuarine and coastal sediments. *Journal of Microbiological Methods*. **2001**, *43*(3): 213-222.

Rashid, M. A. (1985). Geochemistry of marine humic compounds. New York, Springer-Verlag.

Repeta, D. J. and R. M. Boiteau (2017). Organic nutrient chemistry and the marine microbiome. The chemistry of microbiomes: proceedings of a seminar series. Washington (DC), National Academies Press (US).

Rodriguez, G. G., D. Phipps, K. Ishiguro and H. F. Ridgway. Use of a fluorescent redox probe for direct visualization of actively respiring bacteria. *Applied and Environmental Microbiology*. **1992**, *58*(6): 1801-1808.

Samo, T. J., S. Smriga, F. Malfatti, B. P. Sherwood and F. Azam. Broad distribution and high proportion of protein synthesis active marine bacteria revealed by click chemistry at the single cell level (vol 1, 48, 2014). *Frontiers in Marine Science*. **2014**, *1*.

Santander, M. V., B. A. Mitts, M. A. Pendergraft, J. Dinasquet, C. Lee, A. N. Moore, L. B. Cancelada, K. A. Kimble, F. Malfatti and K. A. Prather. Tandem fluorescence measurements of organic matter and bacteria released in sea spray aerosols. *Environmental Science & Technology*. **2021**, *55*(8): 5171-5179.

Sauer, J. S., K. J. Mayer, C. Lee, M. R. Alves, S. Amiri, C. J. Bahaveolos, E. B. Franklin, D. R. Crocker, D. Dang, J. Dinasquet, L. A. Garofalo, C. P. Kaluarachchi, D. B. Kilgour, L. E. Mael, B. A. Mitts, D. R. Moon, A. N. Moore, C. K. Morris, C. A. Mullenmeister, C. M. Ni, M. A. Pendergraft, D. Petras, R. M. C. Simpson, S. Smith, P. R. Tumminello, J. L. Walker, P. J. DeMott, D. K. Farmer, A. H. Goldstein, V. H. Grassian, J. S. Jaffe, F. Malfatti, T. R. Martz, J. H. Slade, A. V. Tivanski, T. H. Bertram, C. D. Cappa and K. A. Prather. The sea spray chemistry and particle evolution study (SeaSCAPE): overview and experimental methods. *Environ Sci Process Impacts*. **2022**, *24*(2): 290-315.

Schill, S. R., D. B. Collins, C. Lee, H. S. Morris, G. A. Novak, K. A. Prather, P. K. Quinn, C. M. Sultana, A. V. Tivanski, K. Zimmermann, C. D. Cappa and T. H. Bertram. The impact of aerosol particle mixing state on the hygroscopicity of sea spray aerosol. *ACS Central Science*. **2015**, *1*(3): 132-141.

Schindelin, J., I. Arganda-Carreras, E. Frise, V. Kaynig, M. Longair, T. Pietzsch, S. Preibisch, C. Rueden, S. Saalfeld, B. Schmid, J. Y. Tinevez, D. J. White, V. Hartenstein, K. Eliceiri, P. Tomancak and A. Cardona. Fiji: an open-source platform for biological-image analysis. *Nature Methods*. **2012**, *9*(7): 676-682.

Sieracki, M. E., T. L. Cucci and J. Nicinski. Flow cytometric analysis of 5-cyano-2,3-ditolyl tetrazolium chloride activity of marine bacterioplankton in dilution cultures. *Applied and Environmental Microbiology*. **1999**, *65*(6): 2409-2417.

Singer, E., M. Wagner and T. Woyke. Capturing the genetic makeup of the active microbiome in situ. *Isme Journal*. **2017**, *11*(9): 1949-1963.

Smets, W., S. Moretti, S. Denys and S. Lebeer. Airborne bacteria in the atmosphere: presence, purpose, and potential. *Atmospheric Environment*. **2016**, *139*: 214-221.

Stokes, M. D., G. B. Deane, K. Prather, T. H. Bertram, M. J. Ruppel, O. S. Ryder, J. M. Brady and D. Zhao. A marine aerosol reference tank system as a breaking wave analogue for the

production of foam and sea-spray aerosols. *Atmospheric Measurement Techniques*. **2013**, *6*(4): 1085-1094.

Vaitilingom, M., L. Deguillaume, V. Vinatier, M. Sancelme, P. Amato, N. Chaumerliac and A. M. Delort. Potential impact of microbial activity on the oxidant capacity and organic carbon budget in clouds. *Proceedings of the National Academy of Sciences of the United States of America*. **2013**, *110*(2): 559-564.

Wang, X. F., C. M. Sultana, J. Trueblood, T. C. J. Hill, F. Malfatti, C. Lee, O. Laskina, K. A. Moore, C. M. Beall, C. S. McCluskey, G. C. Cornwell, Y. Y. Zhou, J. L. Cox, M. A. Pendergraft, M. V. Santander, T. H. Bertram, C. D. Cappa, F. Azam, P. J. DeMott, V. H. Grassian and K. A. Prather. Microbial control of sea spray aerosol composition: a tale of two blooms. *ACS Central Science*. **2015**, *1*(3): 124-131.

Williams, T. J., F. Joux, F. M. Lauro, S. Matallana-Surget and R. Cavicchioli (2011). Physiology of marine oligotrophic ultramicrobacteria. Extremophiles Handbook. K. Horikoshi. Tokyo, Springer Japan**:** 1179-1199.

Chapter 7. Conclusions and Future Work

7.1 Synopsis

The studies in this dissertation investigate the transfer of humic-like substances (HULIS) and proteinaceous substances from seawater to sea spray aerosol (SSA). Using laboratory mesocosms and advanced SSA generation methods, current understanding of these fluorescent materials and microbes, their physicochemical properties, and factors leading to their sea-air transfer has been vastly improved. By coupling two commonly used fluorescence techniques, a fluorescence signature for SSA was identified and provides a framework for future work to use fluorescence spectroscopy to study SSA in the real, complex atmosphere. Additionally, by examining the temporal evolution of different fluorescence signatures in the seawater, the sea surface microlayer (SSML) and SSA, factors affecting sea-air transfer were found to be unique for each class of molecules investigated. Specifically for HULIS, marine bacterial enzymes were found to be likely drivers for changes in humic substance chemistry and for sea-air transfer. By combining fluorescence and seawater size distributions, EEM spectroscopy was found to be a reliable indicator for HULIS relative abundance despite natural marine aggregation processes. The presence of cations was found to play a major role in the reliability of fluorescence, likely due to the shielding of fluorescent moieties. Finally, with respect to seawater microbes, a technique for measuring metabolic activity for microbes in SSA in a laboratory setting has been developed. Using this approach, metabolically active microbes were detected in SSA and are shown to exhibit changing activity that reflects seawater microbial dynamics.

7.2 Conclusions

7.2.1 Tandem Fluorescence Measurements of Organic Matter and Bacteria Released in Sea Spray Aerosols

While SSA has been identified as a source of biological particles in the atmosphere, studying these bioaerosols is challenging in the real atmosphere due to interference from additional non-marine sources [*Despres et al., 2012; Frohlich-Nowoisky et al., 2016*]. In Chapter 2, SSA fluorescence was investigated by combining two commonly used techniques: online single particle fluorescence with a Wideband Integrated Bioaerosol Sensor (WIBS) and offline bulk fluorescence using excitation-emission matrix (EEM) spectroscopy. A unique fluorescence signature for isolated SSA was characterized and shows similar trends in response to changing ocean microbiology, demonstrating the potential to effectively use WIBS aerosol measurements in combination with EEM bulk solution measurements. More importantly, this study revealed, for the first time, a size segregated emission of fluorescent species in SSA. The fluorescence signature for marine bacteria isolates was also characterized and was found to exhibit similar peaks to those found in isolated, nascent SSA, suggesting that marine bacteria contribute to SSA fluorescence. The characterization of SSA fluorescence in this study provides a valuable basis for future studies to investigate marine-derived biological aerosols in the real atmosphere.

7.2.2 Factors Controlling the Transfer of Biogenic Organic Species from Seawater to Sea Spray Aerosol

Fluorescence signals corresponding to specific classes of organic matter have been identified in SSA [*Mostofa, 2013*]. Chapter 3 provides an overview of how the signals for these molecular classes change over the course of a phytoplankton bloom across the bulk seawater, the

SSML, and the SSA. Specifically, the three classes: chlorophyll-a, protein-like substances, and HULIS, have been shown here to exhibit major differences in terms of when these molecules are observed in SSA over the course of a phytoplankton bloom. These differences provide new insights into the factors that control their ejection from seawater to SSA.

The temporal trends in SSA for these different signals together reveal three specific aspects of the sea-air transfer of organic matter. First, the lack of correspondence for signals in SSA with the main peak of chlorophyll in the bulk seawater suggests that phytoplankton are not the main drivers for sea-air transfer of organic matter, but instead play a role in producing the precursors for the molecules that are ultimately transferred to SSA. Second, the trends in SSA differ from the respective trends in bulk seawater, suggesting that factors in addition to concentration are vital for ejection. Processes that change size or chemical properties, such as microbial degradation or increased surface adsorption, likely play a major role in transfer [*Cochran et al., 2016*]. Lastly, each molecular class was identified in SSA at different times, suggesting that the sea-air transfer of different molecular classes is affected by factors unique to each class. The temporal behavior of these fluorescence signals revealed that sea-air transfer is driven by processes in the ocean that transform the organic matter into species more suitable for transfer.

7.2.3 Bacterial Control of Marine Humic-like Substance Production, Composition, Size, and Transfer to Sea Spray Aerosols During Phytoplankton Blooms

In Chapter 4, the physicochemical properties of HULIS in seawater are investigated over the course of multiple phytoplankton bloom mesocosm experiments. All experiments showed a correlation between humic fluorescence and dissolved organic carbon. Additionally, size

fractionation experiments revealed that over 80% of the humic signal remained in the smallest size fraction even after the peak of intense phytoplankton blooms. Thus it is likely that the HULIS in SSA originates from the dissolved organic matter pool.

The enzymatic processes occurring in seawater alter the chemical nature of organic matter and can affect transfer to SSA [*Wang et al., 2015*]. However, no studies have investigated the link between enzyme activities and HULIS production, their chemical composition in seawater, or their transfer to SSA. In the mesocosm experiments described in this work, HULIS intensity was enhanced in the days following bacteria addition compared to a mesocosm with no bacteria addition. This enhancement coincided with a sharp increase in alkaline phosphatase activity. Additionally, these experiments revealed high enzymatic activities that coincide with a spectral shift in seawater HULIS fluorescence and an increase in HULIS in SSA. Thus, the bacterial processing of organic matter plays a major role in altering seawater HULIS chemistry and controlling the transfer of HULIS from seawater to SSA.

7.2.4 Assessing Aggregation as a Potential Artifact Impacting the Fluorescence Intensity of Humic Substances in Seawater

Humic substances are known to form aggregates in the marine environment [*Chin et al., 1998; Verdugo et al., 2004*]. Aggregation results in many chromophores to undergo "aggregation-caused quenching" and decreases their fluorescence intensity [*Lakowicz, 2006; Chen et al., 2019*]. However, not all chromophores exhibit the same effect due to aggregation and the impact of aggregation on humic substance fluorescence has not been fully explored for marine systems. Despite this gap in knowledge, many studies use fluorescence as an indicator for humic substance abundance with the assumption that aggregation does not impact fluorescence

intensity [*Wei et al., 2016; Wang et al., 2017; Yamin et al., 2017; Arai et al., 2018; Kwon et al., 2018*]. Chapter 5 explores the relationship between aggregation and fluorescence intensity for humic substances during laboratory phytoplankton bloom experiments and controlled experiments.

Large daily fluctuations in seawater particle size distributions over the course of multiple phytoplankton bloom experiments, in contrast to the HULIS fluorescence signals, suggest that fluorescence is a robust measurement for HULIS relative abundance despite naturally occurring aggregation processes. Further studies of spontaneous and induced aggregation and EDTA additions suggest the binding of cations likely leads to the shielding of fluorescent moieties, preventing a decrease in fluorescence intensity. The high divalent cation binding in the marine environment [*Mantoura et al., 1978*] suggests that aggregation does not affect HULIS fluorescence. This study can be used to inform future investigations seeking to characterize HULIS abundance in the marine environment.

7.2.5 Metabolically Active Microbes in Sea Spray Aerosols Cycle Inorganic and Organic Carbon Pools: from Single Cells to Bulk Fluorescence-based Analysis During a Phytoplankton Bloom

Bacteria have been shown in previous studies to be transferred from seawater to SSA [*Patterson et al., 2016; Michaud et al., 2018; Malfatti et al., 2019*]. Metabolically active microbes in the atmosphere have the potential to impact aerosol and atmospheric chemistry [*Smets et al., 2016*]. However, the metabolic activity of the microbes in SSA has not been investigated [*Smets et al., 2016*]. Recent work has postulated that microbes in that atmosphere are metabolically active [*Klein et al., 2016; Malfatti et al., 2019*]. Chapter 6 focuses on

investigations into the metabolic activity of microbes in isolated SSA. Metabolic activity was assessed using RedoxSensor Green, a dye that targets reductases in the cell, combined with three different fluorescence techniques: EEM spectroscopy, laser scanning confocal microscopy (LSCM) and flow cytometry. These three techniques were used to study metabolic activity in SSA during a phytoplankton bloom experiment and for marine bacteria isolates. From this study, a method for investigating metabolic activity in aerosols has been proposed and could be applied to future work focusing on airborne microbes in the real atmosphere.

This work reports, for the first time, the identification of metabolically active bacteria in isolated SSA. Further studies monitoring metabolic activity over the course of a phytoplankton bloom experiment revealed that the greatest changes in activity occurred after the peak of the bloom, indicating that SSA activity is directly tied to seawater microbial dynamics. Additionally, analysis of the intensity per cell reveals opposite trends between the activities per cell in the seawater versus the SSA. These trends, combined with size profiles of active microbes, suggest that metabolic activity in SSA is enhanced due to the selective transfer of small, active bacteria. Thus, not only do active microbes play a central role in shaping the inorganic and organic carbon pools in seawater, but the release of the active microbes in SSA can also impact the chemistry of our atmosphere.

7.3 Future Work

In this dissertation, marine microbiology was investigated as the main driver for changing seawater and SSA chemistry. While marine microbiology strongly influences the links between the ocean and the atmosphere, several areas of research have not been fully explored. Three of these areas include: 1) the light-initiated production and *in situ* formation of HULIS in SSA, 2)

HULIS photochemistry and role as a photosensitizer, and 3) the HULIS impact on cloud properties.

Solar radiation drives many atmospheric reaction processes, such as atmospheric ozone and hydroxyl radical formation and secondary aerosol formation [*Finlayson-Pitts and Pitts, 2000; Ervens et al., 2011*]. Previous work has shown that photochemistry has the potential to not only impact the formation of humic substances, but also to influence its breakdown and its climate impacts [*Kieber et al., 1997; Catala et al., 2016; Wang et al., 2020*]. Additionally, previous measurements of HULIS in the ocean have suggested that sunlight impacts HULIS abundance in the ocean's surface water [*Catala et al., 2016*]. Thus future work focusing on the influence of sunlight on the production and degradation of marine HULIS in a controlled setting can fully elucidate the main drivers for HULIS abundance in seawater and SSA. For example, future experiments could examine the light-initiated production of HULIS from both bottom-up (using biomolecules like triglycerides) [*Kieber et al., 1997*] and top-down (with natural seawater complexity) approaches. Comparing these HULIS structures and optical properties to those from seawater, soil, or biomass burning would shed light on the relevance of different sources to atmospheric HULIS. These experiments would be a first step towards unraveling the relative contributions of direct HULIS sea-air transfer and *in situ* formation of HULIS in SSA and in the complex atmosphere.

In addition to the photochemical production of HULIS, previous studies have focused on the role of humic substances as a photosensitizer [*Ciuraru et al., 2015; Shrestha et al., 2018; Tsui and McNeill, 2018*]. In its excited electronic state (often triplet-state), chromophoric dissolved organic matter including HULIS can transfer energy to other molecules to initiate unique reactions in both seawater and SSA [*Chen et al., 2018; Navea and Grassian, 2018;*

Shrestha et al., 2018; Trueblood et al., 2019; Zhou et al., 2019; Luo et al., 2020; Guo et al., 2021]. This energy transfer process also leads to the formation of atmospherically-relevant, highly reactive species, such as HONO [*Bartels-Rausch et al., 2010; Han et al., 2016; Han et al., 2017; Yang et al., 2018; Garcia et al., 2021*]. Thus, atmospheric HULIS has the potential to initiate reactions that can drastically alter marine aerosol and atmospheric chemistry. Future experiments investigating the excited state properties of marine HULIS and mechanisms for photosensitized reactions can improve our understanding of how the ocean transforms atmospheric chemistry.

Lastly, while it is known that HULIS can transfer from seawater to SSA, further studies into the climate and atmospheric chemistry impact of HULIS in SSA are necessary. For example, the formation of HULIS has the potential to affect surface tension [*Kiss et al., 2005*], a variable that has drastic effects on the cloud nucleating ability of aerosols [*Forestieri et al., 2018*]. Thus future experiments monitoring surface tension during HULIS formation or production can directly link the impact of HULIS to SSA cloud properties. In combination with the microbiologically-focused studies described in this dissertation, future work investigating photochemical processes and atmospheric impact can reveal a complete picture of the role of chromophoric organic matter in the ocean and the atmosphere.

7.4 Acknowledgements

Francesca Malfatti and Christopher Lee are acknowledged for assisting in the editing of this chapter.

7.5 References

Arai, K., S. Wada, K. Shimotori, Y. Omori and T. Hama. Production and degradation of fluorescent dissolved organic matter derived from bacteria. *Journal of Oceanography*. **2018**, *74*(1): 39-52.

Bartels-Rausch, T., M. Brigante, Y. F. Elshorbany, M. Ammann, B. D'Anna, C. George, K. Stemmler, M. Ndour and J. Kleffmann. Humic acid in ice: photo-enhanced conversion of nitrogen dioxide into nitrous acid. *Atmospheric Environment*. **2010**, *44*(40): 5443-5450.

Catala, T. S., X. A. Alvarez-Salgado, J. Otero, F. Iuculano, B. Companys, B. Horstkotte, C. Romera-Castillo, M. Nieto-Cid, M. Latasa, X. A. G. Moran, J. M. Gasol, C. Marrase, C. A. Stedmon and I. Reche. Drivers of fluorescent dissolved organic matter in the global epipelagic ocean. *Limnology and Oceanography*. **2016**, *61*(3): 1101-1119.

Chen, Y., X. Zhang and S. X. Feng. Contribution of the excited triplet state of humic acid and superoxide radical anion to generation and elimination of phenoxyl radical. *Environmental Science & Technology*. **2018**, *52*(15): 8283-8291.

Chen, Y. C., J. W. Y. Lam, R. T. K. Kwok, B. Liu and B. Z. Tang. Aggregation-induced emission: fundamental understanding and future developments. *Materials Horizons*. **2019**, *6*(3): 428-433.

Chin, W. C., M. V. Orellana and P. Verdugo. Spontaneous assembly of marine dissolved organic matter into polymer gels. *Nature*. **1998**, *391*(6667): 568-572.

Ciuraru, R., L. Fine, M. van Pinxteren, B. D'Anna, H. Herrmann and C. George. Photosensitized production of functionalized and unsaturated organic compounds at the air-sea interface. *Scientific Reports*. **2015**, *5*.

Cochran, R. E., T. Jayarathne, E. A. Stone and V. H. Grassian. Selectivity across the interface: a test of surface activity in the composition of organic-enriched aerosols from bubble bursting. *Journal of Physical Chemistry Letters*. **2016**, *7*(9): 1692-1696.

Despres, V. R., J. A. Huffman, S. M. Burrows, C. Hoose, A. S. Safatov, G. Buryak, J. Frohlich-Nowoisky, W. Elbert, M. O. Andreae, U. Poschl and R. Jaenicke. Primary biological aerosol particles in the atmosphere: a review. *Tellus Series B-Chemical and Physical Meteorology*. **2012**, *64*.

Ervens, B., B. J. Turpin and R. J. Weber. Secondary organic aerosol formation in cloud droplets and aqueous particles (aqSOA): a review of laboratory, field and model studies. *Atmospheric Chemistry and Physics*. **2011**, *11*(21): 11069-11102.

Finlayson-Pitts, B. J. and J. N. Pitts (2000). Chemistry of the upper and lower atmosphere: theory, experiments, and applications. San Diego, Academic Press.

Forestieri, S. D., S. M. Staudt, T. M. Kuborn, K. Faber, C. R. Ruehl, T. H. Bertram and C. D. Cappa. Establishing the impact of model surfactants on cloud condensation nuclei activity of sea spray aerosol mimics. *Atmospheric Chemistry and Physics*. **2018**, *18*(15): 10985-11005.

Frohlich-Nowoisky, J., C. J. Kampf, B. Weber, J. A. Huffman, C. Pohlker, M. O. Andreae, N. Lang-Yona, S. M. Burrows, S. S. Gunthe, W. Elbert, H. Su, P. Hoor, E. Thines, T. Hoffmann, V. R. Despres and U. Poschl. Bioaerosols in the Earth system: Climate, health, and ecosystem interactions. *Atmospheric Research*. **2016**, *182*: 346-376.

Garcia, S. L. M., S. Pandit, J. G. Navea and V. H. Grassian. Nitrous acid (HONO) formation from the irradiation of aqueous nitrate solutions in the presence of marine chromophoric dissolved organic matter: comparison to other organic photosensitizers. *ACS Earth and Space Chemistry*. **2021**, *5*(11): 3056-3064.

Guo, Z. Y., J. Q. Wang, X. Chen, F. F. Cui, T. T. Wang, C. Z. Zhou, G. B. Song, S. Y. Zhang and J. W. Chen. Photochemistry of dissolved organic matter extracted from coastal seawater: excited triplet-states and contents of phenolic moieties. *Water Research*. **2021**, *188*.

Han, C., W. J. Yang, Q. Q. Wu, H. Yang and X. X. Xue. Heterogeneous photochemical conversion of NO_2 to HONO on the humic acid surface under simulated sunlight. *Environmental Science & Technology*. **2016**, *50*(10): 5017-5023.

Han, C., W. J. Yang, H. Yang and X. X. Xue. Enhanced photochemical conversion of NO_2 to HONO on humic acids in the presence of benzophenone. *Environmental Pollution*. **2017**, *231*: 979-986.

Kieber, R. J., L. H. Hydro and P. J. Seaton. Photooxidation of triglycerides and fatty acids in seawater: Implication toward the formation of marine humic substances. *Limnology and Oceanography*. **1997**, *42*(6): 1454-1462.

Kiss, G., E. Tombacz and H. C. Hansson. Surface tension effects of humic-like substances in the aqueous extract of tropospheric fine aerosol. *Journal of Atmospheric Chemistry*. **2005**, *50*(3): 279-294.

Klein, A. M., B. J. M. Bohannan, D. A. Jaffe, D. A. Levin and J. L. Green. Molecular evidence for metabolically active bacteria in the atmosphere. *Frontiers in Microbiology*. **2016**, *7*.

Kwon, H. K., G. Kim, W. A. Lim and J. W. Park. In-situ production of humic-like fluorescent dissolved organic matter during Cochlodinium polykrikoides blooms. *Estuarine Coastal and Shelf Science*. **2018**, *203*: 119-126.

Lakowicz, J. R. (2006). Principles of fluorescence spectroscopy. New York, Springer.

Luo, M., D. Shemesh, M. N. Sullivan, M. R. Alves, M. S. Song, R. B. Gerber and V. H. Grassian. Impact of pH and NaCl and CaCl2 salts on the speciation and photochemistry of pyruvic acid in the aqueous phase. *Journal of Physical Chemistry A*. **2020**, *124*(25): 5071-5080.

Malfatti, F., C. Lee, T. Tinta, M. A. Pendergraft, M. Celussi, Y. Y. Zhou, C. M. Sultana, A. Rotter, J. L. Axson, D. B. Collins, M. V. Santander, A. L. A. Morales, L. I. Aluwihare, N. Riemer, V. H. Grassian, F. Azam and K. A. Prather. Detection of active microbial enzymes in nascent sea spray aerosol: implications for atmospheric chemistry and climate. *Environmental Science & Technology Letters*. **2019**, *6*(3): 171-177.

Mantoura, R. F. C., A. Dickson and J. P. Riley. The complexation of metals with humic materials in natural waters. *Estuarine and Coastal Marine Science*. **1978**, *6*(4): 387-408.

Michaud, J. M., L. R. Thompson, D. Kaul, J. L. Espinoza, R. A. Richter, Z. Z. Xu, C. Lee, K. M. Pham, C. M. Beall, F. Malfatti, F. Azam, R. Knight, M. D. Burkart, C. L. Dupont and K. A. Prather. Taxon-specific aerosolization of bacteria and viruses in an experimental ocean-atmosphere mesocosm. *Nature Communications*. **2018**, *9*.

Mostofa, K. M. G. (2013). Photobiogeochemistry of organic matter: principles and practices in water environments. Heidelberg ; New York, Springer.

Navea, J. G. and V. H. Grassian (2018). Photochemistry of atmospheric particles. Encyclopedia of interfacial chemistry. K. Wandelt. Oxford, Elsevier**:** 553-562.

Patterson, J. P., D. B. Collins, J. M. Michaud, J. L. Axson, C. M. Sultana, T. Moser, A. C. Dommer, J. Conner, V. H. Grassian, M. D. Stokes, G. B. Deane, J. E. Evans, M. D. Burkart, K. A. Prather and N. C. Gianneschi. Sea spray aerosol structure and composition using cryogenic transmission electron microscopy. *Acs Central Science*. **2016**, *2*(1): 40-47.

Shrestha, M., M. Luo, Y. M. Li, B. Xiang, W. Xiong and V. H. Grassian. Let there be light: stability of palmitic acid monolayers at the air/salt water interface in the presence and absence of simulated solar light and a photosensitizer. *Chemical Science*. **2018**, *9*(26): 5716-5723.

Smets, W., S. Moretti, S. Denys and S. Lebeer. Airborne bacteria in the atmosphere: presence, purpose, and potential. *Atmospheric Environment*. **2016**, *139*: 214-221.

Trueblood, J. V., M. R. Alves, D. Power, M. V. Santander, R. E. Cochran, K. A. Prather and V. H. Grassian. Shedding light on photosensitized reactions within marine-relevant organic thin films. *ACS Earth and Space Chemistry*. **2019**, *3*(8): 1614-1623.

Tsui, W. G. and V. F. McNeill. Modeling secondary organic aerosol production from photosensitized humic-like substances (HULIS). *Environmental Science & Technology Letters*. **2018**, *5*(5): 255-259.

Verdugo, P., A. L. Alldredge, F. Azam, D. L. Kirchman, U. Passow and P. H. Santschi. The oceanic gel phase: a bridge in the DOM-POM continuum. *Marine Chemistry*. **2004**, *92*(1-4): 67-85.

Wang, L., Y. J. Li, Y. Xiong, X. H. Mao, L. Y. Zhang, J. F. Xu, W. B. Tan, J. S. Wang, T. T. Li, B. D. Xi and D. H. Wang. Spectroscopic characterization of dissolved organic matter from sludge solubilization treatment by micro-bubble technologyLei. *Ecological Engineering*. **2017**, *106*: 94-100.

Wang, X. F., C. M. Sultana, J. Trueblood, T. C. J. Hill, F. Malfatti, C. Lee, O. Laskina, K. A. Moore, C. M. Beall, C. S. McCluskey, G. C. Cornwell, Y. Y. Zhou, J. L. Cox, M. A. Pendergraft, M. V. Santander, T. H. Bertram, C. D. Cappa, F. Azam, P. J. DeMott, V. H. Grassian and K. A. Prather. Microbial control of sea spray aerosol composition: a tale of two blooms. *ACS Central Science*. **2015**, *1*(3): 124-131.

Wang, X. K., R. Gemayel, N. Hayeck, S. Perrier, N. Charbonnel, C. H. Xu, H. Chen, C. Zhu, L. W. Zhang, L. Wang, S. A. Nizkorodov, X. M. Wang, Z. Wang, T. Wang, A. Mellouki, M. Riva, J. M. Chen and C. George. Atmospheric photosensitization: a new pathway for sulfate formation. *Environmental Science & Technology*. **2020**, *54*(6): 3114-3120.

Wei, D., H. Dong, N. Wu, H. H. Ngo, W. S. Guo, B. Du and Q. Wei. A fluorescence approach to assess the production of soluble microbial products from aerobic granular sludge under the stress of 2,4-dichlorophenol. *Scientific Reports*. **2016**, *6*.

Yamin, G., M. Borisover, E. Cohen and J. van Rijn. Accumulation of humic-like and proteinaceous dissolved organic matter in zero-discharge aquaculture systems as revealed by fluorescence EEM spectroscopy. *Water Research*. **2017**, *108*: 412-421.

Yang, W. J., C. Han, H. Yang and X. X. Xue. Significant HONO formation by the photolysis of nitrates in the presence of humic acids. *Environmental Pollution*. **2018**, *243*: 679-686.

Zhou, H. X., S. W. Yan, L. S. Lian and W. H. Song. Triplet-state photochemistry of dissolved organic matter: triplet-state energy distribution and surface electric charge conditions. *Environmental Science & Technology*. **2019**, *53*(5): 2482-2490.